# Pulsed Field Magnetometry for High-Speed Characterisation of Rare Earth Magnets

by

Robin Nathan Cornelius

A thesis submitted to the University of Plymouth
in partial fulfilment for the degree of

**DOCTOR OF PHILOSOPHY**

**School of Computing,
Communications and Electronics**

**in collaboration with
Hirst Magnetic Instruments Ltd.**

**July 2005**

**ROBIN NATHAN CORNELIUS**

# PULSED FIELD MAGNETOMETRY FOR HIGH-SPEED CHARACTERISATION OF RARE EARTH MAGNETS

Pulsed Field Magnetometers (PFM) offer large advantages over conventional magnetic characterising equipment for high speed measurement of modern permanent magnet materials. A lack of systematic design procedure and many perceived problems has prevented adoption of the technique. This thesis examines in detail the system components of a PFM, the perceived problems and presents design methodology for critical system components and data processing methods to recover accurate and repeatable material characteristics.

A method for the design of position insensitive gradient coils is presented and compared to a conventional design. By using an inverse Biot-Savat simulation, the coupling from each turn of the pickup coil to the point of interest is calculated and optimum winding positions calculated for homogenous pickup. Problems of thermal expansion due to differential temperatures are considered and a method developed to remove the problem using cooling. The possible origin of the zero signal is presented and a method for nulling of gradient coils to remove this zero signal using an external potentiometer is considered and results demonstrated.

The design and construction of field generation coils are examined in detail and a complete method is developed for the determination of magnetic and electrical characteristics for a given geometry. The effect of skew due to conductor thickness is considered in the model to ensure optimum homogeneity of applied field and the size of the conductor wires are accounted for in a multifilament model. A software tool is created to implement these design methods and the results are compared to physical models with good agreement.

The offline processing of PFM data is considered and methods for the removal of the effects of eddy currents are presented and results demonstrated. By measuring the sample at different rates of change of applied field, two measurements with different eddy current components are generated. This data can be then used to calculate and remove the eddy current component. Careful consideration is given to time aligning the data and insuring the stability of the differential equations.

Possible methods for calibration of a PFM are examined in detail and compared. Methods include standard sample, calibration transfer coils, and the removal of eddy currents in calibration samples by using representative eddy currents in non-magnetic materials. Standard sample and transfer coils have proved successful and produced results with a high degree of agreement compared with conventional systems.

A prototype industrial PFM was built, designed for the high speed characterisation of rare earth materials in an industrial environment. Details of the system are described. Extensive industrial trials were carried out and results from the trials are discussed in detail. Comparisons are made with conventional systems and the PFM is found to have better repeatability and comparable accuracy. Overall the PFM was highly successful and has proved the technology as viable for high speed characterisation of permanent magnet materials. Future work describes improvements to the measurement technique to achieve higher accuracy, such as accounting for distributed demagnetisation factors, and describes the next generation of PFM machines that are to be built due to this work.

# Table of contents

# List of Figures

# List of Tables

# Nomenclature

Table 1 presents the common nomenclature used throughout this thesis. Additional terms are defined where they are introduced.

| Symbol | Description | Unit | Units symbol |
|---|---|---|---|
| R | Electrical resistance | Ohm | Ω |
| L | Inductance | Henry | H |
| F | Capacitance | Farad | F |
| I | Electrical current | Ampere | A |
| i | Instantaneous electrical current | Ampere | A |
| v | Electrical voltage | Volt | V |
| ε | Induced emf | Volt | V |
| N | Number of windings on a coil | | |
| **B** | Magnetic flux density | Tesla | T |
| B | Magnitude of magnetic flux density | Tesla | T |
| **H** | Magnetic field strength | Ampere/metre | $A\ m^{-1}$ |
| H | Magnitude of magnetic field strength | Ampere/metre | $A\ m^{-1}$ |
| **J** | Magnetisation of a magnet | Tesla | T |
| J | Magnitude of magnetisation of a magnet | Tesla | T |
| $\phi$ | Magnetic flux | Weber | Wb |
| $\mu_0$ | Permeability of free space* | Weber/Ampere metre | $Wb\ A^{-1}\ m^{-1}$ |
| $\mathbf{J_E}$ | Eddy current | Ampere | A |
| A | Area | Cubic metre | $m^3$ |
| l | Length | Metre | m |
| t | Time | Second | s |
| T | Temperature | Kelvin | K |

*Table 1 - Nomenclature used in this thesis.*

* The permeability of free space is a constant and is defined in S.I. units as

$4\pi \times 10^{-7}$ $Wb\ A^{-1}\ m^{-1}$

Table 2 contains a number of terms that are commonly used to describe the properties of permanent magnet materials that are used throughout this thesis.

| Symbol | Description | Units |
|---|---|---|
| $BH_{MAX}$ | Energy product; this indicates the maximum energy that a magnetic material can supply to an external magnetic circuit when operating at the optimal point on its de-magnetisation curve. It is the maximum value of B x H in the demagnetisation quadrant. | $J/m^3$ |
| $B_R$ | Remanence; the magnetic induction or magnetisation that remains in a magnetic circuit after the removal of an applied magnetising field due to the magnetisation of the magnet. | T |
| $H_C$ | Coercivity; the demagnetising field, necessary to reduce the observed magnetisation to zero after the magnet has previously been brought to saturation. | A/m |
| $H_{CI}$ | Intrinsic coercivity, The resistance of a magnetic material to demagnetisation. This is the value of H where the where the intrinsic curve intersects the H axis in the second quadrant of the hysteresis loop | A/m |
| $H_{SAT}$ | Saturation; the applied field required to achieve magnetisation. | A/m |
| $\mu_r$ | Relative permeability; a measure of how easy magnetic flux can be conducted by the material, relative to the permeability of free space ($\mu_0$). | |

*Table 2 - Terms used to describe permanent magnet properties.*

# Acknowledgement

The author wishes to thank the following people:-

David Jenkins, David Wilton and Hazel Shute of the University of Plymouth for their supervision and support during this research.

John Dudding, Paul Knell and other members at staff of Hirst Magnetic Instruments for providing the opportunity for this research.

David Edwards and Jockm Kneff of Mecelec Developments Ltd for their contribution to the mechanical handing system that formed part of the end result of this research.

Professor Roland Grossinger of University of Vienna, for constructive discussions during the research.

Beatrtrix Enzberg-Mahlke of Magnetfabrik Schramberg and Wilhelm Fernengel of VAC for providing access to magnet producing factories and for running trials of the prototype system.

Phillip Lethuillier and Jean Toussaint of CNRS, France for discussions on self demagnetisation and pickup coils.

## AUTHOR'S DECLARATION

At no time during the registration for the degree of Doctor of Philosophy has the author been registered for any other University award.

This study was self financed by the author and carried out in collaboration with Hirst Magnetic Instruments Ltd by whom the author was employed during this study.

Relevant scientific seminars and conferences were regularly attended at which work was often presented and several papers were published.

Publications (or presentation or other forms of creative and performing work):-

- UK Magnetic Society, Sheffield seminar - presentation given and paper published in proceedings; "Pulsed Field Magnetometry", November 2001.

- JEMS 2001 – poster presented and paper published in proceedings (author but not presenter); "A Pulsed Field Magnetometer for the Quality Control of Permanent magnets". Journal of Magnetism and Magnetic Materials. pp. 1402–1404, 2002.

- European project meeting – Gloucester, technical presentation on research; "Industrial PFM progress report", 2002.

- IEEE Intermag 2002 – poster presented and paper published in proceedings; "Pulsed Field Magnetometer for industrial use". IEEE Transactions on Magnetics, Vol. 38, No. 5, pp. 2462-2464, September 2002.

- IEEE Intermag 2002 – posters presented and papers published in proceedings (co-author); "Calibration of an industrial Pulsed Field Magnetometer". IEEE Transactions on Magnetics, Vol 38, No 5, pp. 2982 – 2984, September 2002.

- European project meeting – Vienna, technical presentation on research; "Industrial PFM progress report", 2002.

- Seventh international workshop on 1&2 dimensional magnetic measurement and testing, Invited paper presented and published in proceedings (co-author). "Survey of pulsed field measurement technique", PTB-E-81, ISBN 3-89701-992-2, pp. 67-76, June 2003.

- Seventh international workshop on 1&2 dimensional magnetic measurement and testing, Invited paper presented and published in proceedings; "Accuracy and repeatability of an industrial Pulsed Field Magnetometer", proceedings, PTB-E-81, ISBN 3-89701-992-2, pp. 77-80, June 2003.

- European project meeting – Vienna, technical presentation on research; "Industrial PFM progress report", 2003.

All papers that were published in the public domain are attached in Appendix A.

Other conferences attended:-

- UK Magnetics society seminar, "Recent developments in motors and drives for domestic applications" – Leicester, September 2003
- UK Magnetics society seminar, "Magnetic measurements and standards" – Cardiff, April 2004
- UK Magnetics society seminar , "Electrical drive systems for the more electric aircraft" – Bristol , April 2005

External Contacts:-

- Prof. Roland Grossinger – University of Vienna, Austria
- David Edwards and Jockim Kneff of Mecelec Developments, UK
- Beatrtrix Enzberg-Mahlke of Magnetfabrik Schramberg, Germany and Wilhelm Fernengel of V.A.C, Germany.
- Phillip Lethuillier and Jean Toussaint of C.N.R.S.Grenoble, France.

Word count in main body of thesis: 41,062

Signed .....

Date 20-Jan-2006

# Chapter 1 Introduction

## 1.1 Motivation

In 1983, a new magnetic material containing Neodymium, Iron and Boron (NdFeB) was discovered [1]. The material promised new higher efficiency motors in smaller space envelopes than conventional motors. Additional improvements to generators/alternators, actuators and sensors were seen as potential applications. Due to the high price of the NdFeB material, compared to conventional magnets, its use was limited to specialist applications which required the high magnetic energy densities and are not limited by the high cost of their materials.

In the early 1990s Hirst Magnetic Instruments Ltd. (HMI) identified an additional problem that would prevent the wide adoption of NdFeB based magnets, even if the price became acceptable; there was no current magnetic measurement method suitable for the characterisation of the material. The existing standard measurement technique, the permeameter or hysterysgraph, suffered from a number of fundamental limitations that prevented its use for the measurement of NdFeB material. The use of electromagnets and iron yokes, in permeameter systems, places physical limitations on the maximum applied field achievable, making the determination of the intrinsic coercivity of some NdFeB materials very difficult in a permeameter.. The measurement rate of a permeameter has to be limited in order to avoid errors due to the effects of eddy currents. With typical measurement times of 2 to 5 minutes, the permeameter is too slow for high production rate industrial quality control. The problems caused by permeameters made the adoption of quality control standards such as the ISO9000 series difficult and the majority of companies simply ignored the potential benefits of NdFeB materials, such as higher magnetic energy densities and more environmentally stable material, and continued

manufacturing universal motors with ferrite or Alnico materials or companies simply ignored the problem of quality control in order to use NdFeB.

A method of magnetic characterisation known as Pulsed Field Magnetometry has demonstrated the potential to overcome the problems associated with conventional magnetic measurement systems. Pulsed Field Magnetometry suffers a number of fundamental problems that have prevented adoption of the method. These problems include various measurement errors that are a direct consequence of the magnetic characterisation process, such as the effects of eddy currents and self-demagnetisation fields. Other problems have been the lack of systematic design procedures for pickup coils and field generation coils and additional problems are introduced by the requirements of an industrial environment.

A European grant funded project, "MACCHARATEC" [2], was undertaken to address the problems associated with PFM and to create a prototype system suitable for high speed industrial quality control of permanent magnets. The Author was employed by HMI to work on the PFM project. This work involved;

- The creation of a software package for the parametric design of applied field coils for use in PFM systems.
- The design of a position insensitive pickup coil for the detection of the magnetisation of the sample.
- Assessing errors attributed to the method of PFM and creating methods for the minimisation of these errors. These errors include the effects of eddy currents, self demagnetisation and thermal effects.

A prototype industrial PFM system was constructed based on the results of the above work. The Author was actively involved with the design and construction of the

prototype system, including the creation of control and data processing software, high voltage electronics, control electronics and firmware.

This thesis describes the methodology used to design the prototype PFM system, discusses various options for each sub system and why a particular method is selected. Details of the completed industrial system are described and results from industrial trials are discussed in detail.

## 1.2 Literature review

The rapid growth and continuing improvements of new rare earth magnetic materials has led to increased usage in diverse applications such as electric machine rotors, inertia switches and hard disk position sensors. It is necessary to characterise magnetic materials for development or quality control. P. Bretchko and R. Ludwig [3] introduce the problem of measuring modern rare earth magnets and explain that conventional magnetic measurement techniques, which utilise iron cored solenoids, are unsuitable for the characterisation of modern magnetic materials due to a limitation on the applied field caused by saturation of the steel core of the electromagnet. The paper [3] goes on to explain that super conducting magnets are far from ideal, as they are typically limited to fields of less than 100 kOe (1000 kA/m) and also require liquid helium cooling, which causes expensive capital and running costs. The measurement times of conventional systems typically exceeds 5 minutes, making the systems unsuitable for magnet quality control. There are many other examples of the problems with conventional magnetic measurement systems. R. Grossinger et al. [4] shows that static fields with iron yokes of up to 2 Tesla are not sufficient for the measurement of modern magnetic material, and that static hysteresis loops take too much time for industrial process control. Due to the possible speed of the magnet characterisation, PFM is ideal for the measurement of

modern, rare earth permanent magnet materials in the native industrial shapes and at rates suitable for traceable industrial quality control. This is demonstrated by R. Cornelius et al. [5] in which a prototype Pulsed Field Magnetometer that has been designed for use in industry for magnet quality control is presented. The system is capable of measuring 1 magnet every 4 seconds, compared to a typical rate of 5 minutes for a permeameter. The prototype Pulsed Field Magnetometer has been made possible by the work that this thesis describes.

The fundamental principles of Pulsed Field Magnetometry are well understood. A Pulsed Field Magnetometer is essentially a capacitive discharge magnetiser coupled with dedicated instrumentation. A number of authors and groups have considered Pulsed Field Magnetometers as an alternative to conventional magnet characterisation systems such as permeameters and vibrating sample magnetometers. Some of the earliest work on pulsed field measurement systems dates back to the 1970s where E. Bogardus et al. presented a paper [6], where magnetic pulses between 1 μs and 3 ms are used to measure the magnetic moment of ferrofluids. In the late 1980s neodymium iron boron was discovered, this magnetic material had a magnetic saturation and coercive field that was too high for conventional measurement techniques such as permeameters. Pulsed magnetic fields were already used for the magnetisation of magnets and the technology involved could be extended with suitable instrumentation to form a characterisation system. In 1988 R. Grossinger et al. presented one of the first Pulsed Field Magnetometers [7] with emphasis on the measuring system, especially the pickup coils. The paper focuses on the use of a Pulsed Field Magnetometer as a tool for assisting the design of rare earth materials, as the hysteresis and anisotropy field can be easily measured. Prior to this work, R. Grossinger et al. examined the merits and limitations of a pulsed field system for the characterisation of permanent magnets [8]. This paper introduces the problems of the effects of eddy currents and proposes a correction method. It does go on to highlight the advantages of PFM

technology over vibrating sample magnetometers. Other authors have also considered pulsed field systems, and one such author is Min-Seok Song et al. of the Korea Research Institute. Citing earlier work on Pulsed Field Magnetometry, as discussed here, this paper [9] presents a Pulsed Field Magnetometer specialising in high temperature controlled measurements, with the ability to heat specimens up to 200 °C.

The largest problem with Pulsed Field Magnetometry is the measurement errors caused by the effects of eddy currents within the sample being characterised. These errors have prevented the method from being widely adopted. In September 1992, G. Jewell and D. Howe from Sheffield University, working with R. Grossinger and C. Schotzko of Technical University of Vienna presented simulation of the eddy currents in magnets under pulsed fields by employing both axial-symmetry and time-varying boundary conditions to reduce computational time. The results presented in their paper [10] demonstrate simulated instrumentation outputs of a magnet under test showing the effects of eddy currents at different frequencies. However, these results mainly considered the effects of eddy currents induced by the rate of change of the applied field and did not fully model eddy currents caused by the rate of change of magnetisation when factors such as hysteresis are considered. In 2000, C. Golovanov, Gilbert Reyne and Gerard Meunier of Laboratoire d'Electrotechnique de Grenoble, France, R. Grossinger (University of Vienna) and J. Dudding of Hirst Magnetic Instruments, presented a new approach to eddy currents. In this paper [11] a finite element approach is again used but the formulation is chosen for the problem and the electric vector potential (**T**) and the magnetic scalar potential ($\Omega$) are used and the problem is assessed in 3D. The important addition in this paper was the inclusion of the simulation of the magnet's magnetisation and hysteresis. Simulated pickup coil output results were presented and the extra step of considering a method for correcting the effects of eddy currents was considered.

With the theoretical analysis of eddy currents under pulsed field well developed, a practical approach to the analysis of eddy currents and their effects was also considered. In 2001 at the JEMS 01 conference, R. Grossinger et al. presented experimental work where the effects of eddy currents were determined, experimentally, in different (non-magnetic) samples [12]. It confirmed that the effects of eddy currents, in a pulsed field system, were proportional to the conductivity of the sample and proportional to the rate of change of applied field. Results were compared to a finite element simulation and found to be within 10 %. Variations on this work have also been published to the European Commission as part of the European Union funded project MACCHARACTEC [2].

The remaining problem of the correction for the effects of eddy currents has not been well addressed, a report by G. Jewell of Sheffield University [13] gives a method for the correction of the of eddy currents via what has come to be known as the "double pulse technique" or "f/2f method". This report was based on G. Jewell's previous works [10] and [8] and did not fully consider the eddy current effects due to the rate of change of magnetisation in the sample being measured. This report formed the basis of a correction method reported by C. Golovanov et al. in [11] as discussed above. The essence of the report is that by using two pulses of different rates of change of the applied field, it is possible to deduce the eddy current effects, as these will be proportional to the rate of change of the applied field, while the magnetisation of the magnet will be independent of rate of change of the applied field.

Pulsed Field Magnetometry utilises an "open circuit" form of magnetic measurement. This is in common with vibrating sample magnetometers (VSM). The open circuit measurement means that the magnet will generate a self-demagnetising field. This self-demagnetising field will cancel out part of the applied field causing the applied field inside the magnet to be different from the expected field. This problem has been considered by a

number of authors. The original problems of self-demagnetisation factors for ellipsoids and their degenerate forms dates from the work of Poisson. One of the most common magnet shapes, especially for VSMs, is the cylinder and this has led X. Chen, J. A. Brug and R. B. Goldfarb to publish a method for calculating the demagnetising factor of cylinders. The paper [14] presents tables of self-demagnetisation factors for various length to height ratios of cylinders as well as the methods for calculating these tables. Other authors such as R. I Joseph have also considered self-demagnetisation factors with his papers, [15] regarding the demagnetizing field in non-ellipsoidal bodies and [16] which examined ballistic demagnetising factors in uniformly magnetised cylinders. These papers were published in 1965 and 1966 respectively and are both cited by Chen [14].

Many other groups are researching areas related to Pulsed Field Magnetometry such as the Dresden, Insitiitut Fur Angewandte Physik (Institute for Advanced Physics) where they have developed systems to generate magnetic fields up to 100 T in a non-destructive manner [17]. H. Krug et al. provides information on the 1 MJ capacitive discharge system and specially designed solenoids that have to cope with the intense forces involved. These systems are not designed for the measurement of the JH characteristics of permanent magnets, as a Pulsed Field Magnetometer would be, but are used for specific physics research projects. One such use for high field pulsed systems is for the determination of the anisotropy field of permanent magnets. The anisotropy field is the point when all free to rotate domains in the permanent magnet are aligned with the applied field. A method of determining the anisotropy field is singular point detection (SPD). SPD uses successive derivatives of dJ/dH and the singular point is considered as a discontinuity in the function dJ/dH. Various authors have applied the SPD technique to the determination of anisotropy field, G. Asti, in the paper [18], makes the suggestion that singular point detection could be used as a new technique for measuring the anisotropy in polycrystalline samples. Other authors such as R. Grossinger, in the paper [19], consider the effects of temperature on the

anisotropy field of permanent magnets and use the SPD technique to determine the anisotropy field between 150 K and 300 K.

Other groups are using pulsed field systems with super conducting or liquid nitrogen cooled copper coils, and one such example of this is [20] by K. Okuno. This paper examined experimental results from the Japanese low temperate coil with pulsed fields and "extended-condition tests".

The recent work on Pulsed Field Magnetometry has concentrated on the use of Pulsed Field Magnetometers in an industrial environment and the calibration of Pulsed Field Magnetometers. Two papers were presented at the Intermag 2002 conference by R. Cornelius et al. [5] and R Grossinger et al. [21], both these papers are from the same research group. These papers demonstrate practical methods of calibrating both the magnetisation and applied field detection system of a Pulsed Field Magnetometer and the use of a Pulsed Field Magnetometer in a 100 % quality control industrial environment. Much of the work in this thesis has formed the basis of these papers.

The most recent development in Pulsed Field Magnetometry is work with the International Electrotechnical Commission (IEC) and the British Standards Institute (BSI) to achieve international published standards for Pulsed Field Magnetometry systems. An IEC technical report has been published [22] and is based on the developments of Pulsed Field Magnetometry reported in this thesis.

# Chapter 2 An overview of magnetic materials

## 2.1 A history of permanent magnetism

The first permanent magnets known were lodestone ($Fe_3O_4$), an oxide ore of iron that occurs naturally. The magnetic field capability of lodestone is low and large volumes are required to produce a magnetic field of any practical use. Initially lodestone would have found uses as compass needles for navigation.

In the $18^{th}$ century with the advances in the steel making industry, magnetic carbon steels were discovered. Alloying with carbon alone produces soft magnetic steels which are little or no use as permanent magnets. Other alloys such as those including tungsten, to increase the hardness of the steel, and chromium, to reduce the steel's tendency to oxidise, have magnetic side effects. These magnetic carbon steels had far higher magnetic field strengths than loadstone but were easily demagnetised. This resulted in only long shapes being practical for permanent magnets, to reduce the self-demagnetisation effect, or for the magnets to be in closed circuits so there was no self-demagnetising field.

In the 1930s a material named Alnico was discovered. Initially developed for military applications for use in early radar, Alnico or aluminium, nickel, cobalt can be regarded as the first modern permanent magnet. The typical composition of an early Alnico magnet is shown in Table 3. While Alnico has a high magnetic field strength it also has a low coercivity, which meant it suffered from the effects of self-demagnetisation fields and so was easy to demagnetise. Alnico was widely used in motors and loudspeakers and started the development of permanent magnet applications. Alnico is still in use today, loudspeakers being one of its most common applications.

Alnico had one major draw back, its price. Cobalt, at the time, was an expensive element and at 12.5 % of the total magnet, represents a large proportion of its cost. With the majority of the world's supply coming from the "Iron Curtain" part of the world, the Cold War made access to this cobalt resource impossible. In addition the "Cobalt crisis" of the 1970's in Zaire caused the price of Cobalt to jump from less than $3 to over $40 per pound. Zaire was the largest producer of Cobalt outside the "Iron Curtain" and a series of events resulted in concern over the supply of Cobalt. In 1976 the US government ceased sales of Cobalt from the government stockpile. Two years of demand exceeding production reduced the Zairian producers inventories and an invasion of the copper-cobalt mining region in Zaire caused uncertainty in the supply of Cobalt leading to large instabilities in its price. Alternative, non-cobalt based magnet technologies, or ones that made more efficient use of cobalt, were required.

| | |
|---|---|
| Cobalt | 12.5 % |
| Aluminium | 10.0 % |
| Nickel | 18.0 % |
| Copper | 6.0 % |
| Iron | 53.5 % |

*Table 3 - Typical composition of Alnico type magnets showing the distribution of each metal in the alloy.*

## 2.2 Ferrite magnets.

The first "ferrite" magnets were cobalt alloys, although by today's standards they would not be classified as permanent magnets but magnetically soft materials. In use from around 1917 [23], this particular alloy has the highest saturation value of any magnetic material combined with low coercivity, leading to its continual use in specialist applications. It is particularly suitable for pole piece materials and transformer cores

where a high magnetic field is desirable but losses due to hysteresis and reluctance must be kept to a minimum. Later other ferrite alloys were developed such as the barium and strontium ferrites that are still in use today [23]. The use of barium and strontium as alloys increases the magnetic strength of ferrite to a more useful level. Although limited to a maximum of around 5 Mega-Gauss-Oersted (MGOe) the price of ferrite, its magnetic stability and lack of oxidation have ensured that it is still the most common magnet material in use today.

## 2.3 The rare earth materials

The first rare earth materials were samarium cobalt based and have the composition $SmCo_5$, developed by Dr. Karl J. Strnat of the U. S. Air Force Materials Laboratory [23]. The term rare earth refers to the part of the alloy compound, which is found on the Periodic Table in the "rare earth" group of metals. An energy product of up to 18 MGOe was now possible which enabled more efficient magnetic devices.

With changes in the alloys used in samarium cobalt magnets it has been possible to increase the magnetic energy of samarium based magnets up to 32 MGOe, with a mixture of cobalt, iron, copper and zirconium in the form $Sm_2(Co\text{-}Fe\text{-}Cu\text{-}Zr)_{17}$. The $Sm_2Co_{17}$ variety remains very useful today. It has exceptionally high coercive strength and is very hard to demagnetise (it also requires a large applied field to magnetise). This resistance to demagnetisation and its ability to withstand high temperatures has placed samarium based magnets in a very important position in modern technology.

In the early 1980s the Sumitomo Special Metals Company and General Motors almost simultaneously announced the discovery of neodymium-iron-boron magnets (NdFeB) [1]. Neodymium based magnets started a revolution with energy densities almost double that of the previous samarium cobalt generation. With lower manufacture and material costs

compared to samarium based magnets, they found uses in existing applications; improving performance and reducing size, as well as in new applications only now possible, such as very small stepper motors.

NdFeB compounds are available with energy densities over 400 $kJ/m^3$ and coercive strengths over 2800 kA/m but do have one disadvantage compared to samarium cobalt. The curie temperature of NdFeB is in the range 250 - 350 °C while samarium cobalt have typical curie temperatures in the range 700 - 900 °C. This has ensured that samarium cobalt has not been completely replaced by NdFeB as many applications exist where the required operational temperature exceeds the curie temperature of NdFeB.

## 2.4 The future

Research continues into improving magnetic materials although the main focus of "bulk" permanent magnet materials is on improvements to corrosion resistance [24] as well as the fine-tuning of properties to specific applications. Figure 1 shows the development of the modern permanent magnet materials and the improvements in energy densities achieved. It is not expected that there will be any more improvements of the magnitude that neodymium based magnets introduced, as it is believed theoretical maximums are being approached.

Magnetic materials are also used in magnetic recording media and development in this area is very strong. The materials developed by this research, while very valuable, are not considered in this report as they are outside the scope of what Pulsed Field Magnetometers can measure. They tend to be thin-film based materials that are designed to be a maximum of 10s of nanometres thick and are best suited to measurement by super conducting vibrating sample magnetometers where the required high sensitivity is available coupled with the required applied field strength.

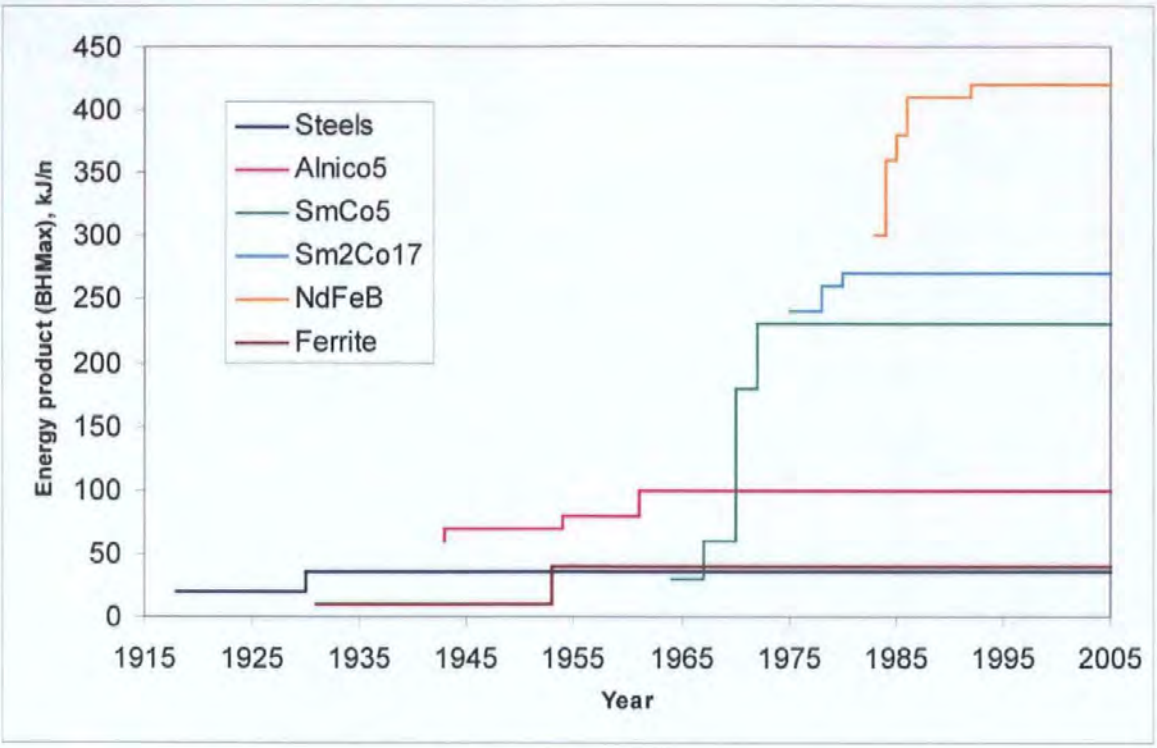


*Figure 1 - Development of permanent magnets, showing types and energy density improvements vs. time [25].*

## 2.5 Properties of magnetic materials

There are a number of properties of magnets that are used to describe the magnetic material. These properties are useful when designing products that utilise magnets and for quality control purposes, i.e. ensuring that the properties of a given magnet are within design tolerances. The main properties of interest are remanence ($B_R$), coercivity ($H_C$), intrinsic coercivity ($H_{CI}$) and the maximum energy product ($BH_{MAX}$). The definition of these terms has already been given in Table 2 and the terms are shown graphically in Figure 2. Chapter 6 gives details on how these parameters are measured.

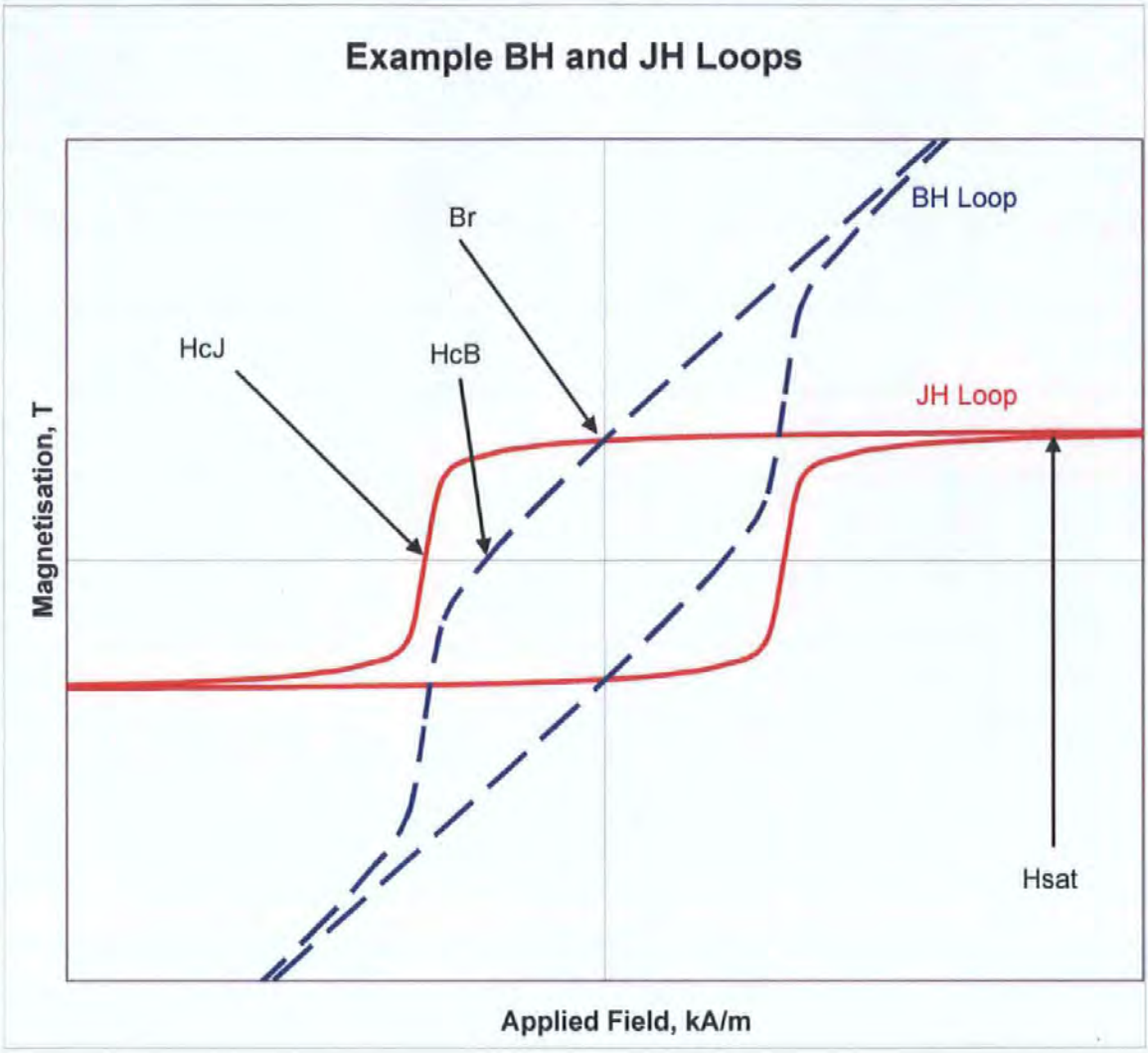


*Figure 2 - Example BH and JH loops showing some of the most critical measurement points. The two loops are related by B=μ0H+J.*

Tables 4 and 5 show a selection of published data for commercially available ferrite, neodymium iron boron and samarium cobalt magnets [26]. They represent typical magnets that can be found in devices utilising magnetic components. The parameter of greatest relevance to this discussion is the $H_{CI}$ values, particularly for the rare earth magnets. It can be seen that values of $H_{CI}$ exist up to 2800 kA/m, in free air this is equivalent to approximately 3.5 Tesla. Conventional magnet characterisation systems such as the hysteresisgraph have limits on the available applied field due to the use of iron pole pieces with a saturation of 2 - 2.5 Tesla. It is therefore not possible to correctly characterise these materials using a hysteresisgraph. Hysteresisgraphs and other conventional magnetic measurement systems and their limitations are discussed in detail in the next chapter.

| Material | Energy Product $(B*H)_{max.}$ | | Remanence $B_r$ | | Temperature coefficient of $B_r$ | Coercivity $H_c$ | | $H_{ci}$ | | Temperature coefficient of $H_c$ | Density | Curie Temp. | Operating Temp. max. |
|---|---|---|---|---|---|---|---|---|---|---|---|---|---|
| | $kJ/m^3$ | MGOe | mT | kG | % / K | kA / m | kOe | kA / m | kOe | % / K | $g / cm^3$ | approx. °C | approx. °C |
| HF 8/22 isotropic | 8,5 | 1,1 | 220 | 2,20 | -0,2 | 140 | 1,76 | 230 | 2,89 | +0,3 | 4,8 | 450 | 250 |
| HF 24/16 | 25,5 | 3,2 | 365 | 3,65 | -0,2 | 175 | 2,20 | 180 | 2,26 | +0,3 | 5,0 | 450 | 250 |
| HF 26/16 | 27 | 3,4 | 380 | 3,80 | -0,2 | 175 | 2,20 | 180 | 2,26 | +0,3 | 5,0 | 450 | 250 |
| HF 28/16 | 30 | 3,8 | 400 | 4,00 | -0,2 | 170 | 2,14 | 170 | 2,14 | +0,3 | 5,0 | 450 | 250 |
| HF 30/16 | 31,5 | 3,9 | 410 | 4,10 | -0,2 | 170 | 2,14 | 170 | 2,14 | +0,3 | 5,0 | 450 | 250 |
| HF 8/26 isotropic | 8,5 | 1,1 | 220 | 2,20 | -0,2 | 140 | 1,76 | 270 | 3,394 | +0,3 | 4,8 | 450 | 250 |
| HF 26/24 | 27 | 3,4 | 380 | 3,80 | -0,2 | 240 | 3,01 | 250 | 3,14 | +0,3 | 4,8 | 450 | 250 |
| HF 28/26 | 30 | 3,8 | 395 | 3,95 | -0,2 | 265 | 3,33 | 275 | 3,45 | +0,3 | 4,85 | 450 | 250 |
| HF 28/28 | 30 | 3,8 | 395 | 3,95 | -0,2 | 280 | 3,35 | 290 | 3,6 | +0,3 | 4,85 | 450 | 250 |
| HF 30/26 | 31,5 | 3,9 | 405 | 4,05 | -0,2 | 260 | 3,33 | 270 | 3,39 | +0,3 | 4,85 | 450 | 250 |

*Table 4 - Summary of commercially available ferrite magnets, demonstrating typical magnetic properties [26].*

| Material | Energy Product $(B*H)_{max.}$ | | Remanence $B_r$ | | Temperature coefficient of $B_r$ | Coercivity $H_c$ | | Coercivity $H_{ci}$ | | Temperature coefficient of $H_{cJ}$ | Density | Curie Temp. | Operating Temp. max. |
|---|---|---|---|---|---|---|---|---|---|---|---|---|---|
| | $kJ/m^3$ | MGOe | mT | kG | % / K | kA / m | kOe | kA / m | kOe | % / K | $g / cm^3$ | approx. °C | approx. °C |
| SmCo5 140/175w | 155 | 19,5 | 880 | 8,80 | -0,042 | 690 | 8,70 | 2000 | 25 | -0,25 | 8,3 | 720 | 250 |
| SmCo5 160/175h | 170 | 21,5 | 925 | 9,25 | -0,042 | 710 | 8,90 | 2000 | 25 | -0,25 | 8,3 | 720 | 250 |
| Sm2Co17 175/160w | 200 | 25 | 1010 | 10,10 | -0,03 | 730 | 9,20 | 2000 | 25 | -0,19 | 8,3 | 825 | 350 |
| Sm2Co17 190/160h | 215 | 27 | 1060 | 10,60 | -0,03 | 790 | 9,90 | 2000 | 25 | -0,19 | 8,3 | 825 | 350 |
| NdFeB 180/250w | 210 | 26,4 | 1050 | 10,50 | -0,09 | 790 | 9,90 | 2800 | 35,2 | -0,5 | 7,6 | 350 | 220 |
| NdFeB 200/220w | 230 | 28,9 | 1110 | 11,10 | -0,09 | 850 | 10,70 | 2500 | 31,4 | -0,5 | 7,6 | 350 | 190 |
| NdFeB 210/250h | 240 | 30,2 | 1110 | 11,10 | -0,09 | 860 | 10,80 | 2800 | 35,2 | -0,5 | 7,6 | 350 | 220 |
| NdFeB 210/220h | 240 | 30,2 | 1115 | 11,15 | -0,09 | 860 | 10,80 | 2500 | 31,4 | -0,5 | 7,6 | 350 | 190 |
| NdFeB 230/220h | 255 | 32,1 | 1160 | 11,60 | -0,09 | 890 | 11,20 | 2500 | 31,4 | -0,5 | 7,6 | 350 | 190 |
| NdFeB 250/125w | 280 | 35,2 | 1230 | 12,30 | -0,11 | 890 | 11,20 | 1400 | 17,6 | -0,6 | 7,5 | 330 | 130 |
| NdFeB 250/175h | 295 | 37,1 | 1240 | 12,40 | -0,1 | 920 | 11,60 | 1900 | 23,9 | -0,6 | 7,6 | 340 | 160 |
| NdFeB 270/125h | 300 | 37,7 | 1280 | 12,80 | -0,11 | 920 | 11,60 | 1400 | 17,6 | -0,6 | 7,5 | 330 | 130 |
| NdFeB 300/125h | 330 | 41,5 | 1320 | 13,20 | -0,11 | 950 | 11,90 | 1400 | 17,6 | -0,6 | 7,5 | 330 | 130 |

*Table 5 - Summary of commercially available rare earth magnets, demonstrating typical ranges of magnetic parameters [26].*

# Chapter 3 The need for Pulsed Field Magnetometry

Society is increasingly dependent on magnetic materials and they are to be found in nearly every aspect of modern life, even if their use is not immediately obvious. The main uses of magnets are as components in motors, generators, sensors and in storage devices such as hard disk drives. Some of the main industries that use permanent magnets are: -

- Automotive
- Aerospace
- Consumer electronics
- Telecommunications

Due to the high price of neodymium iron boron (NdFeB) based magnets, they have been slow to make a serious market impact, despite offering significant performance increases over ferrite and Alnico based magnets.

The automotive industry is today one of the biggest magnet consumers. In the 1950s a car may have contained 1 magnet; today there can be over 200 magnets in a modern vehicle. Some of these magnets are operating in safety critical areas such as ABS sensors and airbag control, while others are used for more aesthetical uses such as loudspeakers. The advantages to the automotive industry, of switching to rare-earth based magnetic materials, are that magnetic components can be smaller, or more powerful, and more efficient. This results in lighter more efficient vehicles or a greater number of features in the same physical space. The current trend towards total computer control and minimising mechanical power transfer also means more opportunities for magnets. With electric water pumps, hydroelectric valves, brake by wire, steer by wire and combined flywheel/alternator systems all starting to appear in cars, the future for magnets never looked brighter, especially for rare earth type magnets.

The relative cost of NdFeB magnets compared to ferrite magnets has traditionally favoured ferrite, but these are not suitable for all the new features being added, as the energy densities of the magnets would result in prohibitively large and inefficient components. With taxes on $CO/CO_2$ emissions from cars, it is in the manufacturers interest to make the vehicles more efficient and one way to do this is to replace ferrite magnets with rare earth magnets to achieve greater magnetic energy densities and be able to manufacture smaller more efficient components.

In consumer electronics, increased legislation has required electrical appliances to be efficiency rated. Washing machines, fridges and many other consumer products are now labelled with their energy efficiency and it is a big selling point. These appliances have gained improvements to efficiencies by better motor design with the use of rare earth magnets instead of Alnico or ferrite magnets.

## 3.1 Quality control

With an increasing number of companies having ISO9000 series accreditation where all procedures and processes are traceable and accountable, how can these companies rely on untested magnets? Some kind of quality control and traceability procedure must be implemented either by them or by their suppliers so they can fully achieve the specifications of the accreditation.

## 3.2 Safety critical magnets

If a washing machine is 10 % slow due to out of tolerance magnets, will the consumer even notice and does it really matter? Although this is annoying to the quality control department it is unlikely anyone would ever notice. If an ABS breaking system is 10 % out of tolerance due to magnet problems or if the air bag inertia sensor is 10 % out of tolerance does it matter now? In the latter two examples quality control is, or should be, mandatory. Even for the example of the washing machine, a magnet quality problem on a

larger scale over many machines would be a problem and could cause their quoted energy efficiencies to be incorrect and damage their commercial image or cause a large scale product recall.

There are numerous applications of magnets in safety critical areas, many in the automotive industry but also in the aerospace industry where a defect could bring down an aircraft or loose a one billion dollar satellite. In safety critical situations it is essential that every component be within specification. While in the case of a billion dollar satellite you could afford the time to test every component and sub-assembly, in the case of the automotive industry this becomes extremely problematic, due to the high volume and the extra costs involved with the testing requirements, any test procedure must be fast, efficient and add value to the product being tested or be a compulsory procedure.

It is desirable to test components rather than finished assemblies as if there is a defect it is cheaper to discard one component than an entire assembly or rework that assembly to fix the component. The automotive industry has also placed pressure on its suppliers so that if their assembly is defective they can become liable for additional down stream costs of their mistake. Many other examples exist even of non-safety critical situations where testing of components is desirable. Hard-disk drive actuator magnets are a good example. A manufacturer of hard-disk drives would not want uncertain magnets in their products as they have reputations built on reliability.

## 3.3 The problem of unlicensed magnetic material

The process of creating many neodymium-iron-boron powders is patented. This has lead to a number of magnet manufacturers creating their own, unlicensed, magnet powders that are then used to form magnets. Many of these companies are based in the Far East. Due to the prices of the "unlicensed" products compared to the "licensed" products, many

companies, including world leaders are using this alternative supply of NdFeB magnets. In one such example Magnequench sued IBM for the alleged use of "illegal" magnets in hard disk drives. The court case demonstrates that even world's biggest players certainly consider these unlicensed magnets as a serious option due to the potential cost savings. Some of the unlicensed producers make good quality magnets, while others make variable quality magnets. The low price of these magnets often persuades the purchasers to choose price over quality. With potential quality problems it makes the testing of the products absolutely necessary.

## 3.4 A solution?

The answer seems simple, for safety/mission critical or high reliability or variable magnet quality situations, test every component and test the rare earth magnets. While the answer is simple, its implementation is not. Conventional magnetic measurement systems have limitations on speed of operation, shapes of samples, limited data output and other "conditions" that make them totally unsuitable for quality control and testing of "industrial" rare earth permanent magnets [5]. Only methods such as batch testing are left and even these may require destructive testing where the component is not tested in its intended end form. This is unacceptable and 100 % of components must be tested using the actual components not representative samples being tested.

A technology called Pulsed Field Magnetometry (PFM) exists [8] and has the potential to measure any magnetic material in its native industrial shape at rates in excess of 1 magnet in 4 seconds. This technology has been slow to develop due to many perceived problems with the method. Pulsed Field Magnetometry relies on exposing the magnetic sample to an intense pulsed magnetic field. This pulse is strong enough to drive the magnet around its major hysteresis curve. During the pulse, instrumentation measures the magnet by

determining the magnet's magnetisation for a given applied field, and its properties are deduced.

PFM systems can detect problems with the manufacture of magnets. Some of the most common problems occur during the powder treatment process. Excess oxidation, incorrect heat treatment or even contamination of the material could all affect the magnetic performance of the final magnet. The PFM can detect these types of problems as incorrect magnetic material properties. Another potential problem with magnets is cracks. If the material has a physical defect then this could fail when the item is assembled in its final product. It is believed that PFM system can detect many of these cracks. A crack in a magnetic material should interfere with the eddy current path and this would result in lower than expected eddy currents within the material. One of the parameters that is calculated by the PFM system during eddy current removal is proportional to conductivity so this can be used as a quality control check. In practice it is very difficult to obtain a magnet with a known crack to test how well crack detection would function.

The major problems with Pulsed Field Magnetometry are eddy currents. Any dynamic magnetic field will induce eddy currents in any electrically conductive material. As magnetic materials can be highly conductive these eddy currents can become significant and cause errors in the measurement of the magnet, due to the magnetic fields the eddy currents themselves generate. There are many additional sources of error that have prevented Pulsed Field Magnetometry from fulfilling its potential, such as the effect of self-demagnetisation, pickup coil design, field generation coil design and calibration.

This thesis rigorously examines the method of Pulsed Field Magnetometry identifying the sources of measurement error and presenting methods to overcome these errors. The thesis

also presents a systematic design procedure for each of the associated sub systems of a Pulsed Field Magnetometer, instead of the "rules of thumb" that have been used until now.

# Chapter 4 Magnetic measurement systems

## 4.1 Conventional systems

Conventional magnetic measurement techniques have limitations that can make them unsuitable for the measurement of modern, hard, rare-earth based magnets, of the sizes and shapes that are used in industry today. Most conventional characterisation systems have extreme size and shape limitations and operate at speeds that are only suitable for laboratory based testing. Many systems are also incapable of generating the fields required to measure modern permanent magnets, although these systems do have other specific usages.

All magnet characterisation systems are based on the same basic principles. A magnet to be tested is driven around part of its hysteresis loop via an applied external field, which is measured and recorded. The magnet's response to the applied field is detected in the form of the magnet's magnetisation, **J**. By plotting the applied field, **H**, against the magnet's magnetisation, **J**, it is possible to deduce nearly all the required magnetic parameters of a permanent magnet material. The commonly required parameters were discussed "Nomenclature". These parameters may be used for quality control or analysis of the material.

The properties of a magnetic material can be deduced by applying a magnetic field to a sample and by measuring the sample's response. Some parameters, such as the saturation of the material, are difficult to obtain for some materials due to the magnitude of applied field required. These difficulties are discussed in this chapter.

Magnet characterisation systems can be divided up in to a two basic categories: closed circuit and open circuit methods. Closed circuit methods do not suffer from the effects of self-demagnetisation. The measurement systems can also be classified into static, slow dynamic and fast dynamic systems as shown in Table 6.

| Measurement method | Closed Circuit | Open Circuit |
|---|---|---|
| **Static** | Uncommon | VSM, AGM, Extraction method. |
| **Slow dynamic** | Permeameter | Uncommon |
| **Fast dynamic** | Infeasible | Pulsed Field Magnetometry<br>Point by Point |

*Table 6 - Basic measurement method classification, separating methods of operation.*

It should be noted that Pulsed Field Magnetometry and Point by Point are the only fast dynamic methods while the other methods rely on static or slow dynamic applied fields. No closed loop dynamic system exists, as it is infeasible to construct one. It would require a soft magnetic material, with a very low electrical conductivity to be used as the pole piece material with sufficiently high saturation to allow the required materials to be measured. Although some low conductivity materials exists, such as produced by the iron powder process, these materials have a usable permeability many times lower than iron and this seriously limits their usefulness in this application. Closed circuit static methods are very uncommon. Although technically feasible, the method has potential complications in magnetisation measurement and no additional advantages over the standard permeameter. An open circuit slow dynamic method is technically possible; however problems arise with sustained high field generation. While super-conducting coils could be used for the field generation, no advantages are gained by this method.

### 4.1.1 Permeameters

Permeameters use an electromagnet to generate the applied field and iron pole pieces to carry the magnetic flux to the sample. Typically coils surrounding an iron yoke are energised with current from power amplifiers to produce a magnetic field. As iron has a much greater magnetic permeability than air, it offers much less reluctance to carrying magnetic flux. The flux is concentrated in the iron resulting in a larger flux density when compared to a solenoid in air. The iron yokes are adjustable to enable the pole pieces to make good contact with the sample to be measured, making a closed magnet circuit. Any flux generated by the magnet will also be conducted through the iron yoke system. This makes the permeameter a closed circuit measurement technique. Figure 3 shows schematically a permeameter system. The drive coil induces a magnetic field to flow through the iron pole pieces and through the magnet.

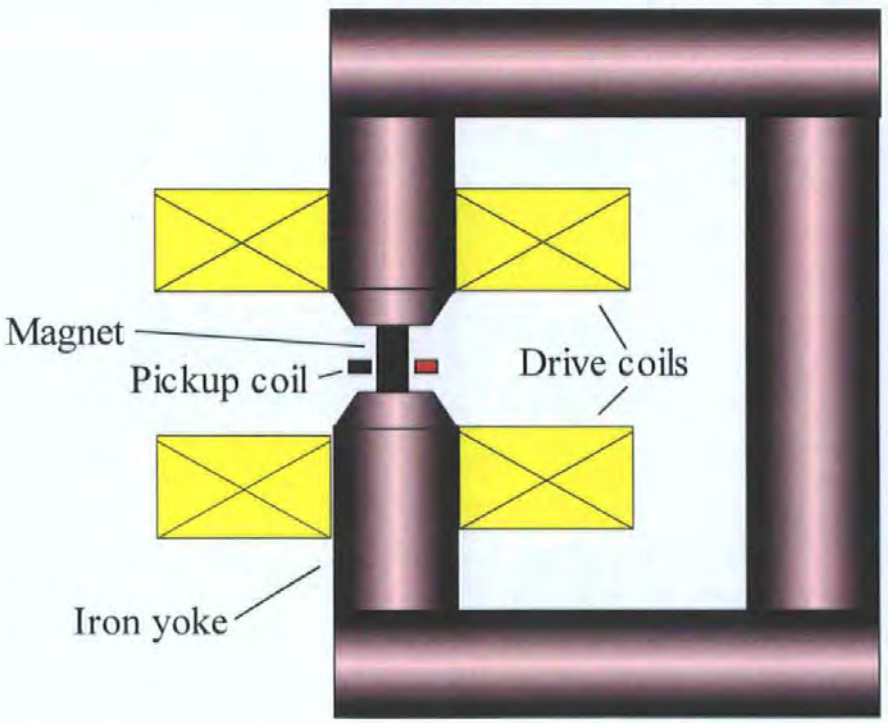


*Figure 3 - Basic configuration of a permeameter, showing field generation coils, iron pole pieces and the location of the sample and pickup coil system.*

The applied field can be detected with either a pickup coil or a Hall element. The magnet's magnetisation is typically detected with a pickup coil. A system of 5 concentric coils can

be used to measure both the applied field and the magnet's induced magnetisation. Figure 4 shows the configuration of a 5 coil combined J and H permeameter pickup system.

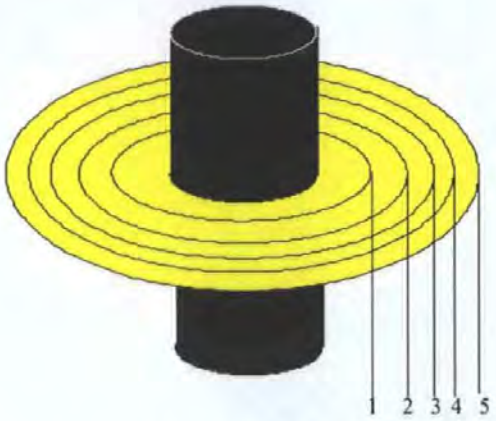


*Figure 4 - Permeameter combined J and H pickup coil system. The 5 individual search coils when added and subtracted in specific combinations provide both the J and the H signal.*

The principle often used in permeameters is to use 5 pickup coils to separate the **J** and **H** signals. By applying Faraday's law of induction it is possible to deduce the operation of a permeameter pickup system. If a coil with a single turn is considered in a uniform, time dependent magnetic field, the induced electromotive force (emf) is given by,

$$\varepsilon = -\frac{d\phi}{dt} \tag{6.1}$$

where $\varepsilon$ is the induced emf and $d\phi$ is the change of flux in time $t$. With each coil having a known number of turns and a known area this becomes,

$$\varepsilon = -N\frac{d\boldsymbol{B}A}{dt} \tag{6.2}$$

where $\boldsymbol{B}$ is the flux density, $A$ is the area of the coil and $N$ the number of conductor turns forming the coil. Two pickup coils, in a uniformly changing magnetic field, will produce the same output if their area turns product is equal.

$$\varepsilon_1 = \varepsilon_2 \text{ if } N_1A_1 = N_2A_2 \tag{6.3}$$

If a magnetised magnet is considered in the air-gap of the permeameter and the permeameter is adjusted so that the pole faces are in contact with the magnet, the magnets flux will be conducted by the iron, forming a closed circuit. No flux will appear across the

air gap, due to the magnetisation of the magnet, all of the flux will be conducted by the magnet. As the flux generated by the magnet, crosses the air gap through the magnet, the output of any pickup coil surrounding the magnet will be proportional to the number of turns but not the area, of the pickup coil.

If the applied magnetic field is considered on its own, the flux flows through the iron yokes and generates a near uniform magnetic field across the air-gap. Therefore the output of any pickup coil within the air gap will be proportional to the number of turns and the area of the search coil.

If coils 4 and 5 have the same number of turns but a different area turns product, and are connected in series anti-phase, the resultant output will be proportional to the applied field and independent of the magnetisation of the magnet, as shown by,

$$\varepsilon_4 - \varepsilon_5 \propto \boldsymbol{H} \tag{6.4}$$

If coils 2 and 3 also have the same number of turns but the difference of their area-turns product is equal to the area-turns product of coil 1 as shown by,

$$(N_2 A_2 - N_3 A_3) = N_1 A_1 \tag{6.5}$$

then if the output of coils 1 and 3 are summed together and this result subtracted from the output of pickup coil 2, the remaining signal will be proportional to the magnetisation of the magnet, and independent of the applied field, as shown by,

$$\varepsilon_2 - (\varepsilon_3 + \varepsilon_1) \propto \boldsymbol{J} \tag{6.6}$$

Due to the volumes of steel in the pole pieces there is a significant limitation on the rate of change of applied field that is practical. This is because of eddy currents that will be induced. This severely increases the measurement time, as the values of $\boldsymbol{H}$ and $\boldsymbol{J}$ can only be determined when there are no eddy currents effects. As iron has a saturation value of 2 - 2.4 Tesla, it is difficult to generate applied fields above this value and this makes the

measurement of materials with coercivity above the saturation of iron error prone. A further requirement is that the pole pieces make good contact with the sample. This requires that the sample has flat ends parallel with the pole pieces to a high degree of accuracy. This limits the shape to a cylinder or other simple cuboid form. The maximum height of the cylinder is determined by the energy available for generating a magnetic field of sufficient magnitude across the air-gap between the pole pieces. As the pole piece gap is increased, the maximum field available for measurement is reduced due to the reluctance of the air gap.

### *4.1.2 Vibrating sample magnetometers*

Vibrating sample magnetometers (VSMs) are designed for the magnetic characterisation of very small samples and can resolve signals from a sample with a magnetic moment as small as a few μEmu. The maximum size of the sample is generally small, due to physical limitations of the vibration process. The sample shape is not limited as with the permeameter, providing the sample can be corrected for the effects of self-demagnetisation.

The applied field in VSMs can be generated in the same way as with permeameters, that is by using iron yokes or more exotic methods, such as super conducting coils, to generate the high fields necessary to measure even the hardest rare earth materials. The use of super conducting coils to generate high fields has its own problems. The systems have a high capital cost, the cryogenic fluids have a high running cost and the measurements still take minutes to complete. This makes VSMs ideal for materials research laboratories where thin films can be characterised at high fields, but long measurement times and running costs are not prohibitive.

Figure 5 shows the configuration of a typical low field VSM. The sample is physically vibrated through a homogenous part of the applied field. A pickup coil is positioned so that the coupling to the sample varies with the vibration. As the sample is vibrated, a sinusoidal output is generated from the J pickup coil. The magnitude of the **J** sinusoidal signal is proportional to the magnetisation of the sample. By placing a reference magnet on the shaft that is being vibrated, and using a second reference coil, a signal can be supplied to a lock-in amplifier and the **J** signal measured with a high degree of accuracy.

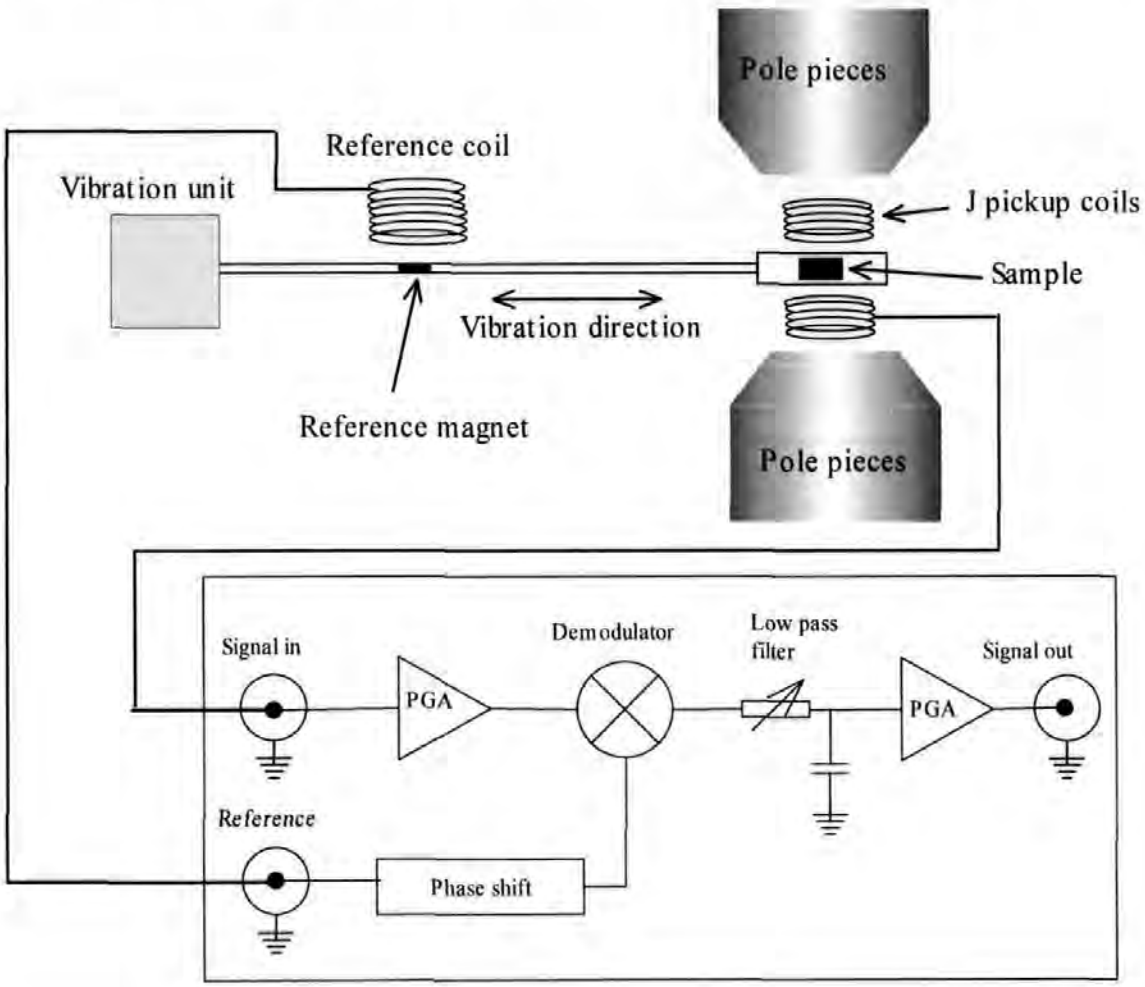


*Figure 5 - VSM applied magnetic field and sample detection principles. The applied field is generated using solenoid coils and a system of iron pole pieces. The sample is vibrated in the magnetic field to produce a dynamic magnetic field that can be detected with search coils and a lock-in amplifier.*

The VSM uses at least one pickup coil to detect the magnetisation of the sample. A second pickup coil may be used to detect the applied field but often a simple Hall element will be used. As the signal detected by the J pickup coil is small, it can have a very poor signal to

noise ratio or be impossible to detect with out the aid of additional processing. Usually a lock-in amplifier is used. Lock-in amplifiers utilise phase and frequency to recover sinusoidal waveforms "buried" in noise. The first stage of a lock in amplifier is a band pass filter coupled with an amplifier. This stage can be used to amplify only signals of the wanted frequency. This signal is then one of the two inputs to the demodulator. By using an additional pickup coil and a small magnet on the vibrator shaft, a reference waveform can be generated. By careful physical design of the vibrator mechanism, a near perfect sinusoidal waveform can be obtained. This reference signal forms the second input to the demodulator stage. Consider the reference signal,

$$S_{ref} = A_{ref} \cos(\omega_{ref} \cdot t) \tag{6.7}$$

where $S_{ref}$ is the reference signal, $A_{ref}$ is the amplitude of the reference signal and $\omega_{ref}$ is the frequency of the reference signal. Now consider the magnet's signal,

$$S_{in} = A_{in} \cos(\omega_{ref} \cdot t + \delta_{in}) \tag{6.8}$$

where $S_{in}$ is the sample's signal, $A_{in}$ is the amplitude of the sample's signal and $\delta_{in}$ is the phase shift of the magnet's signal with respect to the reference signal and $\omega_{ref}$ is the frequency of the reference signal. The demodulator stage is a multiplier that is multiplying $S_{in}$ by $S_{ref}$, which results in an output of,

$$V_{psd} = A_{ref} A_{in} \cos(\omega_{ref} \cdot t) \cos(\omega_{ref} \cdot t + \delta_{in}) \tag{6.9}$$

where $V_{psd}$ is the phase sensitive voltage output that is proportional to $S_{in}$. Assume that the reference signals phase is correctly adjusted and therefore $\delta_{in}$ = 0. By applying the trigometric identity,

$$\cos(\alpha)\cos(\beta) = \frac{1}{2}\cos(\alpha - \beta) + \frac{1}{2}\cos(\alpha + \beta) \tag{6.10}$$

the phase sensitive voltage is given by,

$$V_{psd} = \frac{1}{2} A_{in} A_{ref} [1 + \cos(2\omega t)] \tag{6.11}$$

The voltage $V_{psd}$ is proportional to both the time independent, $A_{in}A_{ref}$, and the 2nd harmonic $A_{in}A_{ref}\cos(2\omega t)$. By applying a low pass filter to remove the time dependent component and as $A_{ref}$ is constant, a static offset remains that is proportional to $A_{in}$. It is then typical to apply another amplification stage to amplify the output of the low pass filter to a useful level.

It is the use of a lock in amplifier to retrieve a signal otherwise buried in noise that provides VSMs with exceptional small sample accuracy and detection abilities.

### *4.1.3 Alternating gradient magnetometers*

Alternating gradient magnetometers (AGMs) are another method designed for small samples. The principle of operation is that the sample is exposed to the applied magnetic field and the physical deflection force is measured using a piezoelectric sensor. This force is directly proportional to the magnetisation of the sample. The method can use the same applied field methods as VSMs and apply super conducting techniques to achieve high applied magnetic fields. The speed of the measurement is a function of any eddy currents induced in the sample and the combined mass of the sample and the deflection measuring apparatus. To achieve a measurement can still take a number of minutes per sample, making the method too slow for industrial quality control.

### *4.1.4 Point by point method*

The point by point method is the closest conventional method to Pulsed Field Magnetometry but still suffers many of the disadvantages of conventional systems. A sample to be tested is magnetised to saturation using an external magnetiser. The sample is then placed in the point-by-point system and a number of unidirectional pulses are applied to the sample to drive the sample down its demagnetisation curve until it's magnetisation is zero. A fluxmeter is used to monitor the flux level between pulses. As the fluxmeter is not attempting to detect the transient of the pulse, the problems of eddy currents and pickup

systems are minimised but not eliminated. Figure 6 shows the applied field pulses used in a point by point system. Each successive unidirectional pulse increases in magnitude to further drive the samples magnetisation towards zero. Figure 7 shows the effect of each unidirectional pulse in the JH domain. The first 3 pulses have reduced the magnetisation of the sample. The magnitude of the 4$^{th}$ pulse was sufficient to partially magnetise the sample in the reverse direction.

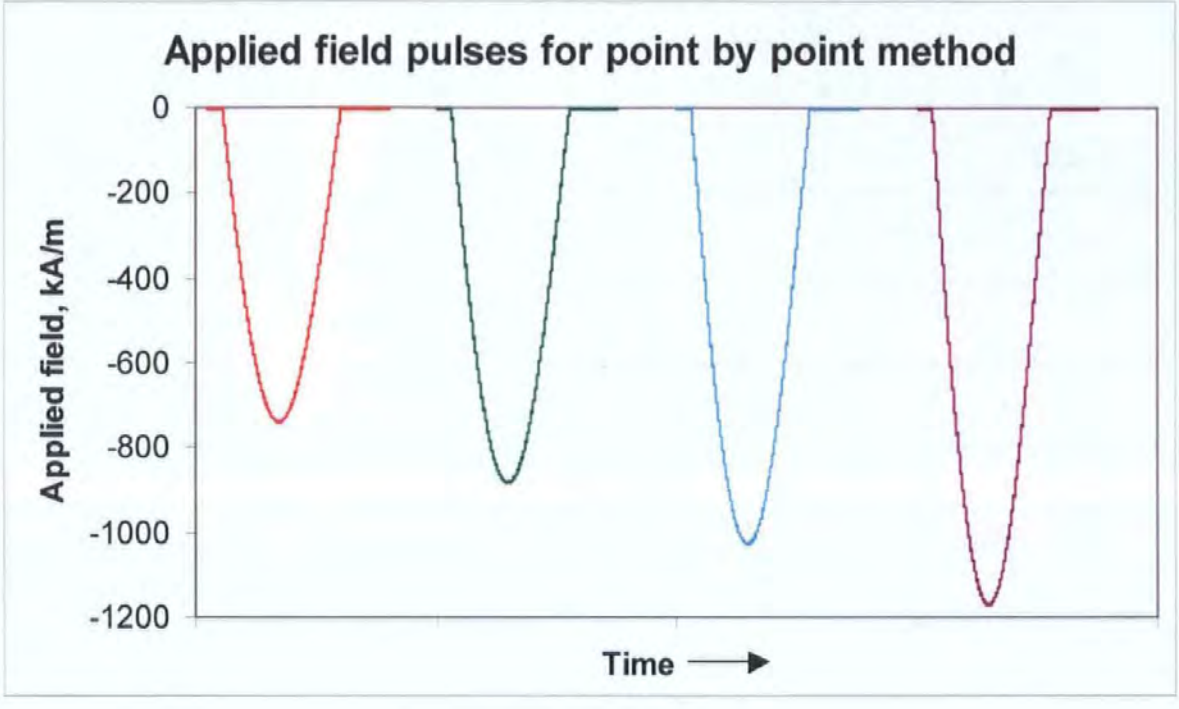


*Figure 6 - Applied field pulses for point by point method. Each successive pulse increases in magnitude.*

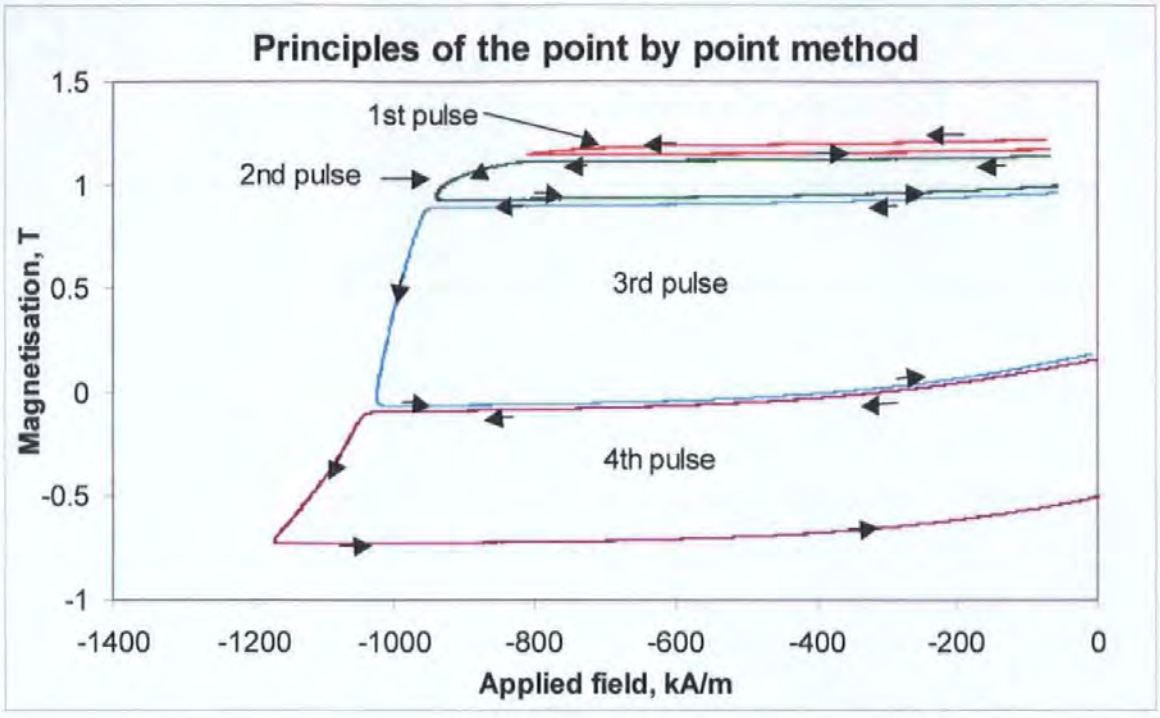


*Figure 7 - Each applied field pulse of the point by point method drives the magnet around a minor loop in the 2nd quadrant resulting in a reduction of the magnet's magnetisation.*

Typically only 3 or 4 pulses are used to drive the magnet to zero magnetisation, but this is based on pre-programmed information regarding the average characteristics of the type of magnet being tested. The magnitude and number of pulses could be optimised for a particular test specimen.

The point by point method only generates enough data for an approximate quality control check, but has its uses as a cheap quality control system for very hard permanent magnets with high saturation values. The method is purely comparative and requires at least one known good sample to use as a reference. The effects of eddy currents, pick-up coil geometry, applied field homogeneity and self-demagnetisation factor make an absolute reading impossible with this type of system.

## 4.2 Pulsed Field Magnetometry

The principle of Pulsed Field Magnetometry is to apply a magnetic field to a magnet and measure the magnet's response, in terms of a magnetisation level. The fundamentals are

the same as any conventional magnetic measuring system. The difference with Pulsed Field Magnetometry and other systems is that the magnetic field is an intense pulse of a short duration. The pickup coil system detects the applied field and the magnet sample's response and passes the signal into data capture electronics. The signal is then subject to analogue and digital processing to produce an accurate calibrated representation of the magnet's response to applied magnetic fields [27].

Figure 8 shows a plot of the applied field against time. Figure 9 shows a plot of the sample's magnetisation against time. In this case a sample of sintered Neodymium Iron Boron.

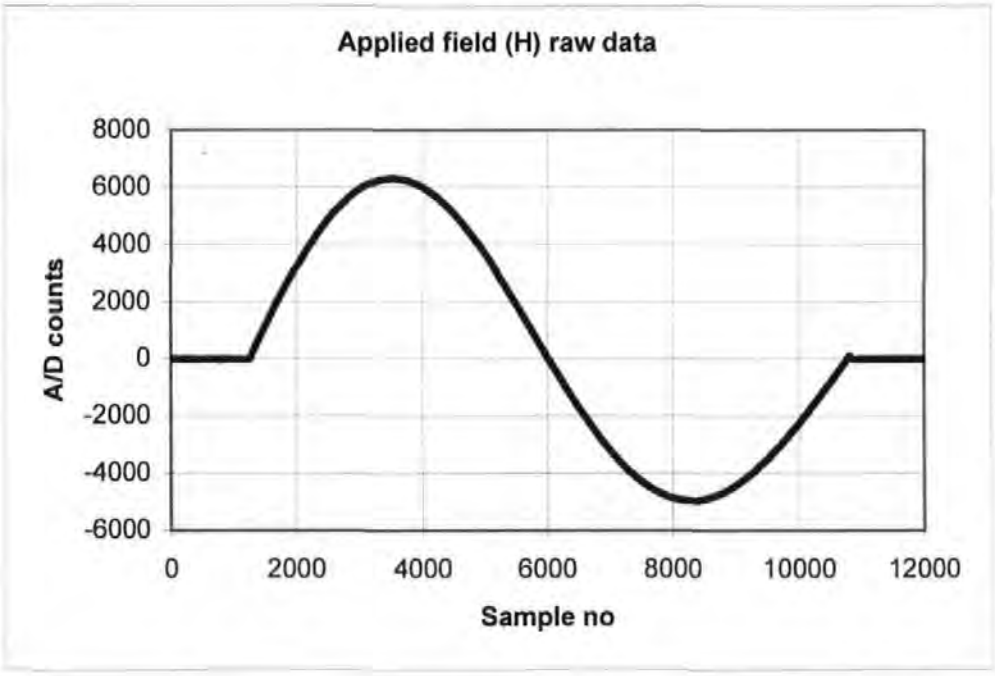


*Figure 8 - PFM H time trace for the measurement of a permanent magnet. The wave form represents the magnitude of the applied field.*

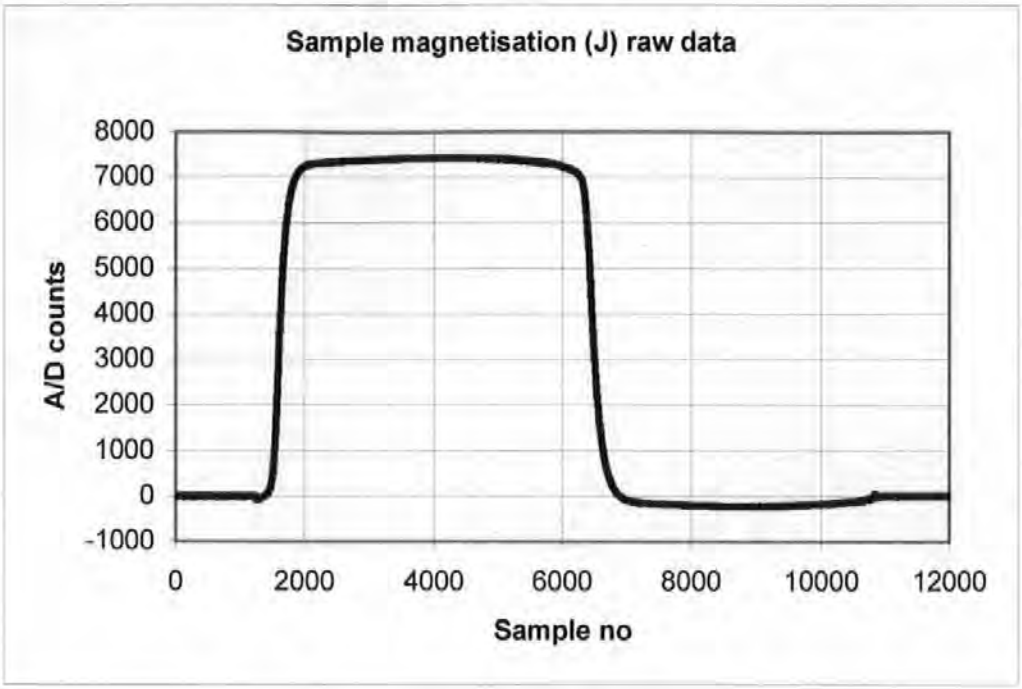


*Figure 9 - PFM J time traces for a permanent magnet. The waveform represents the magnetisation of the magnet as it changes with applied field.*

The problems with Pulsed Field Magnetometry that have prevented wide adoption of the technique are the measurement errors from which the method suffers. The magnetic pulse produces unwanted eddy currents within the samples being measured, the field generation coils and even in the wires that form the pickup coils. These eddy currents cause large distortions to the magnetic field within and surrounding the specimen. This produces deviations from the expected measurement and errors are thus obtained. The method is an open circuit method but unlike VSMs and AGMs, the samples can be relatively large and often complex industrial shapes. This causes the self-demagnetisation field to be complex and the specimens can have a large range of self-demagnetisation factors.

The overall design of PFM system components has, until now, been considered to be something of a "black art". Pickup coils and field generation coils have been designed on 'experience' and a 'feel for what will work' rather that any step by step scientific approach. This thesis hopes to bring a scientific methodology to the design of Pulsed Field Magnetometry components.

## 4.3 Dimensional limitations of PFM measurement systems

As the test specimens are measured in an open magnetic circuit, there is no immediate limit to the size of specimens that can be tested. Both small and large test specimens can be measured providing that eddy current considerations and also the practicalities of the instrumentation are accounted for such as sensitivity and maximum input signal.

Small magnets, in the context of industrial shapes and sizes, are considered to have a volume smaller than 100 $mm^3$. This is typically realised in a cylindrical magnet of dimensions 5 mm diameter by 5 mm high (98.1 $mm^3$). Large magnets are considered to have a volume greater than 21,000 $mm^3$. This size range represents 80 % of the production at Magnetfabrik Schramberg, one of Europe's largest magnet producers.

## 4.4 A comparison of magnetic measurement methods

Table 7 shows a comparison of the measurement techniques discussed. There are very large differences in physical characteristics that make each system only suitable for particular types of magnetic measurement. The parameters are estimates based on the typical specifications of commercially available systems. It should be noted that the methods are considered for use primarily as an industrial quality control system for industrial magnets in their native shapes.

| Method | Typical measurement time | Max field (T) | Sample size range ($mm^3$) | Open or closed | Advantages | Disadvantages |
|---|---|---|---|---|---|---|
| **PFM** | 4 seconds | 20 [2] | 27 – 27000 [4] | Open | Speed, High Field, Any Shape | Eddy Currents Self demagnetisation factor (SDF) |
| **VSM** | 10 - 30 minutes | 3 [1] | < 100 | Open | Sensitivity | Small samples only, SDF, slow |
| **AGM** | 10 - 30 minutes | 3 [1][5] | < 10 | Open | High Sensitivity | Very small samples only. SDF, slow |
| **Permeameter** | 2 - 20 minutes | 3 [1] | 30 -30000 | Closed | Industry standard | Limited shapes, Limited field, slow |
| **Point by Point** | 10 - 20 seconds | 4 - 5 [3] | 30 - 30000 | Open | Speed | Only comparative technique, SDF |
| **Super conducting VSM** | 10 - 60 minutes | 10 - 20[5] | < 100 | Open | High field, sensitivity. | Liquid helium, very slow, high running costs, high capital cost |

*Table 7 - Comparison of measurement methodologies.*

*Table 7 notes:*

*[1] Three Tesla is only achievable with special focusing pole pieces and a reduced pole gap and sample diameter.*
*[2] 20 Tesla is a typical limit for commercial systems. Systems in excess of 50 Tesla have been built.*
*[3] These are not limits but typical maximum values.*
*[4] The size range chosen represented the 80 % size distribution of a typical magnet manufacture. The sizes are not maximum limits.*
*[5] Super conducting versions could be constructed allowing greater fields.*

## 4.5 Magnetic measurement system conclusions

VSMs and AGMs are excellent for the measurement of very small samples typically used in material research and thin film development. The use of super conducting coils allows VSMs to obtain very high magnetic fields in the region 10 - 20 Tesla. Permeameters, the

standard of magnetic measurements, are insufficient to cope with the demands of modern permanent magnet materials or a high speed production environment. Point-by-point methods allow a very crude assessment of magnets, which overcome the limitations of permeameters but dispose of accuracy, calibration and traceability. The optimal and perhaps only current solution is Pulse Field Magnetometry.

The method of Pulsed Field Magnetometry introduces many problems of its own, due to the nature of the method, which conventional methods do not possess. There are methods for reducing these errors by design and by data processing. This thesis highlights the major errors, their sources and ways to prevent or compensate for them, as well as outlining future work in the systematic elimination of measurement errors in Pulsed Field Magnetometry.

# Chapter 5 Magnetic field generation

## 5.1 Purpose

The objective is to generate a magnetic field suitable for the measurement of magnetic samples, as previously discussed. There are a number of requirements of the field generation method that are important to its design,

- Magnitude of the applied field generated
- Temporal characteristics of the applied field
- Spatial homogeneity of the applied field
- Electrical characteristics; inductance, resistance and capacitance
- Electrical current
- Heat generated
- Physical characteristics of the field generator, such as strength and rigidity

## 5.2 Methods of field generation

Nearly all methods of magnetic field generation are based upon an electric current flowing along a conductor. While it is possible to use permanent magnets as the source of the magnetic field, for applications where a fixed magnitude static field is required [28] , they are not useful here as only static fields can be produced, over limited volumes compared to other methods discussed in this section.

### *5.2.1 Pole pieces*

A typical configuration uses iron pole pieces to reduce the reluctance of the magnetic path and to focus the field intensity across an air gap where the sample will be placed. This method is typical in permeameters and non super-conducing VSMs. As iron has a saturation of around 2 - 2.5 Tesla it is impossible to achieve higher flux densities. By use of special focusing pole pieces it is possible to achieve flux densities of about 3 Tesla over

a limited volume of a few cubic centimetres. This is achieved by using a high $\mu_r$ steel such as Vacoflux and by shaping the pole pieces to concentrate the flux over a small volume producing a 3 Tesla flux density, but the homogeneity of the applied field is sacrificed.

The electrical drive circuit would typically consist of a power amplifier with a maximum output in the range of 10 - 20 Amps. Higher currents could be used but the thermal dissipation will become prohibitive as the $I^2R$ losses increase.

This method of field generation is unsuitable for the industrial quality control of rare earth materials for many reasons, the principle reason being,

- It is impossible to generate above 2 - 3 Tesla with iron pole pieces, as the iron will saturate. Rare earth materials require up to 5 Tesla to enable a successful measurement and typically require a minimum of 3.5 Tesla.

- Large iron pole pieces make varying the field problematic, as any change in field will generate enormous eddy currents, therefore the field must be changed slowly and a typical permeameter may take a minimum of 5 minutes to complete its measurement. This length of time is not suitable for industrial quality control implementation, as it would pose a serious limitation on the number of magnets that could be tested, e.g. less than 30 per hour compared to the minimum of 900 per hour demanded by industry.

The use of pole pieces as part of a magnetic field generation system is, despite the above comments, enormously useful. Many applications make use of pole pieces, however in the context of Pulsed Field Magnetometry and industrial quality control systems, not being

able to test rare earth materials, and also having a time limitation as large as this is unacceptable.

### *5.2.2 Super conducting coils*

Super conducting coils are solenoids wound with materials that exhibit super conducting properties when cooled down to very low temperatures. Typical materials used for the superconductor would be niobium-titanium or niobium-tin compounds. These are often wound as a multi-filamentary superconductor twisted within a copper matrix. When cooled down to temperatures as low as 4.2 K - 2.2 K the resistance of the coil becomes effectively zero, however the maximum current is limited by the critical current of the super conducting material. By passing a current of less than 100 Amps through the windings it is possible to generate fields in the region of 10 - 20 Tesla. The reason this is possible is as the resistance of the coil is so small it is possible to get a large number of turns on the coils but with minimal drive voltage requirements and low thermal heating effects. The typical inductance of these types of coils is a magnitude of 10 H – 100 H. This level of inductance is orders of magnitude above that found in conventional air or iron cored coils and is achieved by the high number of windings but without the drawback of high resistance.

Super conducting coils are far from ideal, the superconductor material and the running costs of a liquid helium cryostat contribute significantly to the method's expense. It is problematic to change the field magnitude quickly, due to the reactance of the coils and the importance of maintaining cryostat stability. If the coil or part of the coil becomes non-super conducting, due to thermal effects or exceeding the critical current, the results may be disastrous as the conductor used to make the superconductor will not sustain a significant energy dissipation and could fail. Due to these limitations, the use of super conducting coils tends to be limited to material research laboratories and universities where

the time of the measurement is not as critical as in industry. Super conducting coils would not achieve the magnet characterisation throughput required for industrial quality control in a production situation.

### *5.2.3 Pulsed solenoid coils*

The method uses a conventional solenoid that is designed to have very high radial strength. Copper wire is wound on to a former, forming a solenoid with the required number of turns and number of layers. The outside of the coil is reinforced to provide radial strength and it is typical to use fibreglass for this purpose. A pulse of high current is applied to the coil to generate a magnetic field pulse.

To achieve the field levels required for successful characterisation using Pulsed Field Magnetometry it is necessary to balance the number of turns with the required current to achieve a practical system. It is typical to find coils that require currents of 5 - 10 kA. This current requirement when combined with the electrical properties of the solenoid can result in supply voltage requirements of up to 3000 V. The high current also results in large heating effects due to resistive losses. This can lead to a requirement for cooling of the solenoid to remove excess heat.

The method is routinely used to generate high fields over relatively large volumes. This method has been used to generate fields over 80 Tesla [29]. Fields over 40 Tesla can be problematic as the forces involved can exceed the tensile strength of copper and careful design is required to ensure that the force is transferred into suitable supporting structures [30].

As a pulsed coil system does not require cryogenic cooling and is formed with copper conductors, the cost and associated equipment is a fraction of that of super conducting systems.

Because of the limitations of pole pieces and the associated cost of cryogenic super-conducting coil systems, pulsed solenoid coils are the preferred method of field generation. The detailed design of pulsed coil systems is considered later in this chapter from Section 5.4 onwards.

## 5.3 Power supply for magnetic field generation.

There are a number of possible methods for generating the current required by the pulsed coil, these methods, with their merits and limitations are now considered. The basic aims of the field generation coil for PFM measurements are to,

(i) Generate the highest field possible.

(ii) Keep electrical resistance to a minimum.

(iii) Ensure a good (better than 1 % for the sample region) homogeneity of field.

These considerations are now discussed in detail;

### *5.3.1 Capacitive discharge*

Capacitive discharge is a widely adopted technique for generating large current pulses. By charging a capacitor and accumulating stored energy in a controlled manner over a longer period than the discharge duration, the instantaneous energy demand from the supply is minimised. The potential discharge energy is only limited by the capacitors used to store the charge and the voltage used.

The energy, $E$, stored on a capacitor is given by,

$$E = 0.5CV^2 \tag{5.1}$$

where the terms have their usual meaning. The stored energy and the capacitor's capacitance must be chosen to match with the field generation coil to achieve the desired peak field and pulse duration. There are limitations on the maximum pulse duration due to properties of the field generation solenoid and practical size limits of capacitor banks. It is desirable to keep the pulse duration as long as possible to reduce the effects of eddy currents. There is also a limit of around 40 Tesla where the tensile strength of copper is exceeded by the force due to the magnetic field generated inside the coil. For fields of this magnitude copper alloys are used to provide greater tensile strength in order to withstand the stresses of the magnetic pulse [30].

#### *5.3.1.1 Discharge mechanisms*

The energy discharged from the capacitor to the field generation coil can be delivered in the following forms,

- Decaying sine wave
- Unidirectional pulses (1/2 sine wave)
- Two unidirectional pulses
- Diode clamped
- Resistive

The clamped and resistive configurations are not usually used for measurement of magnetic materials. The clamped configuration is a modification of the decaying sine wave method and places a "freewheel" diode across the solenoid to ensure current flow in one direction only through the solenoid. This is useful for magnetisation applications but causes all of the stored capacitor energy to be discharged as heat into the solenoid. The resistive configuration is unusual, as the reactance of the solenoid must dominate over the resistance to produce significant magnetic field. The resistive configuration is usually used

as a safety circuit to enable the capacitors charge to be "dumped" into an internal resistive load. Figure 10 shows schematically the diode clamped and resistive configurations and Figures 11 and 12 show the current waveforms for the two configurations.

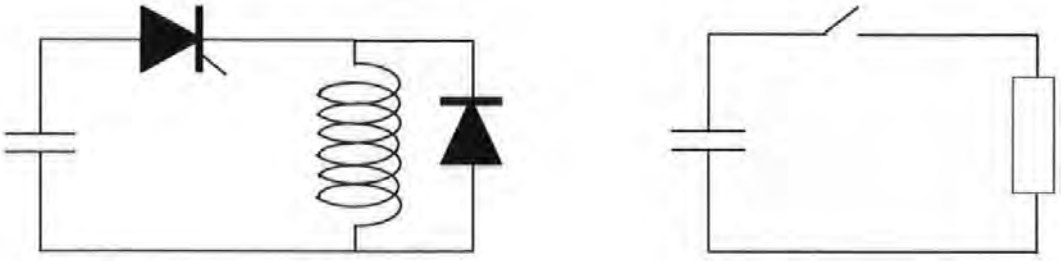

*Figure 10 - The left configurations has a diode in parallel with the coil to cause a unidirectional current flow. A thyristor controls the initial current flow. The right hand configuration simply connects a capacitor to a resistor via a switch causing the capacitors charge to be dissipated as heat into the resistor.*

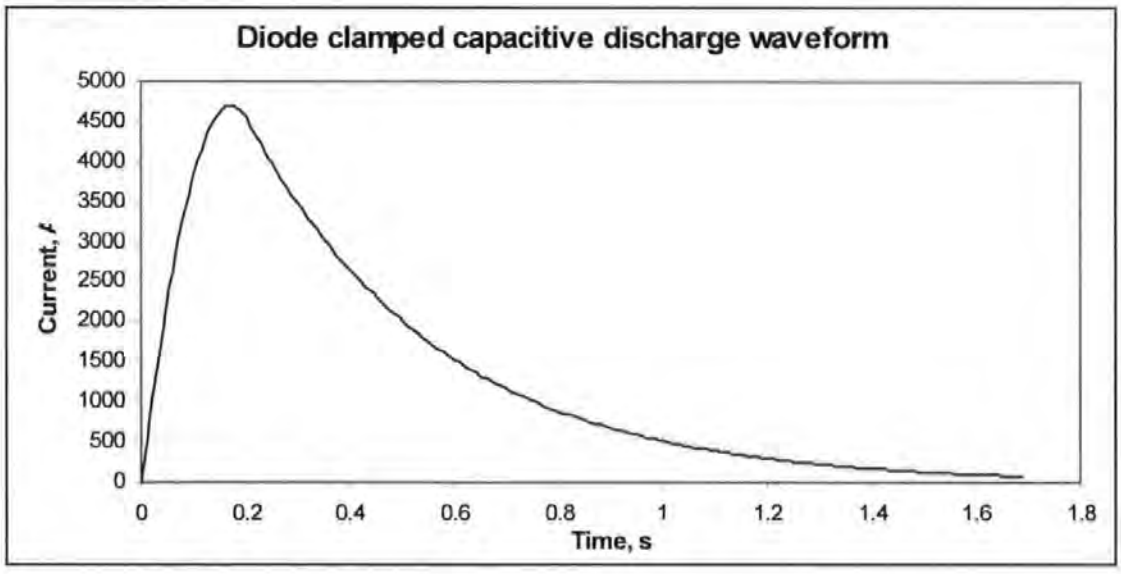


*Figure 11 - Capacitive discharge current waveform with reverse voltage diode clamping. The diode begins conducting when the forward voltage across the device exceeds 0.8 V.*

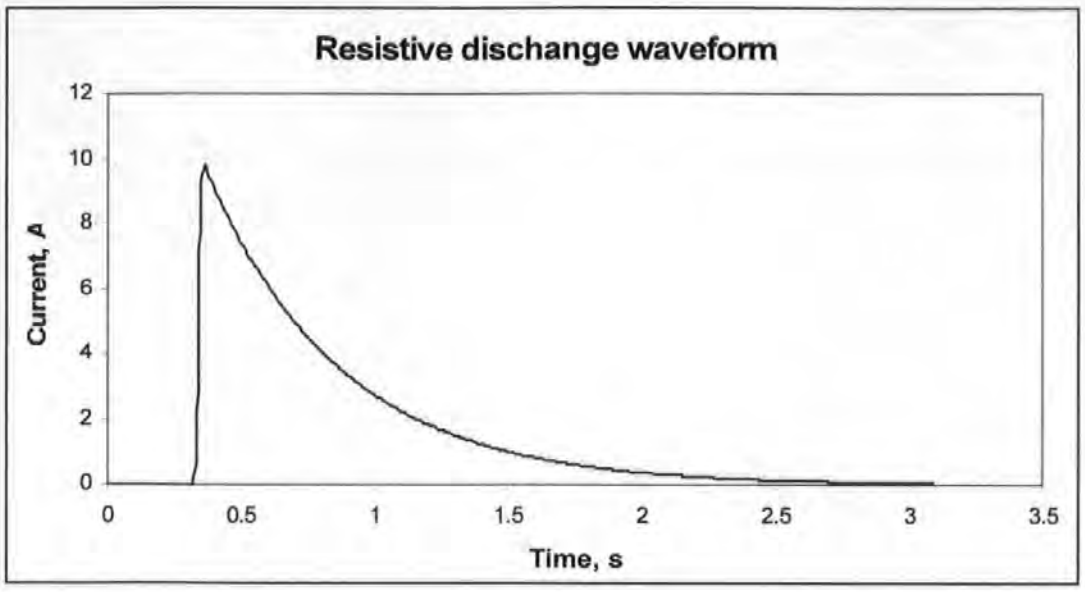


*Figure 12 - Discharge of a capacitor into a resistor. A switch is closed at approximately 0.4 seconds connecting the capacitor to the resistor. The waveform is a simple exponential decay at a rate governed by the resistance of the resistor and the capacitance of the capacitor.*

The decaying sine wave is the simplest of the first three methods. A simple circuit involving a capacitor, the solenoid, a diode and thyristor provide the high current electronics as shown in Figure 13.

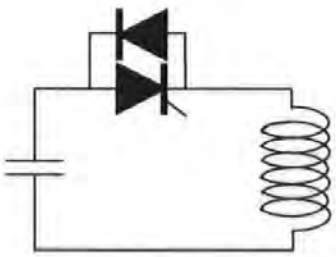

*Figure 13 - Schematic diagram of discharge electronics for decaying sinusoidal output current.*

The current flow i*(t)*, and therefore the resultant magnetic field is described by,

$$i(t) = \frac{V_0}{\omega L}.e^{-\beta t}\sin \omega t \tag{5.2}$$

where i, $t$, $V$ and $L$ have their usual meanings and $\omega$ is given by,

$$\omega = \sqrt{\frac{1}{LC} - \frac{R^2}{4L^2}} \tag{5.3}$$

and $\beta$ is given by,

$$\beta = \frac{R}{2L} \tag{5.4}$$

Due to the resistive losses in the magnetising solenoid, the peak field created in the magnetising solenoid in the reverse direction is reduced, depending on the damping factor $\beta$. It is therefore necessary to apply a higher initial field, to ensure the reverse field is sufficient for the sample under test. Figure 14 shows a typical decaying sinusoidal magnetic field over time. Due to the damping factor, $\beta$, only the start of the waveform is typically useful for magnet characterisation purposes, when applied to a typical field generation coil. Only the first 360° are typically used, as the remaining energy is too low to generate the required magnetic field for an optimised initial applied field.

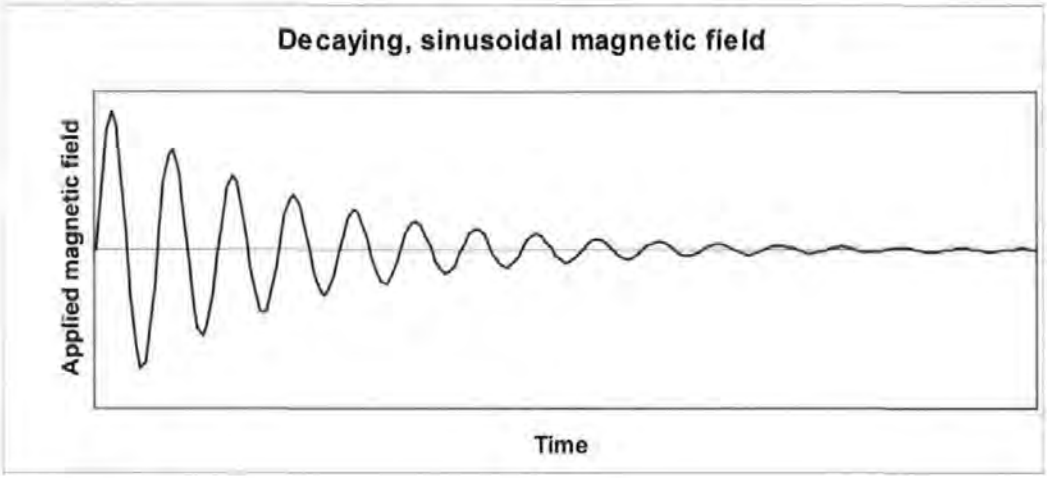


*Figure 14 - Decaying sine wave current waveform. The decay is due to the resistive element of the field generation coil.*

The sine wave technique has the advantage of a continuous process to apply positive and negative polarities and to avoid discontinuities. This is important in the testing of conductive materials where eddy current effects are taken into consideration. It is usual to limit the decaying sine wave to a single "ring", that is, after the first forward conduction cycle of the thyristor, the thyristor is switched off so that only the diode can conduct the reverse current flow. The energy, less the dissipation losses of a forward and reverse cycle, is returned to the capacitor bank.

A single unidirectional pulse is identical to the sine wave (decaying) configuration except only one half-sine wave of current is allowed to enter the field generation coil. The current is described by Equation (5.2 above. The disadvantages of a unidirectional pulse system are that a fully magnetised magnet is required which then must be driven along its demagnetisation curve. A system that is capable of pulsing in both directions can perform the magnetisation itself and hence can start with a de-magnetised sample.

A single unidirectional pulse produces only a partial JH loop from positive remanence back to negative saturation is obtained. This causes additional data processing problems as it is required that the integrators are in a known state at the start and end of measurement in order to determine the constant of integration so that the data can be correctly offset from the origin. This prevents any possibility of digital drift correcting the data and other post-processing techniques used to remove unwanted effects as discussed in Chapter 7.

By applying two pulses with opposite polarity, a full positive and negative field can be applied with identical peak fields in either direction. The overall measurement is accomplished by two separate discharges. Figure 15 illustrates a possible output circuit and an example output current waveform. This approach does have the advantage of achieving the same peak fields on positive and negative pulses. However, two discrete pulses are applied with their inherent discontinuities of current. During the period between the two pulses the magnetisation of the magnet may relax. Depending on the structure of the magnet under test, after the magnet is fully magnetised and the applied field removed the magnet's magnetisation will be at its maximum possible holding value. This value in some materials will relax with time, as some domains partially slip and are no longer orientated in the same direction as the others. Another issue is that the effects of eddy currents will not be continuous. Eddy currents are difficult to quantify and adding extra

discontinuities makes their effect more complex. There is also a requirement for accurate capacitor charging to ensure the discharge energy is symmetrical.

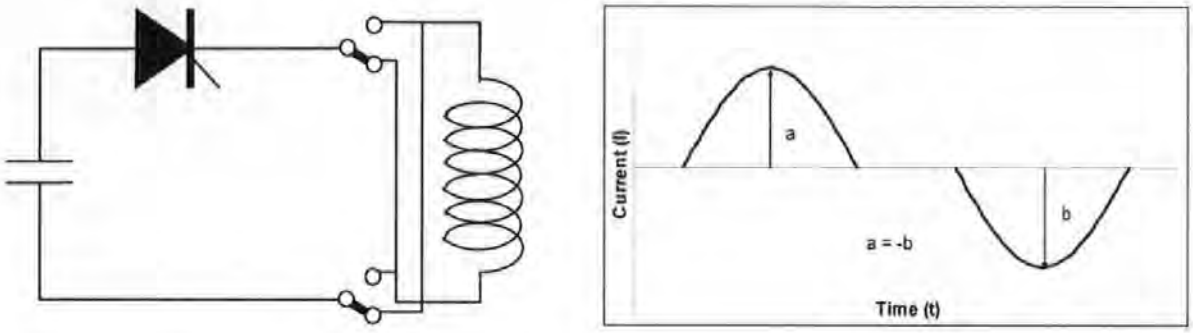


*Figure 15 - Unidirectional pulses (1/2 sine wave) electrical configuration. A single thristor permits a unidirectional current flow and the change-over switch selects the polarity.*

The current flow, during each pulse, is described by the previous Equation 5.2. After the first half sine wave of current flow, the reverse charge that is generated across the capacitors is not permitted to discharge due to the diode characteristic of the thyristor. The capacitor bank is then recharged to the required level and the polarity of the output changed. The current is again allowed to flow, creating a magnetic field with opposite polarity. The resultant current waveform is two half-sine waves of opposite polarity separated by a discontinuity as shown in Figure 15.

#### *5.3.1.2 Comparison of discharge techniques*

The decaying sine wave method exhibits all the properties of a continuous sinusoidal function but resistive losses will cause the current and hence magnetic field to be asymmetrical, thus the negative field will be lower than the positive field. If the field generation current can be represented by a continuous sinusoidal function then the effects due to eddy currents will also be related to a sinusoidal function and hence will become simpler to model. The unidirectional method also exhibits the same sinusoidal properties but only for 0 – 180 degrees of the current waveform. This has the disadvantage that only a unidirectional current and hence magnetic field is generated limiting the possible information in the characterisation process. By adding a second unidirectional pulse of the

opposite polarity, the full 0 – 360 degrees can be utilised with symmetrical positive and negative magnetic fields but with a discontinuity at 180 degrees. This discontinuity can complicate the eddy currents and potentially lead to additional errors. As the period of the discontinuity tends to zero its effects will tend to a decaying sinusoidal waveform, however practical considerations of charging time, current switching and power semiconductor transients ensure the discontinuity remains significantly large.

The preferred approach is a decaying sine wave, particularly in consideration of possible eddy currents in conductive samples the ease of implementation and the reduced discontinuities in the measurement process.

## 5.4 Simulation

The majority of the parameters for field generation coils can be simulated using analytical and empirical means, while still achieving good agreement with physical systems, without resorting to more expensive and time consuming finite element techniques. Although some of the techniques are only approximations based on classical empirical theory, they are more than adequate at the initial design stage and the reduced numerical processing time requirements provides the possibility to run automated design parameter optimisations.

It is necessary to determine the following parameters in order to fully model an applied field generation coil,

- Coil Inductance
- Winding resistance
- Geometric position of the windings forming the coil.
- Discharge current dynamics through the coil
- Magnetic field generated by the coil

The next sections describe the process of determining all of the above parameters and the results are combined into a piece of software called "Aircore" for the parametric design of applied field coils.

### 5.4.1 Inductance

Inductance is one of the more difficult quantities to estimate. With finite element analysis (FEA) a simple model can calculate **B** fields from current carrying conductors. The inductance can then be calculated by integrating **B** over a suitable volume and dividing by half the applied current squared, as given by,

$$L = \frac{\iiint \boldsymbol{B}.dv}{0.5I^2} \tag{5.5}$$

where $L$ is the inductance of the current carrying conductors considered, $\boldsymbol{B}$ is the flux density over the volume and $I$ is the current in the conductors.

The problem with the FEA approach is that a computationally time consuming model needs to be considered for each geometry and unless the geometry has rotational symmetry, a full 3D solution is required. As the model relies on an integral term, for accurate inductance modelling it is desirable to have a large number of elements and extend the calculation volume away from the conductors to ensure an acceptably accurate result. For the initial design stages, estimates of inductance within 5 % - 10 % are acceptable and the computationally time consuming model saved for the final design.

As the required coil shape for Pulsed Field Magnetometry is a multi layer solenoid then the inductance, $L$, can be estimated using Bunnet's formula [31],

$$L = \frac{a^2 N^2}{9a + 10l + 8.4c + \frac{3.2cl}{a}} \tag{5.6}$$

where $a$ is the area of the solenoid windings, $N$ is the number of turns in the solenoid, $l$ is the length of the solenoid, and $c$ is the radial thickness of the windings. This formula has a typical accuracy of better than 5 % for determining the inductance $L$ of multilayer solenoids when the diameter of the solenoid is less than 3 times the length. These dimensional limitations are compatible with the typical dimensions of PFM coils where the diameter is typically equal to or smaller than the length of the coil.

### *5.4.2 Resistance*

By knowing the cross sectional area of the wire to be used, and the total length of the windings, it is possible to estimate the resistance of the wire at a given temperature. The resistance per meter of copper, $R$, can be described by:

$$R = \frac{(1+aT)\sigma}{A} l \tag{5.7}$$

where $a$ is the specific resistance of copper, $T$ is the temperature of the copper in Kelvin, $\sigma$ is the thermal conductivity of copper, $A$ is the cross sectional area of the copper and $l$ is the length of the copper.

Due to the very large currents that are required for the generation of the measurement fields, the energy losses due to copper resistance are considerable. As these losses occur in the form of heating of the copper wire, this effect should be considered in the modelling of the field generation coil. The heating effect will be an almost instantaneous effect and it could be assumed that during the duration of the pulse (a few milliseconds) that all the heat remains within the copper, essentially an adiabatic process. Using the above assumption it is possible to include the effect of adiabatic heating in the modelling of the magnetic field generator in a finite difference, time stepping arrangement, to determine the temperature rise $\Delta T$, which is given by,

$$\Delta T = \frac{1}{C_h \rho A_c L_c} \int i^2(t) R(t) dt \tag{5.8}$$

where $C_h$ is the specific heat capacity of copper, $\rho$ is the density of copper, $A_c$ is the cross sectional area of the conductor used, $L_c$ is the total length of conductor, *i(t)* is the current at time *t* and *R(t)* is the resistance of the copper at time t.

### *5.4.3 Analytical calculation of the applied current waveform*

With the inductance and resistance of the coil predicted it is possible to estimate the field generation current that will flow to generate the magnetic field, by simplifying a Pulsed Field Magnetometer to the equivalent circuit as previously described by Figure 13. The second order equation that describes the relationship between the inductance, resistance, capacitance and the current is given by,

$$\frac{d^2 i}{dt^2} + \frac{R}{L}\frac{di}{dt} + \frac{i}{LC} = 0 \tag{5.9}$$

where the terms have their usual meaning. At the instant the thyristor switches on the current flowing will be 0 A and the rate of change of current will be controlled by only the voltage and the inductance of the coil. This leads to initial conditions, at $t = 0$, of $i = 0$ and $\frac{di}{dt} = \frac{V}{L}$.

It should be noted that many factors have been assumed negligible in this approximation, there can be significant resistance and inductance between the fixture and the capacitor bank, and even internal to the capacitor bank. It is also assumed that the capacitance of the field generation coil can be ignored and that the coil has a relative permeability of 1. It is also assumed that all parameters remain constant during current flow.

The solution to Equation (5.9) has three forms depending on the relationship between *L*, *R* and *C*. Only one form is generally used for the modelling of these types of coils as the other two forms represent huge energy loss due to resistive dampening.

Case 1: Under damped, where $R < 2\sqrt{\frac{L}{C}}$

The current is described by the following equation,

$$i(t) = \frac{V_0}{\omega L} e^{-\sigma} \sin(\omega t) \tag{5.10}$$

where,

$$\sigma = \frac{R}{2L} \text{ and } \omega = \sqrt{\frac{1}{LC} - \frac{R^2}{4L^2}} \tag{5.11) (5.12}$$

Case 2: Critically damped, where $R = 2\sqrt{\frac{L}{C}}$

The current is described by the following equation,

$$i(t) = \frac{V}{L} t e^{-\sigma} \tag{5.13}$$

where the terms $i$, $t$, $V$ and $L$ have their usual meaning and $\sigma$ is described by equation 5.11

Case 3: Over damped, where $R > 2\sqrt{\frac{L}{C}}$

The current is described by the following equation,

$$i(t) = \frac{V}{L(\lambda_1 - \lambda_2)} (e^{\lambda_1 t} - e^{\lambda_2 t}) \tag{5.14}$$

where,

$$\lambda_1 = -\frac{R}{2L} + \sqrt{\frac{R^2}{4L^2} - \frac{1}{LC}} \text{ and } \lambda_2 = -\frac{R}{2L} - \sqrt{\frac{R^2}{4L^2} - \frac{1}{LC}} \tag{5.15) , (5.16}$$

These equations are used in the software package described in Section 5.5 to simulate applied current waveforms for given values of $R$, $L$, $C$ and $V_o$.

### *5.4.4 Coil construction and packing density*

The manufacture of a typical field generation coil will be from solid copper wire. Due to the estimated currents involved and the required resistance, the most suitable wires are the rectangular cross section types. They are more readily available in the cross sections

required and achieve a better packing density close to 1.0 whereas round wire has a packing density of 0.79 as shown in Figures 16 - 18.

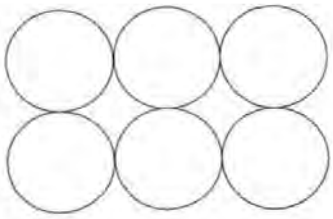

*Figure 16 - Round cross-section wire, packing density approx 0.79.*

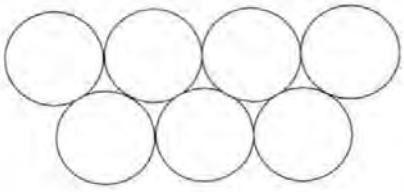

*Figure 17 - Close packed round cross-section wire packing density approximately 0.9.*

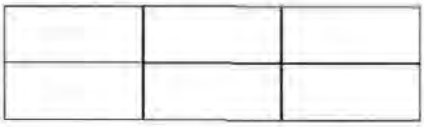

*Figure 18 - Rectangular cross-section wire, packing density close to 1.0.*

As the magnetic field, generated by a solenoid is proportional to both the current flowing through the solenoid and the number of turns of wire on the solenoid, it is often desirable to make a multilayer solenoid to increase the number of turns. Although it is technically feasible to use a single turn with high currents, this is not usually done. In many situations it is possible to design a coil with multiple turns to optimise the required current and minimise the total resistive losses of the coil. This optimised coil will usually have a lower current requirement and lower dissipation than a single turn with high current.

As the wire used to wind solenoids has a finite cross-section, the end of one turn will be displaced by the thickness of the wire from the start of the same turn. This effect will be

carried on for the entire winding layer. This in effect produces a spiral and the magnetic field produced will deviate from classical theory that often assumes concentric circles of wire. The result is that the generated magnetic field will have an off axis component due to the "skew" of the windings. As additional layers are added, they are wound from the opposite end of the solenoid to the previous layer. These have an opposing skew that nearly, but not completely, cancels out the skew from the previous layer. This effect has an impact on the homogeneity of the field generation coil. As homogeneity is an important design parameter it was decided to include this effect in any solenoid coil models. This effect was incorporated into the modelling software described later in order to increase its accuracy to the physical parameters being modelled.

It was decided to analysis the skewed effect to determine the magnitude of any potential problems it may cause to field homogeneity. Figure 19 shows the predicted differences of the magnitude of applied field, between the conventional concentric model and the helix model. Figure 20 shows the effect on the Y and Z components of applied field of the spiral solenoid and the effect due to different numbers of layers forming the solenoid. For both cases, wire with dimensions of 5 mm wide by 3 mm high was selected. Wire of these dimensions was used to construct PFM coils that are discussed later in this thesis.

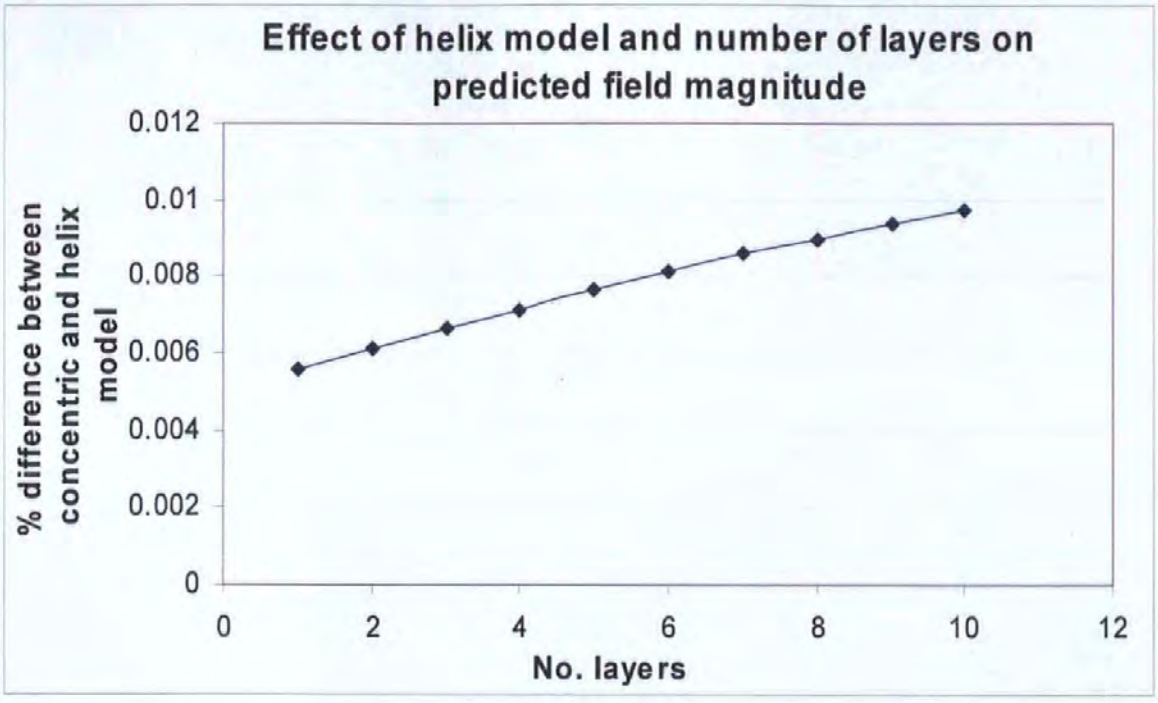


*Figure 19 - % Difference of field at magnetic centre between helix and concentric models of solenoids. The copper wire considered was a 5 mm x 3 mm cross-section. The solenoid had 30 turns per layer.*

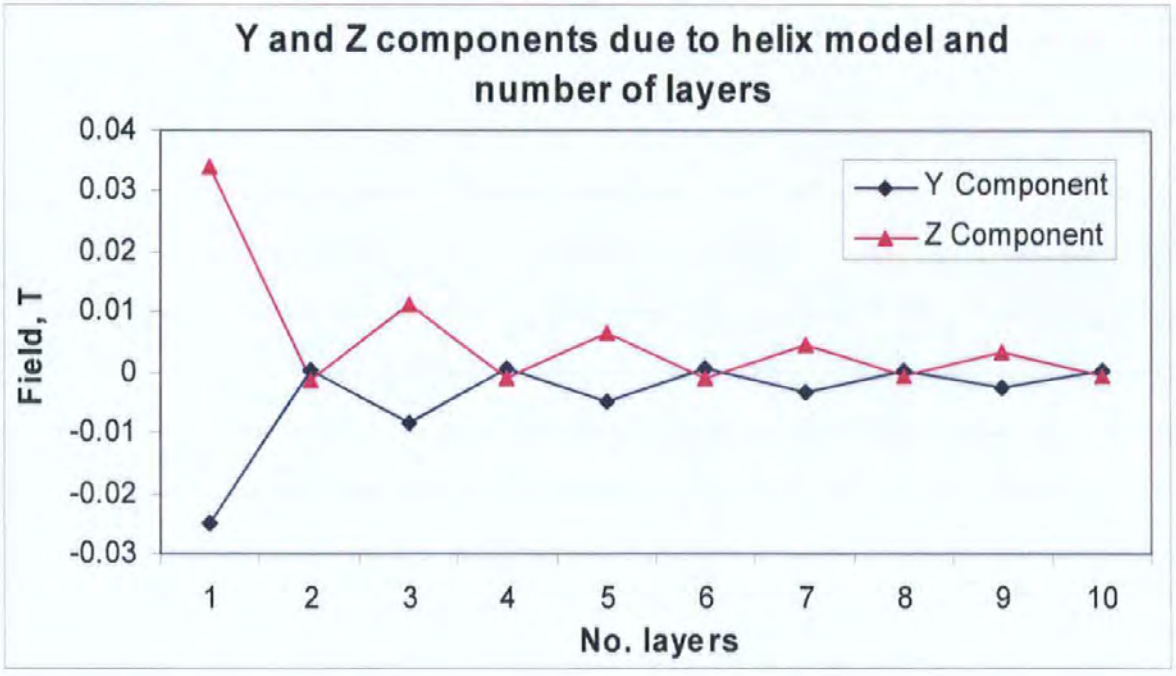


*Figure 20 - Effect on Y and Z components of applied field at magnetic centre due to the helix solenoid model. The copper wire considered was a 5 mm x 3 mm cross-section. The solenoid had 30 turns per layer.*

From Figure 19 it can be seen that the model predicts a small change in the magnitude of applied field between the concentric and helix models. As the number of layers on the solenoid increase, the difference between the two models increases. The magnitude of applied field at the magnetic centre in the helix model is lower than the concentric model. The magnitude of the difference is small, less than 0.01% for 1 to 10 layers. For the particular dimensions of wire used, 5 mm wide by 3 mm high and 30 turns per layer, the predicted effect on the magnitude of applied field is small and the differences between the helix and concentric models can be ignored.

Figure 20 shows a significant effect on the off axis components of the generated magnetic field due to the helix model and the number of layers selected. Fields of up to 34 mT are predicted off the desired axis. It can be seen that for even numbers of layers the effect of the skew is reduced, less than 1 mT is predicted. As the number of layers increases the magnitude of the off axis effects also reduce.

The conclusions from the analysis of the helix and concentric models of solenoids are that for the chosen wire dimensions the effect on the magnitude of generated field is insignificant but the effect on the components of the magnetic field cannot be ignored. When constructing a solenoid coil for PFM applications it is greatly preferred to use an even number of layers to minimise any off axis components that are generated.

### *5.4.5 Geometric modelling*

For the analysis of the magnetic field homogeneity it is necessary to have an accurate representation of the field generation coils geometry. As the coil is to be manufactured from square section conductor, circular conductor is not considered here, although the method of analysis is still valid with slight modification to the geometry equations.

For a square section enamelled copper wire there will be a nominal thickness of copper surrounded by insulating enamel. Figure 21 illustrates the critical dimensions and variables. $C_x$ is the copper $x$ dimension, $C_y$ is the copper $y$ dimension, $C_{mx}$ is the conductor $x$ direction, including copper and enamel and $C_{my}$ is the conductor $y$ direction, including copper and enamel.

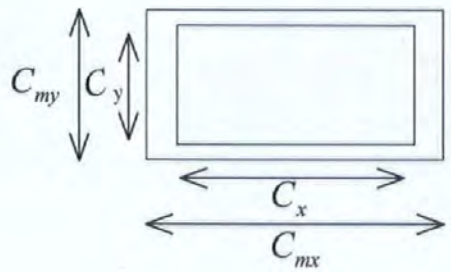


*Figure 21 - Cross-section of enamelled copper wire. The copper and the enamel coating dimensions are shown.*

If we consider a coil made from $g$ layers with $T$ turns of conductor per layer and each turn divided up into $N$ elements, that is wound onto a former of radius $r$, and we define the geometric centre of the coil, in Cartesian coordinates as:

$$X_{WE0} = -T \times \frac{C_{MX}}{2} \tag{5.17}$$

$$Y_{WE0} = 0 \tag{5.18}$$

$$Z_{WE0} = r + \frac{C_{MY}}{2} \tag{5.19}$$

we can specify the coordinates for any element, N, using the following equations:

$$X_{we} = \eta(E-1)\frac{C_{MC}}{N} + (I_{TN} - 1)C_{MX} + X_{WE0} \tag{5.20}$$

$$Y_{we} = \frac{(r + C_{MY})(I_{LN} - 1)}{2} \sin((E-1) \times 2\frac{\pi}{N}) \tag{5.21}$$

$$Z_{we} = \frac{(r + C_{MY})(I_{LN} - 1)}{2} \cos((E-1) \times 2\frac{\pi}{N}) \qquad (5.22)$$

where $\eta$ is 1 for odd numbered layers and −1 for even numbered layers, $I_{TN}$ is the incremental turn number being considered and $I_{LN}$ is the incremental layer number being considered. These equations allow the calculation of the geometry of solenoid coils and the data generated from this modelling is used as the input co-ordinates for the calculation of magnetic fields and homogeneity.

### *5.4.6 Magnetic field and homogeneity*

With the current estimated and the potential geometry known it is possible to predict the magnetic field produced by such a configuration. The magnetic field at the geometric centre of the coil can be estimated using empirical techniques. The homogeneity requires a more complex approach. The most obvious choices are finite element analysis and boundary element method analysis. Due to the complex 3D geometry, of the field generation solenoid, it is actually simpler to perform a boundary element method rather than to enter the data into a FEA package and generate a field plot. By using Biot-Savat's law [32] it is possible to calculate the field at a given position away from a current carrying conductor. The magnitude of the magnetic field at a given point, is proportional to the current flowing in the conductor and inversely proportional to the distance from the conductor. The direction of the magnetic field at a given point is the vector cross product of the vector of current flow. Figure 22 illustrates this concept graphically.

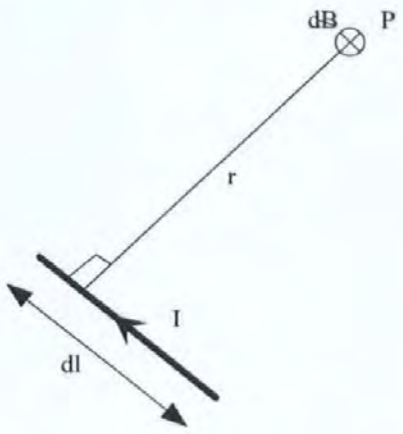


*Figure 22 - The Biot Savat law.*

By using Biot-Savat's law, the incremental field d**B** at point P, from a current carrying conductor is given by,

$$d\mathbf{B} = \frac{\mu_0 I d\mathbf{l} \times \hat{\mathbf{r}}}{4\pi r^3} \tag{5.23}$$

where $\mu_0$ is the permeability of free space, $I$ is the current flowing through the conductor under consideration, $dl$ is an element of the conductor and $\hat{\mathbf{r}}$ is a unit vector from point $P$ to the element $dl$. By integrating around the entire solenoid, it is possible to obtain $\boldsymbol{B}$ at a point, as given by,

$$\mathbf{B} = \oint \mu_0 I d\mathbf{l} \times \frac{\hat{\mathbf{r}}}{4\pi r^2} \tag{5.24}$$

By combining the geometry equations of section 5.4.5 "Geometric modelling" with Equation 5.24 it is then possible to calculate the field produced by a coil at any point in the space inside and surrounding the coil. This can then be used to produce a field profile and ensure the applied field is within homogeneity specifications as well as checking the magnitude of the field within the measurement region.

The wire used for PFM applications usually has a cross-sectional area that is significant enough that it is not representative to model the current flowing through the wire at a

single point. The effect of dividing up the cross-section into firmaments was considered and integrated into the final modelling software. Figure 23 shows how the conductors were divided up. The overall current was assumed to be spread equally between the filaments. The Biot-Savat approach previously discussed was then used to calculate the current due to each filament. Figure 24 shows the effect of increasing the number of conductor filaments on the magnitude of applied field at the magnetic centre. The wire considered was 5 mm wide by 3 mm high. The solenoid had 10 layers and 30 turns per layer wound on to a former of 50 mm.

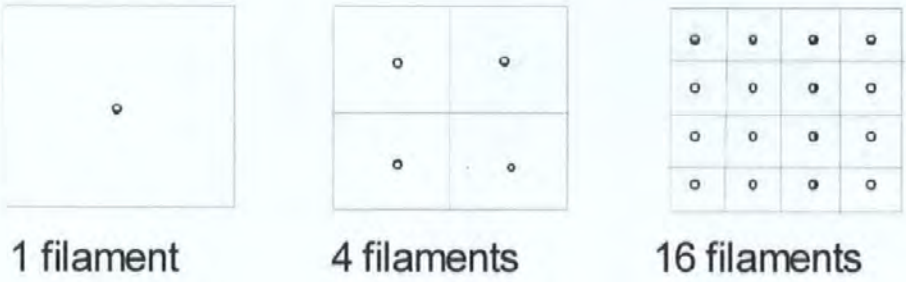


*Figure 23 - Conductor divided up in to filaments*

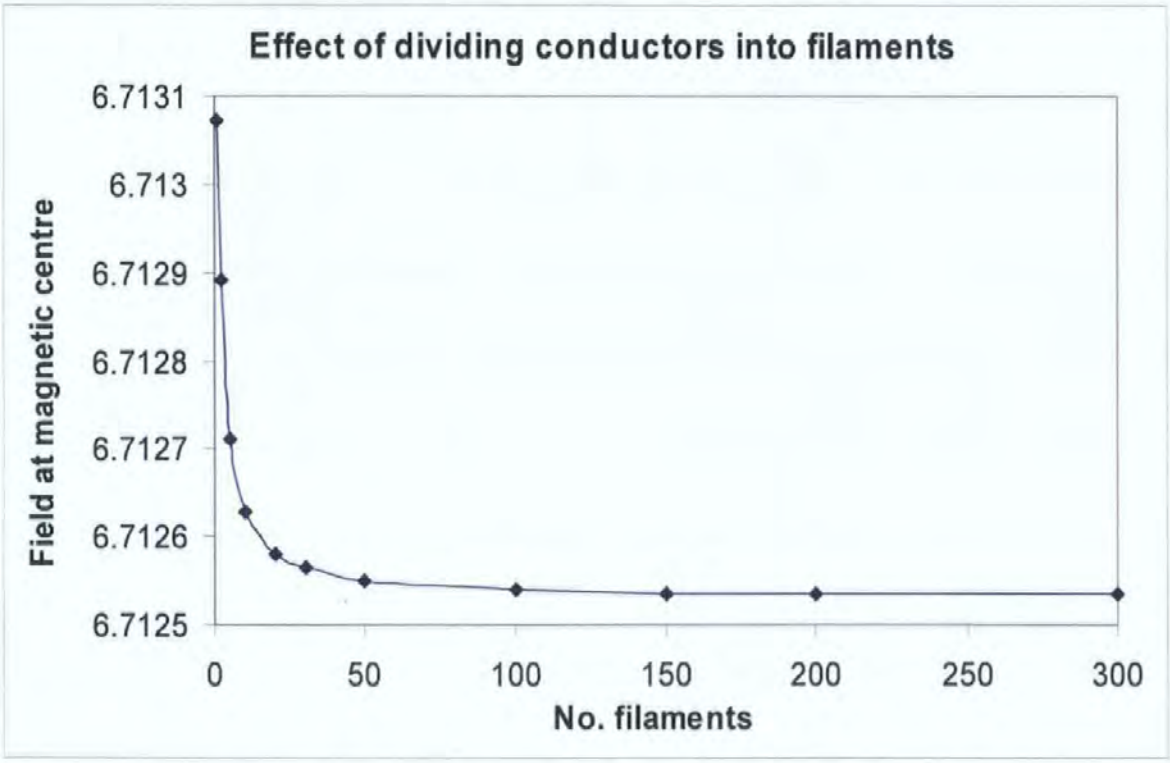


*Figure 24 - As the number of filaments increase the field at the magnetic centre starts to decrease and converges at 200 to 300 filaments.*

It can be seen that the number of filaments has an effect on the simulated magnitude of applied field and as the number of filaments increase the field at the magnetic centre decreases towards a convergence point. The overall effect for this particular geometry of solenoid and wire dimensions is small, approximately 0.008% between 1 filament and 300 filaments. For each given wire size and solenoid geometry the sensitivity to filament number should be accessed and a sufficient number of filaments for the accuracy required should be selected.

### *5.4.7 Cooling*

As the coil's temperature is increased due to resistive $I^2R$ losses, the problem of increased resistance and even over temperature failure become an issue. It is also highly desirable to maintain a stable thermal environment for the sample measurements. The previous modelling of the heating process of the solenoid places an estimate for a temperature rise of approximately 4 degrees Celsius per pulse, for a coil with an initial temperature of 25 degrees Celsius. This equates to a heating energy of up to 12 kJ per pulse. For cooling to be successful, a fluid of a lower temperature must be in contact with a surface to be cooled. Due to the construction of the field generation coils, the external diameter is wrapped in fibreglass for radial strength and the inner diameter is required for pickup coils and magnets. Therefore the only solution is to create the entire coil with spacers between the layers to allow a fluid to pass.

The copper windings have a maximum potential of 3000 V so any fluid would have to be non conductive which prohibits water based fluids. It is also desirable that the fluid has low viscosity, to enable large flow rates to be achieved, and high thermal conductivity. Cryogenic fluids were not used because there were concerns that if the coil was cooled down to cryogenic temperatures it would become very brittle and the forces exerted on the conductors would cause them to mechanically fail. It was decided to use conventional

coolant. A synthetic oil based fluid was chosen and this was "Therminol D12", a non-conductive fluid with a viscosity similar to water and excellent thermal properties. The fluid was pumped under pressure through the field generation coils then back to a header tank and a forced radiator system to remove excess heat.

The cooling method proved successful and it was possible to remove much of the dissipation energy from the coils. When running a single pulsed field coil at the maximum possible rate of a discharge every 5 seconds the coil reached a maximum temperature of 60 °C. This is within the thermal specifications of all materials used in the construction of the pulsed coil and would provide a sufficient margin for changes in ambient temperature.

## 5.5 Aircore - a software package for pulsed solenoid design optimisation

The modelling tools previously discussed were integrated into a software package for ease of computation and automation [30]. The package was called "AirCore" and was generalised to be suitable for the modelling of any air-cored solenoid type coil, not just for field generation coils used in PFM measurements. Figure 25 shows a screen shot of AirCore showing typical parameter entry and results windows. The software fixed the level of required data to a series of 7 design parameters. For the field generation coil the following data is required,

- Conductor size and insulation thickness.
- Number of conductor layers.
- Number of turns per layer.
- Former outside diameter.
- Interlayer insulation thickness.
- Initial ambient temperature.

Additional data was required for the energy source; capacitive discharge, constant current or AC current could be accounted for in the simulation. For the purposes of PFM coils only capacitive discharge will be considered: The require drive parameters are,

- Capacitance
- Voltage

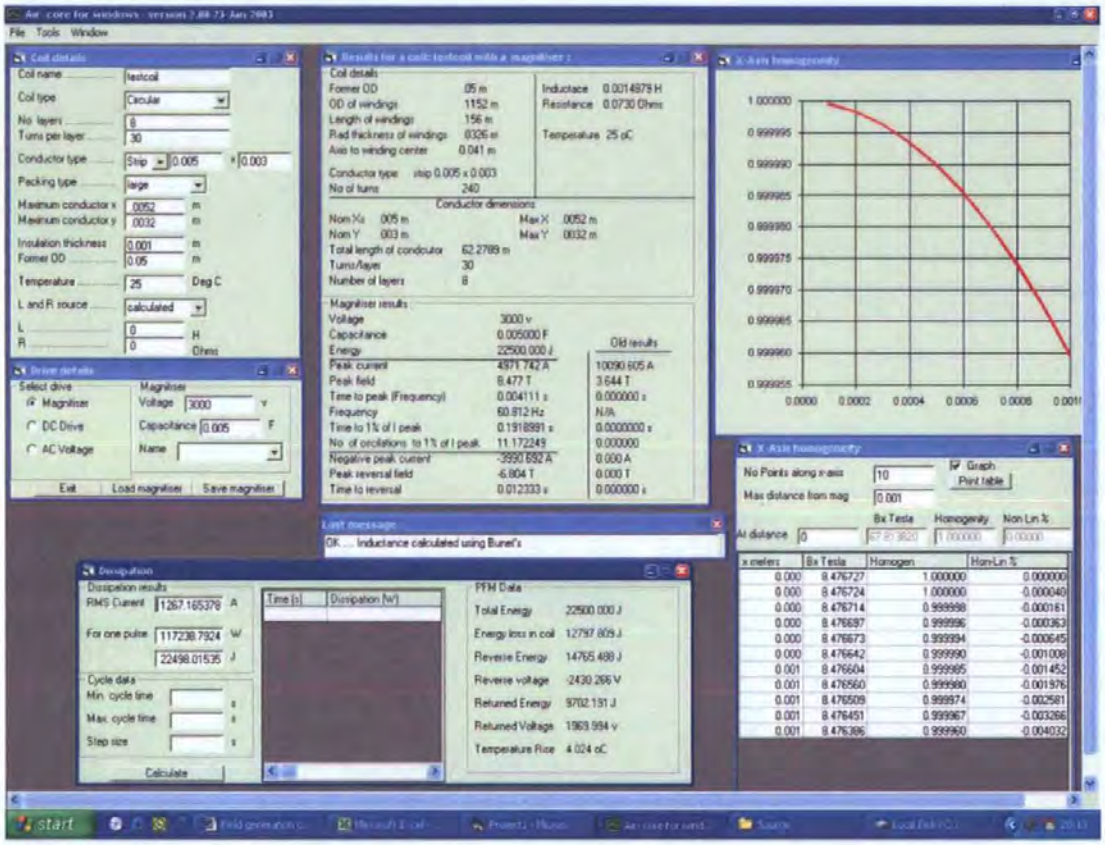

*Figure 25 - Screen shot of the Aircore program. Aircore was created for the design and parameter optimisation of air cored fixtures [33].*

### 5.5.1 Case study of Aircore program

Some examples are now given of the practical application of the modelling tools discussed in this section. A requirement was for two coils with an internal bore of approximately 50 mm that could generate peak fields of 7.5 Tesla and 8.5 Tesla. A 5 mF capacitor bank rated at 3000 V was available. Table 7 gives some examples of predicted electrical and magnetic parameters and the values measured when the coil was constructed.

| Name | No Turns | No Layers | Peak Field (T) | Calculated Inductance (uH) | Calculated Resistance (mΩ) | Measured Field (T) | Measured Inductance (uH) | Measured Resistance (mΩ) |
|---|---|---|---|---|---|---|---|---|
| Coil "long" | 30 | 8 | 7.5 | 1820 | 77 | 7.35 | 1808 | 110 |
| Coil "short" | 30 | 4 | 8.5 | 602 | 42 | 8.3 | 678 | 60 |

*Table 7 - Aircore results compared to physical coils.*

The measured resistance includes the effects of the coil termination and solder joints and hence is greater than the predicted value. The results in Table 7 are typical of the accuracy obtainable from Aircore, proving the assumptions used in the modelling process are acceptable for the level of accuracy required by this type of modelling tool.

The measurement of the actual applied current was not available due to the magnitude of the currents involved. If the applied current measurement was available this would have been useful in assessing the difference between the calculated applied field and the measured applied field and in determining if this discrepancy is due to the modelling of the applied field or due to the modelling of the electrical characteristics or a combination of the two.

### *5.5.2 Homogeneity of field.*

Accurate measurements require that the entire volume of the sample is exposed to a magnetic field which is as homogenous as possible. In practice, it is possible to carefully control and quantify the field distribution through out the sample region. It was a design criteria that any field generation coil must be capable of producing a field with a homogeneity of better that 1 % over the volume of the maximum sized sample.

If the homogeneity of a point is defined as the ratio of the magnetic field at the magnetic centre of the coil to the magnetic field at the point of interest, then Figure 26 shows a plot of homogeneity based on the coils discussed in Section 5.5.1, over the sample measurement volume. The plot shows the homogeneity from the magnetic centre to a point 15 mm along the central axis of the coil. It can be seen that the homogeneity at a distance of 15 mm from the magnetic centre is better than –1 %. The maximum size of magnets that the system was designed to measure was 30 mm and the design criteria was to have a homogeneity with in +/-1 % over the volume of the largest possible magnet, so in the X-axis the system achieves the design criteria.

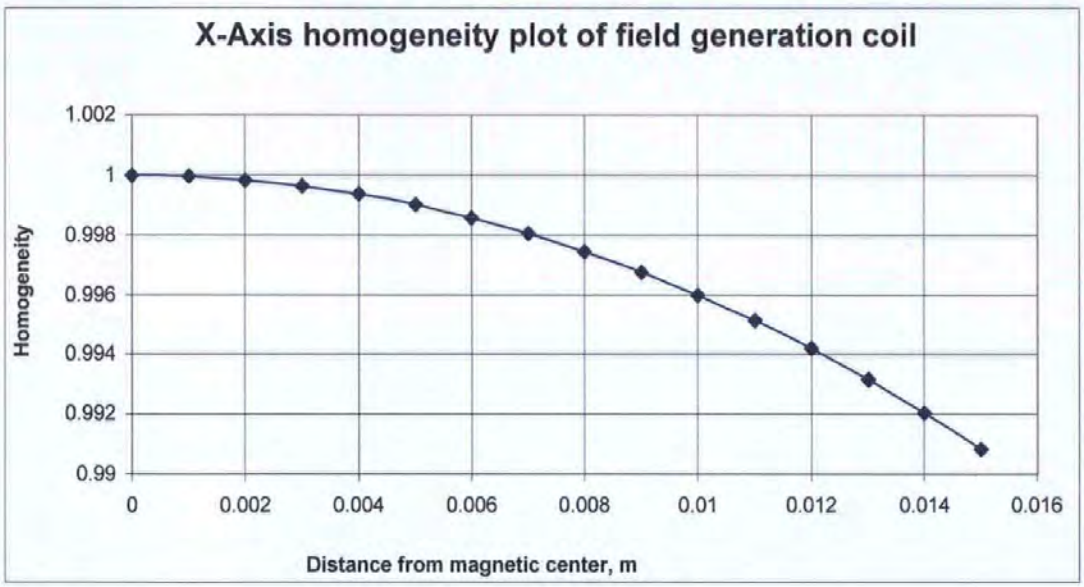


*Figure 26 - Field generator axial homogeneity.*

Figure 27 shows part of the Y/Z axis radial homogeneity from the magnetic centre to a point 15 mm along the coils radius. A radius of 15 mm was chosen as the maximum sample diameter was 30 mm. If the homogeneity was found to be greater than 0.99 in both the X and Y/Z axis then the coil design was satisfactory. The maximum sample diameter the system was designed for was 30 mm, comparing this to the model results shows a homogeneity of +0.5 % at a distance of 15 mm from the magnetic centre. This is with in the deign criteria of 1 % homogeneity in the Y-axis and the design is considered successful.

Combined into a two dimensional plot the homogeneity is shown in Figure 28. This plot is a cross-section of the homogeneity of the field generation coil. It has radial symmetry about the y-axis and represents the entire volume where it is possible to place samples for characterisation. The plot shows that the entire region has a homogeneity of better that 1 % and therefore the coil design meets the homogeneity specification.

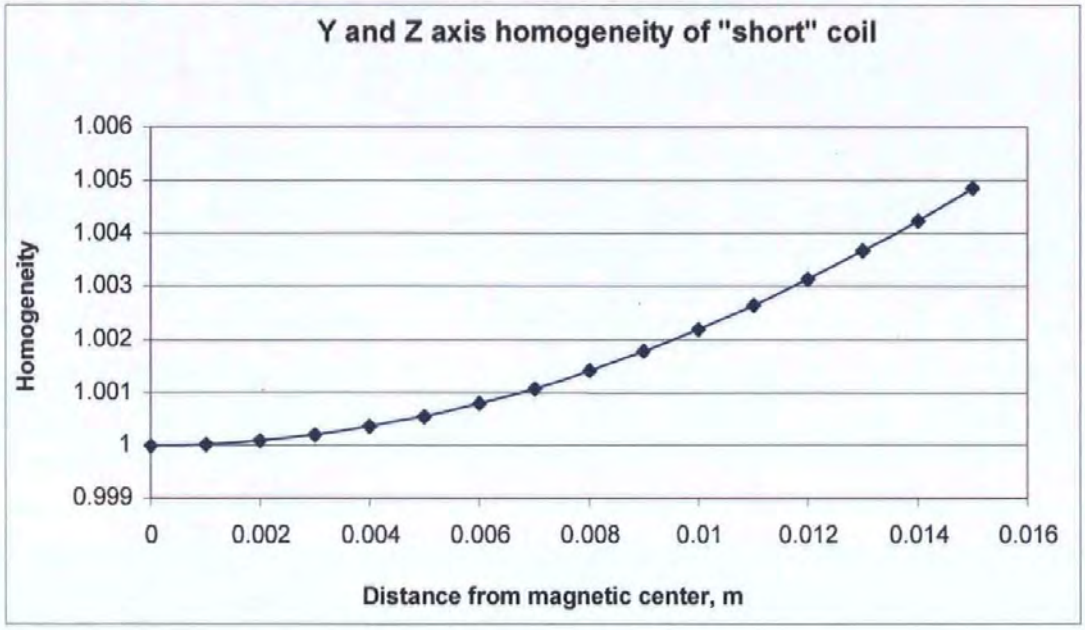


*Figure 27 - Y and Z axis field generator radial homogeneity.*

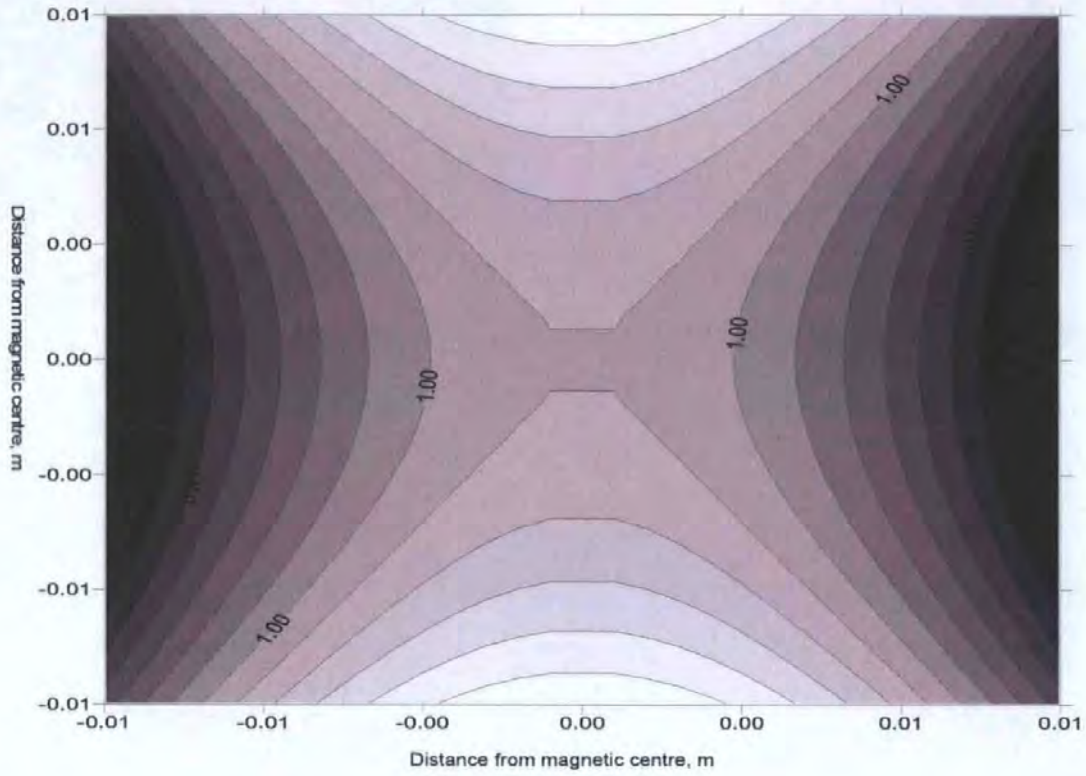


*Figure 28 - 2D contour plot of field generator homogeneity over a 30 mm diameter 30 mm long volume. The magnetic field over the entire volume is within 1 % of the magnetic centre.*

## 5.6 Summary of magnetic field generation

The most appropriate method of magnetic field generation was determined to be a pulsed solenoid coil. The alternatives considered, iron pole pieces and super conducting solenoids were unsuitable for this application. Pole pieces were rejected due to the limited applied field obtainable and the problem of eddy currents within the pole pieces during field transients. Super conducting solenoids were considered too expensive in terms of initial capital cost and running costs when compared to pulsed solenoid coils and in addition the typical high reactive inductance of super conducting coils inhibits rapid applied field changes.

The method of energising the applied field coil was selected as capacitive discharge with the power electronics configured to give a decaying sine wave. The decaying sine wave

was considered the most appropriate discharge type as a single discharge can drive a sample to be characterised completely around its hysteresis loop with no discontinuities.

Methods of modelling the inductance, resistance and coil geometry were presented as tools for the design of pulsed solenoid coil and methods for calculating the resultant magnetic field distribution were presented. These tools were combined into computer software to automate the procedure with comparisons of modelled and measured parameters giving good agreement.

# Chapter 6 Sample magnetisation and applied field measurement

To characterise magnetic materials it is necessary to measure the magnetisation of the test specimen and the applied field simultaneously, as it is the determination of **J** (magnetisation) vs. **H** (applied field) that provides the data for the characterisation process. The materials are to be characterised in terms of coercivity ($H_C$), intrinsic coercivity ($H_{CI}$), remanence ($B_R$) and maximum energy product ($BH_{MAX}$). As previously discussed in Chapter 2, Figure 2 shows two hysteresis plots. The solid plot represents the magnetisation (**J**) of the magnet vs. applied field (**H**) while the dashed plot represents total magnetic flux density (**B**) vs. applied field (**H**). **J**, **B** and **H** are related by the equation,

$$\mathbf{B} = \mu_0 \mathbf{H} + \mathbf{J} \qquad (6.1)$$

The maximum energy product, ($BH_{MAX}$), is determined by multiplying the magnetic flux density (**B**), by the applied field (**H**), in the region where $\mathbf{B} > 0$ and $\mathbf{H} < 0$. The largest product of **B** and **H**, in this region, is the maximum energy product. Remanence is determined by the sample's magnetisation at zero applied field and is therefore simply the positive value of **J** when $\boldsymbol{H}=0$. Coercivity and intrinsic coercivity are given by the value of the applied field necessary to cause $\boldsymbol{B}=0$ and $\boldsymbol{J}=0$ respectively

Two sensors are requires, one for the determination of the applied field and one for the determination of the sample's magnetisation. It is vital that the sensors have sufficient resolution, bandwidth and dynamic range to cope with the range of applied fields and sample sizes that are expected to be seen in an industrial PFM system. It is also important that only the signal of interest is detected and that far-field and near-field interference is rejected to the maximum extent possible to preserve signal integrity.

## 6.1 Types of magnetic sensor

There are a number of sensors available for the detection of magnetic fields. Each type of sensor has optimal operating conditions such as frequency response, resolution and maximum applied field and if used appropriately, these conditions will narrow down the choice of sensor. It should be noted, that in the case of the applied magnetic field, the magnitude of the field is unusually high in this case. In fact fields up to 10 Tesla are required. Many magnetic field sensors are designed for lower field levels than encountered in Pulsed Field Magnetometry, often less than 3 Tesla as this is the upper limit for conventional static fields and many sensors concentrate on resolution into the sub micro Tesla (μT) range. A number of possible detectors are considered in this section for the detection of applied field and magnetisation, these are:-

- Hall Sensors
- Pickup coils
- Magnetoimpedance type sensors
- Fluxgate devices

### *6.1.1 Hall sensors*

Hall effect sensors are semiconductor based devices and detect magnetic fields using the Hall effect principle. Hall effect devices are typically fabricated into an integrated circuit. They are directionally sensitive point measurement devices with a small active measurement area. The Hall effect is caused by the Lorentz force. An electron moving at a velocity, $v$, perpendicular to a magnetic field will experience a force, $\boldsymbol{F}$, normal to the direction of movement and the applied magnetic field, $\boldsymbol{B}$. Figure 29 shows a graphical representation of the Lorentz force on a single electron travelling through a magnetic field.

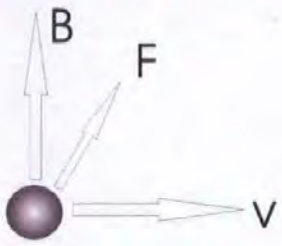


*Figure 29 - Lorentz force considered on a single electron.*

The Lorentz force ***F***, can be described by,

$$\mathbf{F} = -q\mathbf{v} \times \mathbf{B} \tag{6.2}$$

where ***B*** is the applied magnetic field, ***v*** is the velocity of the electron and ***F*** is the force experienced by the electron. Figure 30 shows the Lorentz force when considered on a section of semiconductor with current flowing between two opposite faces of the die and with a magnetic field normal to the current. A voltage is produced that is normal to the current and the applied field. The electrons in the current flow will drift away from the natural current path, due to the Lorentz force, inducing a voltage that is proportional to the magnitude of the applied field and the magnitude of the current flowing. Suitable instrumentation can detect this voltage differential and with amplification and calibration, an absolute measurement of magnetic flux density can be determined.

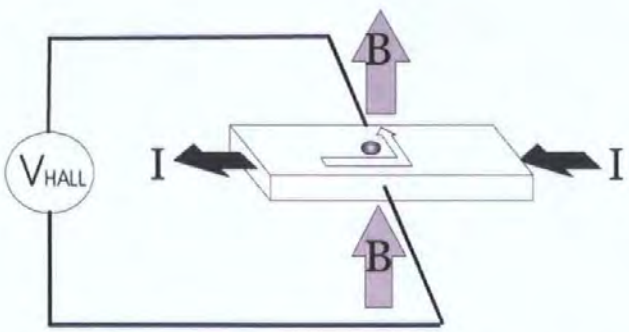


*Figure 30 - Lorentz force on a slab of semiconductor material, placed in a magnetic field with a current flowing through the semiconductor.*

Hall effect devices are typical composed of either Gallium Arsenide (GaAs) or Indium Arsenide (InAs) as these semi-conductor materials exhibit a large Hall effect compared to

other materials. GaAs and InAs devices can have an output as high as 2 Volts per Tesla but GaAs devices have a sensitivity limit of approximately 10 nT. InAs devices tend to have a higher sensitivity than GaAs devices and typically have a noise floor of approximately 1 nT. When a hall effect device is coupled with a suitable Gaussmeter that is designed to measure applied fields of at least 8 T, it is typical to see a resolution of 1 mT. One such Gaussmeter is the model 2100 from Magnetic Instrumentation [34]. This instrument has a quoted range of 30 Tesla with a $4^3/_4$ digit resolution.

### *6.1.2 Pickup coils*

Pickup coils are the simplest of magnetic sensors discussed in this section. The principle of operation of a pickup coil is Faraday's law of induction. Pickup coils are simple to manufacture and require only the required number of turns of wire encompassing the required area. If a single loop of wire is considered in a homogenous time dependent applied field, the induced emf, $\varepsilon$, is given by,

$$\varepsilon = -\frac{d\phi}{dt} \tag{6.3}$$

where $\varepsilon$ is the induced emf and $\frac{d\phi}{dt}$ is the rate of change of magnetic flux. The induced emf is the differential of the flux with respect to time. As the required measurement parameter is typically the flux and not the differential of the flux, an integrator will be used after the pickup coil to integrate the emf with respect to time to obtain the flux. Once the flux is known it is possible to calculate the flux density if the area of the pickup coil and how many turns it contains are known and the field can be considered to be homogenous. In a homogenous field the integrated output is directly proportional to the magnitude of the magnetic flux density B, which is given by:

$$B = N.A\int\frac{d\phi}{dt} + C \tag{6.4}$$

where $N$, the number of turns of wire on the pickup coil and $C$ is the unknown constant of integration. If a suitable origin or boundary condition is known, this can be an absolute measurement of magnetic flux density. The issue of the boundary conditions of this integration is considered in section 7.2

The output of a given search coil is a function of the number of turns that form the search coil and the area encompassed by the coil. The search coil itself, does not have a sensitivity limit and the ability to detect magnetic fields is determined by the instrumentation that is measuring the induced voltage output of the search coil. The design of the search coil can aid the implementation of the instrumentation, for example by ensuring that the search coil is shielded from unwanted signals (interference). The shielding can be a simple electrostatic and/or electromagnetic screen that surrounds the pickup coil.

Figure 33 shows a comparison of the operating range for the magnetic sensors discussed here. The pickup coil is shown having an operating range from the femto Tesla (fT) to the Tesla region. This represents a dynamic range of greater than $10^{12}$ but in practice, a search coil will be designed for a particular application and coupled with dedicated instrumentation designed for that purpose and therefore have a greatly reduced, usable, dynamic range. The measurement bandwidth of a pickup coil is also a function of the pickup coil and the required interconnections and instrumentation. The pickup coil can be considered to be an inductor with a small resistance. Typically a type of shielded cable such as coax will be used to connect the pickup coil to the instrumentation. The coax cable has its own capacitance and resistance. Figure 31 shows a schematic representation of a pickup coil, interconnection cable and instrumentation as used in a typical PFM application.

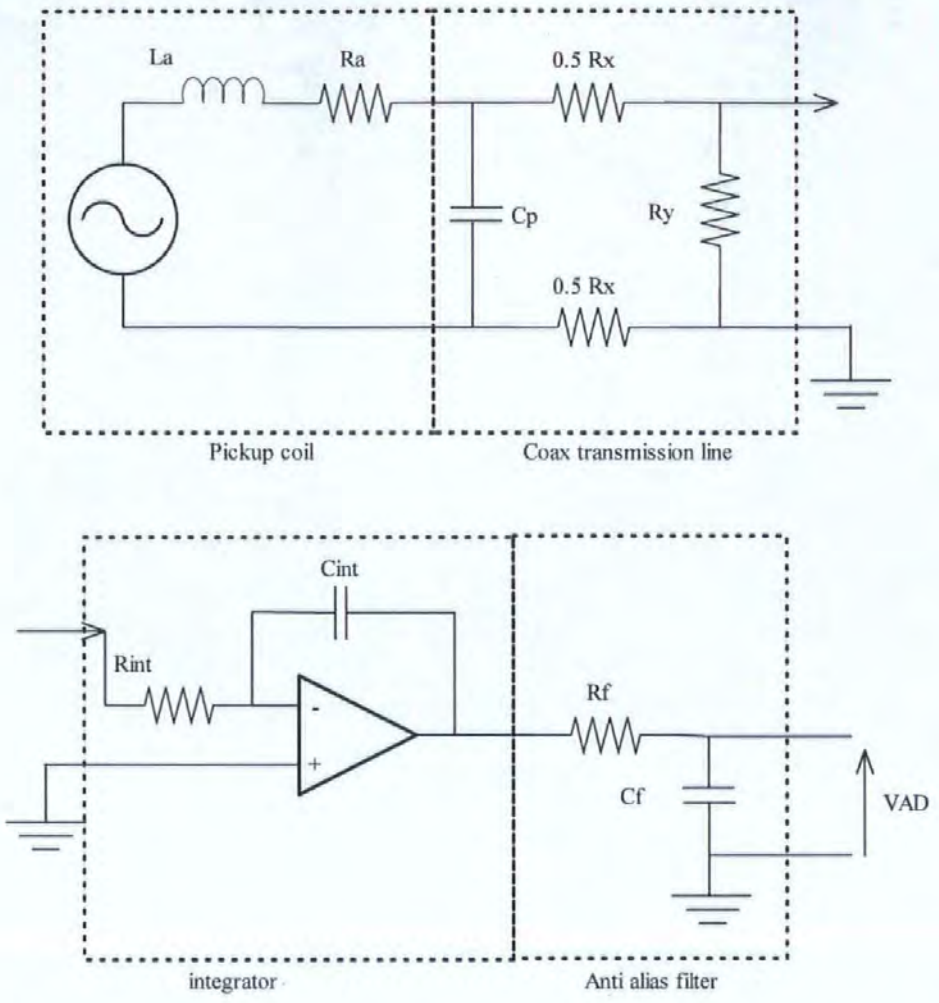


*Figure 31 - Schematic representation of pickup coil, coax transmission line, differential integrator and input anti-alias filter.*

If the pickup coil and the coax are considered then the pickup coil and transmission line will have a transfer function approximated by Equation 6.5. The integrator will have a transfer function approximated by Equation 6.6 and the anti alias filter will have a transfer function given by 6.7.

$$H(s) = \frac{R_x}{(R_X + R_y)} \cdot \frac{1}{(1 + s\frac{L_a}{R_a} + s^2 L_a C_p)} \tag{6.5}$$

$$H(s) = -\frac{1}{sR_{\text{int}}C_{\text{int}}} \tag{6.6}$$

$$H(s) = \frac{1}{1 + sC_f R_f} \qquad (6.7)$$

These transfer functions can be used to determine the useable bandwidth of a given pickup coil and instrumentation system. Typically the limiting factor will be the anti-alias filter that is required to prevent the possibility of aliasing of data when sampling into the A/D converter.

### *6.1.3 Fluxgate devices*

Fluxgate sensors have a diverse range of applications. Originally invented around 1930, they have found uses in navigation systems, submarine detection, geophysical surveys and airborne magnetic field mapping.

Fluxgate sensors work by exciting a ferromagnetic core with an alternating magnetic field. The applied magnetic field drives the ferromagnetic core into saturation. A second coil, coupled to the drive coil via the ferromagnetic core, develops an output that is a function of the hysteresis and saturation of the material. In the presence of no external field the applied drive current necessary to saturate the core in either direction is symmetrical. As an external field is introduced the saturation levels of the ferromagnetic core is biased causing the saturation current to be asymmetrical. The output winding is compared to the input drive current and the asymmetry is directly proportional to the external magnetic field.

Figure 32 shows an example fluxgate sensor topology as developed by The Imperial College Cassini Magnetometer Group [35]. The oscillator generates the drive current that will drive the magnetic core around its hysteresis loop. The output from the pickup windings and the drive signal are fed in to a demodulator to perform phase sensitive discrimination followed by an integrator to recover a DC only signal as a function of

applied field. Additional gain and calibration stages are also shown to give a multi-range calibrated sensor.

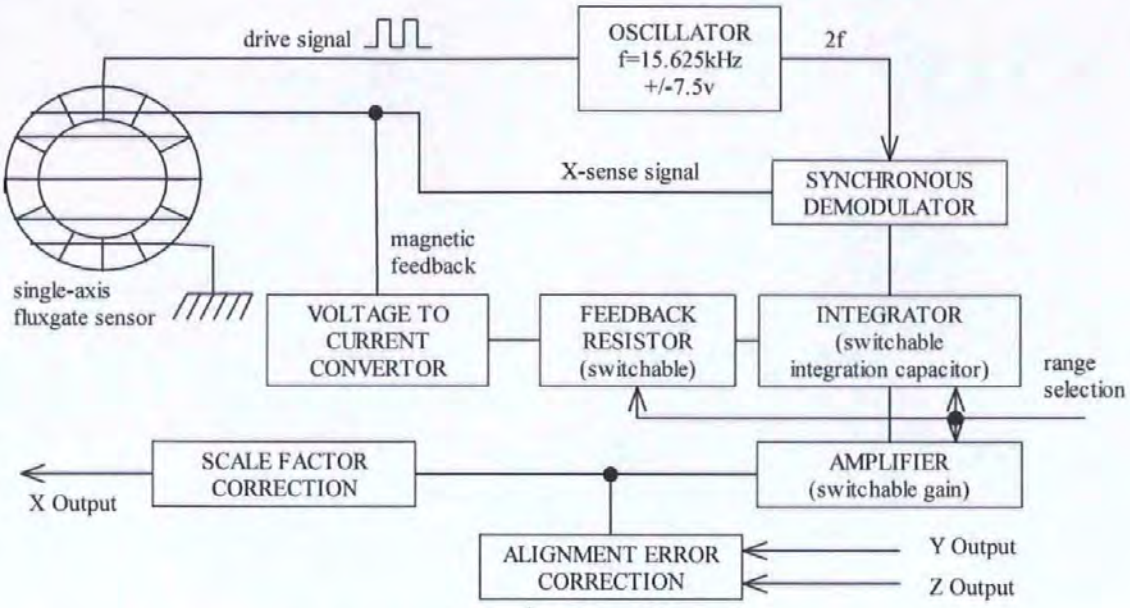


*Figure 32 - Example fluxgate topology, as developed by The Imperial College Cassini Magnetometer Group [35].*

By using materials with low coercivity and a "square" hysteresis curve, that is materials that have a high, and almost linear d**J**/dt from negative saturation to positive saturation, then high sensitivity systems can be achieved. Due to the reliance of a magnetic material for magnetic field sensing this imposes serious limitations on the maximum applied field that a flux gate device can measure.

### *6.1.4 Magneto-resistance and impedance devices*

The most basic magneto-resistance device is the anisotropic magneto-resistive (AMR). The devices are made of a nickel-iron alloy (Permalloy), which is deposited on a substrate as a thin film and patterned as a resistive strip. Typically four of these devices will be configured in a Wheatstone bridge arrangement and this will allow measurement of both field magnitude and direction along a single axis. Magneto-resistive devices have a high measurement bandwidth, typically in the 10 Mhz range.

Other forms of magneto-resistive devices exist such as Giant Magneto-Resistance (GMR) where a multi-layer system of ferromagnetic alloys and non-magnetic materials are used to increase the sensitivity of GMR by 70 % compared to AMR devices. The primary uses of these types of sensors are as read heads in hard disk drives, due to their small size and high sensitivity. Magneto-resistance devices have one major limitation, they are unipolar and therefore the resistance of the device is related to the magnitude of the applied field and not its direction.

Other forms of magneto-impedance (MI) devices utilise AC signals and measure the impedance change of the material to determine applied magnetic flux density. AC magneto-impedance devices are also extremely sensitive but suffer from the same limitations as AMR and GMR in the context of Pulsed Field Magnetometry.

### *6.1.5 Comparison of devices*

Magnetic field detection devices have various advantages and disadvantages that affect their suitability for use in a Pulsed Field Magnetometer system. Table 8 shows the key factors that determine the usefulness of a particular sensor and Figure 33 shows the designed operating flux density of the sensors. Point measurement is considered a disadvantage as during the determination of the magnetisation it is necessary to measure the entire sample and not just a specific region. The limitations on bandwidth of the search coil should not impose a problem as the applied frequencies are in the 10s to 100s of Hertz region. The search coil has the widest dynamic range and has an operating range that is closer matched to the flux densities encountered in Pulsed Field Magnetometry than any other sensor. The fluxgate sensor is not suitable because the bias magnet required limits the maximum applied field. The Hall effect sensor and AMR type sensors while not specifically useful as the main measurement sensor could be employed as local point source measurements for the evaluation of local effects in magnets under pulsed fields and

utilised for further work. Because of the reasons discussed, the search coil is considered the most suitable magnetic field detector for PFM systems, for both the magnetisation (**J**) and the applied field (**H**).

| | **Advantages** | **Disadvantages** |
|---|---|---|
| **Search coil** | Dynamic range limited only by external electronics | Bandwidth limitations due to inductance of coil |
| **Hall Effect** | | Point measurement<br>Eddy currents<br>Calibration issues at high field |
| **Fluxgate** | Good low field performance | Large physical size<br>Based on biasing a sensor magnet (risk of sensor damage/ limit on applied field)<br>Point measurement<br>Limited bandwidth |
| **AMR**<br>**GMR**<br>**MI** | Good low field performance<br>Good bandwidth | Unipolar<br>Point measurement |

*Table 8 - Comparison of magnetic sensor types considered as sensors for Pulsed Field Magnetometry.*

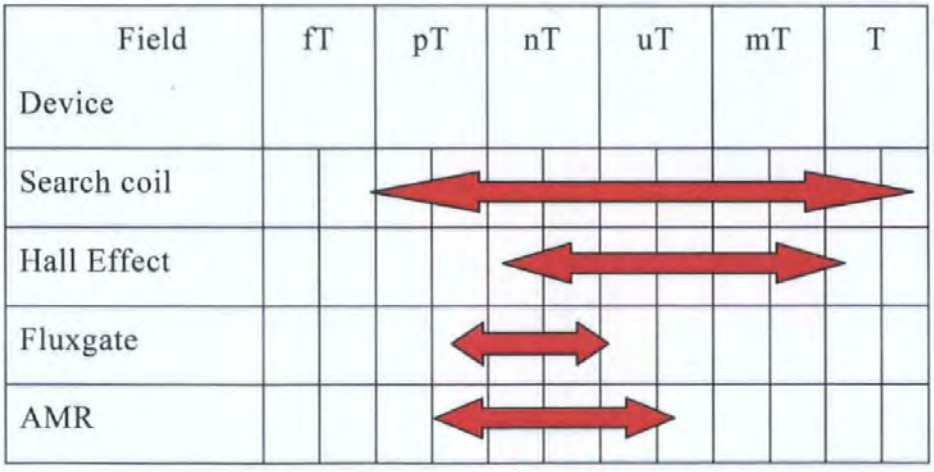


*Figure 33 - Magnetic sensors and their magnetic field detection range based on typical commercially available sensors.*

## 6.2 The magnetisation sensor

The magnetisation sensor, when realised as a search coil, consists of two (or more) coils connected in series opposition forming a gradient coil. The coils have an equal area turns product but different coupling to the test specimen and so measure only a proportion of magnetisation of the test specimen and none of the applied magnetic field.

Two identical air cored coils that are connected in electrical opposition, in a field generator that can produce a homogenous magnetic field, should produce no output for a time dependent applied field. If the magnetic sample to be tested is introduced into only one of the coils, and the time dependent field is applied, the output will be proportional to the magnetisation of the sample. Ideally, the homogeneity of the pick-up coil's response should be uniform over the maximum expected test volume. This minimises position sensitivity and reduces the possibility of error due to sample position and also allows the comparison of unlike shapes.

There are a number of possible methods to create a J pickup coil. The most common methods are the linear gradient and the radial gradient arrangements. These are now discussed in detail.

### *6.2.1 Linear gradient pickup coils*

Figure 34 shows a typical arrangement of a linear gradient pickup coil. This arrangement requires two coils that are connected in series but in anti-phase so that in a dynamic homogenous field, with no magnet present, the sum of the emf induced in both coils is zero. If a magnet is introduced into only one coil, then this coil will have a high degree of coupling to the magnet, the 2nd coil will have a lower coupling to the magnet and therefore

a net emf output is produced from the two coils. The output in this situation is directly proportional to the magnetisation of the magnet.

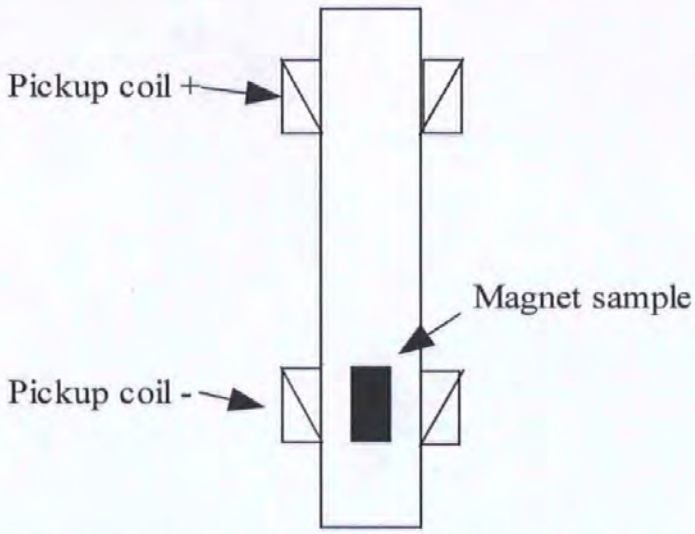


*Figure 34 - Linear gradient pickup coil arrangement. Two identical coils are connected in series opposition.*

The requirements for a linear gradient system are that the two coils produce the same emf. when no magnet is present. A typical method to achieve this is to use two coils of equal area turns, with the two coils spaced evenly with respect to the magnetic centre of the field generation coil. If the sample was positioned at the magnetic centre of the field generation coil then the 2$^{nd}$ coil would likely be in a region of lower applied field and its area turn product would need to be adjusted accordingly to ensure the two coils have equal emf. output for no sample.

While it is easy to control the number of turns forming a coil, controlling the area is more difficult. The simplest solution for this problem is to use the non-homogeneity of the applied field generator along its central axis. The field will be at a peak at the geometric centre and will decrease along the central axis with distance away from the centre point. By positioning the linear gradient coils symmetrically about the geometric centre and allowing a very fine axial movement it is possible to cause one coil to see a slightly higher

field than the other. By adjusting the vertical position of the coils it is possible to cancel out any effect of area differences between the two coils.

The linear gradient coil has a highly non-homogenous pickup and is extremely position sensitive. This makes calibration of linear gradient coil systems difficult as a calibration specimen of the same shape and size of each sample is required. This often means limiting the shape and size of the samples to simple cylinders. While this may be suitable for some quality control laboratories it defeats some of the "non-destructive" aim of industrial Pulsed Field Magnetometry.

Linear gradient coils can be made to be extremely sensitive as it is straightforward to add more turns to each coil, with each additional turn increasing the sensitivity. While it is also possible to adjust the area of the coils to increase sensitivity, this is usually not possible due to the physical constraints of the clear bore diameter of the field generation coil that will surround the pickup coil.

### *6.2.2 Radial gradient pickup coils*

The radial gradient coil, is more complex than the linear gradient design and features two concentric coils. As with the linear gradient coil pair, the inner and outer coils require the same turns area product and to be connected in anti phase series to produce a net emf of zero when located in a dynamic yet homogenous applied field with no magnet sample present. If a magnet sample is inserted inside the pickup system then the coupling from the magnet to each coil is different, thus generating a net emf that is proportional to the sample's magnetisation (J) only.

Figure 35 shows a typical radial gradient coil with the inner longer than the outer, caused by the necessity to balance the area-turns product of the inner and the outer coil. The outer

coil has a greater area and hence requires fewer turns than the inner coil. One problem with radial gradient coils is the exact compensation, as it is not possible to change the number of turns to anything but an integer and once the coil is constructed, changing the area becomes very difficult. Methods exist for the compensation of radial gradient coils and these are discussed in section 6.3.

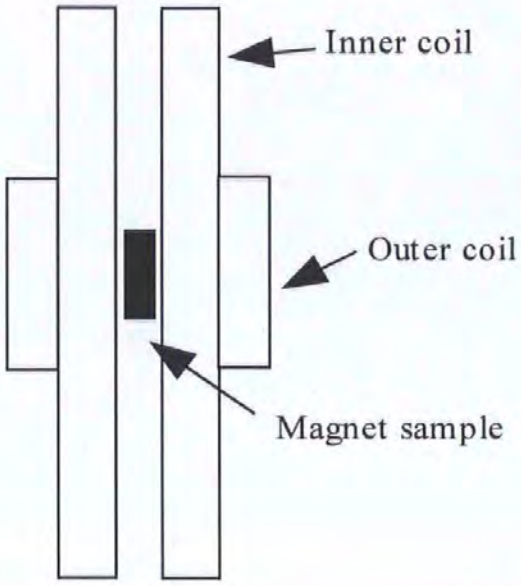


*Figure 35 - Radial gradient pickup coil. Two concentric coils with equal turns-area product are connected in series opposition.*

Despite the apparent lack of advantages of the radial coil over the linear arrangement and in fact a disadvantage due to compensation difficulties, this section proceeds with its analysis of the concentric type of coil. It is during this further analysis and refinement of the concentric coil that its advantages become apparent.

## 6.3 Compensation of radial gradient coils

With radial gradient pickup coils it is more of a challenge to achieve perfect turns/area matching of the inner and outer coils. As the number of turns can only be an integer and the area is dependent on tolerances of the winding surface, a small mismatch always occurs. A number of methods exist for the exact compensation of the J coil, these are known as:-

- Split turn method
- External turn
- Variable turn.

The split turn method was the first attempt to overcome the compensation problems of the concentric gradient pickup system, designed by Dr Letillieur of CNRS laboratories. A series of pins were placed on the inner and outer coils and the inner and outer coil rotated relative to each other and then a link placed between the inner and the outer coil. This provided additional resolution, smaller that one turn, to aid compensation. The CNRS coil was also designed to minimise the capacitive coupling between the inner and outer layers by control of the winding placement.

In practice the split turn method was not successful and compensation proved very difficult. Once the best compensation was achieved the resultant signal contained harmonics due to the coil not rejecting broadband far field interference. This attempt at a radial coil design was abandoned and other approaches investigated.

The external turn method used an additional coil connected in series with the main coil pair. The additional coil is placed in a homogenous region of the field generator, away from the magnet sample and rotated off-axis. The off-axis rotation will cause only the on-axis vector to be detected. The coil's output will be at a maximum when the coil is at 90 degrees to the applied field. If the coil is rotated, then as its alignment becomes perpendicular with respect to the applied field, its output will tend to zero. If the coil is rotated further, its output will increase but with the opposite polarity to its original position. When the coil is exactly 180 degrees from its starting position, its output will be at a maximum but with an inverted sense. The exact angle can be set to provide optimum compensation. This method is successful, and providing the (main) radial coil can be

constructed with a compensation error less than one turn, then this is a viable method of compensation. The extra compensation winding takes up extra physical space which is at a premium inside the field generation coils and so was ruled out due to this constraint.

With the failure of the split turn method and the external turn method considered impractical a new method was conceived to overcome the limitations of the previous two methods. By ensuring that the turns area ratio error between the inner and the outer is less than one turn, an extra turn can be added to the outer coil. By introducing a potentiometer to attenuate this extra turn, the potentiometer can be set exactly to allow the correct proportion of the extra turn to cancel out the error on the inner coil, providing optimum compensation. Figure 36 shows a schematic of the variable turn method. The potentiometer is located in a box external to the pickup coil to ensure that the applied magnetic field does not induce unwanted currents within the potentiometer. All the interconnection wires are tightly twisted to minimise any unwanted pickup. This method has proved successful in production, and compensation is a straightforward process of making a measurement of sample magnetisation and then noting the magnitude of the zero-signal, before then adjusting the potentiometer until a minimum is achieved.

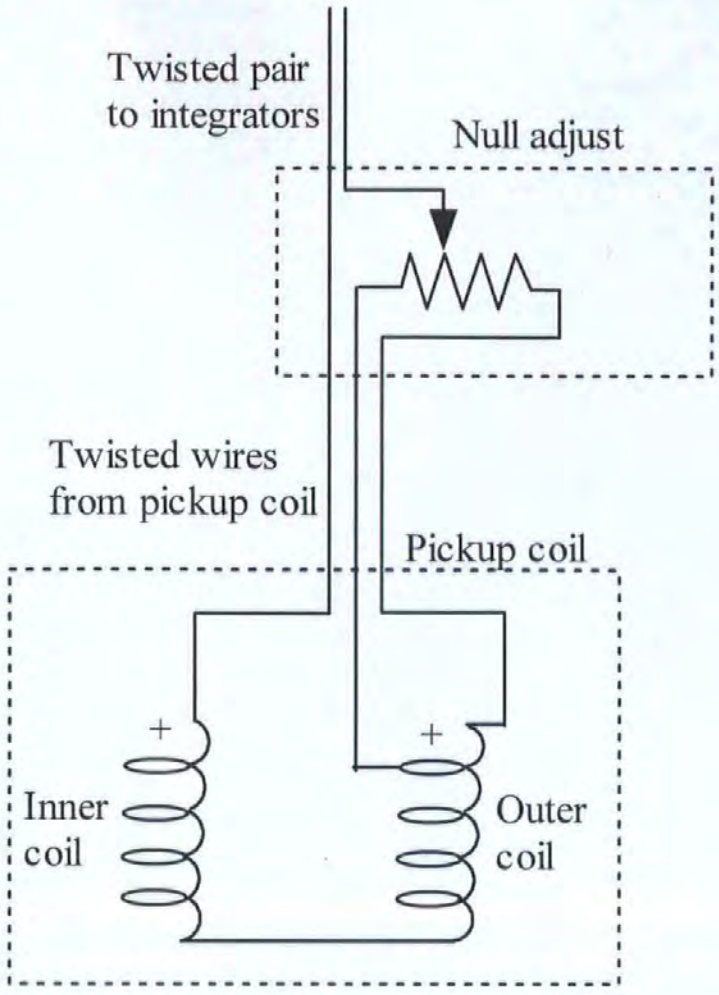


*Figure 36 - Schematic of variable turn method of compensating radial gradient coils. The output of an auxiliary turn is attenuated using a potentiometer to achieve equal output of the inner and outer coils.*

## 6.4 Zero signals

With a perfectly compensated J coil system, it is observed that a measurement with no magnet will produce a signal from the J instrumentation. This signal is proportional to the magnitude of the applied field but is phase retarded by 90 degrees. Figure 37 shows (in blue) a typical zero signal for a well compensated system. If the compensation is not perfect then an additional component is superimposed on the zero signal which is directly proportional to the applied field. The red and green waveforms in Figure 37 are from the same pickup coil as the blue waveform but the pickup coil's compensation is not optimal and the J pickup coil is detecting a proportion of the applied field.

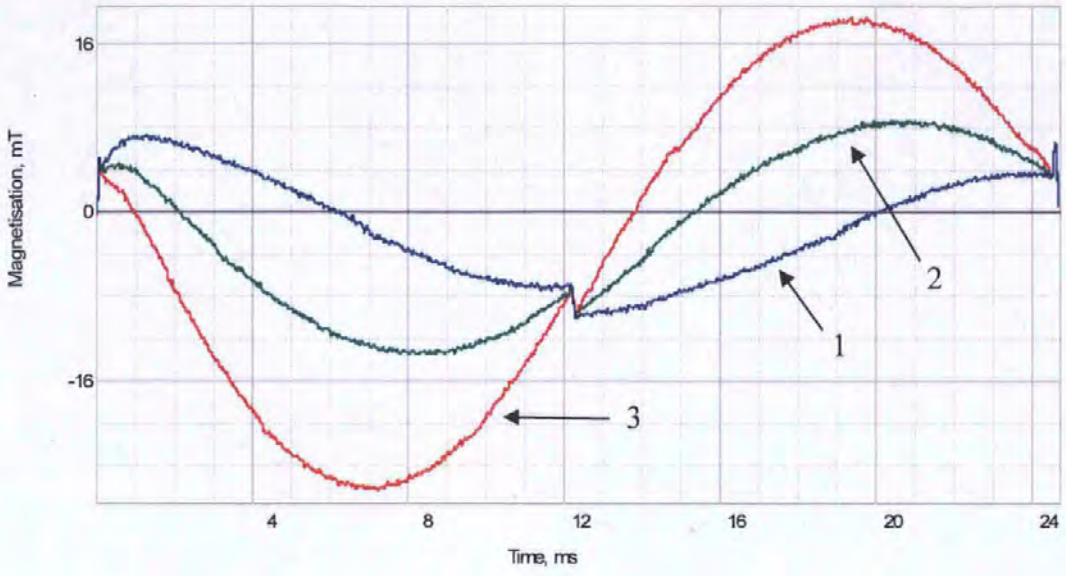


*Figure 37 - Zero signal measurement. The blue (1) waveform represents the zero signal from an optimally compensated pickup coil, compensated using the variable turn method. The green (2) and red (3) waveforms represent non-optimal compensation of the pickup coil.*

The exact source of the zero signals has been debated for some time. It was believed that it was eddy currents within the conductors of the field generation coil causing the effect. To prove this hypothesis a finite element model of a field generation coil was created and a harmonic simulation implemented. The model assumed axial symmetry that neglects the "skew" of the wires used to form the field generation coil. Figure 38 shows the finite element model used to assess zero signals in field generation coils. A representative current and frequency were assumed and the eddy currents assessed by looking at the imaginary domain of the resultant flux density. A field generation coil with an inside diameter of 30 mm was modelled. The coil was constructed from 5 mm x 3 mm square section wire and had 9 layers and 18 turns per layer. A gap of 0.2 mm was left between each conductor block to allow for the enamel that is used to insulate this type of wire. In the model each conductor was assumed to be carrying a harmonic current of 8000 A at 100 Hz. This is an approximation of a PFM system during discharge, but does not include the damping effect due to real resistive losses. The copper conductors are modelled with a conductivity of 58

MS/m (pure copper). It was not possible to couple the conductor blocks to behave as a complete circuit due to the limitations of the FEA package available. This limitation would cause the eddy currents to lack constraint and the sum of the eddy currents would not be zero in all paths. This would add some error to the results, so it should be noted that this is a first order model of the effects of eddy currents. Figure 39 shows results of the finite element harmonic assessment and it is clear that a significant effect exists in the region of the sample and the pickup coils. While the magnetic field magnitude of the eddy current effect is small compared to the applied field magnitude, the effect is "near field" and will not be completely rejected by the gradient coils thus generating a zero signal. If the same model is repeated and the conductivity of the copper reduced the effect tends to zero as conductivity tends to zero, thus proving this to be an effect related to self generated eddy currents in field generation coil.

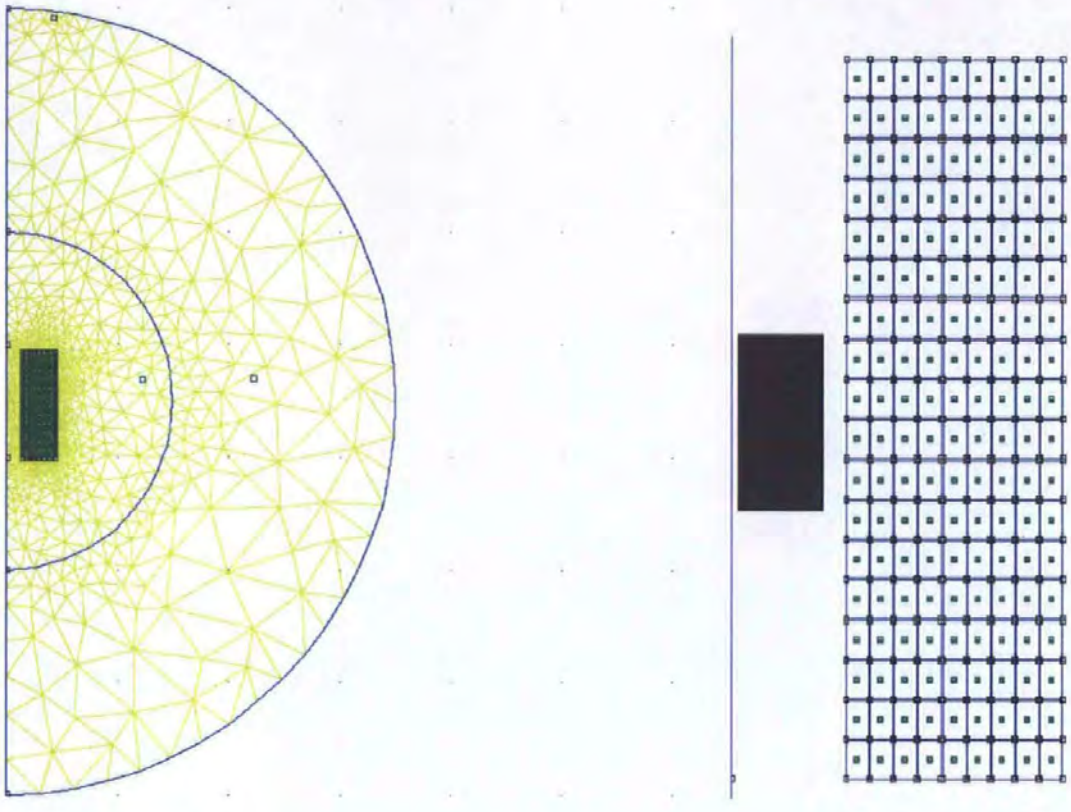

*Figure 38 - Finite element model of field generation coil, each conductor is represented individually as a 5 mm x 3 mm cross section wire. A total of 8 layers and 18 turns per layer were modelled to closely match the industrial PFM coils that were implemented. The right hand image shows the entire model and the left hand image shows a magnification of the conductors. The current was assumed to be 8000 A at 100 Hz, similar to actual PFM conditions.*

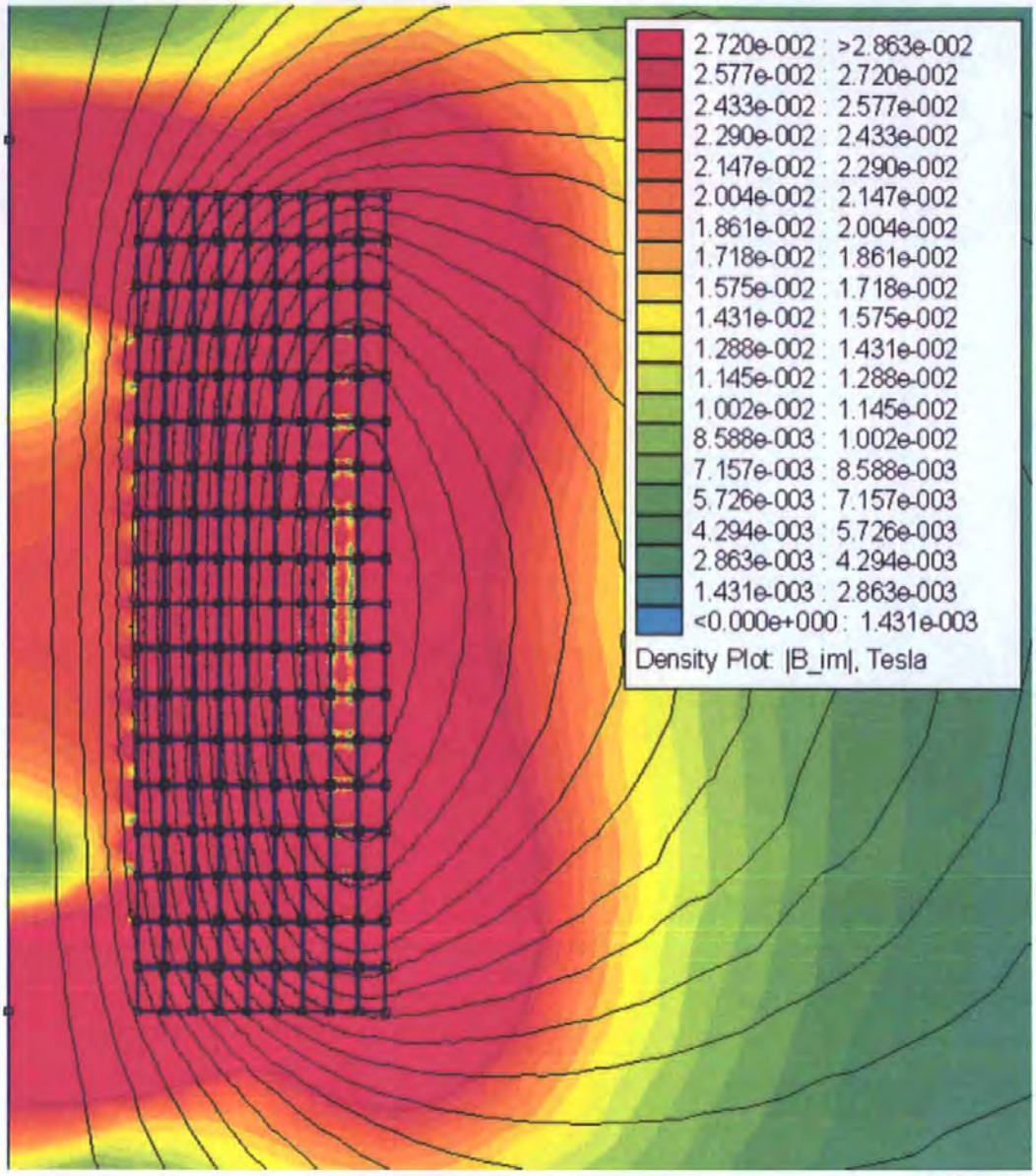


*Figure 39 - Plot of imaginary (out of phase) flux density in region of field generation coil. It is clear that a significant effect exists in the region of the sample that would not appear as a far field effect and hence would not be rejected by the gradient coil.*

In order to determine if this effect is the zero signal, a representative pickup coil was modelled inside the field generation coil to assess the magnitude of the effect. A radial gradient coil was considered with winding diameters of 20 mm and 23.8 mm. The inner coil was modelled with 98 turns and the outer coil 69 turns. The area turns product for the inner and outer coils was equal and hence no signal should be detected in a homogenous applied field. The flux linkage to the inner and outer coils was considered and the difference between the two flux linkages was taken to be the magnitude of any detected signal. Table 9 shows the results of the simulation.

| | Real component of flux (Volt seconds) | Imaginary component of flux (Volt seconds) |
|---|---|---|
| **Inner coil** | -0.40 | 0.0013938 |
| **Outer coil** | -0.40 | 0.0014173 |
| **Difference** | 0 | 0.0000235 |

*Table 9 - Flux linkage and resultant output of simulated pickup coil.*

It can be seen from Table 9 that in the imaginary domain the difference between the inner and outer coils is 23.5 μVs, this is the resultant signal from the radial gradient coil due to eddy current effects within the field generation coil. If the signal is assumed to be purely sinusoidal then it is possible to estimate the output of the integrator that would be connected to the pickup coil and calculate the magnitude of the zero signal.

It is typical to use integrators in a PFM system with effective gains between 100 and 100,000. If a gain of 5000 is considered (A typical value for the J channel) this would produce a sinusoidal voltage after the integrators of approximately 120 mV. With a dynamic range of +/- 12V and an analogue to digital resolution of 14 bits, this equates to a signal with a magnitude of 80 A/D counts. This zero signal is lower than many typical zero signals measured on the PFM system but it is not unreasonable. Typical zero signals may be 2 to 4 times larger. This could be a result of the lack of higher order effects and circuit coupling in the eddy current model but the model does indicate that the origin of the zero signal is indeed eddy current with in the copper of the field generator's conductors.

In order to reduce the zero signal alternative types of conductor were considered for the field generation coil. One such conductor was Litz wire, this is a multi-stranded individually insulated wire that is typically used for RF applications where the high frequency nature of the application suffers from eddy current problems. By forming the

conductor out of many smaller conductors the cross sectional area available to eddy currents is significantly reduced. A prototype field generation coil was wound using Litz wire and initial trials were undertaken to assess any potential benefit. The coil was constructed in a normal fashion with the conductor securely held in place with a combination of potting, resin and fibreglass. The initial results from the Litz wire tests were not promising. The resultant zero signal was reduced in magnitude but it was not repeatable. It was concluded that the individual strands of the Litz Wire were moving with respect to each other and despite securing the Litz wire as a whole the individual strands were free to move. As the magnitude of the zero signal with the Litz wire was still significant, an unrepeatable signal was unacceptable as it could not be removed by processing. Litz wire was considered inappropriate for pulsed field generation coils unless the individual strands could be secured. No further testing was carried out with Litz wire.

During the testing of the radial gradient coil arrangement it was discovered that the zero signal was not repeatable and would vary depending on the usage of the system. If the system was left for a period it was found that the zero signal magnitude would return to the original position and repeated measurements would cause the same error pattern. Figure 40 shows this change over 11 measurements on a PFM12 system. The change represents a significant error even over a couple of measurements and makes the zero correction procedure much harder, as the zero signal will be different from the sample measurement to the zero measurement.

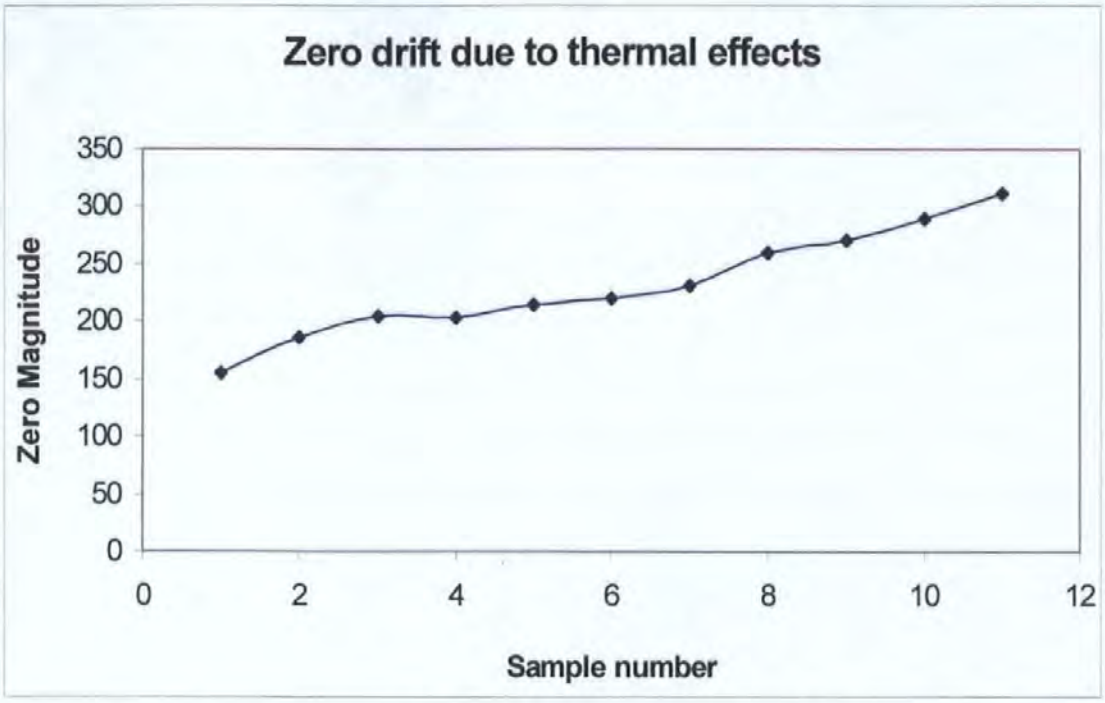


*Figure 40 - Zero signal magnitude change with repeated measurements.*

This result was attributed to the extreme sensitivity of the radial gradient coil to changes in area. As a typical measurement pulse could raise the field generation coil by as much as 4.8 K after a number of pulses a thermal gradient develops across the field generation coil. The pickup coil is physically coupled to the field generation coil therefore thermal effects of the field generation coil ensures that the pickup coil heats up. The inner of the pickup coil is exposed to ambient temperature while the outer is heated by the field generation coil acting as a heat source, generating a thermal gradient across the pickup coil. The temperature of the pickup coil would cause a very small thermal expansion of the pickup coil former causing the outer coil area to increase. The inner coil area would also increase, but due to the thermal gradient, only by a fraction of the outer coil. This expansion caused an imbalance in the area turns product of the inner to outer pickup coil and caused the zero signal phase and magnitude to change. Figure 41 shows a simplified cross-section of the field generation and pickup coils that demonstrate the paths heat flow can take.

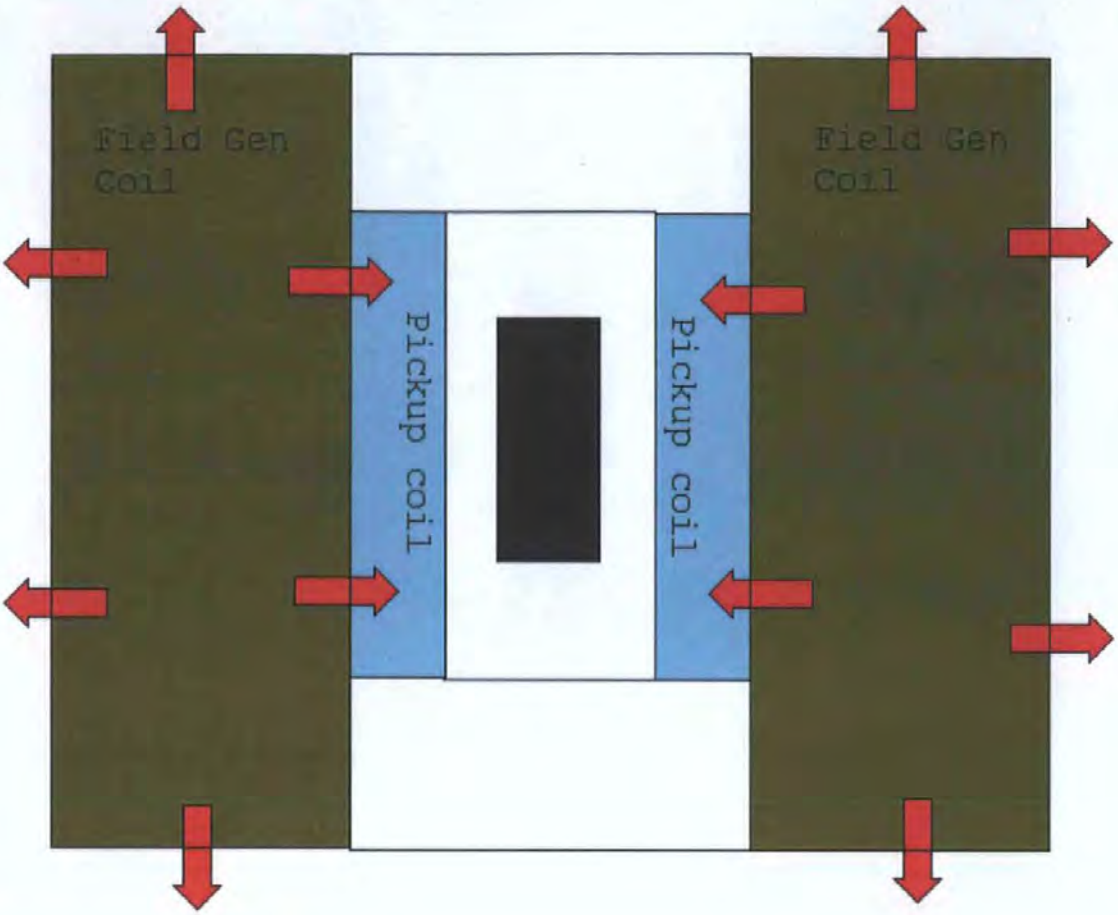


*Figure 41 - Simplified cross section of field generation coil and pickup coil demonstrating thermal heating problem. Heat from the applied field coil will cause a temperature gradient across the pickup coil.*

The solution to the problem of pickup coil thermal effects is to thermally de-couple the pickup coil from the magnetisation coil. A possible implementation would be to use a thermal control system to maintain the pickup coil windings at constant temperature. An implementation of this is presented in Section 9.3.

An additional solution to the thermal expansion problem would be to use alternative materials in the construction of the pickup coil in order to select materials that have a lower thermal expansion coefficient. Table 10 show the coefficient of thermal expansion for the materials used to construct the pickup coil. The pickup coil is formed from glass fibre and

epoxy resin with copper windings forming the coil. Alternative, non-magnetic wire such as titanium could be substituted for the copper. Titanium has a linear expansion coefficient of 11.9 cm/cm/°C × $10^{-6}$. The most likely dominant source of the expansion with in the pickup coil is the epoxy resin, the resin has the highest thermal expansion coefficient of all the materials used. The ideal solution would be to utilise a pickup coil former with a lower thermal expansion coefficient such as a ceramic based material and to use a material for the wire with a lower thermal expansion coefficient such as titanium.

| **Material** | **Coefficient of linear thermal expansion cm/cm/°C x $10^{-6}$** |
|---|---|
| Copper | 17 |
| Glass | 8.5 |
| Epoxy resin | 30 - 100 |

*Table 10 - Coefficient of thermal expansion of materials used for the construction of the pickup coil.*

## 6.5 Position sensitivity

To ensure acceptability of the Pulsed Field Magnetometry method it is important that measurements of sample magnetisation are repeatable. One of the largest factors effecting repeatability is sample position with respect to the pickup coil. It is not always possible or convenient to ensure that samples are located exactly in the sample place for consecutive measurements, especially in an industrial environment where such systems will be deployed. A mechanical handling system will be responsible for the insertion of samples into the measurement coils and absolute position cannot be guaranteed, samples could be displaced by +/- 5 mm from the centre position. For this reason it is highly desirable to minimise the pickup coil's dependence on sample position. As no system can achieve perfect results, it was decided to allow a variation on pickup coil output of up to +/- 1 %

due to position dependence. This is a very tight tolerance for pickup coils but it was considered essential to the success of Pulse Field Magnetometers in an industrial environment.

The concentric pickup coil, implemented in the industrial PFM system, was designed to minimise position sensitivity, so that absolute magnet position deviations would not cause any significant errors to the measurement process. If the pickup coil is considered to be a magnetic field source and modelled as such using the Biot-Savat law, it is possible to calculate for any given pickup coil geometry the coupling between the pickup coil and a given point in space. If the coupling factors are assessed over the volume of interest then the relationship between position and pickup coil output can be determined. As a radial gradient coil is being considered, it is necessary to calculate the coupling factors for both the inner and outer pickup coils and to then subtract these factors to produce an overall factor for the gradient coil. It is important that the radial gradient coil rejects the applied magnetic field, which is considered homogenous. Therefore it is necessary to ensure that the turns area product of the inner and outer coils are equal so that cancellation will occur.

A computer model was developed to design the optimum pickup coil for minimising position sensitivity. The model was based on a Biot-Savat approach and worked by assuming the pickup coil was a magnetic source. Each turn of the pickup coil could have its position independently specified so as to allow the arbitrary placement of windings. The coupling from each turn to a position of interest was considered and by summing the coupling for all the turns, the coupling from a given point to the pickup coil was determined. This approach was repeated for a 2D grid of points that covered the entire area of interest. This area was set to be the maximum sample volume. It was assumed that rotational symmetry existed along the central axis of the pickup coil so a full 3D solution was not required. Multi filaments were not considered for the pickup coil as it is typical to

create pickup coils from wire with a small diameter so the distributed current effect should be insignificant in this case.

By assuming various positions for the pickup coil windings and assuming a nominal current flow through the pickup coil, the coupling factor was determined for the inner and outer coils. The actual pickup of the radial gradient coil is the difference between the inner and outer coupling factors.

Figure 42 shows two coils, coil A is a traditional radial gradient coil and coil B has been improved for homogenous pickup. With the traditional design of radial gradient coil the length of the outer is controlled by the required number of turns for area-turns balancing with the inner and the diameter of the wire used.

Figures 43 show the results of the model for pickup coil A. The Y-axis represents distance across the pickup coil's diameter and therefore has radial symmetry. The X-axis represents the central axis of the pickup coil. The region modelled is a 30 mm by 30 mm area that represents possible locations for samples. It can be seen that with a traditional design of radial gradient coil the homogenous region (shown by the hatch shading) covers an area of approximately 10 mm by 10 mm in the centre of the coil. Along the X axis the homogeneity reaches a worst case of -14 % with in the 30 mm x 30 mm sample region.

Figure 44 shows the results of the model for pickup coil B. The region modelled is the same as Figures 43 with a 30 mm x 30 mm area tested for homogeneous pickup. It can be seen that the results from coil B show significant improvement over coil A. The entire 30 mm x 30 mm region is all within 1% homogeneity. The worst case is -0.8 % in the corners of the sample region.

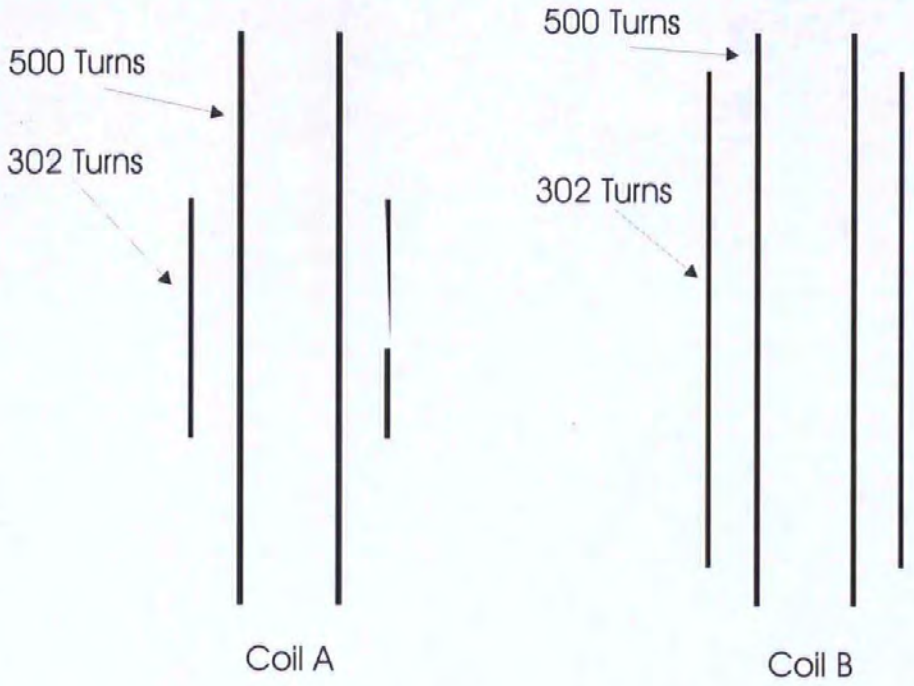


*Figure 42 - Two radial gradient coils. Coil A is a traditional design and coil B has been modified for improved position sensitivity. Both coils have the inner windings at 35 mm diameter and the outer windings at 45 mm diameter. The inner in both cases is 60 mm long. Coil A has an outer of approximately 36 mm long and coil B has an outer of 52 mm long.*

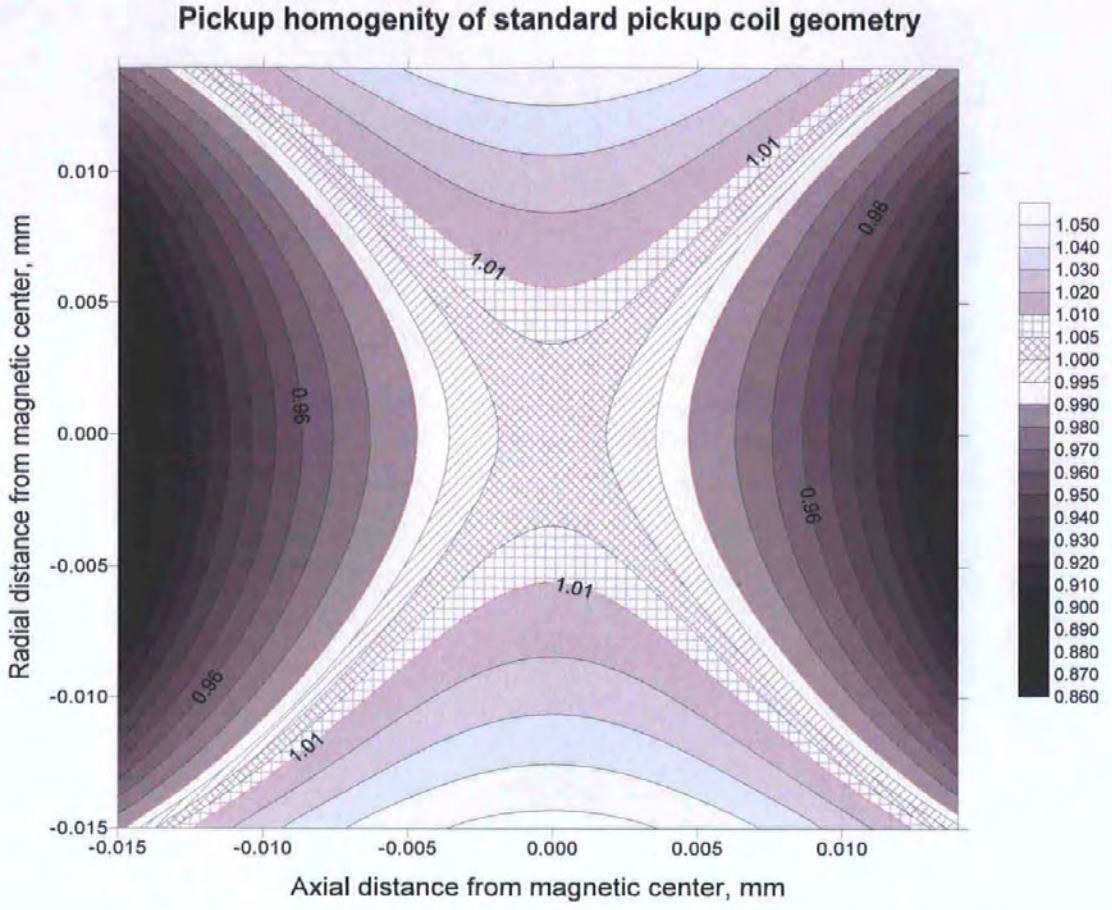


*Figure 43 – Positional sensitivity of a radial gradient coil constructed in a traditional manor with the outer greatly shorter than the inner. The hatched regions show the area of 1% homogeneity.*

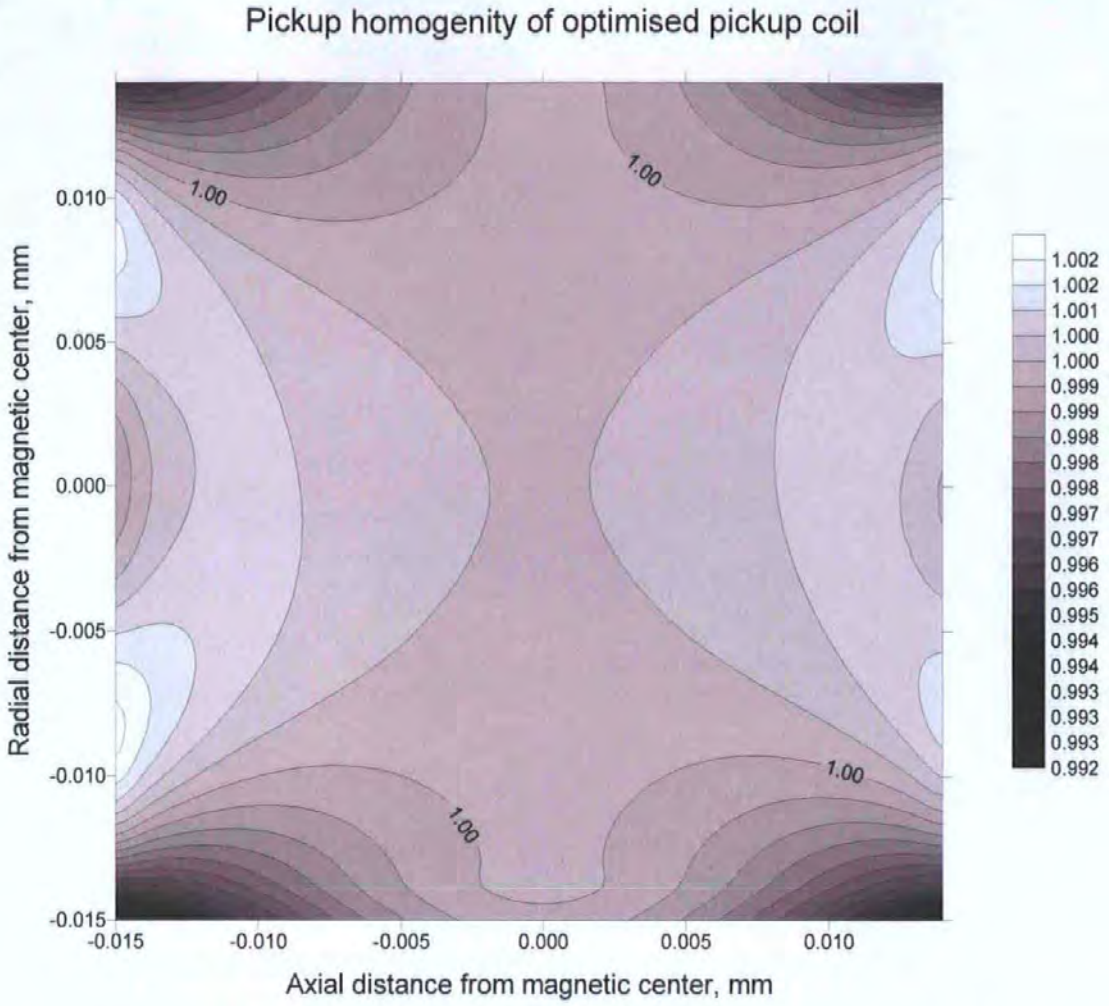


*Figure 44 – Positional sensitivity of a radial gradient coil constructed with the length of the outer optimised. The entire area is better than 1% homogeneity.*

The results from Figures 43 and 44 show that a significant improvement can be made to radial gradient coils by optimising the pickup of the inner and outer coils so as when then interact as a gradient coil the overall positional sensitivity is minimised. The overall aim in reducing the position sensitivity is to match the homogeneity of pickup of the inner and outer coils. If the inner and outer coils have a similar homogeneity profile then the differential homogeneity will be more uniform. The results presented here demonstrate that conventional gradient coils, with careful design, can be given a large homogenous pickup region with out simply increasing the dimensions of the coil.

## 6.6 Magnetic field sensors conclusions

Due to the reasons discussed in Section 6.1.5, pickup coils are the most suitable magnetic sensors for both the magnetisation and the applied field detection for pulsed field type applications where the field can be as high as 20 Tesla. Of the two types of gradient coil considered for the magnetisation sensor, the radial coil is considered the best choice for industrial applications. The lack of sensitivity to position that can be designed in to a radial gradient coil of this type is a large advantage for both industrial and "real world" applications and this advantage outweighs the small extra complication of the nulling procedure involving an external potentiometer.

Temperature dependence provides an additional complication for the radial coil arrangement and the solution to this is to prevent the pickup coil from changing temperature. A practical solution to this is demonstrated in Section 9.3 where an oil cooling solution is presented.

As discussed in Section 6.1.2, pickup coils require dedicated measurement electronics that are selected to work with the pickup coil to produce the best dynamic range and resolution at the required field levels. Details of the measurement electronics are now discussed in detail.

## 6.7 Transient instrumentation, integration and digitising hardware

The outputs of the pickup coils are the derivatives of magnetic flux with respect to time. For the applied field pick-up coil, the coil's output voltage, $V_H$ is proportional to,

$$V_H \propto -\frac{dH}{dt} \tag{6.8}$$

where $H$ is the applied magnetic field. The magnetisation pickup coil's output voltage, $V_J$, is proportional to,

$$V_J \propto -\frac{dJ}{dt} \qquad (6.9)$$

where $J$ is the samples magnetic magnetisation. As $V_J$ and $V_H$ are time dependent signals, because they are derivatives of the wanted signal, it is necessary to remove the dependence on time to recover just the components of interest. This can be achieved with integration. Two approaches may be used, analogue or digital.

Analogue integration uses a capacitor to act as the integration device, this is usually achieved with an operation amplifier. A classical circuit is shown in Figure 45. The disadvantage of analogue integrators is that they suffer from drift, that is unwanted noise signals will also be "integrated". The noise signal can cause the capacitor to build up a charge, this charge will increase until the capacitors voltage is equal to the supply rails. Drift can be compensated for by applying a DC offset voltage to the input of the integrator to compensate for the noise. The noise is often thermal related and will change with ambient temperature so it is necessary to update the drift offset frequently. The drift compensation process is automated by the control software on the PC. By sampling from the integrator for a period of time, the drift rate can be determined by measuring the slope of the captured data. By changing the DC offset by an amount proportional to the drift rate, the optimal drift compensation can be determined and applied to the integrator.

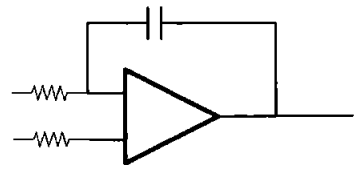

*Figure 45 - Analogue integrator schematic. An analogue integrator is simply an op-amp with a feedback capacitor that accumulates charge, performing the summing or integration of input signals.*

Analogue integration does have some major advantages; with appropriate design the integrator can handle large transient voltages of hundreds of Volts and still successfully

integrate, providing the transient doesn't exceed the maximum Volt-second product of the integrator. An analogue integrator can cope with very fast events and these will still be successfully integrated. After the analogue integrator an analogue to digital (A/D) converter is used to capture the data for further processing and analysis in software.

Digital integrators use an A/D converter to measure the "differential" signal and then software will sum every reading taken from the A/D to provide integration. Digital integrators do not have the same problem of drift as analogue integrators. Although drift will appear during the summation process it is very easy to remove and there is no real danger of saturation, as with a capacitor, as it is possible to use numbers with as much precision as required. Digital integration requires a small overhead in data processing time, but compared to other processing in a PFM system this is considered insignificant.

Digital integrators suffer from a number of disadvantages. It is necessary to operate the A/D converter at a greater rate than with analogue integrator to ensure that all high frequency transients are captured with sufficient resolution to enable good integration. The dynamic range of a digital integrator can be lower than an analogue integrator and it requires a high resolution A/D to ensure that the quantisation level does not exclude low level events from the integration. There is also a limited input range to the A/D of a digital integrator so external protection and attenuation circuitry may be required.

Both analogue and digital integrators have been successfully used for the integration of the signal from pickup coil systems. Providing their limitations are known and understood either can be designed into a system successfully.

After the signal has been detected by the sensors and processed and captured by the measurement electronics it is then possible to apply "offline" processing to the data to

correct for errors, apply calibration factors and to determine the characteristics of the material measured. The details of signal processing are discussed in detail in the next chapter.

# Chapter 7 Signal processing

Signal processing is a critical part of Pulsed Field Magnetometry and utilised to eliminate, or reduce to insignificant levels, errors attributed to PFM. In order to convert the data from the "raw measurement", into a calibrated accurate representation of the magnet's characteristics, it is necessary to process the data to account for; zero signal correction, loop positioning, self demagnetisation factor correction, filtering and the correction of eddy current effects. These are now considered in detail.

## 7.1 Zero signal

As discussed in Section 6.4, a PFM system that performs a measurement without a test specimen, will observe a signal. For a well designed and constructed system, this signal should be small compared to the magnitude of samples to be measured, but if not compensated for could still cause measurement errors. This signal should also be reproducible. This signal is generally known as the "zero signal." and is caused by the effects of eddy currents in any conductive material in the region of the applied magnetising field. Conductive material includes the copper wire forming the field generation coil, which, due to its physical location, produces an eddy current closely coupled to the pickup coil system that is not rejected by the gradient coil used for magnetisation detection.

The magnitude of the zero signal can be expected to change in magnitude for different applied fields, but the shape of the zero signal should remain constant. On early PFM systems the shape was observed to vary. In a well compensated PFM system the magnetisation gradient coil should reject the applied field and produce an output proportional to, only, the magnetisation of the sample being characterised. If compensation is not perfect, a proportion of the applied field signal will couple with the magnetisation signal. This parasitic applied field signal will add to the zero signal producing a signal that

does not have constant shape with respect to the applied field. It has also been discussed in Section 6.4 that the compensation of the magnetisation gradient coil can be effected by factors such as local heating effects. Having a zero signal that is applied field or time dependent makes a correction procedure very difficult, it is therefore recommended to take steps to minimise factors that can effect the magnetisation gradient coil compensation, as discussed in Section 6.3

To remove the effects of the zero signal, it is necessary to subtract a valid zero signal from the data. The amplitude of the zero signal can limit the minimum size of test specimens to be measured by providing an effective sensitivity limit to the instrumentation system, greater in magnitude than the base noise floor. A simple approach to zero signals is to make a "zero" measurement and then subtract this information from all subsequent **J** measurements. After a set time period or number of measurements further zero signals can be measured to ensure accurate zero information and monitor zero signal changes.

Figure 46 shows an applied field waveform and the resultant zero signal. The zero signal represents a peak value of +/- 40 counts in a system with a +/- 8192 count range, an error signal of approximately 1 %. It should be noted that the zero signal is 90 degrees out of phase with the applied field signal. The reason for the phase shift is that the zero signal is due to the effects of eddy currents within the solid copper windings that form the field generation coil. The zero time trace also shows a discontinuity around samples No 7500. This discontinuity is believed to be a semiconductor event related to the thyistor and snubber circuits. On the particular hardware this data was captured on this event was repeatable and did not scale with applied field or increased magnetisation signal. The event was not investigated further as it was repeatable and small and could be removed with the zero signal subtraction.

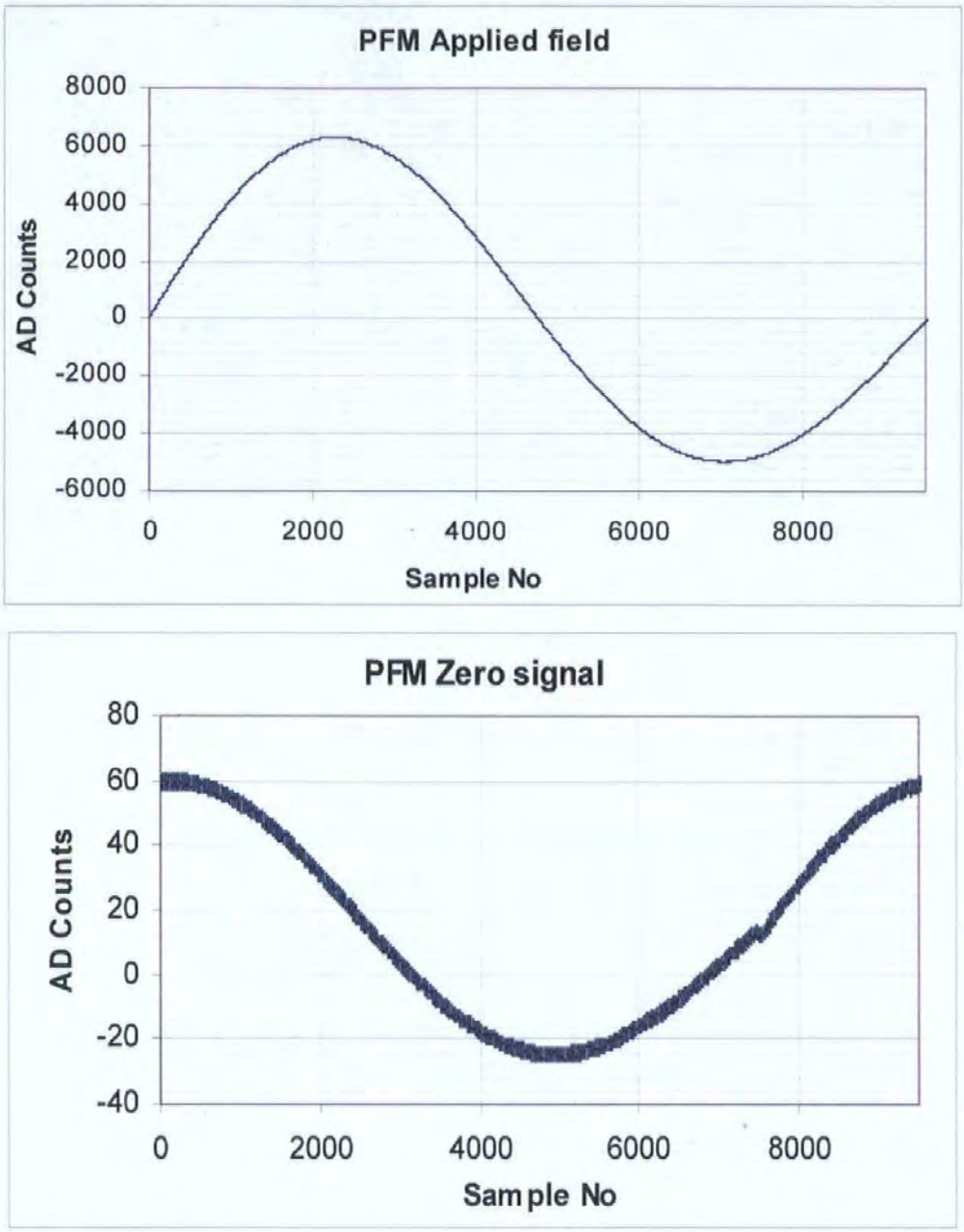


*Figure 46 - PFM J time traces of an applied field signal and a zero signal. Note the zero signal is two orders of magnitude below the applied field signal. The noise floor of the instrumentation is visible on the zero plot.*

## 7.2 Loop positioning

As the pickup coil, by its nature, is AC coupled to the signal of interest and recovered by integration, the offset position of the measured signal is unknown. It is necessary to

determine the constant of integration in order to determine the absolute value of **J** and **H** with respect to time.

The applied field can be assumed to start and end at zero field, or at least at the same magnitude subject to any offsets due to the earth's magnetic field. This level of offset is considered insignificant for the determination of the parameters for industrial quality control. If the system was to be adapted for low coercivity and soft material measurements then an external "nulling" field may be required. Typically, the sample will not be in a "virgin" condition so the origin position of **J** is not known. To obtain the correct position for the JH loop in the JH domain, two approaches can be used; sample displacement and centring. In practice both approaches can be implemented and switched on and off as necessary and even combined if required.

### *7.2.1 Sample displacement*

It is typical when using pickup coils and integrating fluxmeters to integrate the pickup coil's outputs as a magnetised sample is placed inside or removed from the coil. This produces an absolute measurement with a traceable origin. This technique can also be used in Pulsed Field Magnetometry. If the magnet is fully magnetised before it is placed inside the measurement system, the instrumentation can be set to measure the injection of the sample. By resetting the integrators before the sample is injected, then measuring during sample injection and the characterisation process, the **J** data should have a useable origin. If only one field generation coil is used for magnetisation and measurement then the sample can be measured as it is removed from the system.

The disadvantages of a sample injection system are mechanical complications and the possible errors that can be introduced due to integrator drift, as the integrators are required to measure for an extended period. An advantage of this approach is that the data measured

during sample injection should be related to a total flux approach, which is often used as a one point quality check of magnets. The total flux measurement uses a Helmholtz coil pair and a fluxmeter, the sample is rotated in the coil and the maximum flux determined. Having an additional parameter that is related to existing quality control procedures has additional commercial benefit.

### *7.2.2 Data centring*

If the magnet test specimen has been satisfactorily saturated with both positive and negative fields, and the measurement data is considered to be symmetrical, the midpoint between the positive and negative remanence values can be considered to occur at $\mathbf{J} = 0$. This approach seems empirically to operate satisfactorily with all industrial magnets and materials tested to date. With "exotic" materials this approach may be prone to errors if the saturation value was asymmetrical for positive and negative applied fields or if the BH curve was asymmetrical for positive and negative applied fields, but no materials that exhibit this behaviour have yet been observed. There are problems, however, if saturation is not achieved with both a positive and negative applied field as the resultant minor loop deviates from the expected major loop position and will lead to a centring error.

The approach of data centring has the advantage of enabling captured data to be centred by post processing of data and therefore the operation can be scheduled for periods of mechanical handling and capacitor bank charging to maximise total system operation rates.

## 7.3 Self demagnetisation

Permeameter/Hysteresisgraph systems which are often regarded as the industry standard for magnetic characterisation produce closed loop measurements [Section 4.1.1]. It is therefore highly desirable to enable PFM systems to produce data that is directly equivalent to these "industry standard" systems. The PFM produces an open magnetic

circuit measurement. In order to obtain a $JH_{int}$ or $BH_{int}$ measurement, where the suffix $_{int}$ indicates the applied field inside the magnet, it is necessary to apply a self-demagnetisation factor correction [14].

If a magnetised magnet is considered in a homogenous applied field, then the flux density inside magnet is given by,

$$J_{int} = J + \mu_0 H \tag{7.1}$$

where $J_{int}$ represents the flux density within the magnet in Tesla, $J$ is the magnetisation of the magnet in Tesla, $\mu_0$ is the permeability of free space and $H$ is the applied field in amps/metre. This simplified view does not include the divergence of the $J$ and $H$ fields, that is lines of magnetic flux do not have a singular source or sink point and form closed loops around their source. The divergence of the $H$ field can usually be ignored as it is insignificant in the region of interest, due to the design of the applied field coil producing homogenous fields in the sample region. The divergence of the $J$ field cannot be ignored and has a significant effect on self demagnetisation factors. Figure 47 shows a finite element analysis representation of a magnetised magnet (in 2D). It can clearly be seen that the flux lines of the magnet "curl" around to form closed loops. This figure has rotational symmetry about the central vertical axis.

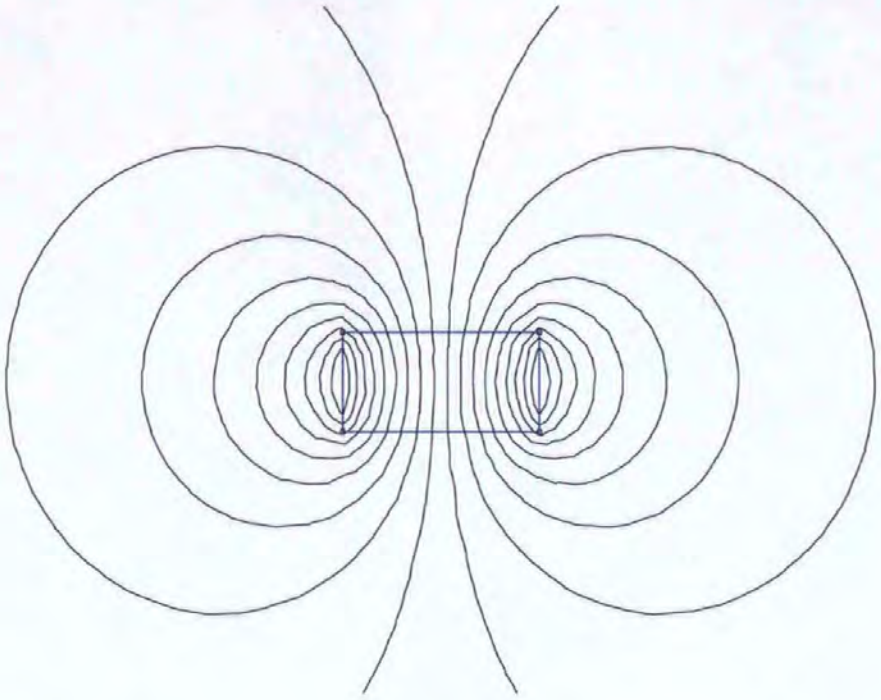

*Figure 47 - Magnetisation of a magnet showing the x and y components of the flux.*

As only a proportion of the magnets magnetisation is aligned with the applied field. Equation 7.1 is inaccurate in an open magnetic circuit. It is often useful to consider the effects of self-demagnetisation from the perspective of the applied field. As it is the dependence of $\boldsymbol{J}$ on $\boldsymbol{H}$ that is being determined, it is desirable to calculate the magnet's internal field and superimpose this with the external applied field to calculate the internal applied field, $\boldsymbol{H}_{int}$. If a factor, N', is considered that represents the proportion of the magnetisation that superpositions with the applied field, then Equation 7.2 gives the field inside the magnet.

$$\boldsymbol{H}_{\text{int}} = \boldsymbol{H} + (1 - N')\frac{\boldsymbol{J}}{\mu_0} \tag{7.2}$$

It is convenient to express the proportion of J that sums with H as shown by Equation 7.3.

$$N = 1 - N' \tag{7.3}$$

The term $N$ is also referred to as the ballistic demagnetisation factor. The self-demagnetisation factor, $N$, depends on the geometry of the test specimen. For regular

shapes, self demagnetisation factors can be determined using look up tables as published in [14].

A problem with the application of self demagnetisation factors is the fact that for most shapes a single factor is not applicable. Only a sphere has a uniform demagnetisation factor. Other shapes such as cylinders have a range of demagnetisation factors that are geometry dependent. This leads to the problem of different parts of a sample being at different positions around the samples JH loop. Figure 48 shows the variation in flux density, across the centre of an equal aspect ratio cylinder magnet. It can be seen that a large variation exists of approximately 23 %.

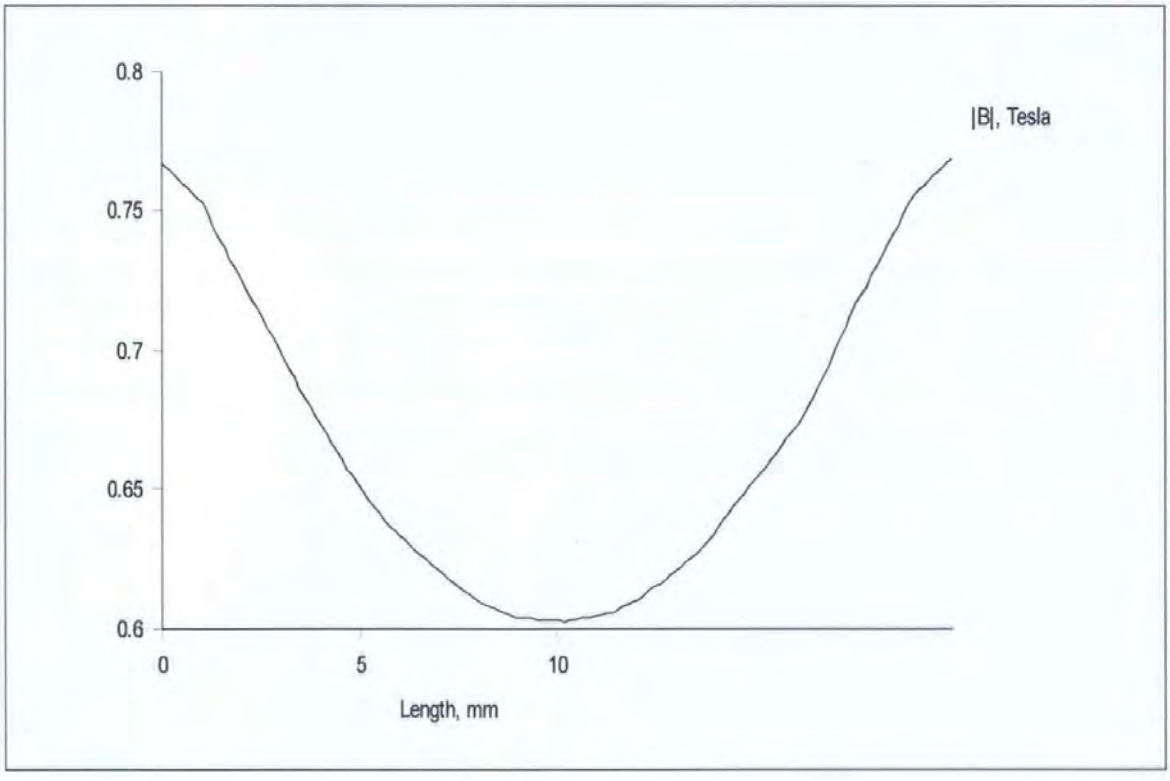


*Figure 48 - The variation in flux density due to distributed demagnetisation factors on a 20 mm diameter, 20 mm long cylinder of NdFeB.*

The results of this distribution of demagnetisation factors is a slight "rounding" of the JH characteristic, for some materials, in the 2nd quadrant of the JH loop. This distribution does not appear to cause difficulty in extracting critical magnetic parameters, as demonstrated in

the results but future work will look at removing this effect by post data processing techniques.

An additional complication exists with self-demagnetisation correction and that is one of "differential permeability". The problem is that the permeability of magnetic material ($\mu$) is dependent on the JH characteristics of the magnet specimen being evaluated and varies with net applied field. Although the field generation coil is providing an approximation of a homogenous applied field, the magnet's own magnetisation field is not homogenous as discussed previously in this section. The net applied field causes the magnet to have a non-singular permeability and as it is permeability that determines how easy it is for magnetic flux to pass through the material, permeability also shapes the path magnetic flux will take through the material and thus affects local and global self-demagnetisation factors.

It is possible to model magnetic materials using finite element analysis and if a non-linear model that includes magnetic hysteresis effects is used, then an approximation of the effects of differential permeability can be determined. The problem is that for a PFM measurement, the magnetic characteristics of the material are what is being determined and without this information it is impossible to predict differential permeability effects and calculate an accurate self-demagnetisation factor. Fortunately the majority of very hard magnetic materials such as the rare earth NdFeB magnets have linear permeability characteristics between remanence ($B_R$) and the coercivity point ($H_C$) thus reducing the issue of differential permeability for these materials.

The actual magnitude of the effects of differential permeability has not been determined and further work will continue in this area to assess the potential problems and find solutions.

## 7.4 Filtering

It may be necessary to filter signals to reduce the effects of system noise, particularly when small test specimens are measured and it is also mandatory to filter signals before an analogue to digital converter to prevent the possibility of breaching the Niquist limit and causing aliasing of the data. It is often desirable to use two filters in the system, an analogue anti-alias filter that has a corner frequency somewhere below the mid-way point of the sampling rate of the data capture card and a digital filter. The digital filter can have adjustable parameters to cater for a wider range of situations than a fixed analogue filter, such as unexpectedly high *dJ/dt* during the measurement or external interference adding extra noise to the measurement. It also allows easy assessment of the effectiveness of different filter types and different corner frequencies by the modification of the algorithm.

It is very important that the design of filters used does not introduce phase shifts to the measured data and can apply an appropriate frequency cut off. A suitable filter may be a Bessel type filter as this has optimum phase preservation but a high order filter may be required to ensure a good cut off. Filtering must not have too low a corner frequency, as this will dramatically distort the measurements. Appropriate filter frequencies are dependent upon the rate of change of the magnetisation signal (*dJ/dt*), which in turn is dependent upon the magnet material characteristics, and the rate of change of applied field (dH/dt), as well as the frequency of any system noise.

## 7.5 Eddy currents

As a dynamic signal is applied to the sample under test, eddy currents can be induced in conductive materials. The resultant eddy current that may occur can create magnetic fields which can introduce errors into the measurement. Two approaches are used to address this effect; eddy current correction by a "Best Fit" approach and eddy current correction by measurement.

Eddy currents in a conductive body are described by the following equation,

$$\nabla \times \mathbf{J} = -\sigma \frac{d\mathbf{B}}{dt} \tag{7.4}$$

where the terms have their usual meaning. For a given class of magnetic materials (and expected range of conductivities) maximum test specimen diameters and frequency of applied field can be chosen to reduce eddy current effects to levels that have insignificant effects on the result of the measurement. In practice the physical constraints on the values of capacitance, inductance and minimum sample sizes prevent the creation of Pulsed Field Magnetometers with frequencies low enough to not have significant eddy current effects. It is therefore necessary to correct for the effects of eddy currents.

### *7.5.1 Eddy current effect correction by a "Best Fit" approach*

If certain assumptions are made about the magnetic material under test, a "correction" can be applied to the measurement to compensate for the assumed eddy current effects [36]. By making assumptions that the sample conductivity, geometry and the eddy current paths are known, it is possible to make an analytical approximation of the effects of eddy currents. An approximate solution of the governing equations can be generated for a particular test specimen geometry and can be used to approximate the effects of eddy currents. This effect can then be subtracted from the measured signal. The approximation, however, only solves for first order effects. Higher order effects are assumed negligible and any imperfections or non-homogeneity of test specimen will be neglected. If a single pulse measurement is made it is possible to then estimate and subtract the eddy current effect error from the measurement. This cannot, however, be considered a valid measurement as any imperfections or non-homogeneities have not been accounted for and these can greatly effect the eddy currents that may flow in the sample, hence the effects and error caused by the eddy currents will deviate from the theoretical values and an erroneous correction may be made.

### 7.5.2 Eddy current correction by measurement

Eddy currents are proportional to the rate of change of applied field, the rate of change of magnetisation, the conductivity and surface area of the test specimen perpendicular to the applied field. Eddy currents are also effected by higher order effects such as the rate of change of magnetic field generated by the eddy currents themselves and even eddy currents generated in the copper of the field generation coils, due to rate of change of magnetisation. The following equation describes the eddy currents inside a conductive sample during the magnetisation pulse:

$$\nabla \times \mathbf{J}_C = -\sigma \left( \frac{d\mathbf{H}}{dt} + \frac{d\mathbf{J}_m}{dt} - \frac{d\mathbf{E}}{dt} \right) \tag{7.5}$$

where $J_c$ is the Eddy current, $H$ is the applied field, $J_m$ is the magnet's magnetisation, and $E$ is the magnetic field due to eddy currents.

If two pulses of differing *dH/dt* are applied to the same test specimen then the eddy currents and the measured effects of those eddy currents will be proportional to the *dH/dt* of the two applied pulses [12]. Each pulse will have an eddy current error proportional to the *dH/dt* of the pulse combined with the real signal. If the signals from the two pulses are vector subtracted then the two magnetisation signals cancel out, as does part of the eddy current error. The remaining proportion of the eddy current error is proportional to the difference in *dH/dt* between the two pulses. Since the *dH/dt* of the two pulses are known, this change in error can be scaled and used to subtract the eddy current error to find the static curve that is free from the effects of eddy currents. As the same sample is used for both pulses, all imperfections and non-homogeneities of the material will be accounted for.

Eddy current processing has seen some of the biggest improvements in PFM technology. Processing problems have previously occurred because the short and long measurements do not have a common applied field reference, as the two applied fields are at different

*dH/dt* it is there for important that correct time alignment is performed to ensure that the effects of eddy currents in the short and long waveforms are correctly compared. The effects of self demagnetisation must also be considered as the field inside the magnet is actually a sum of the magnetisation and the applied field as previously discussed. It is important to correctly calibrate the applied fields to ensure that the peak value of H is as close as possible for the short and long waveforms or the correction functions have problems where the short and long waveforms have identical values. A large problem in the eddy current processing is that the fundamental equations are "unstable" it is necessary to look at the ratio of the derivatives of dH/dt and dJ/dt for the short and long waveform. As the gradient of one of the waveforms approaches zero the ratio of short and long either tends to zero or tends to infinity. It is important to limit these events to ensure asymptotes are not generated in the final processed waveform. Figure 49 shows the f/2f process in detail. J and H points are time aligned with in the JH domain and the differential between the two f and 2f waveforms is used to extrapolate to the eddy current free position.

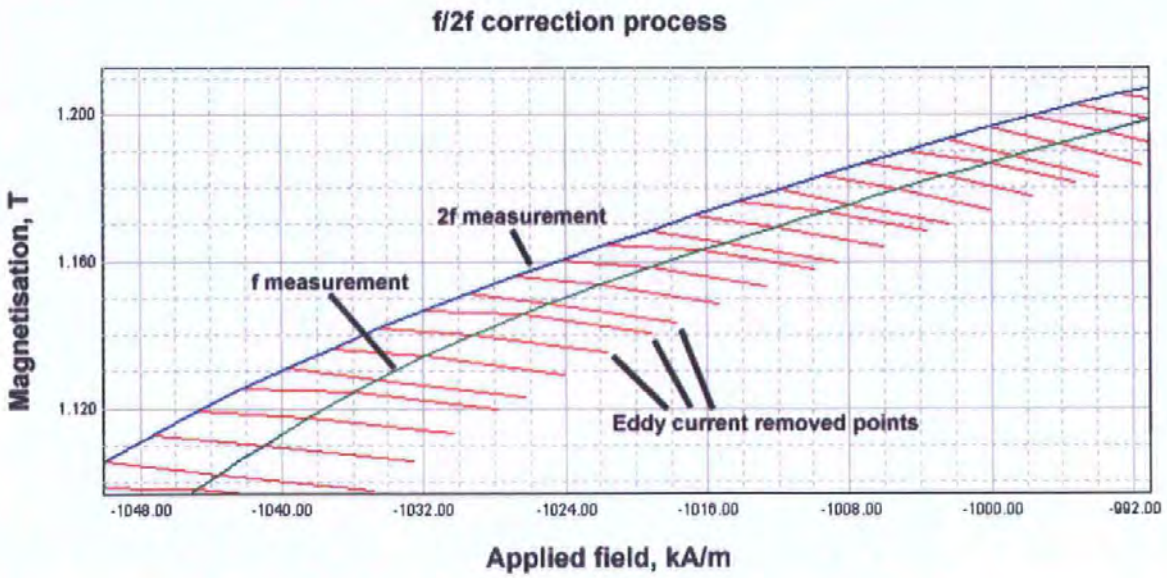


*Figure 49 - f/2f eddy current removal process. Points are time aligned within the JH domain then extrapolated to determine the JH loop that is free from the effects of eddy currents.*

Figure 50 shows the measurement of a sample of neodymium iron boron, measured at two frequencies represented by the two outer loops. As the eddy current effects increase, the loops become "fatter" pushing the measured data further away from the origin. The correction method enables the eddy current to be deduced and removed to obtain the resultant inner loop which is eddy current free. The pulse with the lower rate of change of field is known as the "long" pulse. The pulse with the higher rate of change of field is known as the "short" pulse.

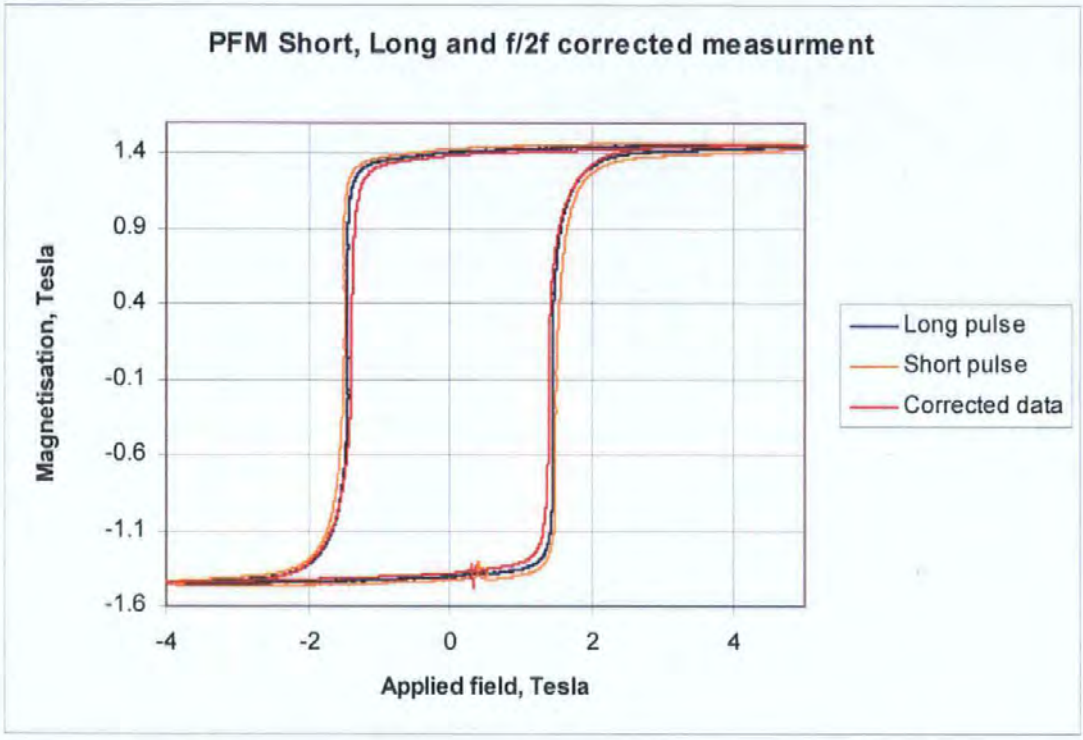


*Figure 50 - PFM JH loops of a sintered NdFeB permanent magnet. The graph shows the "long" and "short" measurement together with the f/2f corrected data.*

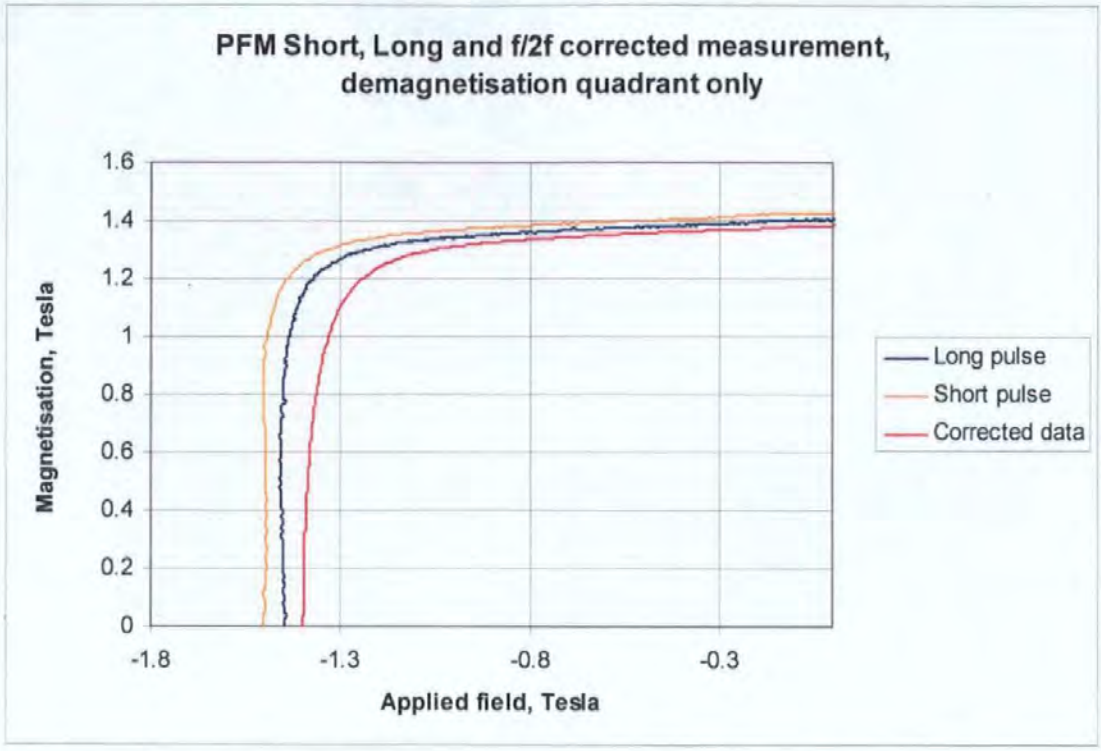


*Figure 51 - Detail of demagnetisation quadrant, showing "short", "long" and f/2f corrected data.*

The eddy current correction procedure described here has been successful in practice and this method was implemented in the prototype industrial PFM system described in Chapter 9. Results from the PFM system, with eddy current effect correction, are presented and discussed in Chapter 10.

Success has been achieved applying the eddy current correction procedure to magnetically soft materials such as nickel. Investigations show that the correction procedure is successful in the saturation regions of the material. Figure 52 shows detail of the saturation region of an eddy current effect corrected nickel and the two original "long" and "short" measurements.

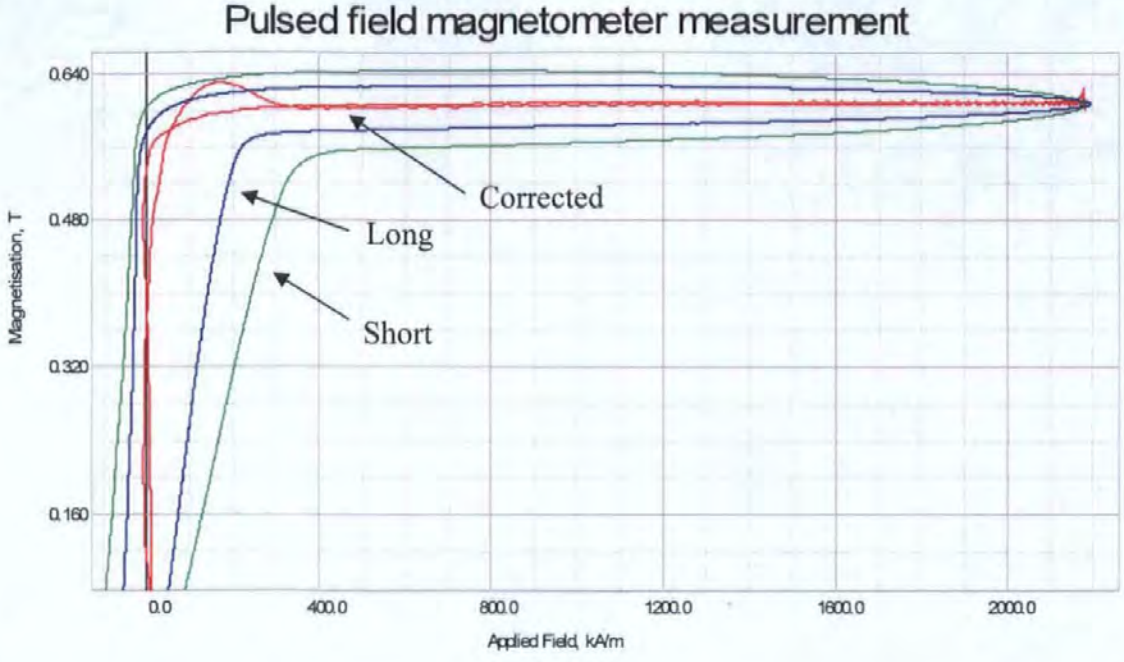


*Figure 52 - Eddy current corrected nickel. The f/2f processing has removed the majority of the effects of eddy currents within the nickel sample except for an overshoot as the nickel enters saturation.*

Figure 53 shows the full hysteresis loop for the eddy current corrected nickel sample. It is observed that in the saturation region the correction appears successful at removing eddy currents. In the region of high $dJ/dt$ the correction is also successful but it can be seen that there is an overshoot as the nickel enters saturation.

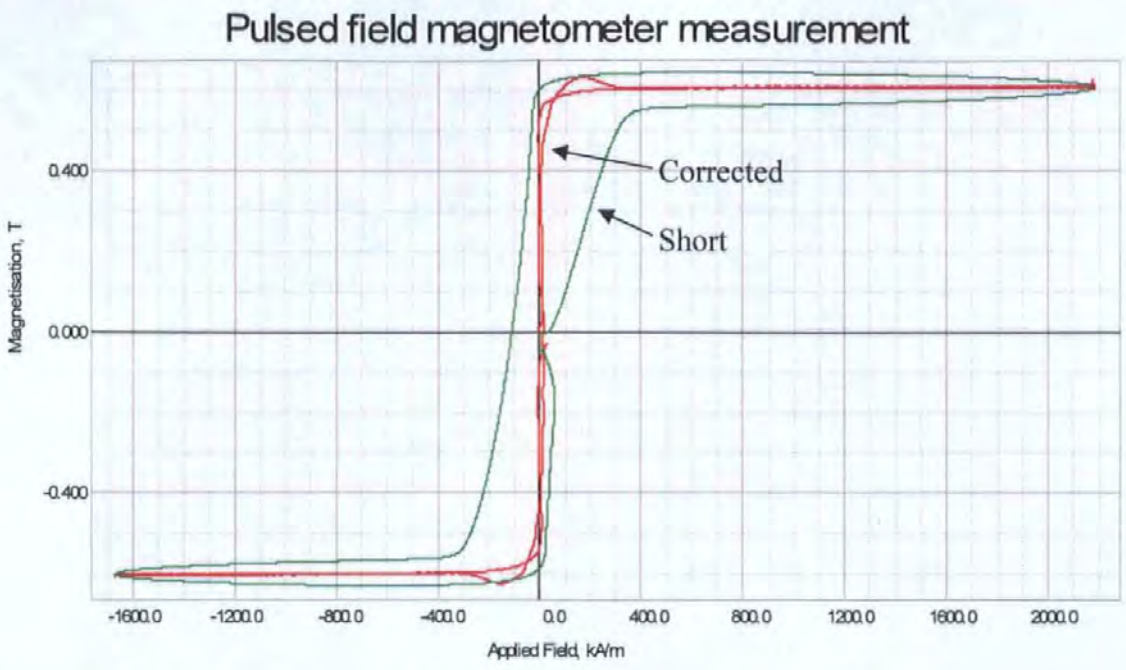


*Figure 53 - Full hysteresis loop for an eddy current effect corrected nickel. The corrected data is shown in red and the "short" measurement data is shown in green. The "long" data is not shown for clarity.*

The eddy current correction by measurement is selected as the most suitable method to compensate for the effects of eddy currents as shown by the results presented. Work is ongoing to improve the eddy current correction process for use with soft materials such as the nickel.

## 7.6 Temperature

As magnetic materials exhibit a temperature dependency, it is necessary to consider thermal effects and the temperature of samples in PFM systems. The temperature of the test specimen may vary from ambient to a higher temperature due to heating effects. Test specimens can be heated from sources that can introduce errors by changing the temperature of the specimen.

As a permanent magnet is driven through its hysteresis loop, effects to the internal domain structure within the magnet material produce heat. The area contained within a complete

hysteresis loop represents the energy required to drive a magnetic material around its hysteresis loop, and this energy will be converted into heat during every magnetic field "pulse" applied to the sample. An additional source of temperature effects may also be eddy currents circulating in the test specimen during characterisation, this will create a heating effect and this will change the specimen temperature.

For a NdFeB magnet with dimensions 10 mm diameter by 10 mm length, a temperature rise of approximately 1.8 K per has been observed when driven completely around its hysteresis curve by a PFM system. The PFM system used had an applied field period of 18 ms. The same magnet was also tested on a system with an applied field period of 4 ms and the temperature rise was found to be 2 K. A magnet of the same material but of dimensions 20 mm diameter by 20 mm long was also characterised on the 18 ms applied field PFM system and its temperature rise was determined to be approximately 1.8 K. This shows that the rise in temperature is dominated by the magnetic effects with in the structure of the magnet and that eddy current effects only have a small contribution to sample heating.

The temperature of the test specimen can be determined by a number of methods that are now discussed in detail.

### *7.6.1 Methods of temperature measurement*

A thermocouple can be mounted in contact with the specimen under test. This approach can have the disadvantage of introducing magnetic eddy currents or instrumentation errors attributed to potential eddy current effects distorting the magnetic field. These effects can be minimised by ensuring no magnetic materials are used in the temperature probe and interconnections and ensuring the volume of electrically conductive material is kept to a minimum. If a "bare" thermocouple is encapsulated in epoxy or another similar material

then this can form the basis of a probe that will not introduce errors to the measurement process.

There are a number of factors that affect the accuracy of determining the sample's temperature via a thermocouple. It is important to ensure a good contact between the temperature probe and the test specimen, which may prove a problem for automated mechanical handling systems. It is necessary to "protect" the measurement electronics of the thermocouple reader to ensure they are not damaged by any voltages inducted into the probe or interconnections during the characterisation process. It is also important to consider the effects of the thermal mass of the "probe" including the material encapsulating the thermocouple as this could introduce a delay, or significantly effect the measurement of the sample's temperature.

An optical window can allow a temperature measurement to be made with a non-contact device utilising a reflected inferred detector to monitor the samples temperature. This has the advantage of being an easily automated and totally non-contact method, but poses difficulties in exposing an optical path to the sample due the construction of the field generation coil, pickup coils and sample holder. The method has proved impossible in practice. The surface of many sintered NdFeB materials is a highly reflective granular structure; this has the effect of scattering the inferred beam decreasing measurement accuracy. The physical size of the detector is also prohibitive as there is limited space due to the bore of the field generation coil.

The temperature of the fluid within the sample area can be measured by means of a thermocouple at close proximity to the specimen under test. Provided that this temperature is stable for a sufficient period of time, the specimen can be considered to be at the fluid temperature. In order to determine this temperature stabilisation period, a test specimen

can be mounted with a thermocouple inside it. By monitoring the fluid temperature, and monitoring the response time of the test specimen, a safe stabilisation period can be determined for test specimens of equal mass and geometry. This method has the advantage that the sample is "controlled" to a specified temperature by the fluid and provides the possibility to specify the characterisation temperature.

## 7.7 Signal processing conclusions

Chapter 6 has discussed in detail methods of detecting and capturing **J** and **H** signals from a PFM system during the characterisation process. These signals are recorded on a PC system and then processed "offline" to eliminate, or reduce to insignificant levels, errors attributed to PFM. This chapter has discussed in detail the process for removing the zero signal, determining the origin of the hysteresis loop, compensating for the effects of the self demagnetisation factor and removing the effects of eddy currents. After minimising the effects of eddy currents and other "errors", it is necessary to scale the data by the appropriate calibration factors to obtain **J** data in Tesla and **H** data in Amps/metre. The next chapter discusses in detail the process of determining these calibration constants.

# Chapter 8 Calibration

It is necessary to calibrate any measuring instrument so that the results obtained can be related back to actual physical phenomena. In a PFM system it is necessary to take the voltage induced in the pickup coil, integrated by the integrators and captured by the analogue to digital converter card and convert this value into magnetic units. This then enables values such as remanence and coercivity to be obtained.

The method of calibration involves the determination of the correct scaling factors to convert the raw data from the analogue-to-digital converter into magnetic units. It is necessary to make two calibrations, the H or applied field channel and the J or magnetisation channel. While it would be possible to calculate individual calibration constants for the pickup coil, the integrators and the analogue to digital converter this is not done and instead a "lumped" calibration constant is calculated for each channel, J and H.

Any calibration procedure requires a reference or base line so that the error between the measuring system under calibration and the accepted base line value can be calculated. This error can then be used to adjust the calibration constant to minimise the error between the measuring system and the base line. It is the selection of a suitable base line that has previously proved a problem for Pulse Field Magnetometry. This chapter examines in detail, possible base line references for both the J and H channel and considers the practical implementation of these methods.

## 8.1 H channel calibration

The calibration of the H channel pickup system involves the determination of the applied field generated by the field coil in the sample measurement region and comparing this to the field detected by the H channel measurement system within the PFM. Essentially, the

H calibration factor is the required conversion from sample counts in the analogue-to-digital converter to applied field in kA/m. The determination of the applied field can be problematic as the majority of magnetic sensors are calibrated in a static field and this can cause errors when these devices are used in dynamic fields. An additional problem is that the applied field can be as high as 8 - 10 Tesla and many sensors are not designed for this operating range.

A number of possible methods for determining the applied field are now considered as alternatives for H channel calibration; Hall effect based sensors, calibrated search coils and direct current measurement.

### *8.1.1 Hall sensor*

Hall sensors have been previously discussed as methods of applied field determination for conventional magnetic measurement systems, where the applied field is static or quasi-static. To measure the applied field in a PFM system requires that the hall sensor be placed in the same position as test samples inside the PFM. The PFM can then be operated in a normal manner, generating a decaying sinusoidal magnetic field which is detected by the hall sensor.

Hall elements by their nature are conductive and being exposed to a transient magnetic field can induce eddy currents within the Hall element. This can introduce measurement errors when compared to the static field within which the Hall probe was calibrated. Hall elements are only linear with in a certain range of flux density and are not usually specified for operations over 1 - 2 Tesla. As Pulsed Field Magnetometry utilises fields of typically 3 - 7 Tesla, this out of specified operating range could also be a source of error. An

additional source of error is that during the magnetic pulse, voltages could be induced in the hall sensor or interconnecting leads and this could cause measurement errors.

### *8.1.2 Integrating fluxmeter*

By calibrating a pickup coil, using external conventional techniques, this coil could be used to calibrate the H channel [21]. A pickup coil of arbitrary area-turns product can be very accurately calibrated in an electromagnet to determine the area-turns product. The field of the electromagnet can be determined with an Nuclear Magnetic Resonance (NMR) meter or other suitable, high resolution, static magnetic field measuring device. By setting the electromagnet to produce a flux density across its air gap and then changing to a different air gap flux density, the integrator can successfully measure the change in magnetic flux. The NMR can accurately determine the starting and ending fields as these are both static DC levels. The induced emf ε, produced by the search coil is given by,

$$\varepsilon = -\frac{d\phi}{dt} \tag{8.1}$$

where the terms have their usual meaning. As the search coil has an unknown area $A$ and has $N$ turns the induced emf. becomes,

$$\varepsilon = -N \cdot \frac{d\boldsymbol{B}}{dt} \cdot A \tag{8.2}$$

The integrating fluxmeter integrates the induced emf and displays a reading of $\int \varepsilon$ that is determined by,

$$\int \varepsilon = -N \cdot A \cdot d\boldsymbol{B} \tag{8.3}$$

where $N \cdot A$ is the area turns product of the coil and d**B** the change in magnetic flux density between the two settings of the electromagnet.

The calibrated search coil can be placed inside the applied field generator, in the sample position, and used with integrating fluxmeters to accurately determine the actual applied

field inside the pulsed field generation coil. The applied field generator can be used at full field so there are no additional errors due to calibrating at non-operation field levels.

### *8.1.3 Current measurement*

By applying a DC current to the solenoid and measuring the associated DC field, the field / current characteristics of the magnetising solenoid can be determined. A simple Hall effect based Gaussmeter could be used to determine the static flux density at a given DC current.

As the peak current necessary to generate a magnetic field of the magnitude necessary for Pulsed Field Magnetometry will be of the order of thousands of amperes, the DC applied current will be a fraction of the operational current. A peak current measurement can be used to deduce the field when the high current pulse is applied. A non-contact device such as a current clamp, or a low value shunt resistor could be used. Unfortunately this technique involves differences between DC and pulsed currents of orders of magnitude and assumes there are no other differences between a static and dynamic current measurement.

### *8.1.4 Plastic bonded permanent magnet.*

A bonded magnet sample of known coercivity can be used to calibrate the applied field. Placing the magnet inside the applied field generator and detecting the magnet's magnetisation in the normal way using the J and H search coils will obtain an un-calibrated reading. As the sample's coercivity is known (the applied field that will drive the magnet's magnetisation back to zero magnetisation) it is possible to work out the calibration factor from the difference between the un-calibrated applied field necessary to drive the sample to zero magnetisation and the known coercivity value.

The influence of magnetic viscosity and the temperature dependence of the coercivity would need to be small, or significant errors could be introduced. If the magnet's temperature dependence is known then a temperature correction can be performed to

remove temperature related errors. It is also assumed that the plastic bonded magnet has a low enough conductivity so that the effects of induced eddy currents are insignificant.

## 8.2 J channel calibration

The J channel calibration involves accurately determining the magnetisation of a magnet that is placed within the sample measurement area of the applied field generator so that a suitable calibration factor can be determined for the J pickup system. The J calibration has previously proved problematic and a number of possible methods are now considered:

### *8.2.1 Test specimen with known magnetic moment.*

The measurement of the magnetic moment of a sample can be established using an integrating fluxmeter and calibrated Helmholtz coil. If the J coil system is connected to the integrating fluxmeter and the test sample, previously measured, inserted into the measurement position, the fluxmeter will measure the coupling coefficient of the J coil to the sample. This can then be used to determine the calibration factor. Various geometries can be used to check the uniformity of the coupling coefficient.

### *8.2.2 Non-conductive magnet material with known saturation*

If a non-conductive sample with known magnetic moment is obtained then this could simply be measured in the PFM system to determine the calibration factor required [21]. The material would have to be a very low conductivity sample, such as ferrite or iron oxide. Suitable materials would be a $Fe_3O_4$ sample or a commercially available ferrite magnet such as a Phillips 3C30. Both have low conductivity and known magnetic moments at a given temperature. Ferrite magnets have a lower Curie temperature than rare-earth type permanent magnets and therefore exhibit a far greater temperature dependence. A change of 10 K from ambient can cause a change in saturation value in excess of 1 %. This approach assumes the effects of eddy currents are insignificant as the material has a relatively low conductivity.

### 8.2.3 Test specimen combination

The conventional calibration method for the J pickup system on vibrating sample magnetometers is a sample of pure nickel, where pure is considered to be better than 99.99 %. Pure nickel has a well-defined magnetic moment of 53.22 EMU/cm$^3$ and is highly electrically conductive allowing eddy currents to be generated. The effects of these eddy currents are highly visible around the saturation region where the measurement is critical, and these effects need to be removed from the nickel measurement. A technique for achieving this previously involved compensating for the eddy current effects in the J signal by subtracting a proportion of an eddy current only signal away from the combined magnetisation and eddy current signal of the nickel.

By creating a pure nickel and a pure copper sample of equal dimensions, the copper can be used to generate an eddy current only signal suitable for the correction of the nickel signal. A nickel sample can be measured in a static arrangement to determine its magnetisation. By measuring the eddy currents in a similar shaped copper test specimen, a proportion of the copper eddy current can be subtracted from the nickel measurement, to give an eddy current free standard measurement. As complex as this technique appears to be, it can give excellent results.

Figure 54 shows the measurement of a conductive solid nickel sample in a PFM system. The result contains errors due to eddy currents, evident throughout the measurement as a "bulging" of the loop. The nickel measurement should be a single line but the effects of eddy currents have given the appearance of hysteresis and caused an effect in the saturation region where the magnetisation is no longer single valued for a given applied field. The effect in the saturation region is the most problematic as it is now impossible to see what the true value of nickel saturation is.

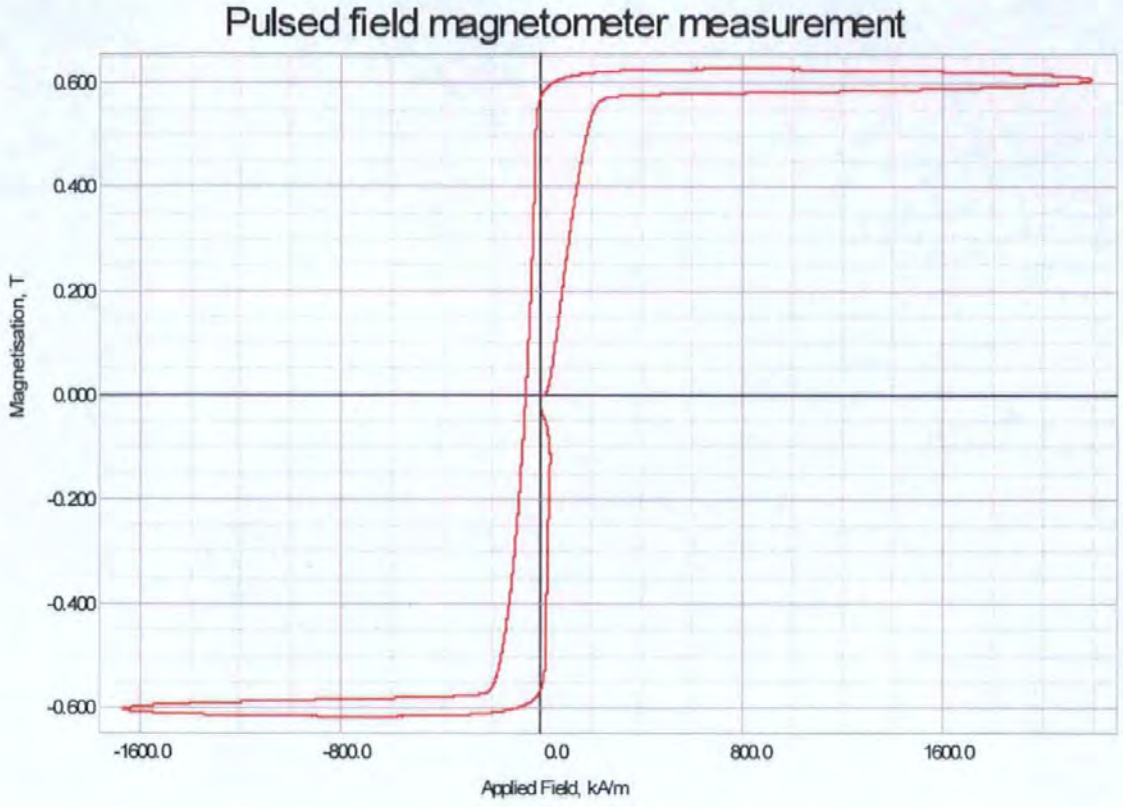


*Figure 54 - PFM nickel JH loop including eddy currents. The eddy current effects manifest themselves as a fattening of the loop. Nickel has no hysteresis and so should be a continuous single line.*

Figure 55 shows a measurement of a pure copper sample and Figure 56 shows a copper corrected nickel measurement. The trace represents the nickel sample after a proportion of the eddy current has been subtracted from the nickel sample results to remove the eddy current effects in the saturated region of the nickel characteristic. The subtraction of a proportion of copper's eddy current **J** signal from the nickel signal has greatly reduced the effect in the saturation region. It is now possible to extract the saturation value of the nickel and use this as a reference for calibration.

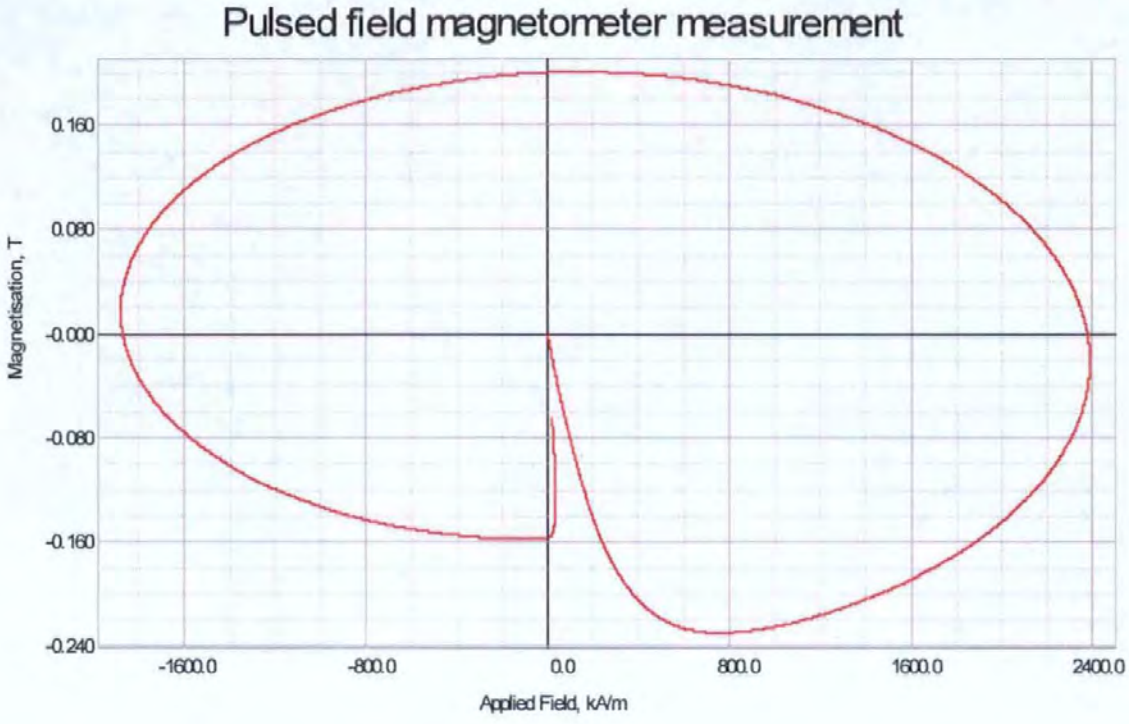


Figure 55 - PFM copper JH loop. The **J** component consists entirely of eddy current effects

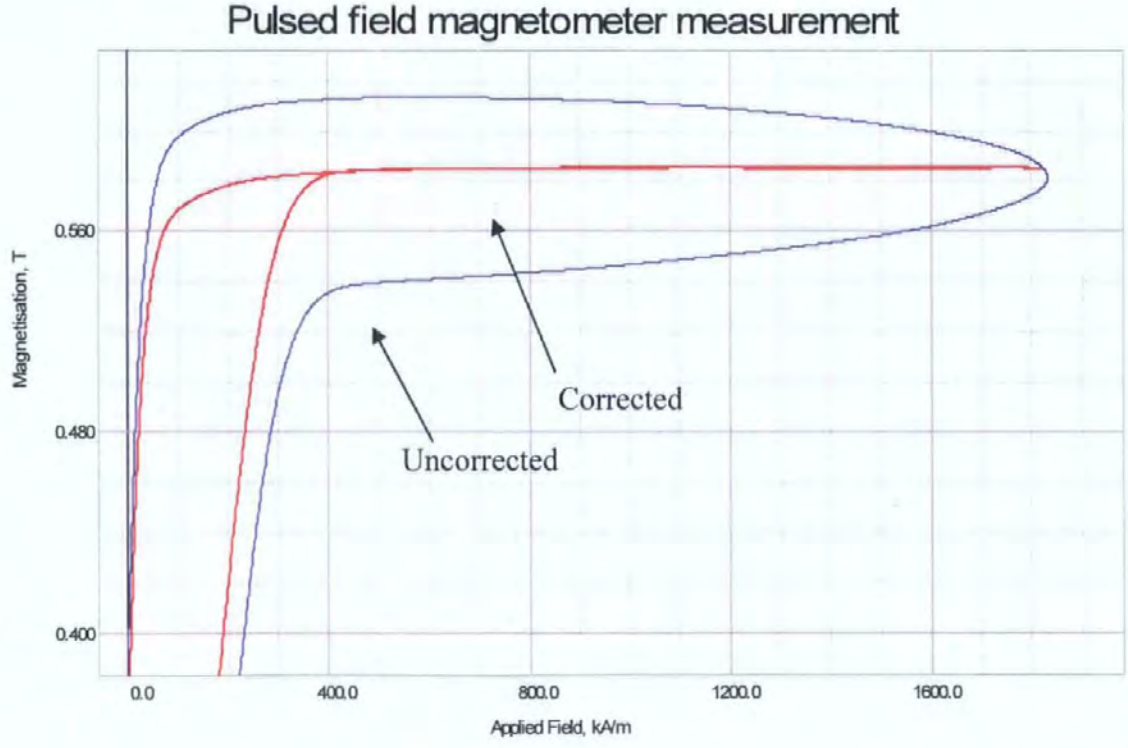


*Figure 56 - PFM eddy current "corrected" nickel sample. The **J** saturation value is now determinable as the effects of eddy currents have been removed.*

As copper has a greater conductivity than nickel, its eddy current signal, for the same sample size sample under the same measurement conditions, is larger. Only a proportion of the copper's **J** signal can be subtracted from the nickel **J** signal. It has been found in practice that the proportion of the signals is close to the ratio of conductivity of the samples. This needs further investigation to determine the exact factor, as this method looks very promising. Table 11 shows the conductivity of copper and nickel. The ratio between the two elements is 4.11. Advantages may be gained by using an alternative material to copper so that the ratio between the conductivities is different. It would be preferred to use a material with a lower conductivity than copper. If a PFM system was constructed with a high rate of change of applied field, there is concern that as the magnitude of the eddy currents increase, higher order effects may influence the eddy current effects and the eddy currents in the copper may become unrepresentative of the eddy currents within the nickel. The ideal solution would be to use two materials with identical conductivity as this would result in similar eddy currents in both materials and reduce any potential problems that may be caused by the eddy currents behaving differently in the two materials.

| **Material** | **Conductivity MS/m** |
|---|---|
| Copper | 58.8 |
| Nickel | 14.3 |

*Table 11 - Conductivity of copper and nickel.*

### *8.2.4 Calibration discussion*

The most successful methods for calibration of the H channel have been the calibrated search coil method. This method is preferred as a dynamic instrument is being used to calibrate a dynamic system; a static calibrated system is not being forced to make a

dynamic measurement. Other advantages of the method are that it is possible to make a very accurate determination of the area-turns product of the calibration search coil, and it is even possible to use the same integrating fluxmeter to make the search coil calibration and also to be used for data acquisition in the PFM system. This ensures that any integrator-based errors are taken into account as part of the calibration.

The Hall effect gaussmeter based measurement has its uses as a lower accuracy calibration system. It can be used for a rough check of the applied field, or a very quick first pass calibration. Its advantages are its simplicity and speed – a sensor is placed inside the coil, the coil is pulsed and the gaussmeter shows the reading.

The most successful methods for calibration of the J channel have been the methods based on test samples. The copper corrected nickel appears to give good results and systems calibrated using this method have produced excellent accuracy when compared to conventional systems. The results from a system calibrated in this manner are presented and discussed in Section 10.1 . The advantage of using nickel, as part of the calibration is that the method is similar to the way conventional VSMs and permeameters are calibrated and obvious similarities exist. This will make the method more acceptable in the community as it is not radically new.

The use of a single sample such as ferrite or iron oxide has also been successful [21] but the method is more suitable for laboratory-based systems where additional time and care to ensure temperatures are stabilised and at the correct level can be ensured, as the samples exhibit temperature dependence.

# Chapter 9 The industrial PFM

A fully operational prototype Pulsed Field Magnetometer was built to satisfy the needs of industrial magnet producers as part of a DG12 European funded project [2]. The methodology presented in this thesis was used for the design of the field generation coil, magnetic sensors, and instrumentation, as well as for the data processing parts of the control software. As the European project partners included magnet manufacturers, they were consulted on their requirements of a system designed for 100 % quality control. The size, shape and range of their production were considered as well as required magnet characterisation rate and types of magnet materials to be tested. Based upon the discussions with the industrial magnet manufactures the following outline specification was agreed: -

- Cycle time less than 5 seconds per magnet
- Peak (reverse) measurement field greater than 5 Tesla
- Maximum sample diameter 30 mm
- Maximum sample height 30 mm
- Minimum sample diameter 5 mm
- Minimum sample length 5 mm
- No temperature controlled environment, but ambient conditions would be monitored and compensated for.

The cycle time was a compromise between usability and cost. The single largest cost component in the PFM system is the capacitor bank. The original proposal for the industrial implementation of a PFM featured four independent capacitor banks with four field generation coils. Each field generation coil would have a discrete purpose: -

- Magnetisation
- "Long pulse" measurement (f)
- "Short pulse" measurement (2f)
- Demagnetisation

The "long" and "short" measurement coils apply the two different d**H**/dt fields for the eddy current correction procedure. The four quarters of the system would operate independently but as a sequential pipeline. Because of the cost of the capacitor bank, approximately £5000, and the duplication of the control and high voltage systems for each bank, it was decided to use a single capacitor bank but retain the four, field generation coil system by multiplexing the single capacitor bank to each of the coils.

Figure 57 shows the functional concept of the industrial PFM system. Magnets are loaded at the magnet loading station and then progress through a magnetisation process "Mag" through to the two characterisation processes named "f" and "2f" and finally through a demagnetisation process "Demag" to allow safe handling on exit from the system.

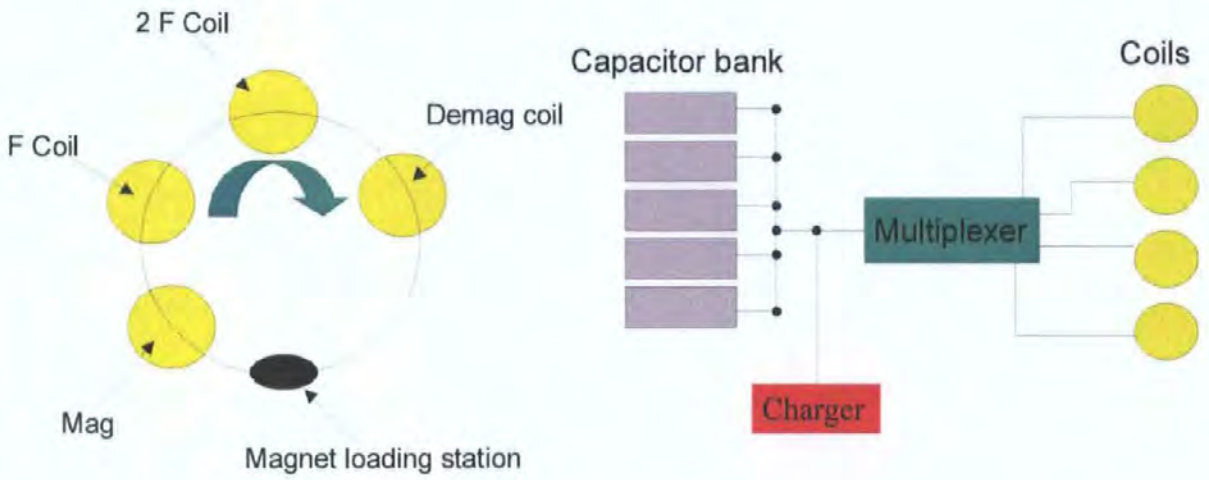


*Figure 57 - Functional concept of industrial PFM. Samples will pass from the loading station through the "Mag", "f", "2f" and "Demag" coils before returning to the loading station. Each coil is serviced by one capacitor bank that is multiplexed between the coils.*

The (minimum) peak measurement field of 5 Tesla was decided upon after consideration of the available field generation energy and the required applied field necessary to saturate even the hardest rare earth magnets that were available from the producers. As the applied field is a single 360 degree (decaying) sine wave then the minimum peak value refers to the value at 270 degrees, the value at 90 degrees was approximately to 6.4 Tesla. Figure 58 illustrates the amplitude of an applied field waveform with respect to time and shows the maximum and minimum peak field positions.

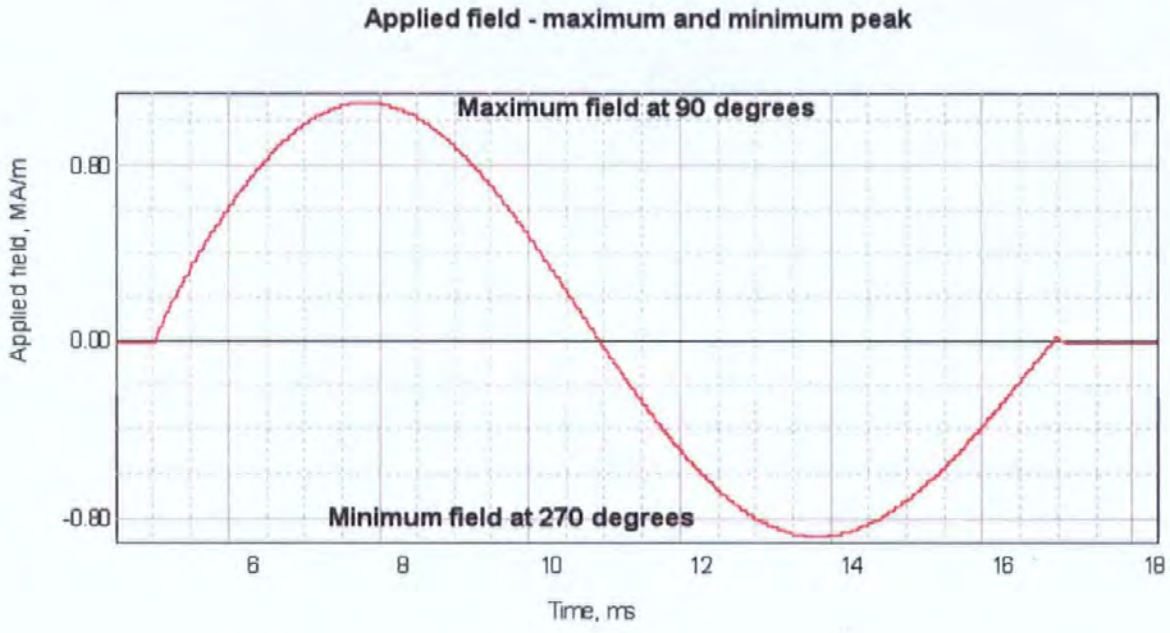


*Figure 58 - Positions of maximum and minimum peak applied field.*

The size limits of 30 mm length by 30 mm diameter were chosen to allow 80 % of a particular magnet manufacture's production to be testable by the machine. As the project was a proof of concept there was little point stretching to 100 % of production at this time. The size limit is essentially dictated by the field generation coil and the available energy. To allow a bigger size range requires a large bore field generation coil and more capacitor bank energy to achieve the required field levels, which equates to significant added cost.

A temperature-controlled environment was not implemented due to prohibitive cost and it would offer limited additional value to a quality control system. From Section 7.6 it is known that the temperature rise of a NdFeB magnet was approximately 2 K per measurement. It was believed that this temperature changes encountered would not affect the measurement results significantly. The prototype machine was to be operated in a temperature controlled quality control laboratory and so ambient conditions were controlled. As the system was to be operated at a constant ambient temperature and would have a constant operational speed, any temperature effect would be constant between samples. A method of determining ambient temperature was added to the system, a simple thermocouple in free air, and the temperature correction factors given for each material type were used in the post data-acquisition processing.

## 9.1 Capacitor energy generation and recovery

The only practical way to charge a 5 mF capacitor bank to 3000 V at high speed is by using a switch mode charger. These are readily available items and typically used for rapid capacitor charging in laser systems and x-ray applications. Switch mode chargers have significant advantages over phased control step up systems including, the ability to gang chargers in parallel to produce higher output currents, lower mains input power factor distortion and have smaller physical footprints. The system selected was a Lambda EMI Model 802, capable of 8000 J / s at maximum voltage. This equates to a time of 5.6 seconds to fully charge a 22.5 kJ capacitor bank. With an expected cycle time of less than 5 seconds, the charger on its own is too slow to provide the required energy to the capacitor bank. Due to budget constraints a larger power supply was not available. If each coil did require the full 22.5 kJ at a rate of 1 magnet every 5 seconds, the total power dissipation from the 4 coils would be 18 kW. In reality the coils all require different energy levels in order to achieve their desired function and this energy level is often far from full power.

The inductance of the field generation coils is typically orders of magnitude greater than the field coils resistance at the rates of change of current considered here, it is the inductance that limits the applied field current and not the resistance, therefore, only a proportion of the applied field energy is lost as dissipated heat. Much of the capacitor bank energy is returned to the capacitor bank, as described in section 5.3.1, and after a discharge this energy can be reused on the next pulse. With use of the "Aircore" design software [33] it is possible to predict the energy losses in a field generation coil and also the returned energy on the capacitor bank. This design data was used to optimise the four applied field coils and arrange the firing order to ensure that sufficient energy was returned to the capacitor bank after each pulse to allow all four coils to be fired from just one charge of the bank. After the final discharge in the sequence, the energy remaining provides a significant proportion of the energy required for the next sequence of discharges, greatly reducing time and energy dissipation by approximately 400 % compared to a sequence requiring four complete recharges.

Figure 59 shows the capacitor bank energy level after each pulse along with the time necessary to recharge the capacitors to full. As each discharge takes less than 50 ms, the charging and discharging sequence will fit into the 5 second time frame. In practice, it is necessary to recharge the capacitor bank only after the "demag" pulse as due to the pulse sequence there is sufficient recovered energy after each stage for the next pulse. By ensuring that the mechanical handling and data processing runs in parallel with the charging it is possible to meet the cycle time requirement.

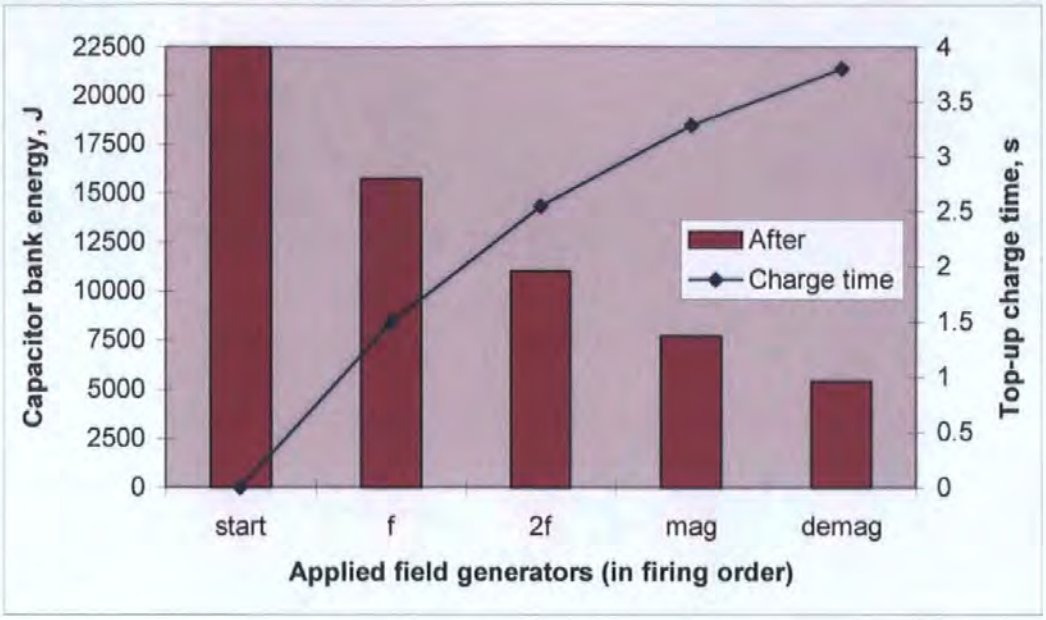


*Figure 59 - Capacitor bank energy and charge time for maximum energy. The bar chart shows the energy on the capacitor after each stage and the line graph shows the time it would require to recharge the bank to full after each stage. The capacitors start at the fully charged value of 22.5 kJ and decrease with each pulse stage.*

## 9.2 Implementation of field generation coils

The field generation coils were designed using the methods described in Chapter 5. The only additional design feature was the introduction of a fluid path to allow the energy due to resistive losses to be extracted. The coils were wound with 0.5 mm spacing between each layer of copper to allow cooling fluids to penetrate the coil and remove heat due to resistive losses in the coil. The coils were designed with a 50 mm clear bore to allow a 30 mm sample space after a pickup coil was fitted. Each of the four field generators required for the industrial PFM were identically constructed. The coils have four power connections to enable the correct windings to be selected so any particular coil could be used for pre-magnetisation, f, 2f or demagnetisation functions by changing the power connections.

The coil was designed to achieve a peak field of 6.4 Tesla when connected to a 5 mF capacitor bank charged to 3000 V. The energy loss due to resistance of the windings resulted in a reverse peak field of approximately 5 Tesla, resulting in approximately 30 %

of the applied energy being lost as heat dissipated into the cooling system. The mechanical construction of the coil featured fibreglass layers wrapped around the final winding layer to provide radial strength to withstand the magnetostrictive forces encountered during the field generation pulse. The maximum expected current was around 5 - 6 kA producing adiabatic heating (to the copper windings) of approximately 2.5 K per pulse.

Figure 60 shows an assembled applied field generator with pickup coil in place. The four power connections are illustrated as is the cooling pipe system. The high voltage connections are exposed as brass studs so that large cables can be securely bolted to the terminals. The cooling fluid terminals feature integrated temperature sensors so that the control system can monitor the coolant temperature at the outlet of each field generation coil.

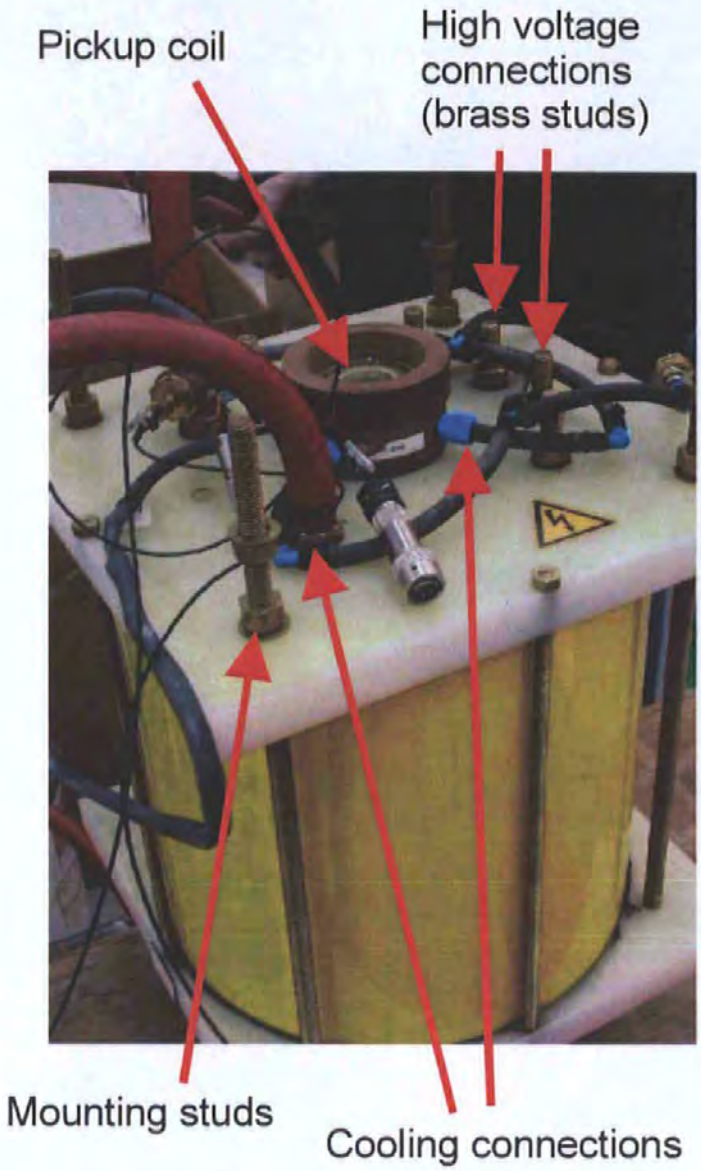


*Figure 60 - Assembled industrial PFM applied field generator, with pickup coil fitted.*

## 9.3 Implementation of pickup system

The pickup coil system was designed using the information presented in Chapter 6. A radial concentric hum-bucking or gradient coil was selected due to the advantages presented in Chapter 6. Due to the thermal problems caused by dissipation in the applied field generators, it was necessary to shield the pickup coil from the thermal effects. As discussed in Section 6.4, "zero signals", the zero signal detected by a radial gradient coil is adversely effected by temperature changes, causing a temperature dependent zero signal.

To minimise the temperature effects on the zero signals two methods were used to minimise the problems encountered: -

- Bulk heat extraction from the applied field coil
- Active heat shielding within the pickup coil

and these are now discussed.

Bulk heat extraction from the applied field coil is necessary to achieve the high operational rates required by industrial PFM systems, and the cooling system implemented would remove the heat from the applied field coil. This would help the zero signal problem but the temperature changes encountered in the field generation coils, even with cooling, still cause temperature dependent errors within the pickup coil. For a field generation coil starting at ambient, approximately 20 °C after a few hours of operation the coolant temperature had reached approximately 50 °C. This still represented a significant temperature change for the pickup coil and so active heat shielding was implemented.

Figure 61 shows graphically the concept of bulk heat extraction realised by passing coolant through the field generation coils. The active heat shielding of the pickup coils is achieved by forcing the pickup coil winding surface and windings to be at a constant temperature greater than the applied field generator. In this way the pickup coil temperature could be maintained regardless of the actual dissipation effects within the applied field generator. As the pickup coils only have a small amount of coolant, the thermal mass of this coolant is low and therefore relatively easy to control with a simple heater and a "Eurotherm" type temperature controller. By removing the heat from the field generation coil and protecting the pickup coil with a coolant jacket, raised above ambient, the pickup coils could be protected from changes in heating of the field generation coil.

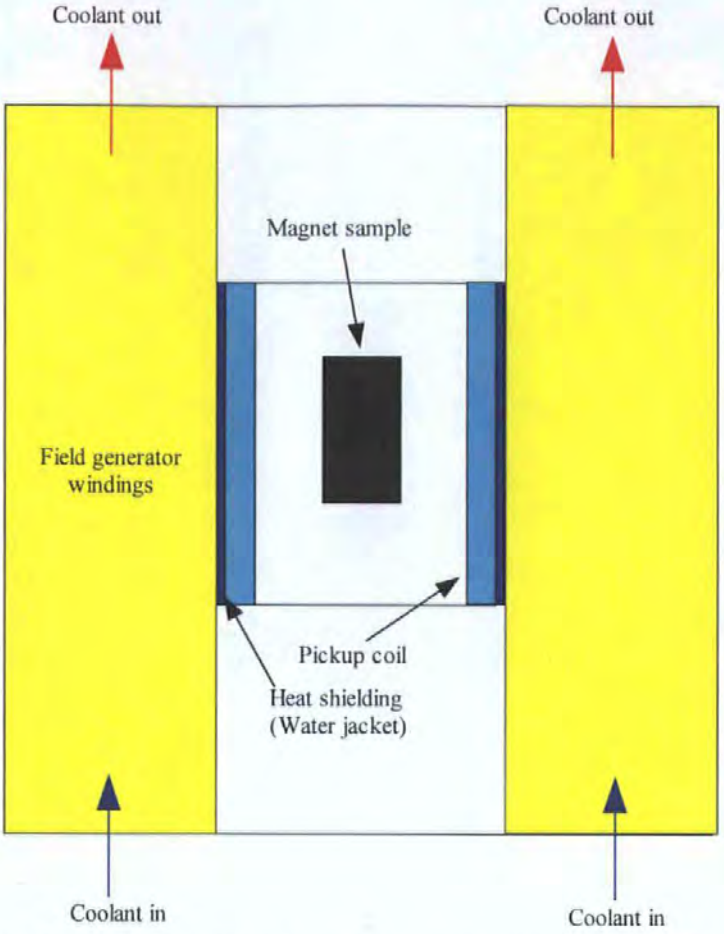


*Figure 61 - Pickup coil thermal solution. A cross-section through the applied field generator and pickup coil showing fluid surfaces and heat extraction.*

The same coolant as used for the applied field generator cooling was used for the pickup coil's controlled temperature, but the fluid was in its own temperature controlled circuit. The pickup coil's formers were designed to allow the fluid to pass through out the pickup coil and cause as even heating as possible. Temperature sensors were also embedded within the pickup coil fluid pathways in position that would not interfere with the pickup coil's function. Figure 62 shows the pickup coil fluid pumps, heater and reservoir. Each pickup coil had its own coolant circuit for independent control.

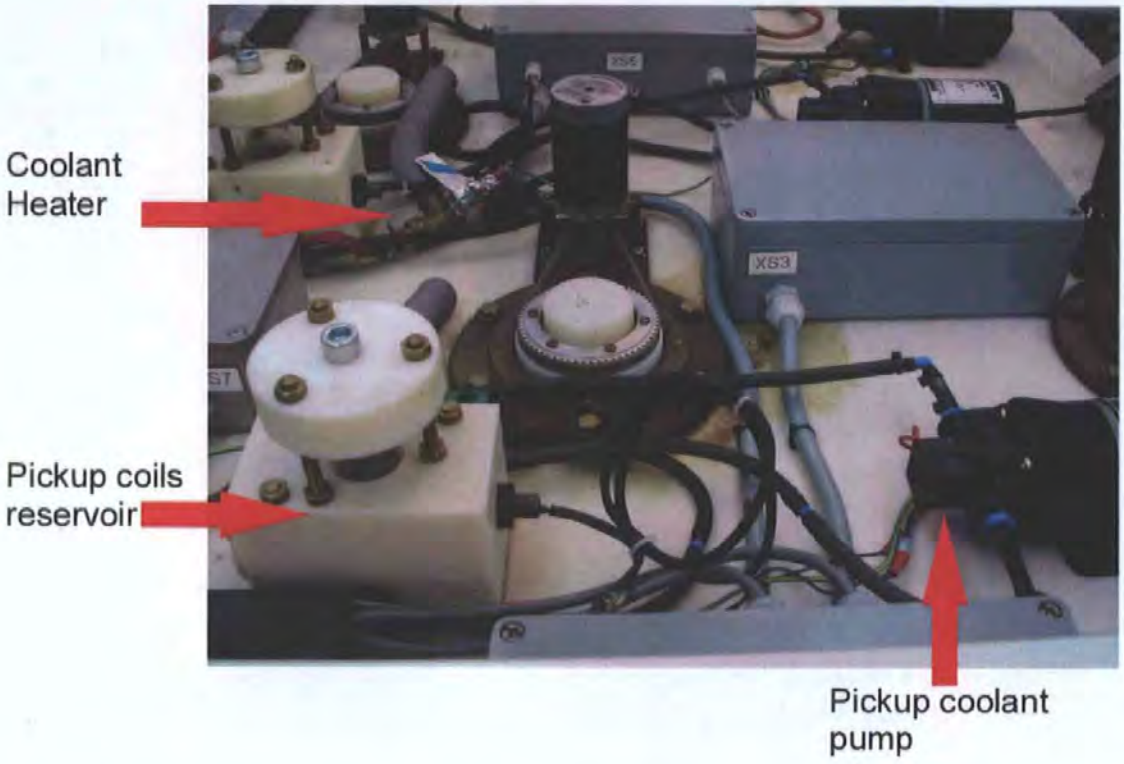


*Figure 62 - Pickup coil fluid pumps, heaters and reservoirs fitted on top of the industrial PFM system. 3 sets of fluid pumps, heaters and reservoirs are fitted on top of the machine together with various support electronic and interconnections.*

## 9.4 Mechanical handling

The Mechanical handling system was developed by Mecelec Developments Ltd, in collaboration with Hirst Magnetic Instruments as part of the MACCARATEC project [2]. The objective for the mechanical handling system were to provide a quick and efficient mechanism for loading magnet samples into the PFM system for measurement, as well has hiding the complexity of the Pulsed Field Magnetometer from the operator.

The basic principle of the mechanical handing system was a rotating table design, as shown in Figure 63. Each of the four field generation coils would be in static positions above the table and the magnets can be rotated around to each position sequentially, and also be raised up via cylinders to the operating position inside the field generation coils. The magnets would progress from the operator loading station to the magnetisation station

and then on to the two measurement and demagnetisation stations before being returned to the operator with a pass or fail status and the complete characteristics logged to a database for comprehensive record keeping of quality control and measurement data.

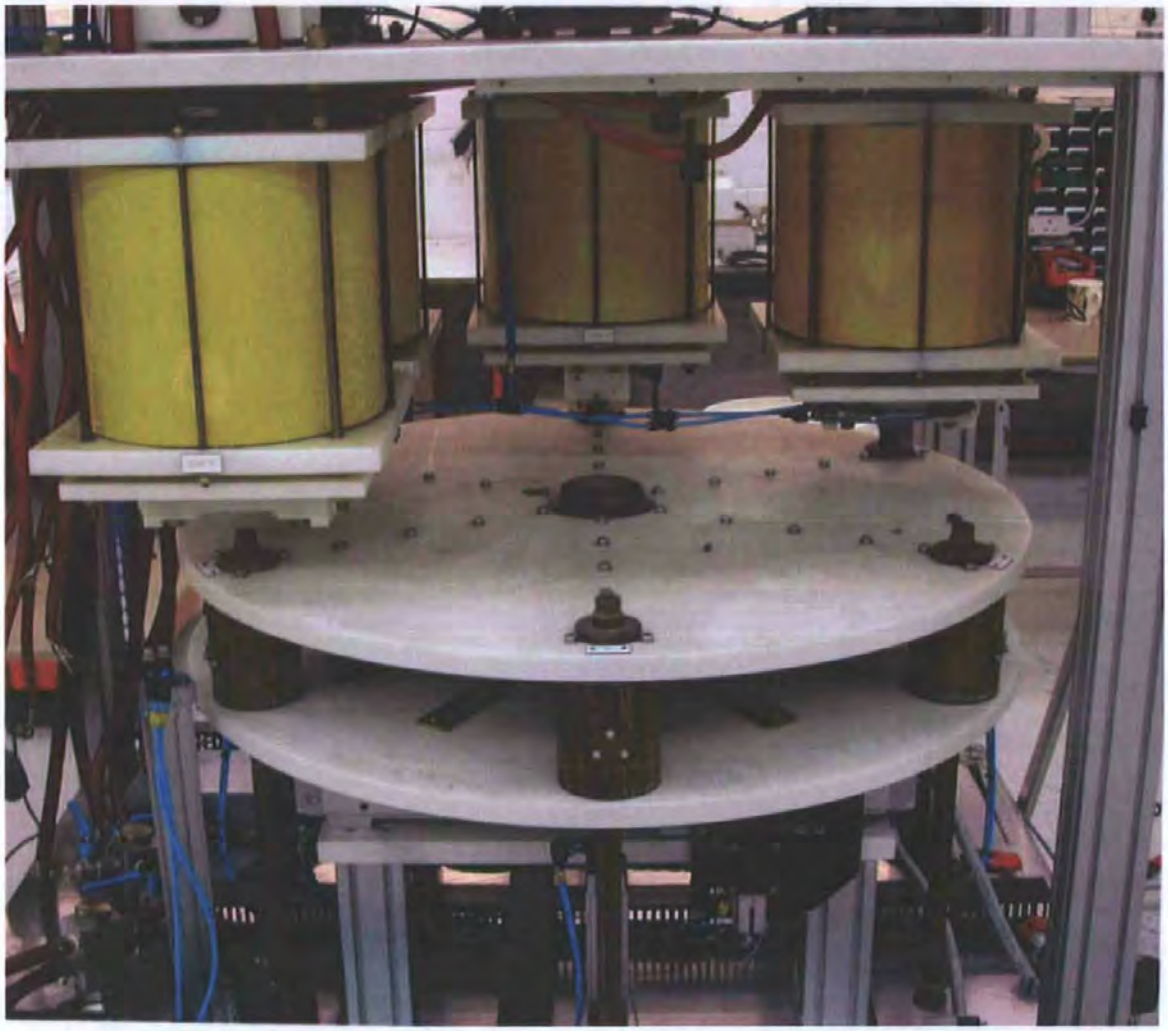

*Figure 63 - The mechanical handling system is centred around a rotating table system for moving samples from the operator's loading station in to each measurement coil. The table can be seen in the centre of the machine. Rods, actuated by cylinders lift the magnets into the measurement position inside the field generation coils.*

Each of the four field generation coils featured adjustable end-stops so that magnets raised up into each coil would automatically be in a central position with respect to the field generation coil and pickup coil. This is particularly important for larger magnets where a static end-stop would not ensure all parts of the magnet sample were within the homogeneity bounds of the pickup coil. The end stops were driven by servo motors on the

top of the system and controlled by the PC software. When a new magnet was selected all the end stops would automatically adjust to the optimum position.

The mechanical handling system was controlled by a PLC system and was essentially an autonomous unit requiring only a few handshake signals with the controlling PC to ensure that magnet rotation only occurred after a successful discharge and measurement sequence.

## 9.5 Software

At the heart of the PFM system was a complex piece of software written especially for the industrial PFM system. The software controls the PFM hardware, data capture, data processing, data storage and a full user interface with data viewing and data recall. The code was completely written in C++ and operated within the Microsoft Windows environment.

Communications with external hardware was via a number of routes. A high speed A/D converter provided the two analogue channels needed to capture the output from the measurement integrators. The high speed A/D converter also had an I/O port that was used to interface to 24 V logic and the PLC system that ran the mechanical handing section of the machine. Serial ports were used to communicate with the PLC system to monitor temperatures at various points around the system. Two additional RS232 ports were used to communicate with the analogue integrator's micro controller and the micro controller in the high voltage control equipment.

A multi-threaded approach to software writing was implemented to allow communication, database access, user interface and data processing tasks to run simultaneously so that measurement data collected from each of the four pickup coils was recorded and collated.

Once a complete set of data was collected the processing tasks would apply eddy current removal procedures and self demagnetisation factor corrections etc. to produce a "error free" version of the collected data. This data would be recorded in the database and displayed on PC's screen with each new measurement updating the display every 5 seconds.

## 9.6 The complete system

The completed prototype industrial PFM system consisted of 4 discrete blocks;

- High voltage cabinet
- Instrumentation and PC cabinet
- PLC Control cabinet
- Mechanical handling system

Figure 64 shows a schematic plan view of the layout of the PFM system. The high voltage control cabinet contained the switch mode charger, the capacitor bank and discharge multiplexor, as well as the micro controller system that governed the operation of the charging system. The instrumentation cabinet contained the sensitive equipment such as the integrators. The PC was also in this cabinet away from the high voltage system. On the front of the PLC control cabinet were various status displays monitoring the temperature sensors throughout the system and from the PLC controller. The mechanical handing cabinet was enclosed in clear polycarbonate to allow visual inspection of the components but to protect personnel from the high voltages, moving parts and magnetic fields. The magnetic field strength surrounding the field generation coils was also considered for health and safety regulations. The Health Protection Agency's Radiation Protection Division has set guidelines of 4.2 G (42 mT) for continuous exposure to a 60 Hz magnetic fields, in industrial and commercial applications. The PFM does not generate a continuous

60 Hz magnetic field, but a transient, decaying magnetic field of similar frequency, therefore the guideline figure of 42 mT is highly conservative in this application. The actual field measured at a distance of 1 m is, a peak of, 8 mT and is therefore well within the guidelines.

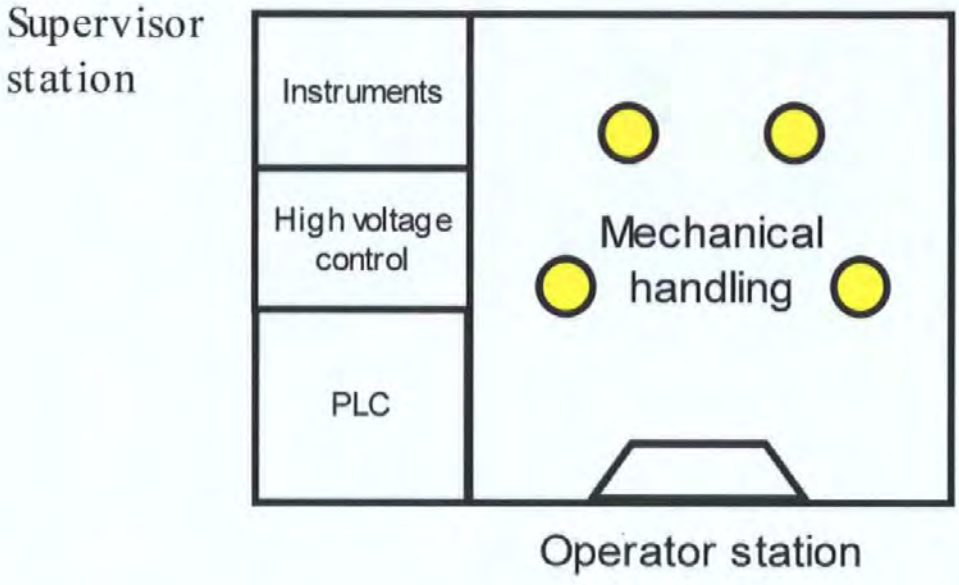


*Figure 64 - Plan view of industrial PFM. The supervisor station has access to the computer system for data recall, calibration and system set-up. The operator has access only to a small control panel with pass and fail indication and start buttons.*

Figures 65 and 66 show photographs of the completed industrial PFM system. Figure 65 shows a view of the PLC and mechanical handling control cabinet and Figure 66 shows detail of the operator station. The yellow field generation coils can be seen behind the protective plastic screen and the rotating table can be seen in the lower half of the machine.

*Figure 65 - Completed industrial PFM, showing operator station, mechanical handling control cabinet (front) and high voltage cabinet (left rear)*

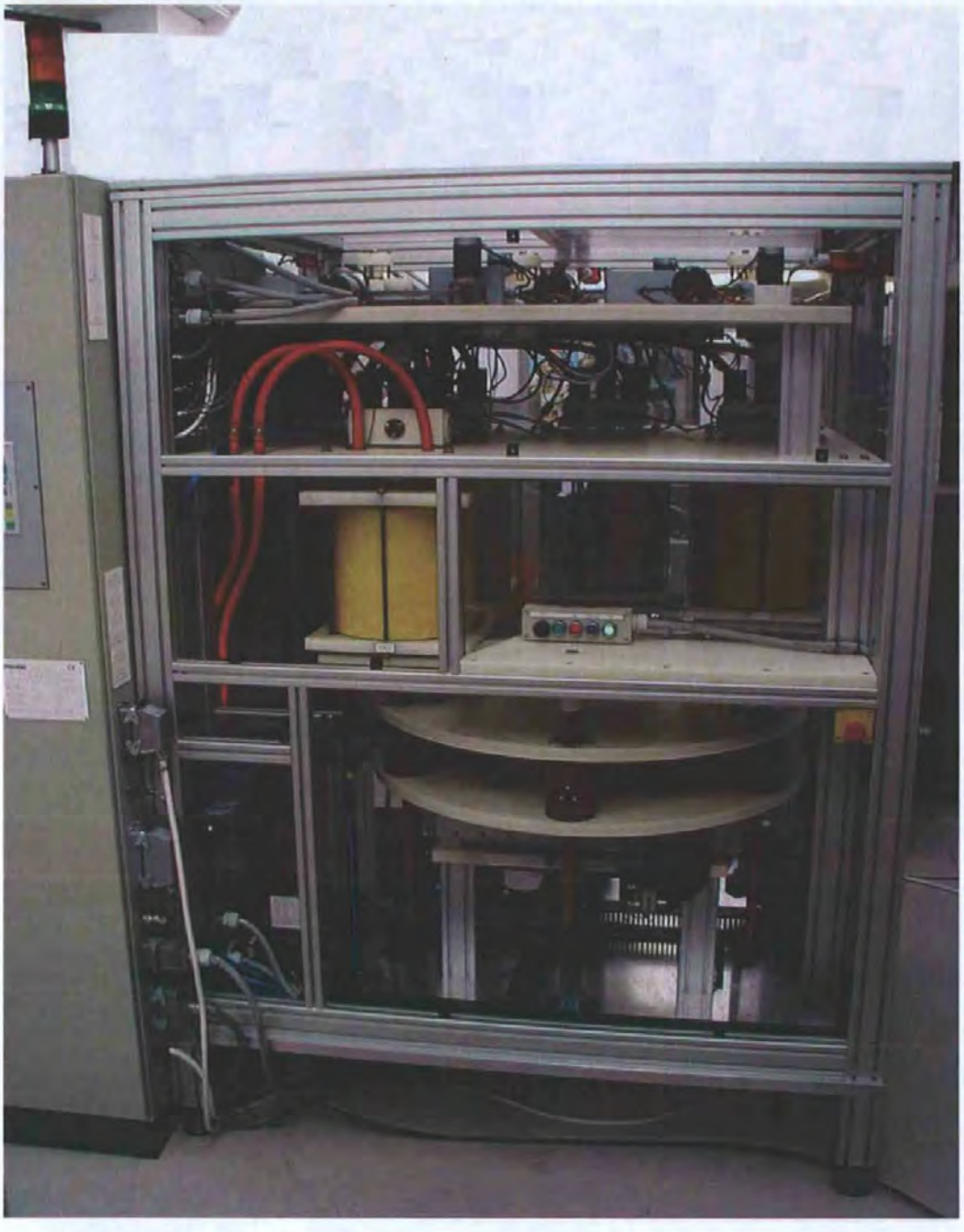

*Figure 66 - Completed industrial PFM showing operator station. The (yellow) field generation coils are visible behind the polycarbonate. Magnets are loaded in front of the visible indicator lamps*

Once completed the prototype system was shipped to a major German magnet manufacture, Magnetifabrik Schramberg, where it entered trials in an industrial magnet producing environment for a period of 12 months. The trials investigated the accuracy, repeatability, ease of operation and durability of the system.

## 9.7 PFM industrial trials

During the first few months, many problems were encountered with software bugs in the PFM control software and the PLC controller code. There were a number of mechanical problems related to the rotating table and sample insertion mechanism. Magnets could get jammed inside the measuring coils, which was an issue. The fluid selected for the coolant "Therminol-D12" was found to be highly corrosive to many standard pipe materials. This caused a number of pipe failures and the pipes were changed for a neoprene based material that was resistant to the coolant. These type of problems are to be expected with a system as complex as a PFM and upgrades and repairs were preformed "in-situ" at the magnet factory.

After the initial problems were resolved the system achieved a good level of performance. Different magnet types, shapes and sizes were tested on the machine to check long-term system performance, from both a measurement and mechanical standpoint. The mechanical handling system performed well and did the required job of loading magnets into the field generation / pickup coil assemblies. The high-speed capacitor charging and discharge multiplexing system was successful and provided no operation problems. The overall cycle time for the system was 5 - 6 seconds. This was just slower than the target of 5 seconds but was considered acceptable for a prototype system.

The data collected by the PFM system when under trial was very successful. The data and the systems accuracy and repeatability are discussed in detail in the next chapter, "Results and discussion".

# Chapter 10 Results and discussion

For PFM systems to become accepted by the academic and industrial community it is necessary to demonstrate that the systems have acceptable accuracy, repeatability and reliability where the terms are used with the following definitions;

- Accuracy is defined as the difference between a measurement and the accepted value of that measurement, expressed as a percentage of full-scale range.
- Repeatability is defined as the maximum difference between a series of identical measurements, using the same equipment, expressed as a percentage of full-scale range.
- Reliability is defined as the ratio of time that the machine is shut down for repair to the time the machine is operational.

It is also necessary to demonstrate the systems are easy to operate from both an operator's and supervisor's perspective and to ensure the price of the system reflects the value it will add to product tested.

The measurement performance of the PFM system discussed in Chapter 9, appeared to meet the initial requirements and this is discussed fully in the sections "Accuracy" and "Repeatability". The system stood up to the industrial high speed environment in which it was tested. The high voltage system, field generation coils, pickup coils and their associated cooling also proved very effective in operation, with the cooling system removing excess heat. No errors due to pickup coil zero drift were noticed, proving the pickup coil temperature control was successful.

## 10.1 Accuracy

The results from a PFM system have been compared with conventional systems as a test to validate the PFM method [37]. Various size samples have been compared on a PFM and a conventional system.

Figures 67 and 68 show the measurement of the same magnet sample on a permeameter and then on a PFM system. The magnet material was a bonded NdFeB ring with dimensions, outside diameter 21 mm, inside diameter 16 mm, length 23 mm. The Magnet material was manufactured and the permeameter measurement made by Magnetfabrik Schramberg. The permeameter was a Permagraph model 6.e manufactured by Magnet-Physik Dr. Steingroever GmbH.

It can be seen from Figures 67 and 68 that the results from the PFM agree closely with the permeameter system, for the limited range of applied field the permeameter can produce. The permeameter measurement is divided into discrete field steps while the PFM measurement is continuous. At the maximum applied field of the permeameter there is a deviation from the PFM measurement. This is due to the saturation of the permeameters pole pieces starting to effect the measurement, which limits the permeameter's maximum applied field.

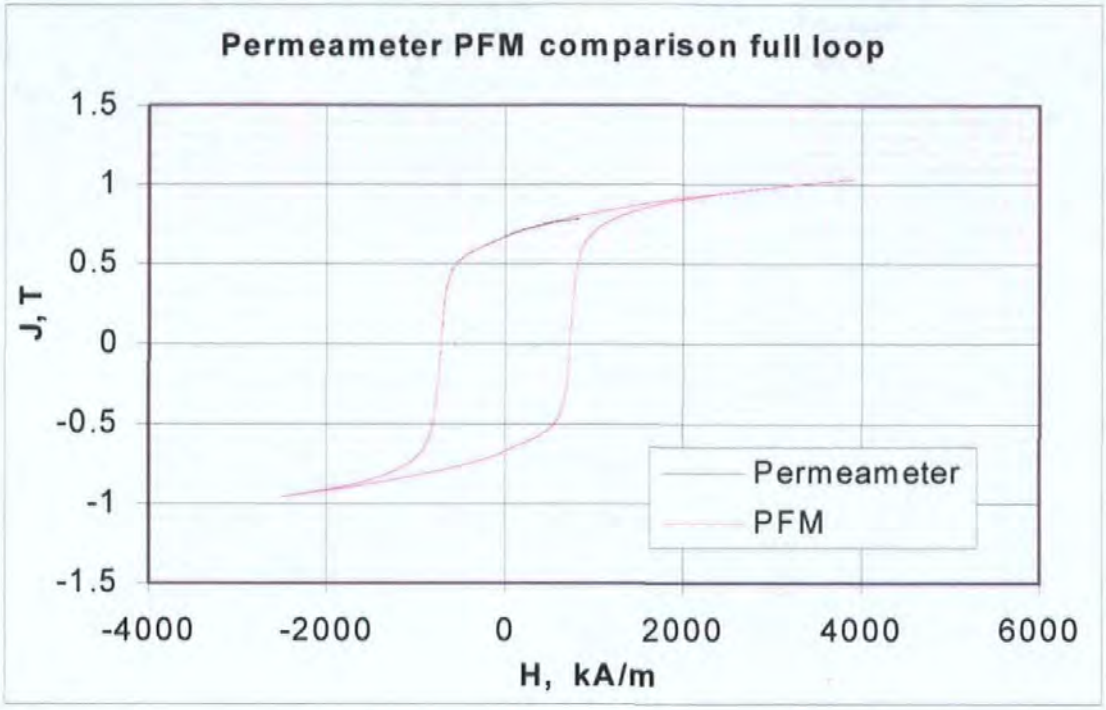


*Figure 67 - The results of a permeameter and a PFM measurement of a "large" sample. At this scale it is impossible to distinguish between the two measurement methods.*

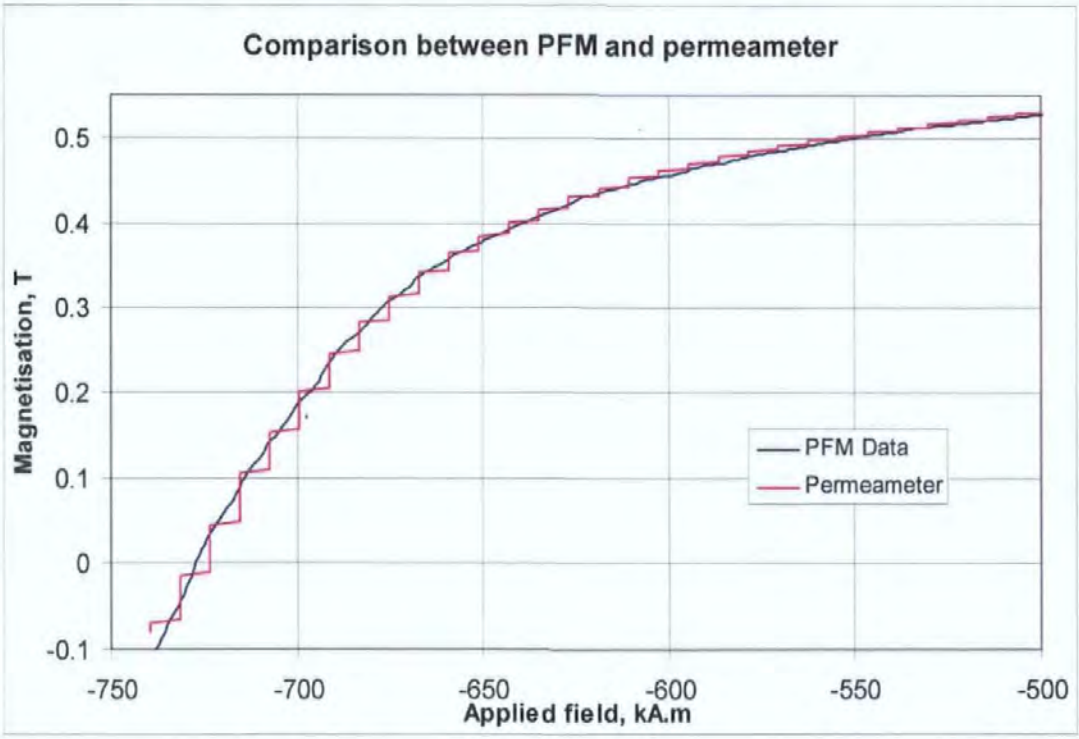


*Figure 68 - Detail of the 2nd quadrant (demagnetisation) of the permeameter and PFM measurement comparison. It is now possible to see the differences between the permeameter and PFM measurement systems. The PFM measurement is continuous while the permeameter data shows discrete steps.*

Figure 69 shows the comparison of a magnet sample measured on a PFM and a super conducting extraction magnetometer of the same magnet. The magnet was a sintered

NdFeB cylinder magnet of diameter 5 mm, length 10 mm, manufactured by Magnetfabrik Schramberg. The extraction method measurement was performed by Laboratoire Louis Neel, CNRS, Grenoble. Figure 70 shows the detail of the 2nd quadrant. At this scale it is possible to see the differences between the PFM and the extraction magnetometer. The largest errors are a maximum of approximately 1.2 % and these can be seen as an offset in the X direction. It is likely that temperature differences between the two measurements accounts for a large proportion of the error

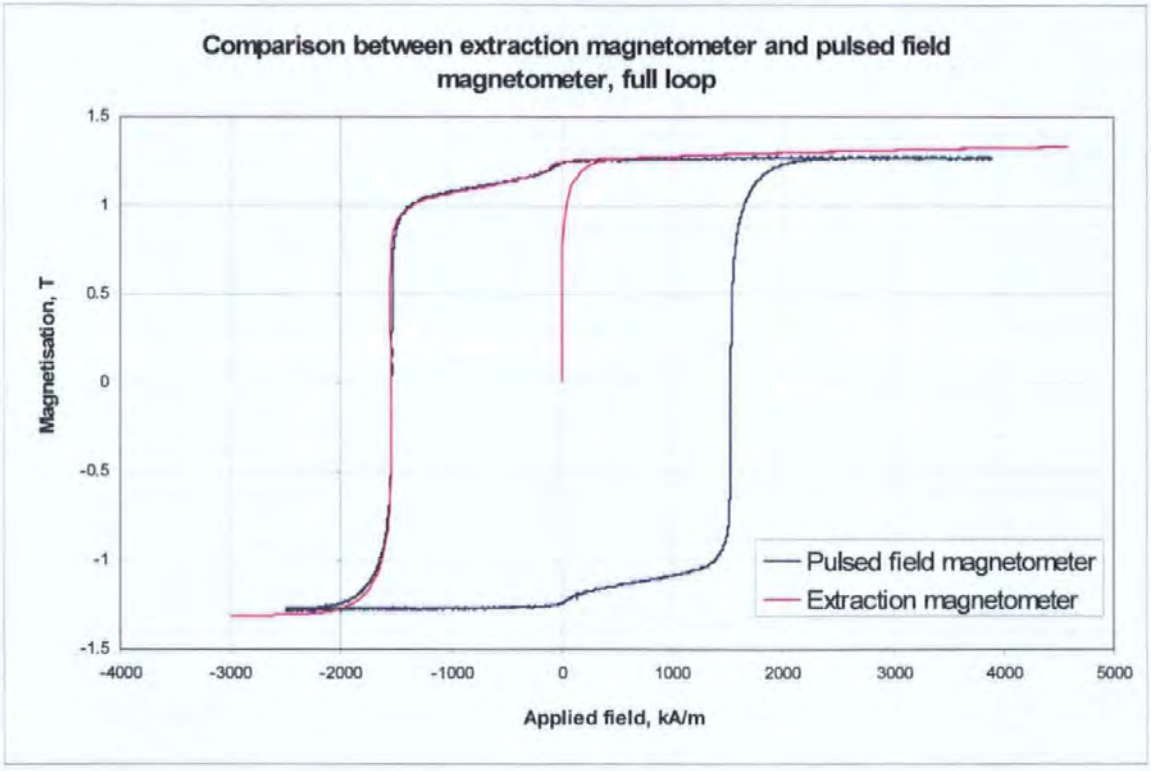


*Figure 69 - Comparison of a "small magnet" measured with a super conducting, extraction method magnetometer and a PFM.*

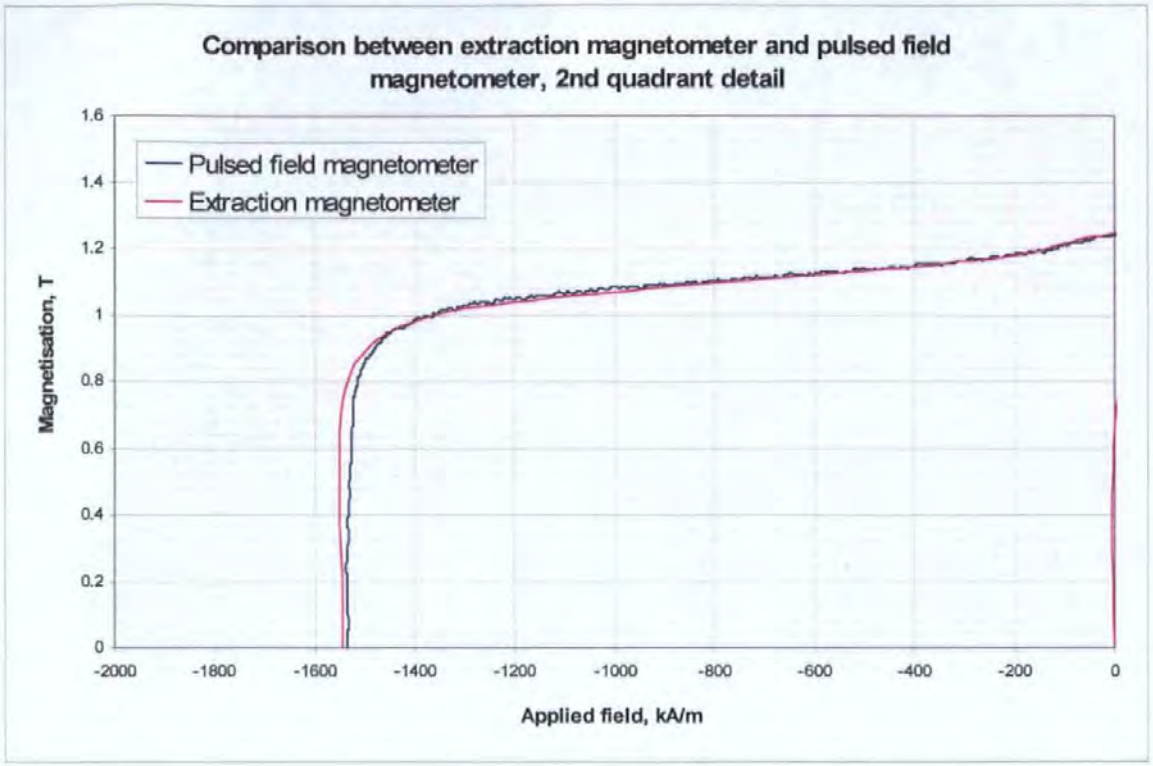


*Figure 70 - 2nd quadrant detail comparison of a "small magnet" measured with a super conducting, extraction method magnetometer.*

The results from the PFM system agree quite closely with the results from the extraction magnetometer. Some differences exist in the high-applied field regions where it appears the extraction magnetometer has "rotated" the data adding an artificial slope to the saturated region, which should be flat. The data in the demagnetisation quadrant does however show good correlation between the two measurement systems. Although it has not been possible to have a repeat measurement on the extraction magnetometer, CNRS Grenoble agree that the slope is an artefact of their extraction magnetometer, due to integrator drift, and not a function of the magnetisation of the magnet.

A comparison between a NIM2000 permeameter and a PFM system was also performed. The NIM2000 is manufactured by the Chinese National Institute of Metrology. A number of Neodymium iron boron magnets were tested on the NIM2000 system at the Chinese National Institute of Metrology. These magnet samples were transported to the

experimental Pulsed Field Magnetometer in Falmouth, England where a comparison was performed. The samples were all 10 mm diameter by 10 mm long cylinders. Table 12 shows the measured results from both the NIM2000 and the PFM system. Table 13 shows the agreement between the two systems for each material.

| Material | NIM2000 | | | PFM | | |
|---|---|---|---|---|---|---|
| | $B_R$ (T) | $H_{CI}$ (kA/m) | $BH_{MAX}$ (kJ/m3) | $B_R$ (T) | $H_{CI}$ (kA/m) | $BH_{MAX}$ (kJ/m3) |
| **Nd154** | 1.320 | 1583 | 321 | 1.318 | 1571 | 323 |
| **Nd153** | 1.371 | 1128 | 347 | 1.362 | 1131.2 | 343 |
| **Nd155** | 1.313 | 1579 | 317 | 1.311 | 1539 | 320 |
| **Nd152** | 1.367 | 1122 | 346 | 1.363 | 1108 | 346 |
| **Nd157** | 1.188 | 2191 | 261 | 1.185 | 2176 | 262 |
| **Nd159** | 1.212 | 2176 | 272 | 1.216 | 2174 | 275 |

*Table 12 - Comparison of measurement results between NIM2000 permeameter and a PFM system.*

| Material | Agreement | | |
|---|---|---|---|
| | $B_R$ | $H_{CI}$ | $BH_{MAX}$ |
| **Nd154** | 0.152 % | -0.758 % | -0.465 % |
| **Nd153** | 0.661 % | -0.283 % | 1.166 % |
| **Nd155** | 0.293 % | 1.227 % | -0.029 % |
| **Nd152** | 0.253 % | 0.680 % | -0.305 % |
| **Nd157** | 0.253 % | 0.680 % | -0.306 % |
| **Nd159** | -0.329 % | 0.064 % | -1.127 % |

*Table 13 - Agreement of results presented between a NIM2000 permeameter and PFM system.*

The results show a good agreement especially for $B_R$. Larger differences exist with the comparison of $H_{CI}$. One possible source for these differences is temperature. NdFeB

magnets typically exhibit a temperature coefficient for $H_{CI}$ of between 0.6 % and 1 % per °C. Therefore a difference of 2 – 3 °C between the sample temperature in the permeameter and the PFM could account for the difference. Another possible source for the difference is repeatability. A PFM typically has higher system repeatability than a permeameter, as discussed in Section 10.2. Permeameters repeatability is typically around 1%, as shown in Table 19, and the variation due to this repeatability alone could account for the majority of the differences between the PFM and the permeameter, with a repeatability contribution from the PFM as well the entire difference could be repeatability distribution. Another very important potential source for the difference is the fundamental limitation of the permeameter. As discussed throughout this thesis permeameters are not suitable for generating the high fields necessary to determine $H_{CI}$ for very hard rare earth magnets. Of the batch of magnets compared, the highest $H_{CI}$ value is 2192 kA/m and this would therefore require an applied field of 2.75 T which is extremely high for a permeameter. However there is no correlation between values of $H_{CI}$ and agreement between the two systems so it is likely that the differences are a combination of temperature effects on the sample and repeatability distribution of the two systems.

## 10.2 Repeatability

To assess the repeatability of the prototype PFM system a single sample was measured many times and the data recorded in full for each measurement. The data was processed and the results for $B_R$, $H_{CI}$ and $BH_{MAX}$ obtained. These points were compared between the measurements and analysed to determine the distribution of data throughout the system. It should be noted that the repeatability measurement is based on the total performance of the measurement system. Individual components have not, at this stage, been assessed for their contribution to the measurement uncertainties.

For the purpose of the analysis, only data points of high importance are considered, these measurement points are remanence ($B_R$), intrinsic coercivity ($H_{CI}$) and the maximum energy product ($BH_{max}$). It is these values that are considered pertinent and are the characteristic points quoted on magnet data sheets and used for design specifications. It should also be noted that $B_R$ occurs at $\boldsymbol{H} = 0$ and $H_{CI}$ occurs at $\boldsymbol{J} = 0$, so these values will assess the individual **J** and **H** measurement channels performance while $BH_{MAX}$ will assess a combined performance.

The sample measured was a HF24/23 hard ferrite of cuboid form and dimensions 12 mm x 12 mm x 6 mm (height). A hard ferrite was chosen for the test instead of a rare earth magnet so that the same magnet could be measured by a conventional system such as a permeameter for comparison. A total of 334 readings were made over a period of 3 days. The ferrite was run through the entire f/2f process even through the eddy currents within the ferrite are very low. This was in order to make the repeatability testing representative for all types of specimen including those that require f/2f processing to remove the effects of eddy currents. The actual results of the f and 2f measurement for the ferrite show good agreement and the difference between the measurements is within the noise band of the measurement system.

Figure 71 shows the JH characteristics of the sample used for the measurement and Table 14 summarises the measurements in terms of $B_R$, $H_{CI}$ and $BH_{MAX}$.

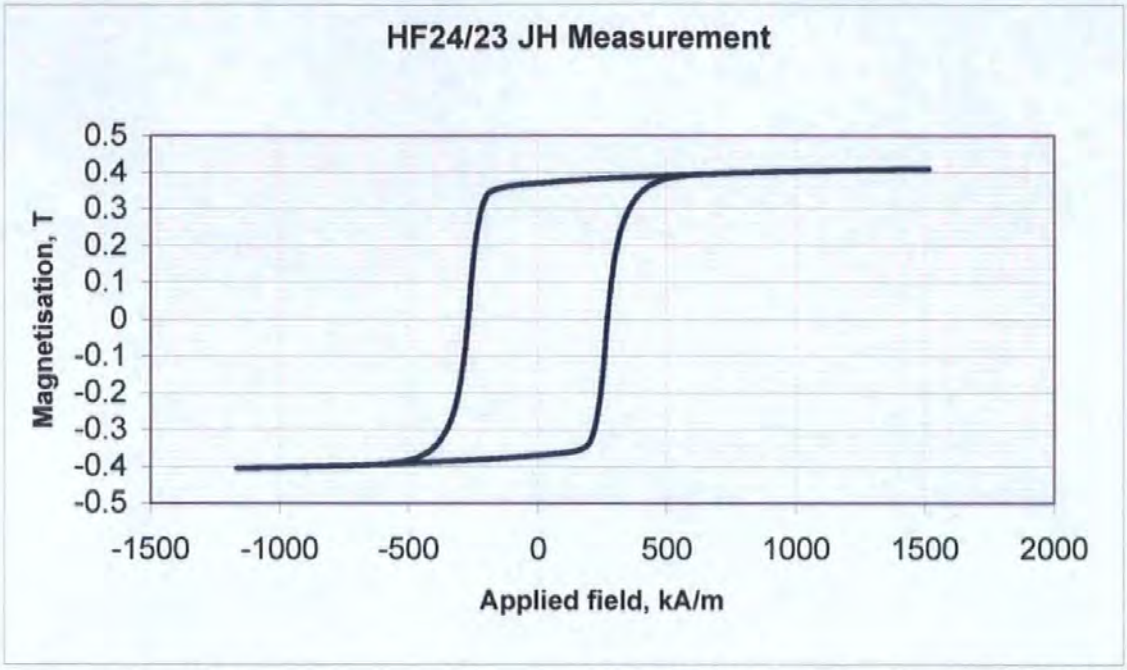


*Figure 71 - JH characteristics of the specimen of HF24/23 used for the repeatability analysis.*

| Parameter | $B_R$ (T) | $H_{CI}$ (kA/m) | $BH_{MAX}$ (kJ/m$^3$) |
|---|---|---|---|
| **Mean** | 0.355 | -230.26 | 23.55 |
| **Maximum** | 0.356 | -220.50 | 23.76 |
| **Minimum** | 0.353 | -234. 99 | 23.38 |
| **Spread** | 0.00296 | -14.49 | 0.380 |
| **Standard deviation** | 0.00057 | 4.29 | 0.074 |

*Table 14 - Results of 334 measurements of HF24/23. The critical parameters were automatically extracted by the measurement software.*

To calculate the repeatability it is necessary to know the full scale reading for the measurement range used. The J and H integrators and the analogue to digital converter (A/D) both have a maximum input level and in a well designed system this is matched to facilitate maximum use of the dynamic range. As these two components are the limiting factor for the full scale range it is not unreasonable to assume that when these devices are at their maximum, that is the maximum value that can be measured. The maximum output of the A/D converter is a known constant for a particular device. If the A/D converter value

is scaled by the system calibration constants, that converts A/D counts into magnetic units, then the full scale reading can be calculated. This calculation is given by the equation,

$$F = \frac{\alpha}{\beta} \times C \tag{12.1}$$

where $F$ is the full-scale reading, $\alpha$ is the maximum analogue to digital converter value and $C$ is the calibration constant and $\beta$ is the gain selected. It does not matter if the calibration constants are incorrect as the same calibration constant is used for the measurement of repeatability and full scale range determination, therefore the calibration constant will cancel out.

The calibration constants in place at the time of the measurement and the selected measurement range are given in Table 15. It should be noted that the J range is on x10000 which is the most sensitive and the H range is suitable for the measurement of any material on the PFM system. Therefore the results are valid as an indication of the performance of the PFM and not just a particular range. Based on the values in Table 15, Table 16 shows the calculated full-scale ranges, which provide the necessary data to calculate the repeatability which is shown in Table 17.

| | **J** | **H** |
|---|---|---|
| **Calibration constant** | 4.279 | 0.397 |
| **Full scale AD count** | +/-8192 counts | +/-8192 counts |
| **Integrator range** | x10000 | x500 |

*Table 15 - Calibration constants and range selection in force during the repeatability analysis.*

| | |
|---|---|
| **J** | 3.506 T |
| **H** | 5148.5 kA/m |

*Table 16 - Full scale range values for the J and H channels as determined by maximum A/D value and calibration constants.*

| | $B_r$ | $H_{CI}$ |
|---|---|---|
| **Repeatability** | 0.084 % | 0.281 % |

*Table 17 - Determined repeatability values, expressed as a maximum spread of a percentage of full scale range, for the prototype industrial Pulsed Field Magnetometer system.*

The repeatability is better that the target maximum of 1 %. The repeatability of $B_R$ is an order of magnitude better than $H_{CI}$ and this is likely to be sample temperature related. Both channels have repeatability better than the typical 1 – 2 % of a permeameter system.

### *10.2.1 System and sample repeatability*

It should be noted that the repeatability discussion in section 12.2 was based on system repeatability, that is the repeatability is considered as a deviation with respect to the full scale range of the measuring equipment. It is very common to also assess repeatability based on sample by sample variation with respect to the mean value of the batch being tested.

If the data in Table 14 is again considered and the repeatability is calculated as a function of the spread with respect to the mean then Table 18 shows the results of sample repeatability.

| Parameter | $B_R$ | $H_{CI}$ | $BH_{MAX}$ |
|---|---|---|---|
| **Sample Repeatability** | +/- 0.415 % | +/- 3.14 % | +/- 0.805 % |

*Table 18 - Sample repeatability for 334 ferrite HF24/23*

From the results in Table 18 it can be seen that the sample repeatability for $B_R$ and $BH_{MAX}$ are better than 1%. The sample repeatability for $H_{CI}$ shows a greater variance. Ferrite exhibits large temperature dependence for values of $H_{CI}$ and as the sample temperature was uncontrolled and not measured it is likely that this is the source of the variation. Like most permanent magnet materials the temperature coefficients for $B_R$ are an order of magnitude smaller than $H_{CI}$ hence why $B_R$ has not been adversely effected in the same manor as $H_{CI}$. The reasons for increased variation in $H_{CI}$ are discussed further in the next section.

### *10.2.2 Distribution of data*

When considering factors such as repeatability it is desirable to analysis the data further to check for abnormalities that may have caused distortion of the results. It also provides an insight into the causes of any measurement errors. The distribution of the data is a function of the measurement errors in the system and one source of error, not considered previously is "noise". Noise is present in all electrical equipment, and in measuring equipment it should be understood so that the limitations of the equipment are known. There are many sources of noise with the most common being :-

- Air-born electromagnetic interference (EMI).
- Ground-born, fluctuations in the ground/earth voltage.
- Thermal noise, internal to passive and semiconductor components.

Due to the nature of PFM, poor design alone can be a source of both air-born EMI and ground-born interference. The most fundamental problems are often earthing problems and

associated ground loops. These can be avoided by following published international standards on electronic machine earthing conventions. It is also important to have instrumentation that has been designed correctly. With large gain stages required to amplify small signals to acceptable levels, any noise before the amplification stage will bury the required data in unacceptable noise. Instrumentation should also have shielding against EMI and take other design precautions to minimise the effect of any EMI picked up. Good design can also minimise the generation and susceptibility to thermal noise. The topic of electronic instrumentation design, although very important, is considered outside the scope of this thesis and will not be discussed further.

Electrical noise may not be the only source of error. In this analysis it is assumed that the magnet sample is 100 % repeatable and any deviation is a fault of the measuring system. Magnets will undergo changes due to oxidation, the ambient temperature, stress history, fatigue and internal microstructure changes. It is not unreasonable to assume that due to the short time span of the experiment the effects of oxidation, fatigue and structural changes can be assumed insignificant but the effect of ambient conditions cannot be ignored. In Section 2.5, Table 5 shows a typical variation of 0.2 %/K for values of $B_R$ (remanence) is shown. The industrial PFM did not implement sample temperature control. Therefore, during the repeatability analysis it would be expected that the sample's temperature be related to ambient conditions thus introducing a potentially large non-measurement system induced error.

Perfectly random noise will produce a normal distribution plot. If the distribution is not normal, this would indicate that a stimuli other that random noise is having an effect on the repeatability and possible the accuracy of the data.

Figures 72 and 73 show the distribution of the remanence ($B_R$) and the intrinsic coercivity ($H_{CI}$) data. It can be seen from the shape of Figure 72 that the distribution is similar to a normal distribution; this would indicate that the scattering of data on the J channel is due to purely low level instrumentation noise.

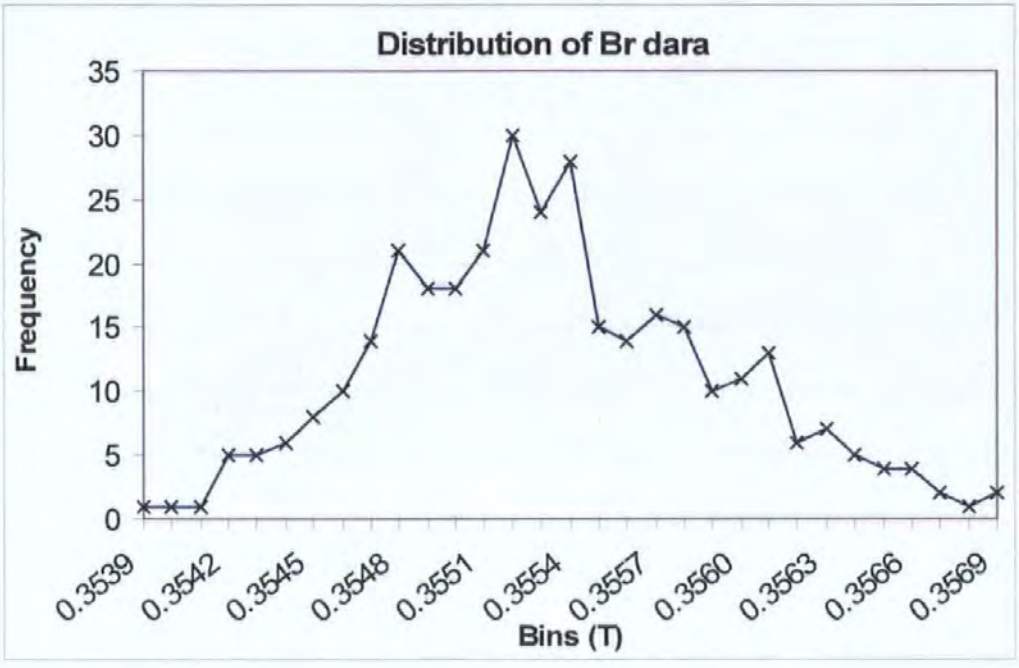


*Figure 72 - Distribution plot of remanence data, $B_R$*

Figure 73 has an unusual shape that does not agree with a normal distribution. It would indicate that there are "preferred" locations for the data and that there is an influence other than simple noise causing the spread of the data. The source of these preferred locations is currently unknown.

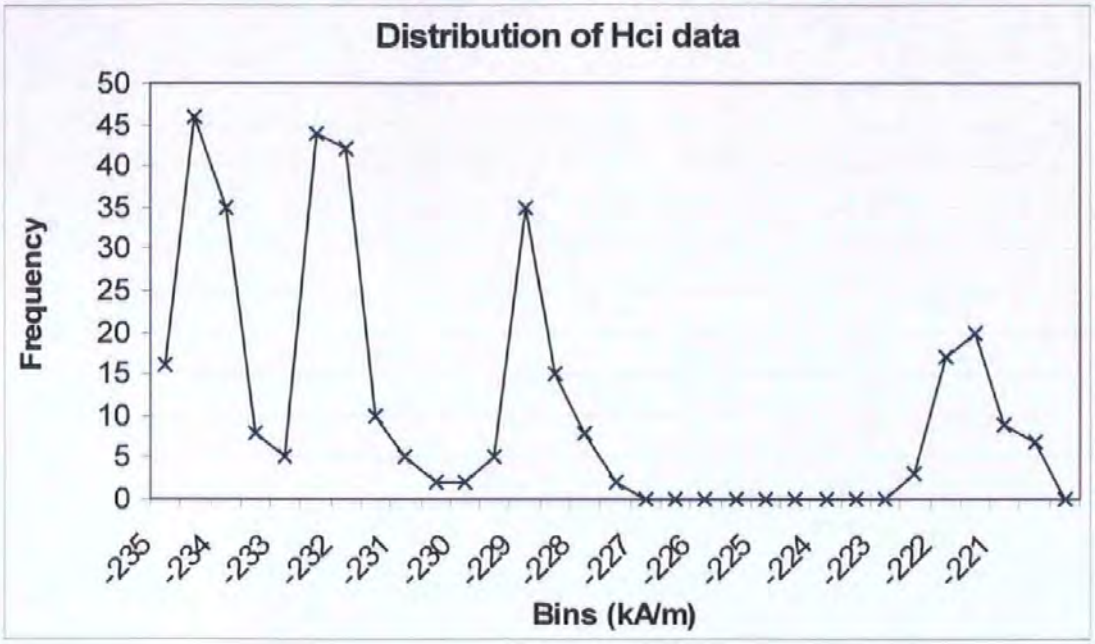


*Figure 73 - Distribution of intrinsic coercivity data, $H_{CI}$*

As the electronics for the J and H measurement channels from the output of the pickup coils to the analogue to digital converter is identical in design, it would be expected that similar characteristics are present in both channels. Therefore, it is assumed that the problem is either related to the pickup coil system or is a magnet property. As the specimen temperature is uncontrolled these preferred locations may be related to temperature effects within the sample, where a change in sample temperature produces "preferred" values for $H_C$.

## 10.3 Comparison to other equipment manufacturers

The goal of the Pulsed Field Magnetometer project was not just to prove the method was scientifically viable but to build, design and test/characterise a system that industry would accept. The main objective was to provide a modern replacement for the permeameter, which is unsuited for modern permanent magnet materials, as discussed in Chapter 3. For industry to accept new technology it must be beneficial and also to add value to their product or reduce costs. Table 19 show the comparison between the repeatability and

accuracy of the PFM system and various commercially available permeameter / hysteresisgraph systems.

| Manufacture | Equipment Type | Repeatability | Accuracy |
|---|---|---|---|
| **Hirst Magnetic Instruments Ltd** | PFM 21 | 0.281 % | +/-1.2 % |
| **Lakeshore [38]** | 7800 Hysteresisgraph | 0.5 % | 1 % |
| **Walker LDJ Scientific Ltd [39]** | AMH-5 Hysteresisgraph | 0.5 % | 2 % |
| **Hirst Magnetic Instruments Ltd [40]** | ARP03 Hystetesisgraph | 1 % | 1 % |

*Table 19 - Comparison of a PFM's accuracy and system repeatability with commercially available permeameter/hysteresisgraph systems*

From the results in Table 19 it can be seen that the PFM is achieving an accuracy that is comparable to permeameter systems and a repeatability that is significantly better. These results are very good for the technology of PFM and demonstrate that the design methods, tools and system improvements to the methods of Pulsed Field Magnetometers as discussed in this thesis are valid.

# Chapter 11 Conclusions and further work

With rare-earth based magnet materials becoming increasingly popular and finding uses in increasing numbers of safety critical and other systems that cannot afford to fail; this thesis has addressed the need for a method of industrial quality control for rare earth based magnet materials. Conventional magnetic measurement techniques are not suited to the measurement speed requirements of industry, and in the case of the industry "standard", the permeameter, are insufficient to measure rare earth materials. The magnetic field levels required for the saturation and demagnetisation of rare earth materials are just too high for closed loop electromagnet based systems that rely on iron and iron alloys with maximum saturations around 2.5 Tesla. The high speed requirement of industry also prohibits the permeameter due to its relatively slow measurement period of a few minutes per sample. Coupled with size and shape limitations this makes the permeameter totally unstable for quality control of rare earth, or high volume, magnet production.

## 11.1 Design

The design of Pulsed Field Magnetometry systems has previously been somewhat of a "black art" and this thesis has presented systematic methods for the design of various sub systems of a Pulsed Field Magnetometer, as well as locating sources of error and discussing methods to reduce or eliminate these errors by design or data processing. Methods have been presented for the systematic design of field generation coils so that the field level, homogeneity and electrical characteristics can be determined and modelled at design time, reducing commercial uncertainty and cost. Pickup coils have been examined in detail with methods for designing a homogenous radial gradient coil presented. Data processing has also been considered in detail and methods proposed and demonstrated to overcome the effects of eddy currents, self demagnetisation fields and zero signals.

The methods presented here were used to build a prototype PFM system as part of a European research project [2]. The prototype system, although functional enough to provide the results for the measurement comparisons, still was not suitable for a commercial product due to additional errors and problems encountered at an early stage. These problems were mainly to do with the pickup coil design and overcome once the methodology presented in Chapter 6 was developed. Once the initial limitations were overcome; a high speed, proof of concept system, optimised for industrial quality control was constructed and used to assess the viability of Pulsed Field Magnetometry in industry.

## 11.2 Measurement comparison

The comparison of measurements between the PFM system and the two static methods shows very good agreement. Permeameters are limited, with hard magnetic materials, to the demagnetisation quadrant only, so a full loop comparison in this case is not possible. However, for one quadrant, comparison was possible and the results agree very well. The deviations that occur towards the top right of the permeameter curve highlight limitations of the permeameter and not of the PFM. The measurement results from the extraction technique also show good agreement with the PFM measurement. The extraction technique is a long process and it is possible to see the effects of integrator drift in the results as a rotation of the hysteresis curve. What is most important in these comparisons is that the shape of the hysteresis curve is unchanged. The method of PFM does not distort the shape of hysteresis curve and the methods of calibration appear to be successful.

The comparison between the NIM2000 permeameter and the PFM system shows good agreement, typically better than +/- 1.2 %. These results prove that a PFM is capable of measuring the same data as a permeameter and that the perceived problems of eddy current effects and open loop measurements can be compensated for and useful results obtained.

The repeatability analysis proves that a PFM system is more repeatable compared to a closed loop system such as a permeameter, even when additional sources of error are reducing the PFM's repeatability. This is a major benefit for the technology. With additional safeguards and improvements to instrumentation noise floors and sensitivity it is expected that this figure still has room for improvement.

## 11.3 Data processing

As well as improvements to the physical design of Pulsed Field Magnetometers, large improvements have also been made in the area of data processing. It is the perceived problem of eddy currents during the measurement that is the largest cause of resistance to the adoption of the technique and it is in the removal of eddy currents that large improvements have been accomplished. Eddy currents can be successfully removed from various rare earth and ferrite materials and significant improvements made with highly conductive and magnetically soft materials such as nickel.

Self-demagnetisation factors have always been an issue for open circuit measurement techniques. They are often ignored when using VSMs but require correction for PFM measurements, where manufacturer's data is often given as closed loop derived BH curves. While the actual self-demagnetisation correction is trivial, the developments in determination of self demagnetisation factors for different shapes, for use in PFM and the knowledge of the potential problems of differential permeability has greatly eased the implementation.

## 11.4 Overall conclusions

Pulsed Field Magnetometry has matured into a viable commercial technique. It has been demonstrated that the system can be used for the quality control industrial magnets in an industrial environment at cycle times exceeding 5 seconds. The methods presented in this

thesis have all been put to test in the construction of a prototype industrial system that has successfully completed trials in industrial environments. This has been possible thanks to the improvements in design of pulsed field components and data processing software developed as part of the research described here. On going work hopes to build upon these achievements to further improve the technique and diversify the range and types of specimens that can be measured.

## 11.5 Future work

Despite the achievements in the development and construction of a Pulsed Field Magnetometer system that are discussed in this thesis, there are still many aspects which can be improved upon. The most notable areas are :-

- Calibration
- International standards for PFM technology
- Eddy current processing improvements
- Self demagnetisation correction improvements

### *11.5.1 Calibration*

Currently two major calibration problems exist. One is the determination of the calibration constant of the H pickup coil and the other is the determination of the calibration constant for the J pickup coil.

The H coil is a simple pickup coil but due to its construction, mounting and size it cannot be directly calibrated in an electromagnet and instead a calibration must be inferred via another device. Because of this limitation the H coil cannot be calibrated directly against NMR, or squid systems as these devices have particular field homogeneity and stability requirements. As discussed in Chapter 8 "Calibration", additional pickup coils have been used to successfully transfer the calibration from an NMR, in an electromagnet, to the PFM H coil. Work is ongoing to determine how this technique contributes to the uncertainties.

The J pickup coil presents greater calibration problems than the H coil. As the J pickup is a gradient coil, the calibration constant is essentially the coil coupling constant. Methods for the determination of the J calibration factor were presented in Chapter 8, but these methods also rely on the transfer of calibration data through methods such as standard samples, which may be effected by time and environmental conditions.

Absolute calibration and traceability remain an issue for Pulsed Field Magnetometers. Discussions with the National Physical Laboratory (NPL) have begun to look at alternative calibration methods or adaptation to existing methods to allow NPL to calibrate subsystems or to calibrate calibration coils/samples so that internationally acceptable calibration certificates can be issued for Pulsed Field Magnetometers providing accuracy and uncertainty figures. As part of this work, it is expected that each measurement system component will be assessed for its contribution to the total uncertainty and that a total uncertainty budget can be systematically discovered.

### *11.5.2 International standards*

International standards are considered highly important for the acceptance of PFM technology. Convention magnetic characterising techniques, such as permeameters and VSMs, are governed by standards with guidelines on equipment and measurement processes.

Due to the successful demonstration of the industrial Pulsed Field Magnetometer, work has started on the creation of an international (ISO) standard. Working with the International Electrotechnical Commission (IEC) and the British Standards Institute (BSI) a technical report has been created [22] that should form the basis of a full international standard. This will state how pulse field measurements will be taken and specifying the type of measuring

equipment to use. The standard will state methods of measurement and include details of appropriate pickup coils, give examples how eddy current effects can be removed and provide the initial basis for the work on PFM calibration standards.

### *11.5.3 Eddy currents*

The eddy current correction process, as discussed in Section 7.5 has proved itself as highly effective in the removal of the effects of eddy currents in pulsed measurements, but improvements can still be made. When attempting to correct a magnetically soft material, such as nickel, the resultant output from the eddy current removal process shows that a higher order term may be missing. It is suspected that there is an inductive effect due to the eddy current path having a finite length, the equivalent to a single turn winding and this causes the error. In the correction process it is assumed eddy currents are a direct consequence of the rate of change of applied field and the rate of change of magnetism, but the rate of change of eddy currents is neglected.

Section 6.4 discussed zero signals and their origin, i.e. eddy currents within the field generation coil's copper windings. Work is ongoing in the minimisation of these eddy currents and methods such as reducing the cross section of the copper wire and using multifilament individually insulated stranded wire is under investigation. This type of wire is commonly used in high frequency applications to minimise the losses due to eddy currents and it is believed that it may reduce the zero signal on PFM systems by reducing the effects of eddy currents.

### *11.5.4 Self demagnetisation factors*

Self-demagnetisation factors remain a potential issue for open loop measurement systems. The method of a global average demagnetisation factor appears to work satisfactorily, as can be seen from the accuracy comparison, but there is still concern over differential permeability effects. The effects are caused by the magnet's magnetisation causing a non-

uniform permeability by placing different parts of the magnet at different working points. Further work is necessary to quantify the magnitude of this effect, as well as other comparisons between open and closed loop systems, to assess any additional impact of the self-demagnetisation effect correction process.

A remaining problem with self demagnetisation factors is the calculation of the factor for irregular shapes. It is believed that a magnet can be modelled in a finite element package and the demagnetisation factor determined by looking at the angles of the flux lines through out the magnet. Some thoughts on the modelling of self demagnetisation effects are given below. This represents some initial ideas and further work is needed to verify and expand this modelling.

If Equation 6.1, from Section 7.3, is modified to allow for the components of the J vector then the flux density inside magnet is given by;

$$J_{int} = J.\cos\phi.\cos\theta + \mu_0 H \qquad (11.1)$$

where $\phi$ is the angle of the flux line with respect to the x axis and $\theta$ is the angle of the flux line with respect to the z axis. The value $cos\ \phi.cos\theta$ should be N, the self-demagnetisation factor. As neither $J$ nor $\phi$ are constant over the volume of the magnet, it is necessary to divide the volume into small blocks over which $J$ and $\phi$ can be considered constant. If there are M blocks then block i is given by,

$$J_{int\,i} = J_i.\cos\phi_i.\cos\theta_i + H\mu_0 \qquad (11.2)$$

It should be noted that Pulsed Field Magnetometry measures the total magnetisation of the magnet and hence measures $\sum_{i=1}^{m} \mathbf{J}_i$ or just $J$. If the angular terms are considered separately then a global self demagnetisation factor can be defined as,

$$N=\sum_{i=1}^{m}\cos\phi_i.\cos\theta_i \tag{11.3}$$

The self-demagnetisation equations can then be reduced to,

$$J_{int} = J + N\mu_0 H \tag{11.4}$$

The term $N$ is also referred to as the ballistic demagnetisation factor. The self-demagnetisation factor, $N$, depends on the geometry of the test specimen. Irregular shapes can have their global demagnetisation-factors calculated using a finite element method to determine the angles of flux, $\phi$ and $\theta$ over a number of elements that represent the magnet shape being considered.

### *11.5.5 Other magnetic materials*

The PFM system was designed primarily for industrial sized, rare earth magnets that required large applied magnetic fields to characterise. It was believed that the majority of samples to be tested would be large single components, such as magnet segments from motors. During the project it has become apparent the high speed and high field nature of the technique has attracted interest from groups wishing to measure soft magnetic materials for quality control and also from groups wishing to characterise thin films and other materials that normally would require a super-conducting vibrating sample magnetometer.

Soft magnetic materials, such as SMC materials from compressed iron powder, are finding increasing uses replacing conventional iron as motor and generator core material. The materials have low conductivity and can be made into complex shapes, unlike standard iron laminations. Work has begun to use technology from the PFM to build a quality control system for SMC components. By applying low fields around 10 - 100 mT at frequencies up to 50 kHz it is anticipated that the eddy current correction process, as

described in Section 7.5.2, can determine the magnetic properties and the conductivity of the material and this information be used for quality control purposes.

Thin films are typically nanometres thick and therefore have a magnetic moment that is considerably smaller than the 5 mm diameter x 5 mm long samples that were stated as the minimum for the industrial PFM. Many thin films consist of rare earth materials and therefore required fields greater than can be produced by a standard electromagnet system. Typically a superconducting VSM is used to characterise these materials because of its extremely high sensitivity and high field capability. PFM systems are capable of the high fields necessary but it would be necessary to design a highly sensitive pickup coil and use modified instrumentation to detect and amplify the magnetisation signal. Part of the ongoing work is to determine the sensitivity limits of PFM technology in order to determine the smallest possible sample size that can be characterised and to develop improved sensors and instrumentation to aid this process.

### *11.5.6 Further system improvements*

Examining the results presented in Section 10.2.2, Figure 73, it was seen that the distribution of the results has an unusual characteristic and this requires further investigation to discover the source of this particular error, as there is a 330 % difference in the repeatability between the two measurement channels. It is anticipated that this work will involve providing a temperature-controlled environment for samples to determine if temperature variation of the samples is causing this effect.

A major draw back for potential buyers of PFM technology is the size of the prototype industrial unit. Further work has begun in reducing the size of the system to a single applied field and pickup system with higher speed charging, mechanical handling and data

processing. This should reduce cost, complexity and remove any issue of measurement tractability between multiple pickup coils, as only one will be used for f and 2f measurements. This should increase the viability and potential benefits of the system.

## 11.6 Ongoing work

The Industrial PFM system described in this thesis has proved technically successful and the results demonstrate the system is suitable for industrial quality control applications. The PFM system discussed here was only intended as a prototype system to test the system in an industrial environment. The components were designed and built specifically for this application and items such as the pickup coils, magnetisation coils, data processing and calibration procedures were all developed for this application and as part of this thesis.

Commercially the prototype system is too expensive. The next generation of Industrial PFM systems are building on the results of the prototype system to simplify and reduce the cost of pulse field magnetometers. The field generation multi coil system is to be replaced with a single coil, with improved cooling and manual or automatic loading options are to be added. The automatic loading system will be based on linear cylinders which will replace the rotating table system previously used. With only one coil to load/unload the mechanical handing becomes simpler and cheaper. The high voltage electronics will be based on the principle used in the prototype machine. The high voltage components selected for the industrial prototype were conservatively selected and lower rated cheaper devices could be selected reducing cost further.

Based on the demonstration and results of the industrial prototype PFM and the improvements made to the technology as a consequence of the work this thesis describes, there are currently orders for 3 of the next generation systems and this demand is expected to grow over the next year.

# References

[1] Croat John Joseph, General Motors Corporation, "High energy product rare earth-transition metal magnet alloys containing boron," E.U. Patent EP0144112-1985-06-12, June, 1985.

[2] "MACCHARACTEC", E.U 4th framework project SMT4-CT98-2212.

[3] P. Bretchko and R. Ludwig, "Open loop Pulsed Hysteresis Graph System for the Magnetisation of Rare-Earth Magnets," *IEEE Transactions on Magnetics*, vol. 36, No. 4, pp. 2042-2051, July 2000.

[4] R Grossinger, B Wittig, M Kupferling, M. Taraba, G Reyne, C. Golovanov, B. Enzberg-Mahlke, W. Fernengel, P. Lethuillier and J. Dudding, "Large bore Pulsed Field Magnetometer for characterizing permanent magnets," *IEEE Transactions on Magnetics*, Vol. 35, No. 5, pp. 3971-3973, September 1999.

[5] R. Cornelius, J. Dudding, P. Knell, R. Grossinger, B. Enzberg-Mahlke, W. Fernengel, M. Kupferling, M. Taraba, J.C. Toussaint, A. Wimmer and D. Edwards, "A Pulsed Field Magnetometer for Industrial Use," *IEEE Transactions on Magnetics*, Vol. 38, No. 5, pp. 2462-2464, September 2002.

[6] E. Bogardus, R. Scranton and D. Thompson, "Pulse magnetization measurements in ferrofluids," *IEEE Transactions on Magnetics*, Vol. 11, No 5, pp. 1364 –1366, Sep 1975.

[7] R Grossinger, Ch. Gigler, A. Keresztes and H. Fillunger, "A Pulsed Field Magnetometer for the Characterization of Hard Magnetic Materials," *IEEE Transactions on Magnetics*, Vol. 24, No. 2, pp. 970-973, March 1998.

[8] R Grossinger, G.W Jewell, J Dudding and D. Howe, "Pulsed Field Magnetometry, " *IEEE Transactions on Magnetics*, Vol. 29, No. 6, pp. 2980-2982, November 1993.

[9] Min-Seok Song, Yoon-Bae Kim, Chang-Suk Kim and Taik-Kee Kim, "Measurement Accuracy of a Pulsed Field Magnetometer Designed for Rare Earth Based Permanent Magnets," *IEEE Transactions on Magnetics*, Vol. 36, No. 5, pp. 3637-3639, September 2000.

[10] G.W. Jewell and D. Howe, "A Method for Assessing Eddy Current Effects in Pulsed Magnetometry," *IEEE Transactions of Magnetics*, Vol. 28, No. 5, pp. 3114-3116, September 1992.

[11] C. Golovanov, G. Reyne, G. Meunier, R. Grossinger and J. Dudding, "Finite Element Modelling of Permanent Magnets Under Pulsed Field," *IEEE Transactions on Magnetics*, Vol. 37, No. 4, pp. 1222-1225, July 2000.

[12] R. Grossinger, M. Kupferling, P. Kasperkovitz, A. Wimmer, M. Taraba, W. Scholz, J. Dudding, P. Lethuiller, J.C. Toussaint, B. Enzbery-Mahlke, W. Fernengel and G. Reyne, "Eddy Currents in Pulsed Field Measurements," *Journal of Magnetism and Magnetic Materials*, Vol 242-245, Part 2, pp. 911-914, April 2002.

[13] G. Jewell, "Eddy current correction procedure," HMI Report, 1993.

[14] D. Chen, J.A. Brug and R.B. Goldfarb, "Demagnetizing Factors for Cylinders," *IEEE Transactions on Magnetics*, Vol. 27, No. 4, pp. 3601-3615, July 1991.

[15] R.I. Joseph and E. Schlomann, "Demagnetizing field in nonelliposidal bodies," *Journal of Applied Physics*, Vol 36, pp. 1579-1593, May 1965.

[16] R.I. Joseph, "Ballistic demagnetising factor in uniformly magnetised cylinders," *Journal of Applied Physics*, Vol 37, pp. 4639 - 4643, Dec 1966.

[17] H. Krug, M. Doerr, D. Eckert, H. Eschrig, F. Fischer, P. Fulde, R. Groessinger, A. Handstein, F. Herlach, D. Hinz, R. Kratz, M. Loewenhaupt, K.H. Müller, F. Pobell, L. Schultz, H. Siegel, F. Steglich and P. Verges, "The Dresden high-magnetic field laboratory – overview and first results," *Physica B*, Vol 294-295, pp. 605 - 611, 2001.

[18] G. Asti and S. Rinaldi, "Singular points in the magnetization curve if a polycrystalline ferromagnet," *Journal of Applied Physics*, Vol 45, Issue 8 , pp. 3600 – 3610, Aug 1974.

[19] R. Grossinger, P. Obitsch, H. Kirchmayr and F. Rothwarf, "Magnetic anisotropy studies of permanent magnets," *IEEE Transactions on Magnetics,* Vol Mag-20, No 5, pp. 1575 – 1577, Sep 1984.

[20] K. Okuno, T. Kato, Y. Takahashi, F. Iida, H. Tsuji, T. Hiyama, S.S. Shen, J.W. Lue, M.S. Lubell and S. Shimamoto, "Experimental results on the Japanese LCT coil in the IFSMTF: Pulsed field tests and extended-condition tests," *IEEE Transactions on Magnetics*, Vol. 24, No 2, pp. 767 - 770, March 1988.

[21] R. Grössinger, M. Taraba, A. Wimmer, J. Dudding, R. Cornelius, P. Knell, P. Bissel, B. Enzberg-Mahlke, W. Fernengel, J. C. Toussaint, and D. Edwards, "Calibration of an Industrial Pulsed Field Magnetometer," *IEEE Transactions on Magnetics*, Vol 38, No 5, pp. 2982 - 2984, September 2002.

[22] "Pulsed Field Magnetometry," Technical Report, BS PD IEC/TR 62331:2005, 2005.

[23] National Imports magnetic products division, "History of Magnetism and Electricity," http://www.rare-earth-magnets.com/magnet_university/history_of_magnetism.htm, 2002.

[24] S. J Lillywhite, A. Walton, A. J. Williams, I. R. Harris, D. J. Kinsey, G. W. Jewell and D. Howe, "An investigation into the corrosion behaviour of Zn coated NdFeB powder," in *International Magnetics Conference Digest of Technical Papers*, 2003, pp. BE12.

[25] Applied Alloy Chemical Group University of Birmingham, "History of Magnetism," http://www.aacg.bham.ac.uk/magnetic_materials/history.htm.

[26] Magnetfabrik Schramberg, "Magnet Material data," http://www.magnete.de/php/p_s_magnetischekenndaten.php.

[27] J. Dudding, "Advances in instrumentation for magnetic measurement," in *Proceedings of the UK Magnetic Society*, June 2000.

[28] M. Kumada, T. Fujisawa, Y. Hirao, M. Endo, M. Aoki, T. Kohda, Y. Iwashita, I. Bolshakova and R. Holyaka, "Development of a model 4 Tesla Diople Magnet," Proceedings of the Second Asian Particle Accelerator Conference, Beijing, China, 2001

[29] G. Aubert, H. W. H. M. Jongbloets, W. Joss, J. C. Picoche, A. Plante, P. Rub and J. C. Vallier, "The High Magnetic Field Laboratory of Grenoble," *IEEE Transactions on Magnetics*, Vol 30, No 4, July 1994.

[30] P. Pernambuco-Wise, H. J. Schneider-Muntau, L. Van Bockstal, L. J. Campbell, D. G. Rickel and J. R. Sims, "Design and Construction of 80 Tesla Internally Reinforced Pulsed Magnets," *IEEE Transactions on Magnetics*, Vol 30 No 4, pp. 2226 – 2228, July 1994.

[31] F. Langford- Smith, "Bunnet's formula for multi layer solenoids," *Radio designer's handbook*, pp. 443, 1953.

[32] W J Duffin, "Biot-Savat's law", *Electricity and Magnetism*, pp. 182, 1990.

[33] Robin Cornelius, "Aircore," Software, 2001.

[34] Magnetic Instrumentation Inc, "Model 2100 Gaussmeter," Datasheet.

[35] The Imperial College Cassini Magnetometer Group, "The fluxgate magnetometer," http://www.sp.ph.ic.ac.uk/cassini/fgm.html, 2002.

[36] Phillip Lethuillier, "*MACCHARATEC progress report*", 2002.

[37] J. Dudding, P. A. Knell, R. N. Cornelius, B. Enzberg-Mahlke, W. Fernengel, R. Grössinger, M. Küpferling, P. Lethuillier, G. Reyne, M. Taraba, J. C. Toussaint, A. Wimmer and D. Edwards, "A Pulsed Field Magnetometer for the Quality Control of

Permanent magnets," *Journal of Magnetism and Magnetic Materials*, Vol 242–245, pp. 1402–1404, 2002.

[38] Lake Shore Cryotronics Inc, "Hysteresisgraph datasheet," http://www.lakeshore.com/sys/hys/hym.html, 2001.

[39] Walker scientific JDJ, "AMH datasheet," http://www.walkerldjscientific.com/Products/Product_Lines/Magnetic_Analysis/Hysteresisgraphs/AMH-specs/amh-specs.html, 2002.

[40] Hirst Magnetic Instruments Ltd, "ARP03 datasheet," http://www.hirst-magnetics.com/products/ARP03.shtml, 2003.

# Appendix A - Published Papers

# Pulsed Field Magnetometer for Industrial Use

R. Cornelius, J. Dudding, P. Knell, R. Grossinger, B. Enzberg-Mahlke, W. Fernengel, M. Küpferling, M. Taraba, J. C. Toussaint, A. Wimmer, and D. Edwards

***Abstract*—An industrial pulsed field magnetometer was developed, focusing on industrial needs. The system is to be used for the complete characterizing of permanent magnets in a production-line situation. The purpose is to create a fast, reliable, and accurate magnetometer for quality control but also, in a later step, as a standard measurement method for magnets.**

***Index Terms*—Eddy currents, hysteresis, measurement.**

## I. Introduction

A PULSED field magnetometer (PFM) was constructed to meet the needs of industrial magnet manufacturers and consumers. Existing measurement systems such as permeameters have limited applied field, are slow (by comparison to PFMs), are limited (generally) to one quadrant, and require samples to have perfectly flat and parallel faces and be of regular shape. PFMs do not have these limitations.

The system was required to cope with a range of sample dimensions up to 30 mm in diameter and 25 mm in height. It was necessary to deal with a range of samples including rare earth and those where the effects of eddy currents could cause a significant measurement error [1].

The industrial magnet producer required rapid production rate measurements, but with the repeatability and accuracy of laboratory-based equipment.

A multiple pulsed magnet system was developed with four coils, one for each major function of the machine: magnetization, demagnetization, and two measurement coils. The maximum field strength for measurements was 6.2 T.

## II. Pulsed Magnets

The prototype system featured four pulsed magnets, each optimized for the required function, magnetization, demagnetization, or measurement. Each pulsed magnet was fluid-cooled to enable the heat energy generated by the $I^2R$ losses to be removed ensuring that the required duty cycle could be met.

The two measurement coils were of different resonant frequency with the capacitor bank, enabling two applied pulses of differing frequency, conventionally known as the short and long pulses.

## III. Energy Topology

The energy used for the magnetic field generation was stored on a 0.5-mF capacitor bank with the voltage being selectable anywhere between 0 and 3000 V. A switched-mode charger provided rapid charging.

A bank of eight power thyristors directed the energy to the four coils and allowed either unidirectional or a full sine wave (decaying) pulse. Typically, the magnetization and demagnetization pulses would be unidirectional and the two measurement coils full wave. If required, the demagnetization pulse could also be a full decaying ringing sine wave.

## IV. Pickup Coils

Each of the pulsed magnets contained a removal pickup-coil cartridge. The pickup system was designed specifically for this PFM and was based on a concentric hum bucking design, with an inner and outer $J$ coil connected in antiphase series [2]. The spacing of the windings of the $J$ coil were critically determined to ensure maximum homogeneity of pickup over the volume where samples are to be placed. The actual homogeneity value is better than 1%. A novel external compensation system allows easy and very accurate compensation of the $J$ coil once fitted inside the pulsed magnet. The applied field sensor or $H$ coil is also integral within the pickup cartridge.

The industrial advantages are that the system is not sample position dependent, meaning that a very quick and not particularly accurate loading system can be used which is ideal for industrial use. If the system compensation drifts with age, the end user of the machine can recompensate. Finally, if the unit is damaged, it can simply be replaced.

## V. Data Acquisition

The output of the pickup coils was connected to differential integrators designed to cope with the large voltage transients during a discharge. The integrators were in turn connected to a two-channel 16-bit 2.5-MHz analog-to-digital board interfaced directly to a PC. The whole system was controlled by a custom software application to handle all necessary data processing and storage.

Manuscript received February 14, 2002; revised May 15, 2002. This work was supported by the European Community (EC) under MACCHARACTEC (European 4th Framework) Project SMT4-CT98-2212.

R. Cornelius was with University of Plymouth, PL4 8AA Plymouth, U.K. He is now with Hirst-Magnetic Instruments Ltd., TR11 4SN Cornwall, U.K.

J. Dudding and P. Knell are with Hirst-Magnetic Instruments Ltd., TR11 4SN Cornwall, U.K.

R. Grossinger, M. Küpferling, M. Taraba, and A. Wimmer are with the Institut Für Experimentalphysik, Technical University of Vienna, A-1040 Vienna, Austria.

B. Enzberg-Mahlke is with Magnetfabrik Schramberg, 78713 Schramberg-Sulgen, Germany.

W. Fernengel is with VACUUMSCHMELZE GmbH, 63450 Hanau, Germany.

J. C. Toussaint is with the Centre National de la Recherche Scientifique (CNRS), BP 166-38042 Grenoble, France.

D. Edwards is with Mecelec Developments Ltd., GL2 5QT Gloucester, U.K.

Digital Object Identifier 10.1109/TMAG.2002.803600.

An important feature was that all samples were logged to a database for 100% sample control. To maximize efficiency and speed of operation, a fully multitasking system was used so that data could be processed during otherwise wasted periods of time such as indexing of the mechanical handling system and charging the capacitor bank. The overall data storage and processing took approximately 2 s, including the eddy-current correction.

## VI. Eddy-Current Correction

As eddy currents are governed by the partial differential equation

$$\mathbf{J}_{\mathrm{EDDY}} = -\sigma \operatorname{curl} \frac{d\mathbf{B}}{dt}$$

where $\mathbf{J}_{\mathrm{EDDY}}$ is the eddy current, $\sigma$ is the material conductivity, and $\mathbf{B}$ the magnetic flux density, any conductive samples will have eddy current in PFM [3]. The eddy currents are proportional to the conductivity of the sample and the surface area perpendicular to the applied field of the sample (in a simple cylindrical example) as well as the rate of change of applied field. The magnitude of the eddy currents and their effects are sufficient in many samples to cause significant errors in the measurement [4]. This is accounted for and corrected in the system using the $f/2f$ method [5]. The $f/2f$ method requires two measurements at different frequencies, hence, the two measurement coils and the information obtained can be used to deduce the eddy-current-effect free measurement.

If two pulses of differing frequencies are applied to the same sample, then the eddy currents and the measured effects of those eddy currents will be proportional to the frequencies of the two applied pulses. The lower frequency pulse is named $\mathbf{F_L}$ and the higher frequency pulse $\mathbf{F_H}$. Each pulse will have an eddy-current error proportional to the frequency of the pulse combined with the real signal. If the signals from the two pulses are subtracted, then the two real signals cancel out as do part of the eddy-current error, leaving only the extra error component that the $\mathbf{F_H}$ has but the $\mathbf{F_L}$ does not

$$\Delta\mathrm{Error} = \mathbf{F_H} - \mathbf{F_L}.$$

With the frequencies of the two pulses known, this change in error can be scaled and used to subtract the eddy-current error to find the static (no eddy-current effects) curve. As the same sample is used for both pulses, all imperfection and nonhomogeneity of the material will be accounted for.

## VII. Mechanical Handling

Fig. 1 shows the handling schematic. The mechanical handing system was a rotational design with push rods to elevate the sample into the pulsed magnets. A loading station allowed the loading of magnets into the system, with a minimum of controls. Magnets would be moved around the system clockwise, being lifted up into each station for the required function then being lowered and moved to the next station. The station order was loading, magnetization, $f$, $2f$, demagnetization, spare, and loading.

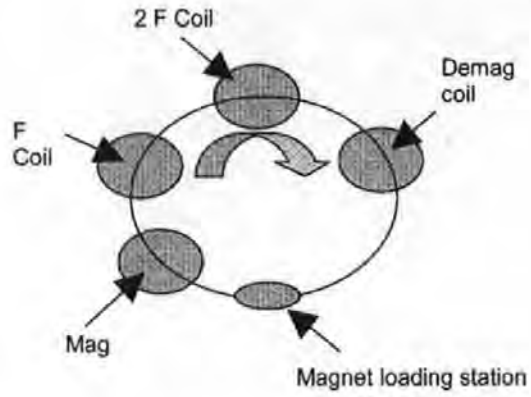


Fig. 1. Handling schematic.

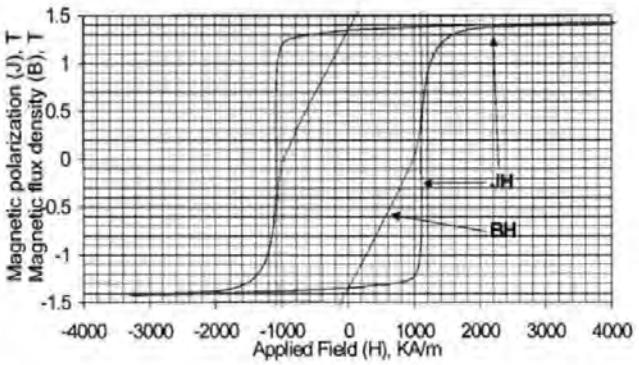


Fig. 2. PFM measurement of NdFeB 270/95h cylinder 20 mm diameter × 10 mm height using a Hirst Magnetic Instruments PFM21. Measurement and magnet manufactured by Magnetfabrik Schramberg. Eddy-current corrected. $JH$ and $BH$ loops shown.

## VIII. Results

The following results are all measured on the prototype industrial PFM21. Eddy-current effect correction is active and correcting where necessary.

Fig. 2 shows an eddy-current-effect corrected NdFeB magnet measured on the industrial PFM system discussed here. The magnet has been fully saturated in both directions and the full hysteresis loop measured with a short and long duration pulse (not shown). Fig. 2 shows eddy-current-effect corrected results as the NdFeB 270/95h is a conductive material and the two actual measurements made on the PFM contained the effects of eddy currents.

Fig. 3 shows the detail of the coercivity point for a different NdFeB 270/95h to Fig. 2. The three lines represent a small section of three full hysteresis loops. The left-most line shows the short duration pulse measurement, the middle line is the longer duration pulse, with less effect of eddy currents, and the right-most line is the eddy-current-effect corrected data.

Fig. 4 shows the demagnetization quadrant of a plastic-bonded ferrite, where there are no eddy-current effects of any significance to the measurement.

These and many other results have been compared to permeameter measurements of the same samples. Agreement is typically better than 1% for all the major points of interest ($BH$ Max, $Br$, $Hcj$, $Hcb$, etc.) for the eddy-current-corrected

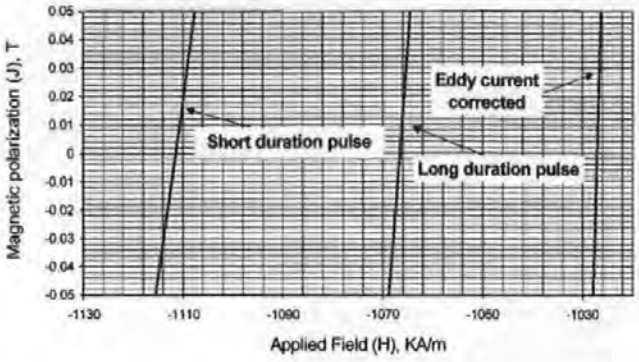


Fig. 3. Short duration, long duration, and eddy-current-effect corrected (from left to right) measurement of a NdFeB 970/95h cylinder 20-mm diameter 20-mm height. Measured using a Hirst Magnetic Instruments PFM21. Measurement and magnet manufactured by Magnetfabrik Schramberg.

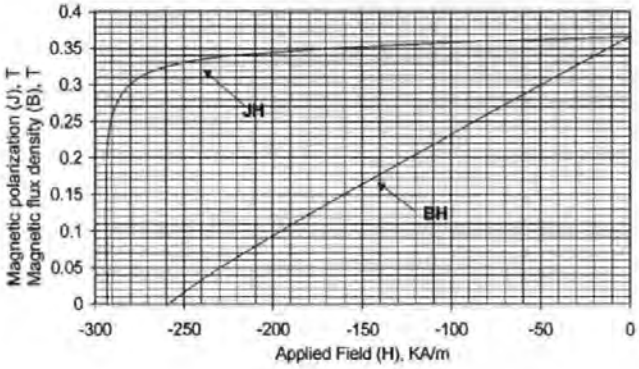


Fig. 4. PFM measurement of a hard ferrite HF24/23 using a Hirst Magnetic Instruments PFM21. Measurement and magnet manufactured by Magnetfabrik Schramberg. Full loop measurement, only demagnetization quadrant is shown for clarity. $JH$ and $BH$ loops shown.

PFM data when compared to permeameter data. The permeameter by its slow measurement procedure has no eddy-current effects.

The shape of the hysteresis curve shows excellent correspondence between the PFM-corrected data and the permeameter's measurement, in the second (demagnetization) quadrant only (due to limitations of permeameter's applied field). Fig. 5 shows a comparison between a permeameter and a PFM for a bonded NdFeB magnet.

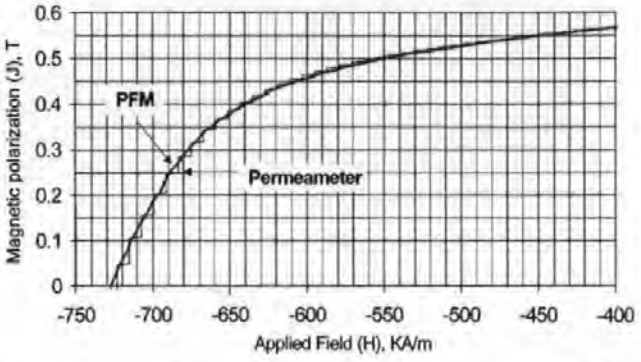


Fig. 5. Comparison between a permeameter and a PFM21. The PFM trace lies with in 1% of the permeameter. The quantization of the applied field can be seen for the permeameter while for the PFM, the trace (eddy-current-effect corrected) is continuous.

## IX. Conclusion

The technology of PFM has matured to the stage where it is a viable magnetic measurement technique. Not only have the results been proven to be accurate and repeatable, but the durability of the technique has been proven in an industrial environment with the experimental machine having completed six months of continuous operation in an industrial environment.

Due to the use of air-cored solenoids, the repeatability is higher than conventional techniques that rely on relative permeability measurements. Repeatability has been found to have a 45% improvement compared to the test permeameter. Absolute accuracy, although apparently better, improvements are still to be determined.

## References

[1] R. Grössinger, E. Wittig, M. Küpferling, M. Taraba, G. Reyne, C. Golovanov, B. Enzberg-Mahlke, W. Fernegel, P. Lethuillier, and J. Dudding, "Large bore pulsed field magnetometer for characterizing permanent magnets," *IEEE Trans. Magn.*, vol. 35, pp. 3871–3973, Sept. 1999.

[2] D. Eckert, R. Grössinger, M. Doerr, F. Fischer, A. Handstein, D. Hinz, H. Siegel, P. Verges, and K. H. Müller, "High precision pick-up coils for pulsed field magnetization measurements," *Physica*, pp. 294–295, < AUTHOR: PLEASE PROVIDE VOL. # AND MONTH > 2001.

[3] G. W. Jewell, D. Howe, C. Schotko, and R. Grossinger, "A method for assessing eddy current effects in pulsed magnetometry," *IEEE Trans. Magn.*, vol. 28, pp. 3114–3116, Sept. 1992.

[4] C. Golovanov, G. Reyne, G. Meunier, R. Grössinger, and J. Dudding, "Finite element modeling of permanent magnets under pulsed field," *IEEE Trans. Magn.*, vol. 36, pp. 1222–1225, July 2000.

[5] R. Grossinger, G. W. Jewell, J. Dudding, and D. Howe, "Pulsed field magnetometry," *IEEE Trans. Magn.*, vol. 29, pp. 2980–2982, Nov. 1993.

# Calibration of an Industrial Pulsed Field Magnetometer

R. Grössinger, M. Taraba, A. Wimmer, J. Dudding, R. Cornelius, P. Knell, P. Bissel, B. Enzberg-Mahlke, W. Fernengel, J. C. Toussaint, and D. Edwards

***Abstract*—An industrial design of a pulsed field magnetometer (PFM) which generates in a bore of 30 mm a maximum field of 5 tesla with two different pulse durations (40 and 57 ms) is described. The field is calibrated using a small pickup coil where the effective winding area is known from a nuclear magnetic resonance calibration. The magnetization is calibrated using $Fe_3O_4$, an industrial ferrite, but also Fe and Ni.**

***Index Terms*—Magnetometer, permanent magnets, pulsed fields.**

## I. Introduction

HIGH-QUALITY permanent magnets, based on rare earth intermetallic compounds such as Sm–Co and Nd–Fe–B, exhibit coercivities between 1 and 5 tesla. These coercivities are too high for Fe-yoke-based hysteresis systems (see, e.g., [1] and [2]). These magnets can neither be fully magnetized nor characterized in commercially available systems. Therefore, industrial producers and users of permanent magnets have a need for measuring systems which allow a fast and reliable online measurements of such magnets.

## II. Industrial Pulsed Field Magnetometer

Based on existing knowledge of pulsed field systems [3], [4], a pulsed field magnetometer (PFM) was developed by Hirst Instruments focusing on the industrial needs. The design was a manual loading system that could charge a 22.5 kJ capacitor bank ($C = 5$ mF) to 3000 V in approximately 25 s, using phase controlled thyristors. Fig. 1 shows a block diagram of the constructed PFM.

The pulse magnet was divided into two sections, which can be pulsed independently, providing long and short duration pulses. The field homogeneity of the two magnets over a length of 30 mm is better than 1%. The eddy currents during magnetization are proportional to $dH/dt$ [5]. By processing the two measurements—conventionally named $f$ and $2f$ [but in practice, the frequencies are nearer $f$ (57 ms) and $1.3f$ (40 ms)]—it is possible to remove the effect due to the eddy currents and produce the direct equivalent of a static hysteresis plot. This is called the $f/2f$ method [6].

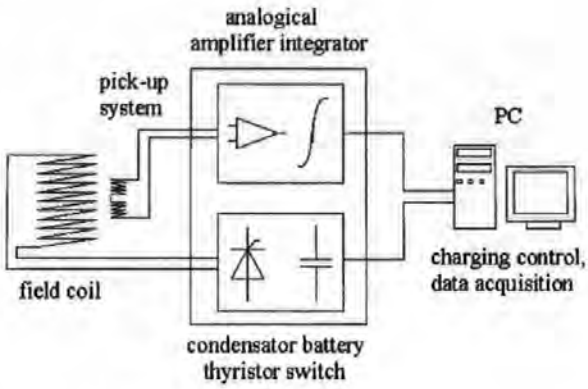


Fig. 1. Industrial PFM block diagram.

The validity and the limits of the $f/2f$ method were investigated by three-dimensional (3-D) finite-element calculations [7]. The design of the J-coil, especially its balancing, is based on an idea published in [8].

## III. Magnetometry

Pulsed field magnetometry is a magnetically open-circuit method of magnetic measurement. This means that the shape of the hysteresis loop is affected by the demagnetizing field. For magnets having a complicated geometry the demagnetizing factor becomes a space dependent function, which can be calculated using a finite-element program [9].

## IV. Calibration

### A. Field Calibration

The field is calibrated using a small (3-mm-diameter, 0.1-mm-high) pickup coil whose effective winding area is known from a nuclear magnetic resonance (NMR) calibration. The induced voltage $u(t)$ is then fitted using (1), in order to determine the field calibration factor $k$ (for the $f$ and the $2f$ pulse), and also the damping factor and the pulse duration (including the effect of the damping)

$$\begin{aligned} H &= H_0.\exp(-at).\sin\omega t \\ u_i(t) &= -N.A.\,dB/dt \\ &= -N.A\mu_0.H_0(d/dt)[\exp(-at).\sin\omega t]. \end{aligned} \quad (1)$$

Manuscript received February 11, 2002; revised May 21, 2002. This work was supported by the EC under the Maccharactec (European 4th Framework) Project: SMT4-CT98-2214.

R. Grössinger, M. Taraba, and A. Wimmer are with the Inst. f. Festkörperphysik, Vienna University of Technology, A-1040 Vienna, Austria (e-mail: rgroess@xphys.tuwien.ac.at).

J. Dudding, R. Cornelius, and P. Knell are with Hirst Magnetic Instruments Ltd., TR11 4SN Cornwall, U.K.

P. Bissel is with the University of Central Lancashire, Preston PR1 2HE, U.K.

B. Enzberg-Mahlke is with Magnetfabrik Schramberg, Schramberg-Sulgen D-78713, Germany.

W. Fernengel is with VACUUMSCHMELZE, Hanau D-63450, Germany.

J. C. Toussaint is with the Centre National de la Recherche Scientifique (CNRS), 38042 Grenoble, France.

D. Edwards is with Mecelec Developments Ltd., GL2 5QT Gloucester, U.K.

Digital Object Identifier 10.1109/TMAG.2002.803199.

TABLE I
SUMMARY OF CALIBRATION RESULTS

| Sample | shape | $\mu_0 H_{max}$(T) T = 57 ms | $<\mu_0 M>$ | $\mu_0 M_{literature}$ | Error (%) | $\mu_0 M$(T) T = 40 ms |
|---|---|---|---|---|---|---|
| $Fe_3O_4$ | Sphere 2r = 5.5 mm | 1.5 | 0.5787 ± 0.001 | 0.569 [10] | +1.6 | 0.5782 |
| Ni | Cylinder D=4; h=8 mm | 1.5 | 0.6259 ± 0.0008 | 0.610 [11] | +2.6 | 0.6322 |

The thus determined damping factor "$a$" can be compared with the circuit derived value $a \approx R/2L$. The calibration factor $k$ was determined as a function of the gain (integrator gain + gain of preamplifier on the ADC-Datel-board) for the two pulses with different time constants. The calibration factor "$k$" gives a relation between the induced voltage and the field of the search coil. At the same time, the integrated voltage (using different gain factors) of the $H$-measuring coil (which is at a different location) on the magnetometer system is recorded.

The calibration factor $k$ was determined as a function of the gain using an analog integrator constructed by Hirst. The scatter of the $k$ factor is below ±1%. This indicates that the linearity of the gain is better than 1%. Using such a procedure, an absolute field calibration of better than 1% is achieved—including the time constants (gain) of the integrator.

### B. Magnetization Calibration

The magnetization is calibrated using well-known materials such as Fe and Ni (in which the eddy-current error causes an uncertainty) or preferably a nonconducting sample such as $Fe_3O_4$ or a soft magnetic ferrite, such as 3C30. All calibration measurements were performed at room temperature. The results of the magnetization calibration measurements are summarized in Table I. To check the reproducibility, the measurements were repeated ten times giving an average value $\langle M \rangle$. Additionally, measurements using a shorter pulse duration (40 ms) were performed, which were generally in good agreement with that of the long pulse. For the metallic samples, an error of 1%–2% due to the eddy currents occur.

*1) Analysis of the Calibration Data:* Table II summarizes the results of the calibration measurements and the deviations from the "true" (literature) values.

The mean value of the deviations $D_{mv} = 1.6\%$ is higher than the "true" values. Therefore, the internal calibration factor of the PFM had to be corrected. It should be mentioned that there were no significant differences in the measured magnetization values when different pulse duration were employed.

The mean value of the deviations $D_{mv} = 1.6\%$ has a standard deviation of 0.95%. The standard deviations concerning the reproducibility gave a mean value of 0.19%. Therefore, the deviation is, in the worst case, 1.14%. This means that the magnetization value could be calibrated with an absolute accuracy of ±1.14%.

### C. Reliability of the Calibration

For testing the reliability of the calibration procedure, a "calibrated sample" from the Physikalisch-Technische Bundesanstalt (PTB) in Braunschweig, Germany, was measured. This sample was an anisotropic barium–ferrite from Magnetfabrik Schramberg with a cylindrical shape, with a height of 10 mm and a diameter of 6 mm. The mass was 1.417 g. The hysteresis measurement was performed by applying an external field of 2 T and a pulse duration of 56 ms. In order to reduce the statistical error, the measurement was repeated seven times.

TABLE II
SUMMARY OF CALIBRATION MEASUREMENT

| **Sample** | $\mu_0 M_{meas}$ | **S** | $\mu_0 M_{literature}$ | **Deviation** |
|---|---|---|---|---|
| **Units** | [T] | % | [T] | % |
| **$Fe_3O_4$** | 0.5787 | 0.2 | 0.569 | 1.6 % to high |
| **Nickel** | 0.6259 | 0.13 | 0.610 | 2.6 % to high |
| **Iron** | 2.1525 | 0.24 | 2.138 | 0.7 % to high |

The mean value of the thus determined remanence magnetization is $B_r = (0.3644 \pm 0.0002)$ T, which corresponds to an error of ±0.05%. PTB gave a remanence value of $B_r = (0.3625 \pm 0.0044)$ T. So the difference between the PFM and the PTB value is about 0.5%, which is smaller than the given calibration error.

In order to test the effect of the pulse duration, the PTB calibrated sample was measured under the same conditions but with different pulse durations (56 and 40 ms). The difference in the remanence magnetization is below 1%.

### D. Influence of Sample Geometry on Magnetization Values

In order to investigate the effect of the sample geometry on the accuracy of the magnetization measurements in the PFM, a set of industrial soft magnetic ferrites with different shapes were used. [Philips (3C30)] All samples were from one charge. This material has a magnetization at room temperature of about 0.55 T, whilst the Curie temperature is about 240 °C. The density is 4800 kg/m$^3$. Since this material is an insulator, there are no eddy-current effects. The chosen shapes are given in Table III.

The samples were measured in an external field with an amplitude of 2 T and a pulse duration of 56 ms. All samples were measured at room temperature (21 °C ± 1 °C) using the same amplification factor and the same mechanical adjustments. Small deviations are visible in the shape of the hysteresis loops, especially where the saturation enters in the high permeability region; see Fig. 2. This is due to the fact that the "mean" demagnetization factor causes an error, which becomes especially significant in this part of the loop.

TABLE III
SHAPES AND MASSES OF THE 3C30 SAMPLES

| Sample | Size | Mass |
|---|---|---|
| Sphere | d = 9.1 mm | m = 1.9065 g |
| small cube | 11.2 x 11 x 0.8 mm | m = 0.5226 g |
| Medium cube | 11.9 x 11.9 x 3 mm | m = 1.9316 g |
| big cube | 21 x 14.6 x 11.9 mm | m = 17.3848 g |

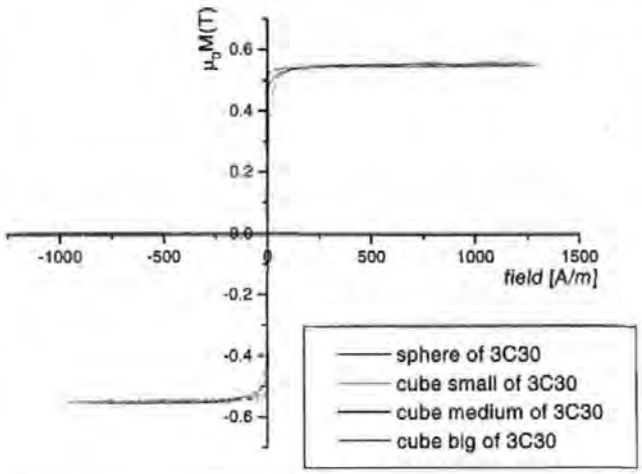


Fig. 2. Hysteresis measurements on 3C30 samples with different shapes.

The results are summarized in Table IV.

The magnetization values of the three different cubes show a difference up to 0.6%. The value for the sphere exhibits the largest difference of 2% with respect to the average value of the cubes. (This may be a result of the grinding process in an air-pressure driven mill. The sample is forced to rotate rapidly in a container of corundum.) It is possible that the surface structure of the sample may have been destroyed. If a disturbed surface layer of 40 $\mu$m is assumed, this could account for the deviation of the magnetization value.

## V. SUMMARY AND DISCUSSION

The field of a PFM is calibrated using a small pick-up coil, where the effective winding area is known from an NMR calibration. Using such a procedure allows an absolute field calibration of better than 1%—including the time constants (gain) of the integrator. The obtained field calibration agrees also within 1% with that of the PTB-calibrated magnet coercivity value.

In principle, nonconducting materials, like $Fe_3O_4$, or a soft magnetic ferrite, like 3C30, are better suited for the calibration. Unfortunately, the temperature dependence of the magnetization of the industrial available ferrite 3C30 is much worse then that of $Fe_3O_4$.

The calibration constants using $Fe_3O_4$, Fe, and Ni agree within 1.6%. The reproducibility of the different magnetization measurements—especially using Fe or Ni samples was better than 0.3%. The error due to eddy currents in the rather long pulse duration (56 ms) is negligible. The zero-signal of the system is less than 10% of the $Fe_3O_4$ sample signal, which has the smallest sample signal. According to these considerations, one can conclude that the sensitivity is sufficient for the PFM to measure Nd–Fe–B magnet samples as small as 0.3 g mass, which corresponds to a cube of 3 × 3 × 3 mm. The PFM is, however, also capable of measuring samples with diameters up to 30 mm.

If one works very carefully, an absolute magnetization calibration within ±1% is possible. Due to the good linearity of the analog measuring electronics and the high resolution of the ADC card (14 bit), a relative measurement—which is most important for a quality control system—with a relative accuracy better than 0.5% is possible.

So, such a PFM is a new and reliable instrument for a fast and reliable measurement of the hysteresis loop of hard magnetic materials. For the first time, a system is commercial available which can be used for an online quality control.

TABLE IV
MAGNETIZATION AT $H = 2$ T OF 3C30 SAMPLES

| Sample | magnetization |
|---|---|
| Sphere | 0.550 T |
| small cube | 0.558 T |
| Medium cube | 0.555 T |
| big cube | 0.557 T |

## REFERENCES

[1] R. Grössinger, Ch. Gigler, A. Keresztes, and H. Fillunger, "A pulsed field magnetometer for the characterization of hard magnetic materials," *IEEE Trans. Magn.*, vol. 24, pp. 970–973, Mar. 1988.
[2] R. Grössinger, X. C. Kou, and M. Katter, "Hard magnetic materials in pulsed fields," *Phys. B*, vol. 177, pp. 219–222, 1992.
[3] R. Grössinger, M. Katter, G. Badurek, and R. Krewenka, "The construction of a highly sensitive pulsed-field magnetometer for measuring hard magnetic materials," *J. Magn. Magn. Mater.*, vol. 101, pp. 304–306, 1991.
[4] R. Grössinger, D. Eckert, E. H. C. Sinnecker, M. Taraba, and G. W. Jewell, "An accurate pulsed field hysteresograph," *Phys. B*, vol. 211, pp. 348–350, 1995.
[5] R. Grössinger, M. Küpferling, P. Kasperkovitz, A. Wimmer, M. Taraba, W. Scholz, J. Dudding, P. Lethuillier, J. C. Toussaint, B. Enzberg-Mahlke, W. Fernengel, and G. Reyne, "Eddy currents in pulsed field measurements," *J. Magn. Magn. Mater.*, vol. 242-245, pp. 911–914, 2002.
[6] G. W. Jewell, D. Howe, C. Schotzko, and R. Grössinger, "A method for assessing eddy current effects in pulsed magnetometry," *IEEE Trans. Magn.*, vol. 28, pp. 3114–3116, Sept. 1992.
[7] C. Golovanov, G. Reyne, G. Meunier, R. Grössinger, and J. Dudding, "Finite element modeling of permanent magnets under pulsed field," *IEEE Trans. Magn.*, vol. 36, p. 1222, July 2000.
[8] D. Eckert, R. Grössinger, M. Doerr, F. Fischer, A. Handstein, D. Hinz, H. Siegel, P. Verges, and K. H. Müller, "The Dresden high-magnetic field laboratory—overview and first results," *Phys. B*, vol. 294–295, p. 705, 2001.
[9] J. C. Toussaint, private communication.
[10] R. Grössinger, D. Eckert, E. H. C. Sinnecker, M. Taraba, and G. W. Jewell, "An accurate pulsed field hysteresograph," *Phys. B*, vol. 211, pp. 348–350, 1995.
[11] J. F. D. Montenegro and E. W. Lee, "The magnetic field dependence of the magnetization of nickel," *J. Magn. Magn. Mater.*, vol. 30, p. 5, 1982.

ELSEVIER

Journal of Magnetism and Magnetic Materials 242–245 (2002) 1402–1404

Journal of magnetism and magnetic materials

www.elsevier.com/locate/jmmm

# A pulsed field magnetometer for the qualitiy control of permanent magnets

J. Dudding[a,*], P.A. Knell[a], R.N. Cornelius[a], B. Enzberg-Mahlke[b], W. Fernengel[c], R. Grössinger[d], M. Küpferling[d], P. Lethuillier[e], G. Reyne[f], M. Taraba[d], J.C. Toussaint[e], A. Wimmer[d], D. Edwards[g]

[a] *Hirst Magnetic Instruments Limited, Tesla House, Tregoniggie, Falmouth, Cornwall TR11 4SN, UK*
[b] *Magnetfabrik Schramberg, Schramberg-Sulgen, Germany*
[c] *VAC, Hanau, Germany*
[d] *Inst. f. Experimentalphysik, Techn. Univ. Vienna, Austria*
[e] *CNRS, PO BOX 166X Grenoble, France*
[f] *Univ. Ensieg LEG, Saint-Martin D'Heres, France*
[g] *Mecelec Developments Limited, Gloucester, UK*

**Abstract**

A pulsed field magnetometer (PFM) for industrial applications was developed. The system has a capacitor bank of 5 mF for energy storage, which can be charged up to 3000 V. The pulse magnet has a bore of 30 mm (including the pickup coil), which is subdivided into two coils and produces a maximum field of 5 T with pulse frequencies of 17.5 and 25 Hz. The magnetisation is measured with a well balanced and temperature stabilised coaxial pickup system. The signal is integrated with a stable analogue integrator with selectable time constants. The signals are connected to a 14bit 5M sample/s two-channel ADC in a computer. For the data handling a C$^{++}$-based computer program was written. The effects of eddy currents on the metallic samples are corrected by using the so-called $f/2f$ method. Here two hysteresis measurements with two different time constants are used to measure the eddy current error. The function and reliability of the system is demonstrated by measuring the hysteresis of standard permanent magnets in the PFM and in a static system. 

*Keywords:* Magnetic measurement; Hysteresis loop; Eddy currents

## 1. Introduction

Industrial producers and consumers of magnets are increasingly demanding that magnets have to be individually tested. The current conventional methods, namely vibrating sample magnetometers (VSMs) and permeameters, have limiting physical constraints. VSMs cannot handle samples of industrial size and conventional VSMs can only produce a relatively low field strength. Super-conducting VSMs can produce higher fields, for rare earth magnets, but require liquid helium cooling and are expensive to operate and still can only measure relatively small samples. Permeameters have a limited applied field that can be generated due to the iron pole pieces. They also cannot measure full hysteresis loops. All conventional systems have measurement times that are unacceptable for industrial process control.

## 2. The system

A pulsed field magnetometer (PFM) was developed to meet the industrial needs. The design was a manual

*Corresponding author.
*E-mail address:* dudding@hirst-magnetics.com (J. Dudding).

0304-8853/02/$ - see front matter 
PII: S0304-8853(01)01247-1

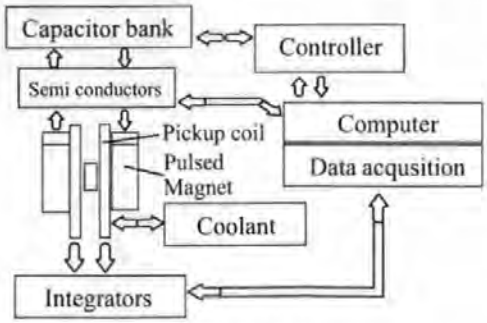


Fig. 1. PFM block diagram.

loading system that could charge a 22.5 kJ capacitor bank to 3000 V in ~25 s, using phase controlled thyristors, upgradable to a 4-s charge using a high frequency switch mode supply. The discharge, data capture and processing all occur in <1 s. Fig. 1 shows a block diagram of the constructed PFM.

The pickup coil was a sealed unit featuring an integral $J$ and $H$ coil with temperature monitoring and fluid pathways that allowed coolant to keep the windings at a constant temperature. The $J$ coil was a radial concentric humbucking coil with an inner and outer coil [2]. The spacing of the pickup conductors was critically determined to provide a homogeneity of pickup better than 1% over the maximum possible area. This ensured that the coil was not sample position dependent, a benefit for industrial measurements where there is no time to accurately position samples to fractions of a millimeter.

The inner and outer windings were accurately wound on to the formers to ensure near-perfect cancellation of the applied field. The outer $J$ coil is "tunable", enabling all external field to be cancelled out, apart from a 90° out-of-phase quadurature component, which was very small (<50 counts out of ±8192 at full voltage, full gain).

Pulsed field magnetometry is an open circuit method of magnetic measurement. This leads to a problem that the magnet's self-demagnetisation field is also included in the measurement. The software, as part of its processing corrects for self-demagnetisation factor. An external piece of software, that accurately calculates the global demagnetisation factor for a given shape, has been developed by one of us (J.C. Toussaint) as part of the research.

## 3. Eddy currents and their correction

The pulsed magnet was divided electrically into two coils that could be pulsed independently, providing a long and short duration pulse. The two pulse durations are conventionally named $f$ and $2f$ but, in practice, the frequencies are nearer $f$ and $1.3f$. The two frequency pulses are used to measure each sample. Both magnets generate the same $J$ signal with respect to the applied field but with the addition of eddy currents. As the eddy currents are related to frequency, by processing of the two measurements, it is possible to mathematically remove the eddy currents effects, producing the direct equivalent of a static hysteresis plot, this is known as the $f/2f$ method [1].

The equations used in the $f/2f$ calculations are as follows:

$$J_{\mathrm{EDDY}} = -\sigma \frac{\mathrm{d}B}{\mathrm{d}t},$$

$$M_{\mathrm{EDDY}} \propto J_{\mathrm{EDDY}},$$

$$M_{\mathrm{MAGNET}} = \mu H + M_{\mathrm{EDDY}}.$$

Magnetic viscosity effects are assumed to be negligible at the frequencies involved. As the measurement occurs at two frequencies it is possible to deduce $M_{\mathrm{EDDY}}$ and to remove its component from $M_{\mathrm{MAGNET}}$.

## 4. Results

The following Figs. 2 and 3 are $f$ and $2f$ measurements of a cylindrical Vacodym 510 magnet, 20 mm in diameter and 7 mm long. The two readings are then processed to obtain the eddy current corrected full loop characteristic. The resulting graph (Fig 4) shows the long ($f$) and short ($2f$) loops presented with the corrected loop (eddy currents removed).

The system is capable of accepting samples up to 30 mm in diameter and 25 mm long within a ±1% pickup homogeneity range, while smaller diameter samples of greater length can be accepted within this homogeneity range.

The two hysteresis measurements with two different time constants are used to calculate the eddy current

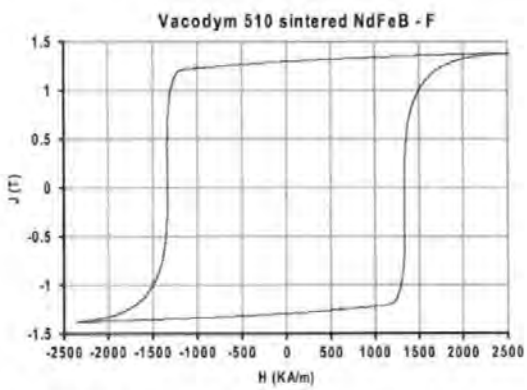


Fig. 2. PFM11 measurement of a Vacodym 510 (sintered NdFeB) cylinder, 20 mm in diameter and 7 mm long (long/$f$ pulse). $H_cJ = 1331.3$ KA/m.

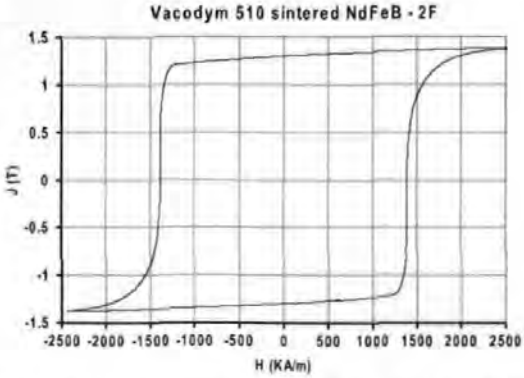


Fig. 3. PFM11 measurement of a Vacodym 510 (sintered NdFeB) cylinder, 20 mm in diameter and 7 mm long (short/$2f$ pulse). $H_cJ = 1385.3$ KA/m.

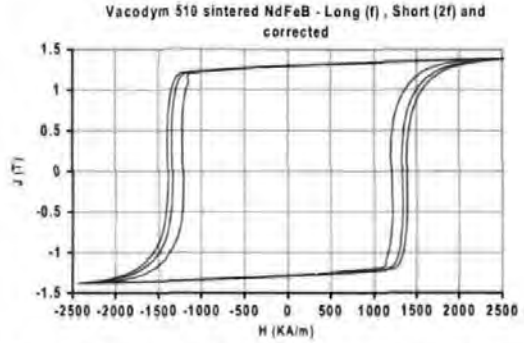


Fig. 4. The results of the $f/2f$ eddy current correction process for a Vacodym 510 (sintered NdFeB) cylinder, 20 mm in diameter, 7 mm long. Corrected $H_cJ = 1207.0$ KA/m.

error. The function and reliability of the system is demonstrated by measuring the hysteresis of standard permanent magnets in the pulsed field magnetometer and comparing it to static systems. Fig. 5 shows a comparison between the data measured on the PFM and a permeameter. There is a very good agreement between the two measurement systems. However, on the right-hand side of the permeameter data, it is possible to see the effects of the pole pieces beginning to enter the non-linear region and hence do not display the true magnetic characteristic. The PFM has no such limitation and hence the curves begin to diverge.

## 5. Conclusions

There is a very good agreement between the characteristics of magnet samples measured on the PFM and

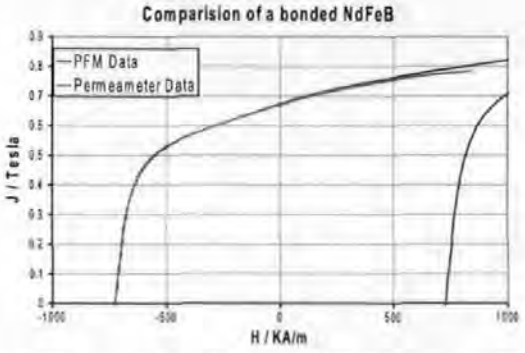


Fig. 5. The comparison of a bonded NdFeB between the PFM and a permeameter. The traces overlay nearly perfectly.

on static systems. The effects of the pulsed field can be seen when comparing two measurements, of a conductive material, at different frequencies. The $f/2f$ method of eliminating the induced eddy currents is very effective for high accuracy measurements. Although the effects of eddy currents in bonded materials are negligible, it can be neglected for many cases, also in sintered materials at the frequencies in the system described here.

For industrial use the charging time of the constructed system is still too slow. By using the switch mode chargers, any desired charging time can be achieved, the only limitation being the maximum cost the industry is prepared to pay.

At high duty cycles the pulsed magnet will be required to dissipate a large amount of energy. This amount is proportional to the energy used to generate the pulse and the resistance of the coil. This will need removing by artificial means. The pulsed magnet has been constructed in such a way as to allow oil cooling, although the present system does not employ cooling.

## Acknowledgements

The work was supported by the EC under the name MACCHARACTEC (European 4th Framework) with the project number SMT4-CT98-2212.

## References

[1] G.W. Jewell, D. Howe, C. Schotzko, R. Grössinger, IEEE Trans. Magn. 28 (1992) 3114.
[2] D. Eckert, R. Grössinger, M. Doerr, F. Fischer, A. Handstein, D. Hinz, H. Siegel, P. Verges, K.H. Müller, Physica B 294–295 (2001) 705.

ELSEVIER

Journal of Magnetism and Magnetic Materials 242–245 (2002) 911–914

Journal of magnetism and magnetic materials

www.elsevier.com/locate/jmmm

# Eddy currents in pulsed field measurements

R. Grössinger[a,*], M. Küpferling[a], P. Kasperkovitz[b], A. Wimmer[a], M. Taraba[a], W. Scholz[a], J. Dudding[c], P. Lethuillier[d], J.C. Toussaint[d], B. Enzberg-Mahlke[e], W. Fernengel[f], G. Reyne[g]

[a] *Institute für Experimentalphysik, Technische Universitat, Wiedner Haupstrasse 8-10, 1040 Vienna, Austria*
[b] *Institute für Theoretische Physik, Technische Universitat, Vienna, Austria*
[c] *Hirst Magnetic Instruments Ltd., Cornwall, UK*
[d] *CNRS, P.O. BOX 166X Grenoble, France*
[e] *Magnetfabrik Schramberg, Schramberg-Sulgen, Germany*
[f] *VAC, Hanau, Germany*
[g] *Univ. Ensieg LEG, Saint-Martin D'Heres, France*

**Abstract**

The eddy-current magnetization of spherical and cylindrical samples of technical Cu and Al were measured in a pulsed field magnetometer using different pulse durations $\tau = 9.1$ and 15.7 ms. Good agreement between the measured eddy-current moment as a function of the applied field with that calculated by a finite element program was found.


*Keywords:* Magnetometry; Eddy currents

## 1. Introduction

Modern high quality permanent magnets such as Sm–Co or Nd–Fe–B-based materials needs rather high magnetic fields in order to measure the hysteresis loop [1,2]. Static fields as available with Fe-yokes (up to about 2 T) are not sufficient. Higher fields, as can be produced by superconducting magnets (10–15 T) are not usual in industrial surroundings. Additionally, static hysteresis measurements take too much time for industrial production control. Therefore, the target of this EC funded project was to develop a fast and accurate pulsed field hysteresograph suitable for industrial applications. Magnetization measurements in transient fields on metallic conducting samples cause eddy currents. These eddy currents influence the shape of the loop and the value of the obtained magnetization. Therefore within the work presented here, eddy currents and the dynamic magnetization caused by these eddy currents were investigated.

## 2. System description

A pulsed field hysteresograph ($\mu_0 H_{max} = 10$ T) using a magnet with a bore of 70 mm diameter for characterizing permanent magnets of technical shapes and sizes at room temperature was developed [3]. The power is delivered by a capacitor battery (8 or 24 mF, $U_{max} = 2500$ V).

The magnet is subdivided into two sections with two layers each in order to allow a variation of the time constant of the system. The capacitor battery with a thyristor/diode switch allows a full wave of the field which is necessary for hysteresis measurements of magnetic materials. The magnet was optimized for low damping resistance; the amplitude of the second half wave is only 25% smaller than that of the first one.

*Corresponding author. Tel.: +43-1-58801-13150; fax: +43-1-58801-13199.

*E-mail address:* rgroess@xphys.tuwien.ac.at (R. Grössinger).

0304-8853/02/$ - see front matter 
PII: S0304-8853(01)01324-5

## 3. Samples

For analyzing the effect of eddy currents in pulsed magnetic fields, spherical samples of technical Al (Al-sample Al2: 5 mm diameter) and technical Cu (Cu-sample Cu2: 7.3 mm diameter) and cylindrical samples of the same Cu (E-Cu HHT F25) and the same Al ($AlMgSi_{0.5}$ F22) were studied. The effect of different dimensions on the magnitude of the eddy currents was determined using Cu samples with different sample radii $r_S$ and heights $h$ (diameter $2r_S = d$ : 2–9.8 mm, height $h = 8$ mm, respectively, $d = 4$ mm and $h$ between 2 and 10 mm). All samples were investigated after a heat treatment at 500°C for 4 h to reduce mechanical stresses. For determining the exact value of the specific resistivity $\rho$ of the samples an accurate 4-point resistivity measurement has been performed. The thus obtained room temperature values were: $\rho_{Cu} = 1.76\,\mu\Omega\,cm$ and $\rho_{Al} = 3.82\,\mu\Omega\,cm$, respectively.

## 4. Results

Fig. 1 shows a measurement comparing the dynamic "eddy-current" moment in a Cu cylinder with that which occurs in an Al cylinder (both: $d = 4$ mm, $h = 8$ mm). Naturally, the eddy currents in the Al cylinder are smaller because the specific resistivity of Al is a factor 1.6–2.2 higher than that of Cu. The shape of the curve shows that a phase shift exists between the field and the dynamic magnetization signal, which is about 90°. The second half pulse has, due to the damping, a lower $dH/dt$ therefore the eddy currents are less. At the beginning of the pulse, a sharp increase of the eddy currents occurs, which can be explained, assuming a dynamic inductivity between the eddy currents and the pulse magnet.

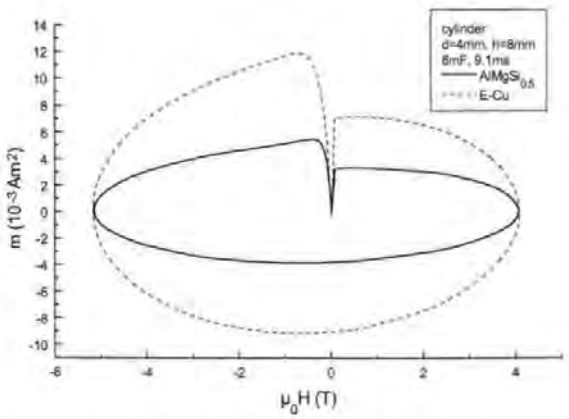


Fig. 1. Hysteresis loop of a Cu (Cu1) and an Al (Al1) cylinders at a pulse duration of 9.1 ms.

## 5. Finite element program (FEMM)

The finite element package FEMM by David Meeker [4] provides a complete set of tools for solving static and low frequency (harmonic) 2D or axial-symmetric problems in electrodynamics. The shape of the hysteresis loop has been verified by this FEMM. Assuming a harmonic oscillating field the program delivers the eddy-current density of axisymmetric samples as a complex function of the sample radius $r_S$ and the value $z$ on the symmetry axis.

The maximum eddy-current density ($J_{max} = J(r_S, z = 0)$) of all samples with different pulse duration have been calculated using FEMM which gives (for not too high frequencies and small samples) a linear radial increase of the eddy-current density and a constant value along the $z$-axis. Under this assumption the magnetic moment $m_{FEMM}$ was calculated.

$$m_{cyl} = \frac{1}{2c} 2\pi h \int_0^{r_S} r^2 j_{max} \frac{r}{r_S} dr = \frac{\pi h j_{max} r_S^3}{4} \tag{1}$$

$$m_{sph} = \frac{1}{2c} 2\pi \int_0^{\pi} \sin^2\vartheta \int_0^{r_S} r^3 j_{max} \frac{r \sin\vartheta}{r_S} dr\, d\vartheta = \frac{4\pi j_{max} r_S^4}{15}. \tag{2}$$

The magnetization is then given by

$$M \approx m/V, \tag{3}$$

where $V$ is the volume of the cylinders

$$V = r_s^2 \pi h. \tag{4}$$

Finally, the magnetization for a cylinder is

$$M = \frac{j_{max} r_S}{4}. \tag{5}$$

Hence, the magnetization is independent of the height of the cylinder.

A similar calculation delivers the magnetization for a sphere

$$M = \frac{j_{max} r_S}{5}. \tag{6}$$

Table 1 gives a comparison between experimental obtained eddy-current amplitudes and theoretical with FEMM calculated values. The general agreement is for the Cu samples of the order of 2% whereas for the Al samples a difference up to 8% was found—see $\Delta m$.

The above described software package FEMM was used to calculate point by point the $H(t)$ profile including the damping of the pulsed magnet. With this method the magnetic dipole moment $m(Am^2)$ due to eddy currents was calculated for cylindrical samples as well as for spherical samples. The results in comparison with the experiments as obtained for the Cu-sphere (Cu2: $d = 7.3$ mm) are shown in Fig. 2. The agreement

Table 1
Comparison of measured ($m_{measured}$) and by FEMM calculated eddy-current density ($j$(FEMM)) and the resulting magnetic moments ($m_{calculated}$) at an applied external field of about 4.4 T for different pulse duration $\tau$ obtained for spherical (Cu2, Al2) and cylindrical (Cu1, Al1) sample geometries ($d = 4$ mm, $h = 8$ mm)

| Sample | Shape | $\tau$ (ms) | $B_{averaged}$ (T) | $J_{max}$(FEMM) (MA/m$^2$) | $m_{measured}$ ($10^{-3}$ Am$^2$) | $m_{FEMM}$ ($10^{-3}$ Am$^2$) | $\Delta m$ (%) |
|---|---|---|---|---|---|---|---|
| Cu1 | Cylinder | 15.7 | 4.425 | 100.61 | 4.98 | 5.06 | 1.6 |
| Cu1 | Cylinder | 9.1 | 4.618 | 181.14 | 9.11 | 9.11 | 0 |
| Cu2 | Sphere | 15.7 | 4.425 | 183.55 | 27.03 | 27.29 | 1.9 |
| Cu2 | Sphere | 9.1 | 4.618 | 330.08 | 49.7 | 49.08 | 1.3 |
| Al1 | Cylinder | 15.7 | 4.425 | 46.36 | 2.18 | 2.33 | 6.4 |
| Al1 | Cylinder | 9.1 | 4.618 | 83.47 | 3.85 | 4.20 | 8.3 |
| Al2 | Sphere | 15.7 | 4.425 | 57.96 | 1.96 | 1.90 | 3.2 |
| Al2 | Sphere | 9.1 | 4.618 | 104.30 | 3.47 | 3.41 | 1.8 |

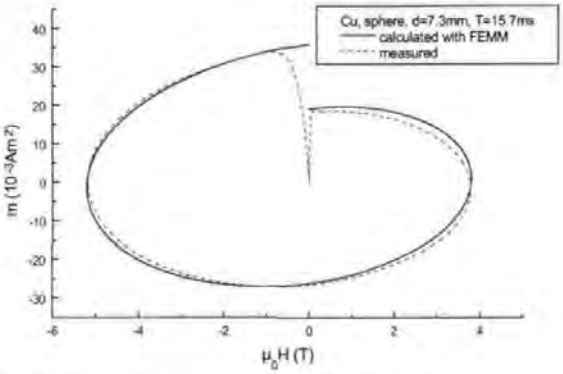


Fig. 2. Comparison of the measured and calculated hysteresis loop of a Cu-sphere (Cu2).

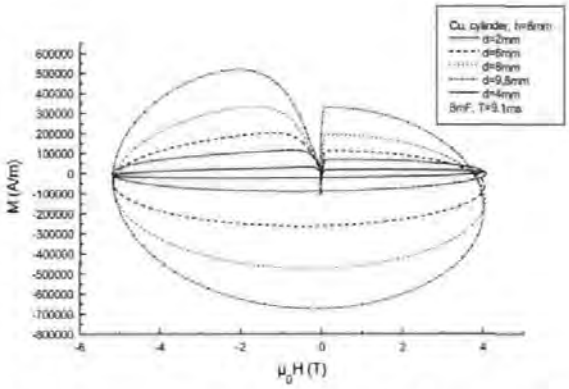


Fig. 3. Comparison of hysteresis loops of Cu-cylinders of different diameters.

between the measured loop and the FEMM calculated curve for the spherical Cu sample is excellent.

To prove the assumption that the magnetization due to eddy-current density increases linearly with the radius but stays constant with the height of the sample, several cylindrical samples of Cu were studied. Fig 3 shows eddy-current measurements ($T = 9.1$ ms) as obtained on Cu-samples with different diameters. In order that all samples have the same electrical conductivity they were heat treated at 500°C for 4 h. It can be shown that the eddy currents increase quadratically with the radius of the sample.

Fig. 4 shows eddy-current measurements ($T = 9.1$ ms) as obtained on Cu-samples with the same diameter but with different heights. In order that all samples have the same electrical conductivity they were heat treated at 500°C for 4 h. As can be seen and in agreement with the above given formulas the eddy currents are (nearly) independent of the height of the sample. Small but systematic deviations can be explained by the increasing $h$ and decreasing sensitivity of the pick-up system.

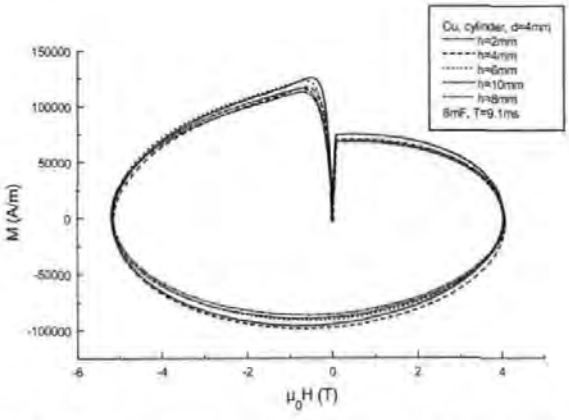


Fig. 4. Comparison of hysteresis loops of Cu-cylinders of different heights.

## 6. Conclusion

For analysing eddy currents in conducting samples, experimental and numerical studies were performed. The experiment showed a hysteresis loop with a phase-

shift of about 90° between field and magnetization, which increases with increasing conductivity and decreasing pulse duration. The shape has been reproduced by a finite element program. The eddy-current density has been analysed with this program and showed a linear radial increase and a constant value along the symmetry axis. This has been verified with the measured data. The absolute values of the measured and the calculated maximum magnetization showed an agreement for the Cu-samples within 2%, for the Al-sphere within 3% and for the Al-cylinder within 8% (see Table 1).

## Acknowledgements

The work was supported by the EC under the name MACCHARACTEC (European 4th Framework) with the project number SMT4-CT98-2212.

## References

[1] R. Grössinger, M. Katter, G. Badurek, R. Krewenka, J. Magn. Magn. Mater. 101 (1991) 304.
[2] R. Grössinger, X.C. Kou, M. Katter, Physica B 177 (1992) 219.
[3] R. Grössinger, E. Wittig, M. Küpferling, M. Taraba, G. Reyne, C. Golovanov, B. Enzberg-Mahlke, W. Fernengel, P. Lethuillier, J. Dudding, IEEE Trans. Magn. 35 (1999) 3971.
[4] D. Meecker, Finite element method magnetics; http://members.aol.com/dcm3c.

# SURVEY OF PULSE FIELD MEASUREMENT TECHNIQUE

**R.Grössinger[1], M. Küpferling[1], M.Taraba[1], A. Wimmer[1], J.Dudding[2], R. Cornelius[2], P. Knell[2], B. Enzberg-Mahlke[3], W.Fernengel[4], J.C.Toussaint[5], D.Edwards[6]**

[1] Inst. f. Festkörperphysik, Techn. Univ. Vienna,
Wiedner Hauptstr. 8-10 ; A-1040 Austria
[2] Hirst Magnetic Instr. Ltd., Cornwall, UK
[3] Magnetfabrik Schramberg, Schramberg-Sulgen, Germany
[4] VAC, Hanau, Germany
[5] CNRS, PO BOX 166X Grenoble, France
[6]Mecelec Developments Ltd. Gloucester, United Kingdom

**Abstract** The construction of a pulsed field magnetometer (PFM) suitable for industrial applications is given. A reliable calibration procedure for the magnetic field strength H and the magnetization M is described. The importance of the demagnetizing factor is demonstrated. The influence of eddy currents on a real magnetization is mathematically described and shown. A possibility to correct this error is shown.

## 1. Introduction

The characterisation of modern permanent magnet materials like SmCo based or Nd-Fe-B type material is difficult because coercivities up to 5 T are possible. The measurement in an Fe-yoke allows fields up to 1.5 T which is not sufficient neither to obtain a full second quadrant demagnetization curve nor to saturate the sample. Additionally each sample needs a special preparation where two plane and parallel surfaces have to be made. In magnet laboratories are sometimes vibrating sample magnetometers available which use a superconducting coil producing fields up to 8T and even more. These magnetometers, which are generally for small samples (few millimeters), need minutes for a hysteresis loop – this time is given by the allowed rise time dH/dt of the magnet. Additionally these systems operate in a magnetic open circuit, which needs a careful correction of the demagnetizing field. Generally a fast measurement of large industrial shaped samples is an open problem.

Recently the use of pulsed field magnetometers (PFM) for characterising permanent magnets in industrial surroundings was successfully tested [1,2]. The advantage of a PFM is that a fast loop measurement (within seconds) of magnet samples is possible. Generally there are two problems when a transient field pulse on a permanent magnet material is applied:
i) Eddy currents – In metallic samples the dynamic moment due to eddy currents causes an error in the measurement of the hysteresis loop.
ii) Magnetic viscosity – also this effect can cause a change of the "true" loop. This effect depends on the actual domain structure and the magnetisation process and consequently on the actual magnet sample.

Additionally the fact that such a PFM is a magnetically open circuit needs a correction for the demagnetizing field. This may be a problem for industrially used shapes like arc segments or tubes.

In the present work the construction of a pulsed field magnetometer is given. The problems due to eddy currents and those of the demagnetizing factor are discussed.

## 2. Industrial pulsed field magnetometer

Fig. 1 shows a block diagram of a pulsed field magnetometer (PFM). PFMs for industrial applications shall be systems which are operating at room temperature and which allow repetition rates of seconds. A pulsed field magnetometer consists of:

a) the energy source, generally a condensator battery, the stored energy is given by $C.U^2/2$. For industrial purpose the maximum charging voltage may be not higher than 3 kV, which allows the use of only one thyristor as a discharge switch. The capacitance determines then the stored energy and also the costs of such a system. In order to achieve fields up to 7 T in a usable volume (20 mm – 40 mm), an energy of about 50 kJ is necessary. The pulse duration shall be as long as possible (longer than 10 ms).
b) the charging unit, which shall generate a reproducible and selectable charging voltage; it determines the repeatability of the achieved field in the pulse magnet. For industrial purpose a short charging time is important.
c) pulse magnet: for an existing energy, the pulse magnet determines, via its inductivity, the pulse duration. Additionally the volume (diameter, homogeneity) limits the size of the magnets which can be measured. A field amplitude of at least 7 T is necessary in order to characterise modern permanent magnet materials. The resistivity of the magnet should be as small as possible for a low damping which is essential for the measurement of a full and closed hysteresis loop.
d) measuring device: this consist of the pick-up system and the measuring electronics (amplifiers, integrators, DC's, data storage). Here a careful design of the pick-up system is very important in order to achieve a high degree of compensation and consequently a good sensitivity. The pick-up system shall be connected directly with the transient recorder using a twisted and shielded pair of wires. If one uses a differential input a good common mode rejection can be achieved. For the analogue to digital conversion at least 12 bits shall be available. For storing the full curve 4k points for the dM(t)/dt and 4k points for the dH(t)/dt signal are generally sufficient. The integration can be performed by hardware or by software, however the use of an analogue and stable integrator is better.
e) electronics: the use of a modern data acquisition on a standard PC allows a software-supported operation of the PFM (charging, discharging and the measurement). For this purpose special software has to be written. The calibration constants as well as the possibility to choose M(H) or B(H) and also to correct online for the demagnetizing factor can be included.

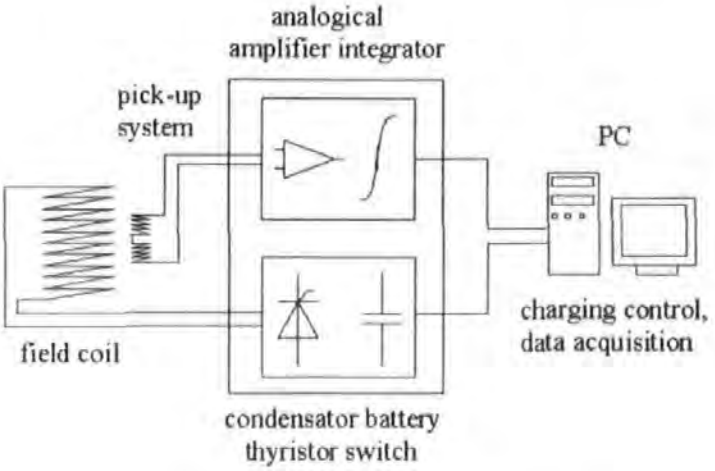


**Figure 1** Typical block diagram of a PFM

## 2.1 Measuring System

In general the law of induction is used for the magnetization measurements. In order to measure the magnetization versus the external field M(H), the influence of the field has to be cancelled. For this purpose several types of construction are possible. The most simple

approach is to measure using a compensated axial symmetric N/N pick-up system. Such a system consists simply of two coils, where both coils have N windings, which are wound antiparallel on the same former. Without a sample, this system delivers a signal that is close to zero. With a sample, the signal is proportional (factor K) to the magnetization M:

$$u_S(t) = u_1(t) - u_2(t) = \mu_0 NK \frac{dM}{dt} \qquad (1)$$

A better possibility is to use a dipole compensated coaxial system. A coaxial system consist of at least two concentric wound coils with different radii, $R_1$ and $R_2$ where, for a dipole compensation, the windings $N_1$ and $N_2$ have to fulfil the following condition: $N_1.R_1^2 = N_2.R_2^2$. Additionally the quadrupolar compensation as well as homogeneity considerations determine the different length of the coils. In all these equations the parameters are quadratic, which means the coils have to be manufactured very accurately.

The advantage of a N/N system is that the field compensation can be made mechanically, the disadvantage that it is rather sensitive to vibrations and thermal effects. The N/N pick-up coil can be adjusted mechanically in order to achieve compensation. The coaxial system is more difficult to compensate.

For large samples a coaxial pickup coil is used for determining the polarization J. The spacing of the pickup system has to be critically determined to provide a homogeneity of the pickup voltage better than 1% over an large area of (20 mm - 30 mm). The pick-up coils are coaxial, dipol compensated with an inner and outer coil. The design of the J coil can follow an idea published in [3]. The outer J coil consists of two sections which makes the coil "tunable", enabling the external field to be cancelled out, except a 90 degree out of phase quadrature component which shall be very small. For systems with high repetition rates it is advantageous to cool the pick-up system, because the compensation is very temperature sensitive.

### 2.2 Magnet Design

It is favorable to divide the pulse magnet into two magnets which can be pulsed independently providing a long and short duration pulse, conventionally named f and 2 f. Another possibility is to use two different pulse magnets with different pulse duration. The general idea here is to measure the loop using two different time constants in order to check if any difference in the shape of the loop can be detected. The origin of this difference can be either eddy currents in the metallic sample or magnetic viscosity. We will concentrate here on the effect of eddy currents.

## 3. Magnetometry

Pulsed field magnetometry is a magnetically open circuit method of magnetic measurement. This means that the shape of the hysteresis loop is affected by the demagnetizing field (see Chapt.3.2).

### 3.1 Calibration

#### 3.1.1 Field Calibration

Important for the reliability of a magnetometer is a careful calibration procedure. The field is calibrated using a small (3 mm diameter, 0.1 mm high) sensing coil which was produced by Magnet Physik. According to an information of this company the winding area of such a coil can be determined with an error of 0,3% for a coil with an area of

approximately 100 cm² and of 0,5 % to 1 % for a coil with a winding area between 3 and 5 cm². This can be improved if a NMR calibration is used. The induction voltage u(t) is then fitted thus determining the field calibration factor (for the f and the 2f pulse) as well as the damping factor and the pulse duration (including the effect of the damping). The fit is performed using the following formulas:

$$H = H_0.\exp(-at).\sin\omega t$$
$$u_i(t) = -N.A.{}^{dB}\!/_{dt} = -N.A\mu_0.H_0\left({}^{d}\!/_{dt}\right)\left[\exp(-at).\sin\omega t\right] \qquad (2)$$

The calibration factor creates a relation between the calibrated search coil, which delivers via the law of induction the voltage which corresponds to the signal in the existing H-measuring coil. Here the integrator is included. The scattering of the k-factor when different gains are used should be below ±1 %. This indicates that the gain linearity is sufficiently good.

### 3.1.2 Magnetization Calibration

The magnetization measuring coil can be calibrated using materials with well known saturation magnetization such as Fe and Ni (thereby the eddy current error causes an uncertainty) but better with a non-conducting sample such as $Fe_3O_4$ or a soft magnetic ferrite – such as 3C30. For magnets with complex shapes a calibration sample of the same shape shall be used. In principle a non-conducting material is better suited. Unfortunately the temperature dependence of the magnetization of the 3C30 ferrite available in industry is much worse then that of $Fe_3O_4$ – see Fig.2.

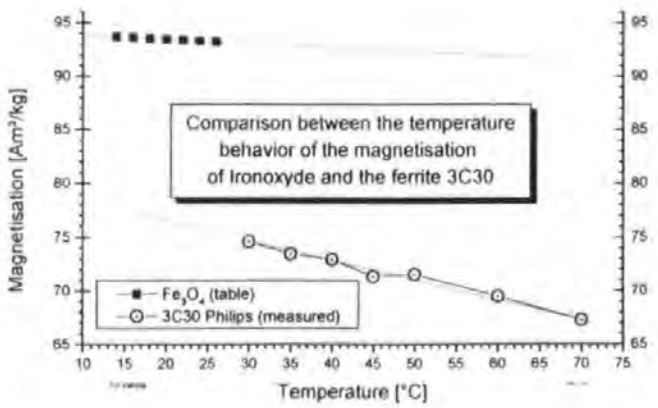


**Figure 2** Temperature dependence of the saturation magnetization of 3C30 in comparison with that of $Fe_3O_4$.

An absolute magnetization calibration is only possible within 2 %. Due to the good linearity of the analogue measuring electronics and the high resolution of a good ADC card (14 bit) a relative measurement – which is most important for a quality control system - with a relative accuracy better than 1 % is possible.
Hysteresis measurements on Fe and Ni cylinders (h = 8mm, d = 4mm) were performed. Fig.3 shows, as an example, the loop as obtained on $Fe_3O_4$. The calibration obtained from the different materials constants agree within 2 %. Also the repeatability of the magnetization measurements, especially using Fe or Ni samples, was only within 2 % which may be a

consequence of eddy currents. In our case the zero signal was about 10 % of the sample sign of $Fe_3O_4$. If one transfers this to a Nd-Fe-B sample one can say that the smallest magnet samp which can be measured with this system has a mass of 0,3 g which corresponds to a cube ( 3 mm x 3 mm x 3 mm in a system which is suited for sample sizes up to 25 mm.

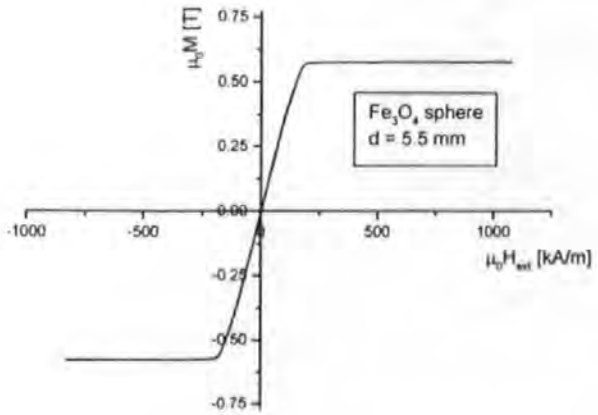


**Figure 3** Hysteresis measurement as obtained on $Fe_3O_4$

To check the repeatability the measurements should be repeated at least 10 times giving an average value <M>. Measurements using a shorter pulse duration f/2f were performed additionally, which were generally in good agreement with those made with the long pulse. For the metallic samples an error of 1 % – 2 % due to the eddy currents occurs. Summarizing one can say that a PFM can be calibrated with an absolute accuracy of ± 1.5 % [4].

**Sample geometry:** In general any magnetization measurement shall only be performed on a spherical or elliptical sample. However especially in industry other sample shapes such as cylinders, cubes, tubes etc. are usual. In this case the effect of the sample geometry on the accuracy of the magnetization measurements in the PFM has to be checked.

### 3.2 The demagnetizing factor

In principle the correction for the demagnetizing factor, $N_d$, is a very important step to get the "true" hysteresis loop as a function of the internal field. Especially important points like the remanence and the working point but also the energy product $(B.H)_{max}$ depend strongly on $N_d$. For simple shapes like spheres or ellipsoids a well defined demagnetizing factor exists. Unfortunately in industry more complex shapes like cylinders, cylinders with holes and also arc segments are used. In this case $N_d$ can become a tensor, corresponding to the symmetry of the sample. For complex shapes a finite element package have to be used in order to calculate the stray field [5].

In order to investigate the effect of the $N_d$ for simple shapes, in Fig.4 the demagnetizing curves in the second quadrant for an anisotropic ferrite HF 24/16 are drawn. The two samples were from the same batch, one was a cylinder and one a sphere. The shape of the loops agrees very well. This means that in this case the use of a constant $N_d$ for the cylinder is sufficient for the correction.

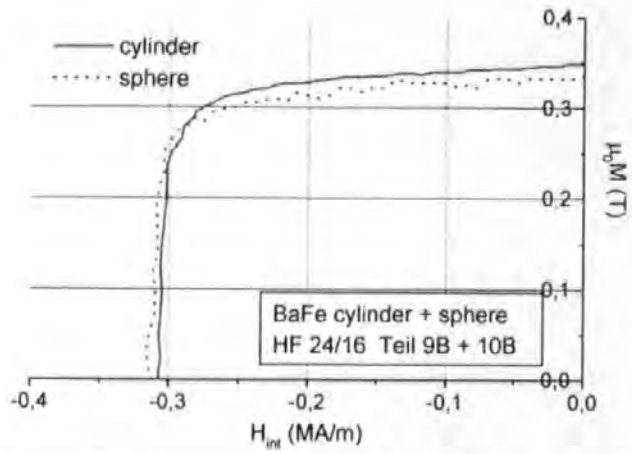


**Figure 4** Demagnetizing curve as obtained on an spherical and a cylindrical anisotropic Ba-ferrite (HF 24/16).

Fig. 5 shows the hysteresis loop as measured on a cylindrical sample with a hole (outer diameter 19 mm, hole: 3.17 mm; h = 2 mm) of plastic bonded Nd-Fe-B type material. Assuming $N_d = 0.45$ gives a remanence of 0.666 T, whereas $N_d = 0.55$ delivers a remanence of 0.682 T. The static value measured in a Fe-yoke was 0.682 T. This demonstrates the problem of such an unknown demagnetizing factor - it seems impossible to say what the correct value for $N_d$ really is.

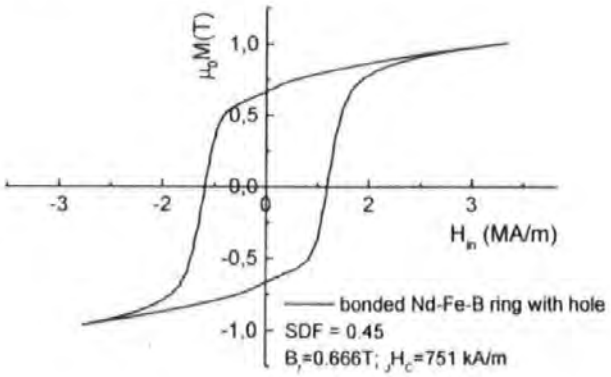


**Figure 5** Hysteresis loop of a cylindrical sample with a hole of plastic bonded Nd-Fe-B type material.

## 4. Eddy currents

A time dependent external magnetic field causes, according to Maxwell equations, in a metallic conducting sample currents ("eddy currents") which create a dynamic magnetic moment which is antiparrallel to the external field as is demonstrated in Fig. 6.

Under the following assumptions a general proportionality between the magnetic moment and dB/dt for axis-symmetric samples can be derived using the Maxwell equations.

1. The external field is homogenous and isotropic in the area of the sample.
2. The conductivity of the sample is not too high – interactions between eddy currents are negligible.
3. The radius of the sample and the magnet are small compared to the wavelength of the external field.

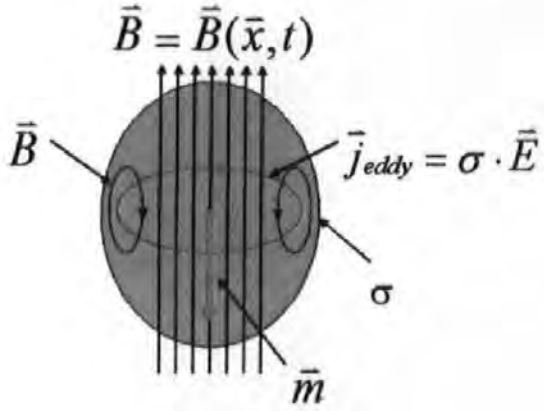


**Figure 6** The principle of eddy currents in a metallic sample.

The measurement corresponds to the superposition of each dipole moment $\vec{m}_i$ which is proportional to $j_i = j(r_i)$. Therefore the total magnetic moment $\vec{m} = \sum_i \vec{m}_i$ is proportional to the total eddy current $\vec{j}$. And finally one can write for a cylinder symmetrical sample (radius $R_S$):

$$m \propto \sigma \cdot \frac{\partial}{\partial t} B_0 \quad \Rightarrow \quad \vec{m} = \int_{sample} \vec{m}(x,t).d^3x = -\frac{\sigma}{16c^2}\frac{d}{dt}B(t)\int_{z_1}^{z_2} R_S(z)^4\, dz.\vec{e}_z \qquad (3)$$

This means that, due to eddy currents, plotting the magnetization versus dH/dt (see Fig.7) of a conducting sample delivers a linear relation where the slope is proportional to σ (specific electrical conductivity) which is equal to 1/ρ (specific electrical resistivity).

In order to test this type of analysis it was tried to plot the magnetization as a function of the derivative of the field changing with time. The result of this type of analysis applied on a Cu and an Al cylinder is given in Fig 7.

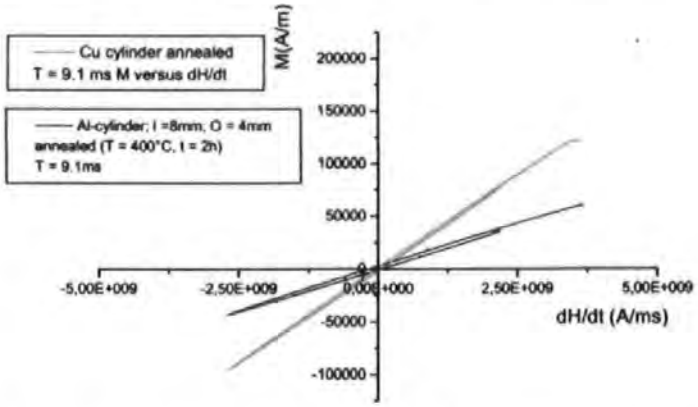


**Fig. 7** Eddy current magnetization versus dH/dt as obtained on a Cu cylinder and an Al cylinder in the annealed state using a pulse duration of 9.1 ms

The slope of the M versus dH/dt curve for the Cu sample is indeed about two times higher than that for the Al. The slope depends also on the geometry of the sample. In all cases a linear M versus dH/dt was found.

The maximum eddy current density ($J_{max} = J(r_{sample}, z = 0)$) of all samples obtained with different pulse duration, and their magnetic moment $m_{FEMM}$, can also be calculated using FEMM designed by David Meeker [6] (2D- finite element software). For not too big samples and not too high frequencies – a linear relation between the eddy current density and the radius r holds, which gives a rather simple solutions for calculating the dynamic eddy current magnetization. Aassuming now a linear radial increase of the eddy current density and a constant value along the z-axis allows to calculate the so-called eddy current magnetization in metallic conducting samples:

$$m_{cyl} = \frac{1}{2c} 2\pi \cdot h \int_0^{r_p} r^2 j_{max} \frac{r}{r_{sample}} dr = \cdot \frac{\pi \cdot h \cdot j_{max} \cdot r_{sample}^3}{4} \tag{4}$$

$$m_{sph} = \frac{1}{2c} 2\pi \int_0^{\pi} \sin^2 \vartheta \int_0^{r_p} r^3 j_{max} \frac{r \sin \vartheta}{r_{sample}} dr d\vartheta = \cdot \frac{4\pi \cdot j_{max} \cdot r_{sample}^4}{15} \tag{5}$$

The magnetization is then given by

$$M \approx m/V, \tag{6}$$

where $V$ is the volume of the cylinders

$$V = r_s^2 \pi h \tag{7}$$

Finally, the magnetization for a cylinder is

$$M = \frac{j_{max} r_s}{4}. \tag{8}$$

Hence, the magnetisation is independent of the height of the cylinder.
A similar calculation delivers the magnetization for a sphere

$$M = \frac{j_{max} r_s}{5}. \tag{9}$$

To prove the assumption that the magnetization increases due to eddy current density linearly with the radius but remains constant with the height of the sample, several cylindrical samples of Cu and Al were studied [7]. Fig 8 shows eddy current measurements (T = 9.1 ms) as obtained on Cu-samples with different diameters.

The measured maximum magnetization can be fitted with a function $f = Cr^2$ (r is the radius of the sample) which gives, as theoretically expected, a quadratic dependence. On the other side, in agreement with the above given formulas, the eddy currents are (nearly) independent of the height of the sample which indeed was experimentally found [9].

The actual hysteresis loop of a metallic permanent magnet shows that, close to the saturation, the effect due to eddy currents is equivalent to that of a metalic non-magnetic sample, scaling only with the electrical resistivity. However, close to the coercivity an additional contribution arises due to the permeability of the material. This can only be corrected by applying a finite element calculation.

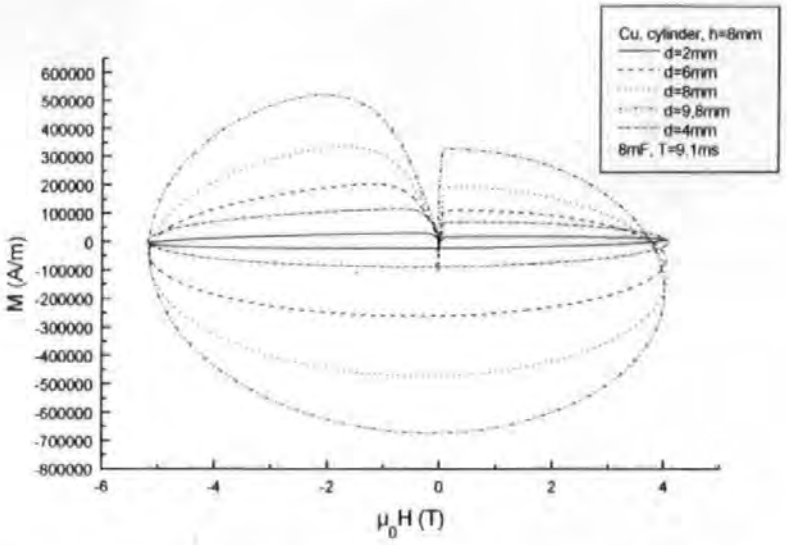


**Fig. 8** Comparison of hysteresis loops of Cu-cylinders of different diameters; The magnetization increases with increasing sample diameter.

## 5. Permanent magnet measurements

The hysteresis loop of each sample is measured with two pulse durations (f and 2f) which shall generate the same J signal with respect to the applied field but with the addition of different dynamic magnetizations due to eddy currents. The eddy currents are related to the frequency, roughly the eddy current magnetization is proportional to dH/dt [7]. By processing the two measurements it is possible to remove the error due to eddy currents producing the direct equivalent of a static hysteresis plot, this is named the f/2f method [8]. This method can be applied under the general assumption that the eddy current error is not too high. The validity and the limits of the f/2f method were investigated by a 3D finite element calculation [9].

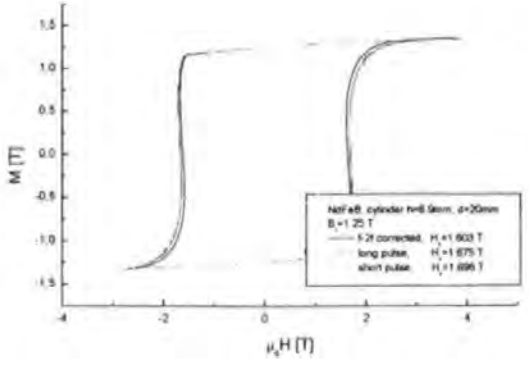


**Fig. 9** Hysteresis loop of a sintered Nd-Fe-B magnet (Vacodym 510)as measured with a f and a 2f pulse and applying the so-called f/2f correction.

For testing the system and especially the f/2f correction a large cylindrical commercial Nd-Fe-B magnet from VAC (Vacodym 510, Charge 210105) was measured – see Fig. 9. This cylinder had a diameter d = 20 mm, and a height of 6.9 mm. The static data measured by VAC were: remanence $Br$ = 1.296 T, the coercivity $\mu_0 H_{CJ}$ = 1,577 T.

The f/2f corrected coercivity value is now 1.603 T which is 2 % too high. The measured remanence value of 1.25 T is about 2 % too high. So the f/2f corrected hysteresis loop as

obtained from a really calibrated system looks very good. Here more measurements are necessary in order to check the reliability of this f/2f correction procedure.

## 6. Summary

The most important parameters determining the dynamic hysteresis measurement in a PFM were discussed. For obtaining the "true" loop the demagnetizing factor has to be considered. An absolute calibration of better than 2 % is possible. The eddy currents in metallic conducting samples scale with the square of the radius of the sample. For permanent magnets with sample dimensions up to 25 mm and for pulse duration which are above 25 ms the so-called f/2f correction procedure can be applied.

### Acknowledgement

The work was supported by the EC under the name MACCHARACTEC (European 4th Framework) with the project number SMT4-CT98-2212.

### Refernences

[1] R.Grössinger, D.Eckert, E.H.C.Sinnecker, M.Taraba, G.W.Jewell
An accurate pulsed field hysteresograph; Physica B 211 (1995) 348 – 350

[2] R.Grössinger, M.Küpferling, A.Wimmer, M.Taraba, W.Scholtz, J.Dudding, P.Lethuillier, B.Enzberg-Mahlke, W.Fernengel, G.Reyne;
The Pulse Field Magnetometer – a tool for characterizing Permanent Magnets;
Proceedings of the 16th International Workshop on Rare-Earth Magnets and Their Applications, Ed by H.Kaneko, M.Homma, M.Okada; Sendai (Japan) (2000) 1129 – 1138

[3] D.Eckert, R.Grössinger, M.Doerr, F.Fischer; A.Handstein, D.Hinz, H.Siegel, P.Verges, K.H. Müller;
High precision pick-up coils for pulsed field magnetization
Measurements; Physica B 294-295 (2001) 705-708

[4] R.Grössinger, M.Taraba, A. Wimmer, J.Dudding, R. Cornelius, P. Knell, P.Bissel, B. Enzberg-Mahlke, W.Fernengel, J.C.Toussaint, D.Edwards;
Calibration of an Industrial Pulsed Field Magnetometer; IEEE Transactions on Magnetics 38(5) (2002) 2982 - 2984

[5] J.C. Toussaint (CNRS Grenoble) private communication

[6] D.Meecker, Finite element Method Magnetics; http://members.aol.com/dcm3c

[7] R.Grössinger, M. Küpferling, P. Kasperkovitz, A. Wimmer, M.Taraba, W.Scholz, J.Dudding, P. Lethuillier, J.C.Toussaint, B. Enzberg-Mahlke, W.Fernengel, G. Reyne
Eddy currents in pulsed field measurements; JMMM 242-245 (2002) 911-914

[8] G.W. Jewell, D. Howe, C. Schotzko, R. Grössinger;
A method for assesing eddy current effects in pulsed magnetometry;
IEEE Trans. Magnetics 28 (1992) 3114 - 3116

[9] C. Golovanov, G. Reyne, G. Meunier, R. Grössinger, and J. Dudding;
Finite Element Modeling of Permanent Magnets under Pulsed Field;
IEEE Transactions on Magnetics July 2000, Volume 36, (04) 1222-1225

# ACCURACY AND REPEATABILITY OF AN INDUSTRIAL PULSED FIELD MAGNETOMETER

**Robin Cornelius[1], Beatrice Enzberg-Mahlke[2], Wihelm Fernengel[3], John Dudding[1], Paul Knell[1], Roland Grosseniger[4], Michal Taraba[4], Alfred Wimmer[4], Jean.C. Toussaint[5], and David Edwards[6]**

[1] Hirst-Magnetic Instruments Ltd, Tregoniggie, Falmouth, Cornwall, UK, TR11 4SN.
[2] Magnetfabrik Schramberg, Schramberg-Sulgen, Germany
[3] Vacuumschmelze GmbH Hanau, Germany.
[4] Inst. F. Experimentalphysik, Techn. Univ. Vienna, Austria.
[5] CNRS, Grenoble, France.
[6] Mecelec Developments Ltd. Gloucester, United Kingdom.

**Abstract** A Pulsed Field Magnetometer (PFM) has been constructed for the purpose of industrial quality control of industrially shaped high coercivity magnets. The accuracy and reproducibility of the system has been carefully examined with the machine under industrial conditions.

## 1. Introduction

With the increasing use of high coercivity rare earth permanent magnet materials in safety critical and other sensitive applications, it has become impossible using existing technology to provide quality control of any significant proportion of a magnet batch or to measure representative sizes and shapes of the magnetic material in its industrial form.

The high cost of rare earth based magnets has driven many consumers to seek cheaper sources of these materials. These cheaper materials come at the expense of the overall quality and variability of the magnets. No practical methods have previously existed to differentiate the quality of industrially shaped magnets other than to integrate the magnet in its finial assembly and test the entire unit.

A prototype industrial Pulsed Field Magnetometer was developed [1] to provide a solution to these problems. The objectives were to have the capability to test high coercivity magnets in their final industrial shapes at rates that is practical for 100 % quality control.

## 2. Error minimisation

The prototype industrial PFM used many techniques to minimise and eliminate errors to improve absolute accuracy and repeatability.

Eddy current effects are perceived as the biggest problem in Pulsed Field Magnetometry. The PFM discussed here used the patented f/2f technique [2] to eliminate eddy current errors. By taking two measurements with different applied field periods, it is possible to deduce the effects of eddy currents and use this information to mathematically predict the B, H curve with no eddy current effects. Figure 1 shows the application of the f/2f process on part of the J, H curve.

The technique of Pulsed Field Magnetometry is an open circuit measurement method and as such, it requires the effects of self demagnetisation fields to be taken into account. Software was developed to calculate the global demagnetisation factor for any given shape. This factor could then be applied to the measurement to correct for the self-demagnetising effect.

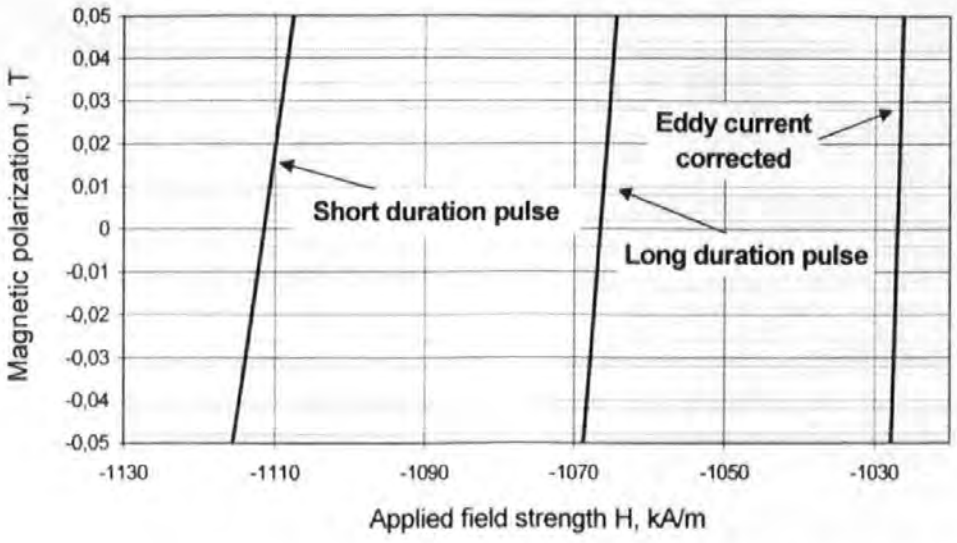


**Figure 1** Eddy current effects at coerciverty due to different duration pulses and correction on a NdFeB 270/95 h sample; f/2f correction

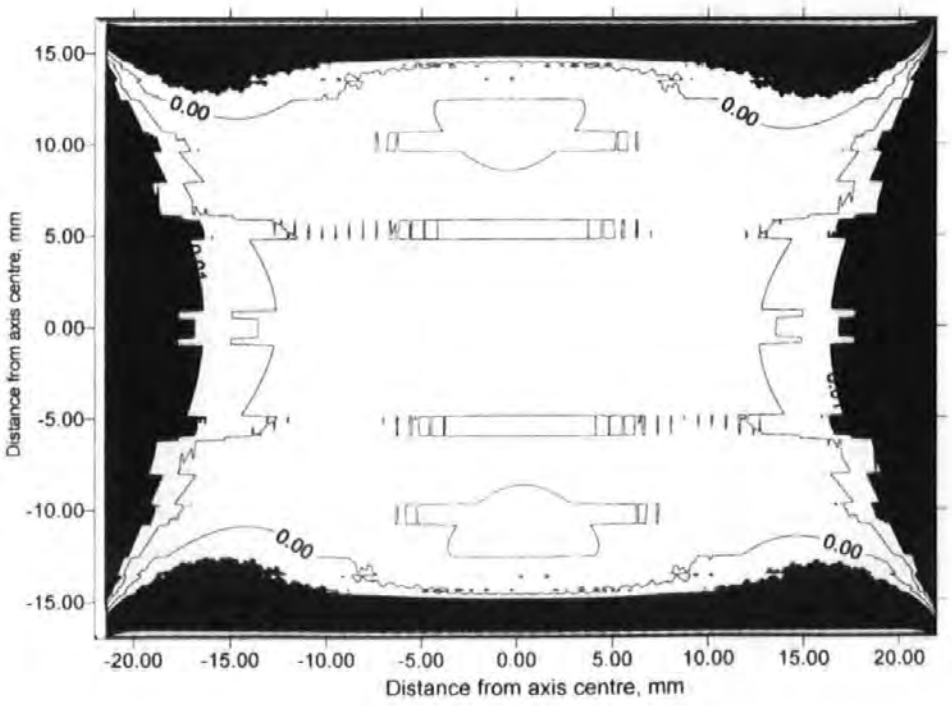


**Figure 2** Homogeneity contours through cross-section of designed humbucking pickup coil. Black area, worse than 1 % homogeneity. White area better than 1 % homogeneity.

The pickup coils were designed to have the maximum homogenous pickup volume possible [3]. By using radial humbucking type pickup coils of a non standard design it was ensured that sample placement need not be 100 % accurate, a requirement for rapid industrial sample loading.

Figure 2 shows the predicted homogeneity of the humbucking pickup coil through a

cross-section of the centre axis. The white area has a homogeneity of better than 1 % while the black area has a homogeneity worse than 1 %. This means that any sample in the white area is not sensitive to sample position placement and will give the same results (within 1 %) if placed anywhere else with in the white region. The pickup coil windings are external to the area covered by figure 2.

Novel external nulling circuits also improved the pickup systems overall accuracy and made adjustment in an industrial environment straightforward, a significant improvement to the conventional techniques of highly accurate pickup coil building or compensation coils that need 'tuning'.

## 3. Results

Figure 3 shows the measurement comparison between a permeameter and the industrial Pulsed Field Magnetometer. The finite field steps of the permeameter can clearly be seen. On "harder" rare earth materials the above comparison would not be possible as the permeameter would reach its applied field limit (due to pole saturation). The PFM does not have these limitations.

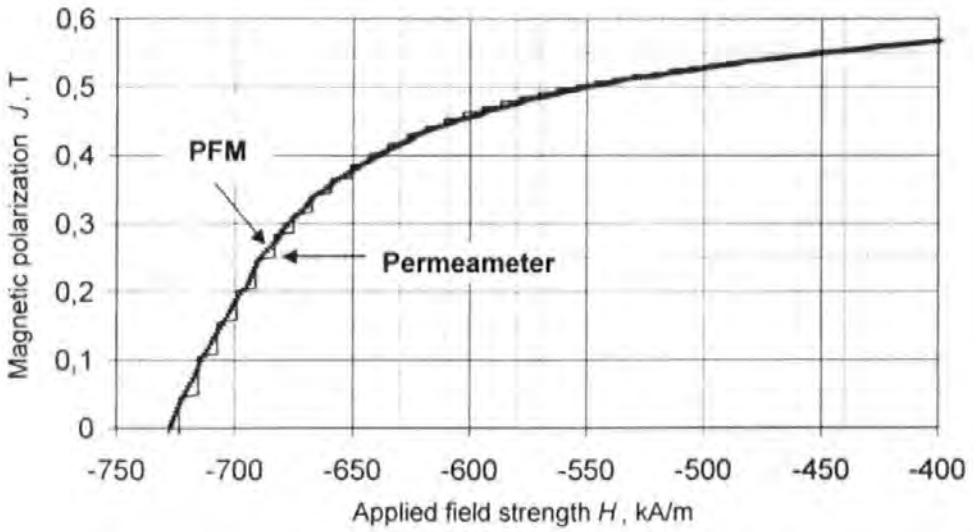


**Figure 3** Permeameter / PFM Comparision (2nd Quadrant) of a bonded NeFeB

## 4. Conclusions

Pulsed field Magnetometry has demonstrated its self as a viable measurement technique and is the only available technique that can handle the range of industrial shaped magnets with high coercivity as well as being capable of 100 % control at industrial production rates.

Early experiments are suggesting that the PFM has a greater repeatability than conventional relative permeability techniques. Absolute accuracy improvements remain impossible to determine as even two permeameters differ by larger amounts than the accuracy attempting to be measured.